The spiral, zigzag, and steady turning maneuvers were selected as the standards on which to base the evaluation of inherent or open loop characteristics of the ship. These three simulated maneuvers were performed for thirteen of the full scale model equivalents for which a complete mathematical model was developed. In addition, simulated stopping maneuvers were conducted, both with and without rudders, for a few representative configurations.

In the following discussions each definitive maneuver is described and simulation results are presented for each configuration. Unless otherwise noted, all of the results pertain to full load displacement of 350,000 tons in calm water of unrestricted depth and width and a rudder deflection rate of 2.33 degrees per second. All derived numerical measures are expressed dimensionally in real time and distance. To utilize the data in analyses involving other ship sizes, the dimensional values can be readily converted to nondimensional values by use of appropriate normalizing factors as indicated in the discussion.

Spirals - The spiral is a definitive maneuver which provides quantitative measures of the inherent directional stability characteristics of a ship. The basic spiral maneuver can be conducted on trials with special instrumentation in the following manner:

1. The propeller speed is adjusted to an rpm corresponding to a predetermined speed, ahead or astern. Once steady rpm is achieved, the throttle settings are held constant for the balance of the maneuver.

2. The rudder is manipulated as necessary until an essentially straight course has been obtained and held for one minute.

3. The rudder is then deflected to about 15 degrees right and held until the rate of change of heading, as indicated by the gyro compass and a stop watch, remains constant for one minute or

longer. The rudder angle is then decreased by 5 degrees and held again until the rate of change of heading remains constant for one minute. The procedure is repeated until the rudder has covered a range of 15 degrees on each side and back again to 20 degrees on the first side. For 5 degrees on either side of zero or neutral rudder angle, the intervals are taken in one degree steps.

For ships equipped with a rate gyro, each rudder setting in Step 3 is held until the heading rate reading on the gyro becomes steady. A similar procedure is followed in the computer simulation.

The numerical measures associated with the basic spiral maneuver are derived from measured values of the steady rate of change of heading versus rudder angle. A plot of these variables is indicative of the inherent directional stability characteristics of the ship. If the plot is a single continuous curve from right rudder to left rudder, the ship is said to be inherently directionally stable. If the plot consists of two branches joined to form a hysteresis loop, such as is shown for a typical series model in Figure 6-12, the ship is said to be inherently directionally unstable. In such cases, the size of the loop height and width, as defined in Figure 6-12, can be used as a numerical measure of the degree of instability; the larger the loop, the more unstable the ship. The height of the loop is a more direct measure of inherent instability since, for a given rudder planform, it will be the same regardless of whether the rudder is all movable or flapped, whereas the width of the loop is affected by the control effectiveness of the rudder as well. However, the width of the loop is a fairly direct indication of probable coursekeeping ability since it governs the envelope of rudder angles which must be employed to keep the ship from swinging from side to side. Typical of single screw ships, there is a shift of the loop to starboard. Therefore, the height of the loop is defined as that taken at the center of the loop or at neutral rather than zero rudder angle.

Simulated spiral maneuvers were performed at approach speeds of 8 and 16 knots for each of the thirteen models for which complete mathematical models were obtained. The numerical measures derived from these maneuvers are compared in Table 6-8. Included are values of the neutral rudder angle or loop center at which the height was measured. As expected from the analysis based on nondimensional dynamic stability indices, all thirteen configurations are inherently directionally unstable as indicated by the existence of the loop.

The effect of L/B variation on the inherent directional stability characteristics of the 350,000 ton hulls can be seen by comparing the numerical measures given in Table 6-8 for ships E, F, and H with L/B = 5.0, 5.5, and 6.5, respectively. Dimensionally, the degree of instability decreases generally with an increase in L/B over the range covered, as indicated by the decrease in loop height. At 16 knots for example, the loop height is decreased from 0.458 to 0.332 deg/sec, from ship E with L/B = 5.0 to ship H with L/B = 6.5. The loop width is about 5 degrees for ships E and F, but only about 3 degrees for ship H.

The effect of B/T variation can be seen from a comparison of the numerical measures in Table 6-8 for either ships E, K, and L or ships G, N, and P with B/T = 3.00, 3.75, and 4.50, respectively. In both cases, the loop height decreases, indicating a decrease in inherent instability, with an increase in B/T. The largest decrease occurs between ships G and P; the loop width also decreases from 7 to 4.5 degrees.

Ships H, J, and P have the smallest degree of inherent instability among the configurations investigated, as indicated by loop heights between 0.32 and 0.33 deg/sec at a speed of 16 knots. Of these, ship H potentially should have the best course-keeping characteristics because of its relatively small loop width of 3 degrees.

The foregoing trends indicated by the dimensional numerical measures differ to some extent from the trends shown by the nondimensional dynamic stability indices discussed earlier. The

trends shown by σ_{1h}", which is based on equal volume comparisons, at least appear to reflect the same trends as exhibited by the loop heights at L/B values above 6.0 and B/T values above 3.75. The differences in trends associated with the loop heights and nondimensional stability indices are attributed largely to the effects of the nonlinearities. It should be emphasized, however, that the range in degree of instability covered by the cases in Table 6-8 is rather small, particularly in terms of the nondimensional indices.

As stated previously, the height and width of the loop obtained from spiral maneuvers are both indicative of the inherent coursekeeping ability of unstable ships. It is quite possible for ships having fairly large loops to maintain course reasonably well, with a properly designed and adjusted automatic control system. However, they may have the tendency to require excessive rudder activity with attendant wear on control machinery and increase in resistance or propulsive power in maintaining a straight course. The size of the loop that can be tolerated and yet give satisfactory overall coursekeeping characteristics can best be established by means of studies performed on a computer simulation facility which include the effects of the helmsman, autopilot, and machinery characteristics associated with the complete control system. The mathematical models provided in Table 6-6 can provide a good basis for such studies.

Zigzags - The zigzag is a definitive maneuver which is intended to provide quantitative measures of the inherent effectiveness of the rudder in making changes in heading or width of path. The handling qualities revealed by this maneuver include the ability to both initiate and check course changes during transient maneuvers. The first half cycle of the zigzag maneuver, known as the overshoot maneuver, provides most of the numerical measures of interest for evaluating handling qualities. A typical procedure for conducting zigzag maneuvers on ships

without the use of special instrumentation is as follows:

1. The propeller speed is adjusted to an rpm corresponding to a predetermined speed. When a steady rpm is achieved, the throttle settings are held constant for the balance of the maneuver.

2. The rudder is manipulated as necessary until an essentially straight course has been obtained and held for one minute.

3. After steady conditions on straight course have been established, the initial heading shown on the ship's gyro compass is noted. The rudder is then deflected at maximum rate to a predetermined angle and held until a predetermined change of heading angle is reached.

4. At this point, the rudder is deflected at maximum rate to the opposite (checking) angle and held until the ship passes through its initial course to complete the overshoot phase of the maneuver.

5. If a zigzag is to be completed, the maneuver is continued until the same heading to the opposite side is reached, whereupon the rudder is again deflected rapidly to the same angle in the initial direction. This cycle is repeated through 3rd and 4th executes of rudder angle changes.

In this discussion a designation such as 20-10 is used to denote a zigzag or overshoot maneuver which is conducted with maximum rudder angles of ±20 degrees and the heading change is 10 degrees. The standard maneuver usually included in maneuvering trials is the 20-20 zigzag, although other combinations are also used. The 5-5 zigzag has been advocated as a means for evaluating directional stability of full-form ships.

Figure 6-13 shows the time history of heading angle and path change obtained from a simulated 20-20 zigzag maneuver with a typical series model. As shown by the figure, the primary numerical measures obtained from the overshoot maneuver are the time to reach execute change of heading angle, overshoot heading angle, and overshoot width of path. The zigzag maneuver

provides the additional measures of reach and period which are more significant for frequency response analyses than establishment of handling qualities. The time to reach the desired heading is a direct numerical measure of ability to rapidly initiate changes in course. The heading and path width overshoots are measures of course checking ability and are indicative of the amounts of anticipation and latitude of error that the helmsman is permitted if he is to retain control within tolerable limits of the maneuver. It should be noted that path width data require elaborate instrumentation and, therefore, are seldom obtained on ship trials, whereas such data are easily acquired in the computer simulations.

Simulated zigzag maneuvers were performed for each of the models for which complete mathematical models were available. The program included 5-5, 10-10, and 20-20 zigzags conducted at approach speeds of 8 and 16 knots. The numerical measures derived from these maneuvers are compared in Tables 6-9 and 6-10 for the 8 and 16 knot cases, respectively. Values for the second and third heading angle overshoots and period for the 5-5 zigzag were not obtained for the 8 knot case due to restrictions placed on computer running time. However, the trends exhibited by these quantities are shown by the corresponding 16 knot case.

Table 6-10 shows that for the 5-5 zigzag maneuver, the second heading angle overshoot in each case is many times larger than the first. This behavior is characteristic of inherently directionally unstable hulls and becomes particularly pronounced when execute rudder angles approach the loop width. This can be seen by comparing the cases of ships B and H with loop widths of 7 and 3 degrees, respectively. The third heading angle overshoot is much smaller than the second, but is considerably larger than the first. The second heading angle overshoot is also somewhat larger than the first for the 10-10 zigzags shown in Tables 6-9 and 6-10. The third overshoot, however, tends to be equal or somewhat lower in most cases. For the 20-20 zigzags in Tables 6-9 and 6-10, the second heading angle overshoot is

generally only slightly higher and the third is only slightly lower than the first. Other general trends shown are that the first overshoots (heading angle and path width) increase with increase in the execute angles, and for a given set of execute angles, increase somewhat with an increase in speed.

The ability to initiate and check a course change rapidly is one of the most important handling qualities of a ship. The first half cycle of the 20-20 zigzag or overshoot maneuver provides an excellent means for objectively evaluating this inherent capability irrespective of human response and instrumentation. On a comparative basis, the best ship is the one which combines the least time to reach the execute heading change with the smallest overshoot heading angle and width of path. These characteristics are not always compatible since they depend both on the inherent control effectiveness and degree of inherent directional stability or instability. The following trends are expected to apply when comparing numerical measures from 20-20 overshoot maneuvers for ships of equal displacement having equal control effectiveness but with different degrees of inherent stability or instability:

1. The time change to reach the execute heading angle change should be about the same.

2. The overshoot heading angle should become smaller as the degree of inherent instability is decreased.

3. The overshoot width and total width of path should both be decreased as the degree of inherent instability is decreased.

These trends can be examined in terms of the numerical measures for the first overshoot phase of the 20-20 zigzag presented for the 16 knot case in Table 6-10c. In general, those ships with the lowest degree of inherent instability have the smallest overshoot angles and those with the highest degree of inherent instability have the largest overshoot angles. For example, ships J and P with the lowest loop heights in Table 6-8 (0.321 and 0.325 deg/sec, respectively) have the smallest overshoot angles (10.4 and 10.6 degrees, respectively). However,

ship B with the highest loop height in Table 6-8 (0.493 deg/sec) has the largest overshoot angle (18.2 degrees). It is also noted that ship J with the least amount of control effectiveness, as indicated in Table 6-5 by the value of cp = 1.74 sec^{-2}, takes the longest time to reach the execute heading angle (84 seconds). However, this does not have much effect on the overshoot angle in this case. The smallest overshoot path widths are generally associated with the smallest overshoot angles. Since the comparisons are based on equal displacement hulls, the longer ships tend to have relatively larger overshoot path widths for equal overshoot angles. For example, ships J and P with overshoot path widths of 1704 and 1502 feet have lengths of 1327 and 1199 feet, respectively.

The trends shown in Table 6-9c for the 8 knot case are similar to those shown in Table 6-10c for the 16 knot case. However, the magnitudes of the overshoots are somewhat smaller in each case and the times to reach execute heading change are considerably longer.

Appendix C, containing sample computer generated plots, and tabulated data summaries, is a synopsis of principal numerical results for 35 degrees rudder angle turns and 20-20 zigzag maneuvers at 8 knot approach speed for all 16 ships operating in deep water.

Turning Maneuvers - The turning circle provides quantitative measures of the effectiveness of the rudder and is the most widely used of the definitive maneuvers. The following is the standard procedure for the conduct of such maneuvers on a ship:

1. The propeller speed is adjusted to an rpm corresponding to a predetermined speed and when steady rpm is achieved, the throttle settings are held constant for the balance of the maneuver.

2. The rudder is manipulated as necessary until an essentially straight course has been obtained and held for one minute.

3. After steady conditions on a straight course have been established, the initial heading on the ship's gyro compass is noted. The rudder is then set to a predetermined angle, e.g. 35 degrees, and held until a change of heading of at least 540 degrees has occurred, at which point the maneuver is terminated.

Figure 6-14 shows path data from a simulated 35 degree starboard steady turning maneuver performed for a typical series model. The numerical measures of primary interest are the tactical diameter, advance, transfer, and steady turning diameter, as defined on the figure; the times to change heading 90 and 180 degrees, and speed loss in turning. All of these measures should be taken into consideration in defining handling qualities associated with this type of maneuver.

Simulated steady turning maneuvers were performed for each of the thirteen 350,000 ton displacement hulls for which complete mathematical models were available. The program included turns with 10, 20, 35, and 45 degree rudder angles. All turns were made to starboard at approach speeds of 8 and 16 knots. The numerical measures derived from the steady turning maneuvers are summarized in Tables 6-10 and 6-11 for approach speeds of 8 and 16 knots, respectively. These numerical measures can be compared to determine the relative turning performance of the thirteen ships.

Figure 6-15 shows the variation with rudder angle of the nondimensional advance, transfer, tactical diameter, and speed in steady turn for ship E. In general, the trends shown are characteristic of those found from maneuvering trials of large tankers. At a 35 degree rudder angle, the steady turning diameter is about 2.8 ship lengths, which is somewhat larger than obtained on some large, unstable tankers. This is attributed to the relatively low aspect ratio rudder used with the series configurations. At a rudder angle of 45 degrees, however, the steady turning diameter is 2.2 ship lengths, which compares favorably with values achieved by modern large tankers. The percentage loss in speed is about 69 and 76 percent for the 35

and 45 degree rudder steady turns, respectively. These losses are in general agreement with losses obtained on trials of comparable ships.

The effect of L/B variation on the nondimensional numerical measures associated with 35 degree rudder starboard steady turns of the series models is shown by Figure 6-16. Within the range covered, the variations in these nondimensional measures with L/B are rather small. For example, the steady turning diameter over a range of L/B between 5.0 and 6.5 is between 2.7 and 2.8 ship lengths. There is an apparent tendency for the nondimensional turning diameters to increase as L/B is decreased below 5.5. As a practical matter, however, even though the nondimensional values are close, the longer ships will require significantly more area in which to turn than the shorter ships, as seen by the dimensional measures in Tables 6-10 and 6-11.

The effect of B/T variation on the nondimensional numerical measures associated with 35 degree rudder starboard steady turns of the series models is shown by Figure 6-17. Here, most of the nondimensional measures show very little change with B/T up to about 3.75, but then increase significantly up to about B/T of 4.50. This is probably due both to the decrease in instability with increase in B/T, as shown for ships G, N, and P in Table 6-8, and the lower movable rudder area ratio used with the B/T = 4.50 ships. From a practical standpoint, the nondimensional increases become even more significant since the length of the standard ships increases with B/T. For example, Table 6-10 shows that, for a rudder angle of 35 degrees, the steady turning diameter of ship N with B/T = 3.75 is about 3100 feet compared to about 3700 feet for ship P with B/T = 4.50.

Stopping Maneuvers - Simulated stopping maneuvers were performed for ships E, H, and L. The propeller rpm time history selected for use in these simulations is typical for large tankers and is given in Figure 6-18. As with the other types of maneuvers discussed earlier, the conditions assumed were calm,

unrestricted, deep water with no wind. The following three types of stopping maneuvers were conducted:

(a) Undisturbed - rudder fixed at zero angle and no activity thereafter

(b) Controlled - rudder manipulated during the maneuver just enough to maintain course

(c) Fishtailing - rudder moved back and forth through a large angle at the maximum rudder rate to aid in slowing the ship

The controlled stopping maneuver was simulated in the subject investigation by setting coefficients Y_*' and N_*' equal to zero. In the absence of outside disturbances or rudder changes, the only force which could cause a change in course is the propeller interaction on the hull which is represented by these coefficients. Simulating the controlled stopping maneuver in this fashion neglects the effect on drag of the rudder changes resulting from the use of a real automatic course keeping control. However, since the rudder changes are generally small, the influence on drag is also small, particularly since the ship is steadily slowing. The head reach obtained from simulating a stopping maneuver this way can be considered to be a maximum for the conditions noted.

The rudder angle and rate used for the fishtailing stopping maneuver were ±35 degrees and 2.33 degrees per second, respectively, since this maneuver is strongly influenced by rudder changes.

Figure 6-19 shows typical path trajectories resulting from simulated stopping maneuvers conducted on ship E with each of the three aforementioned modes of rudder use. The numerical measures derived from such maneuvers conducted for the three ships are summarized in Table 6-13. It should be noted that the fishtailing stop produced the minimum head reach by a substantial margin but resulted in only a slightly greater side reach than

the undisturbed stop. The large drift angle produced by the first rudder swing in the fishtailing stop helps to slow the ship quickly.

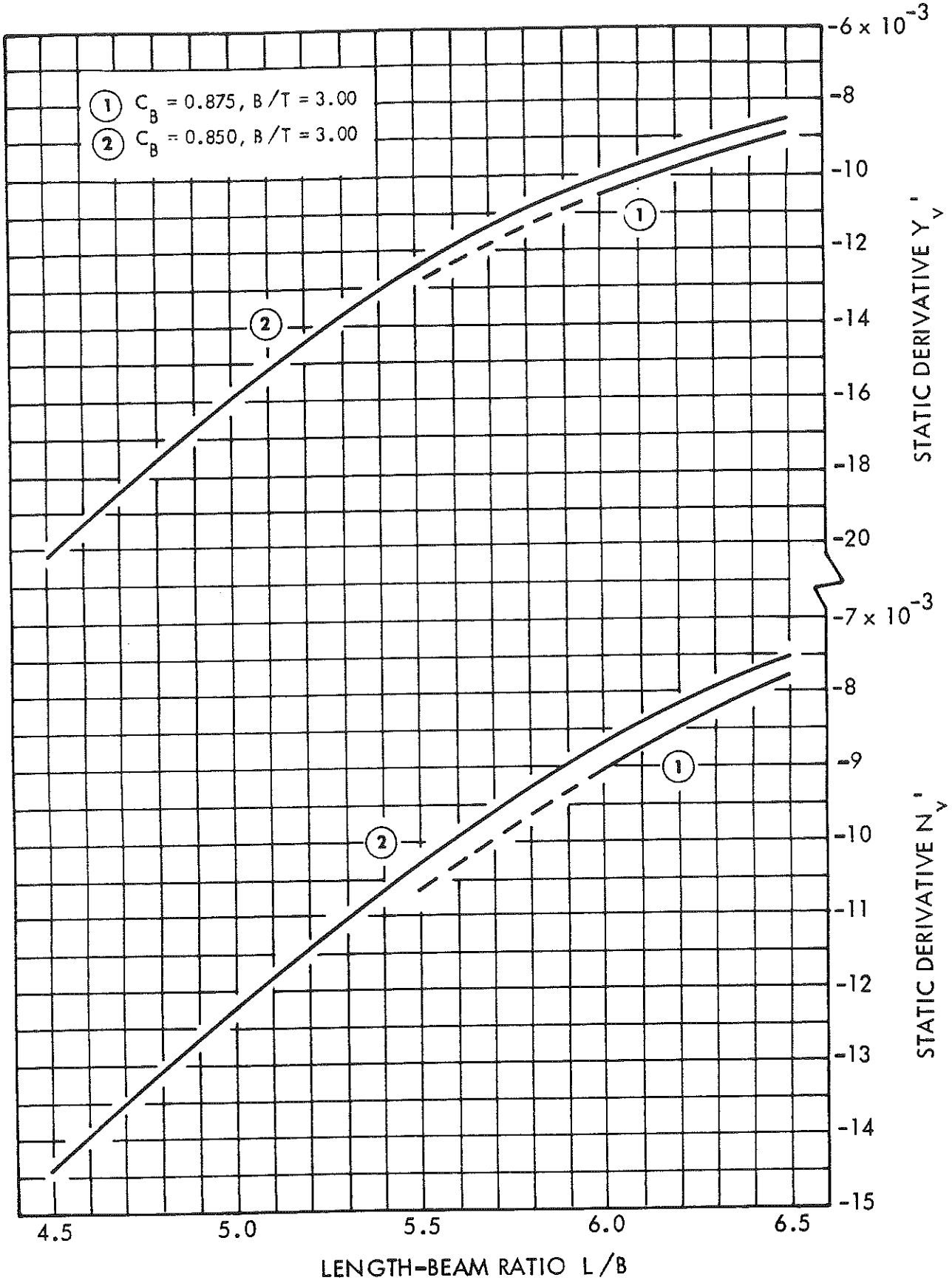

(a) Static Derivatives

FIGURE 6-1 - EFFECT OF L/B VARIATION ON STATIC, ROTARY AND ACCELERATION DERIVATIVES - BARE HULL

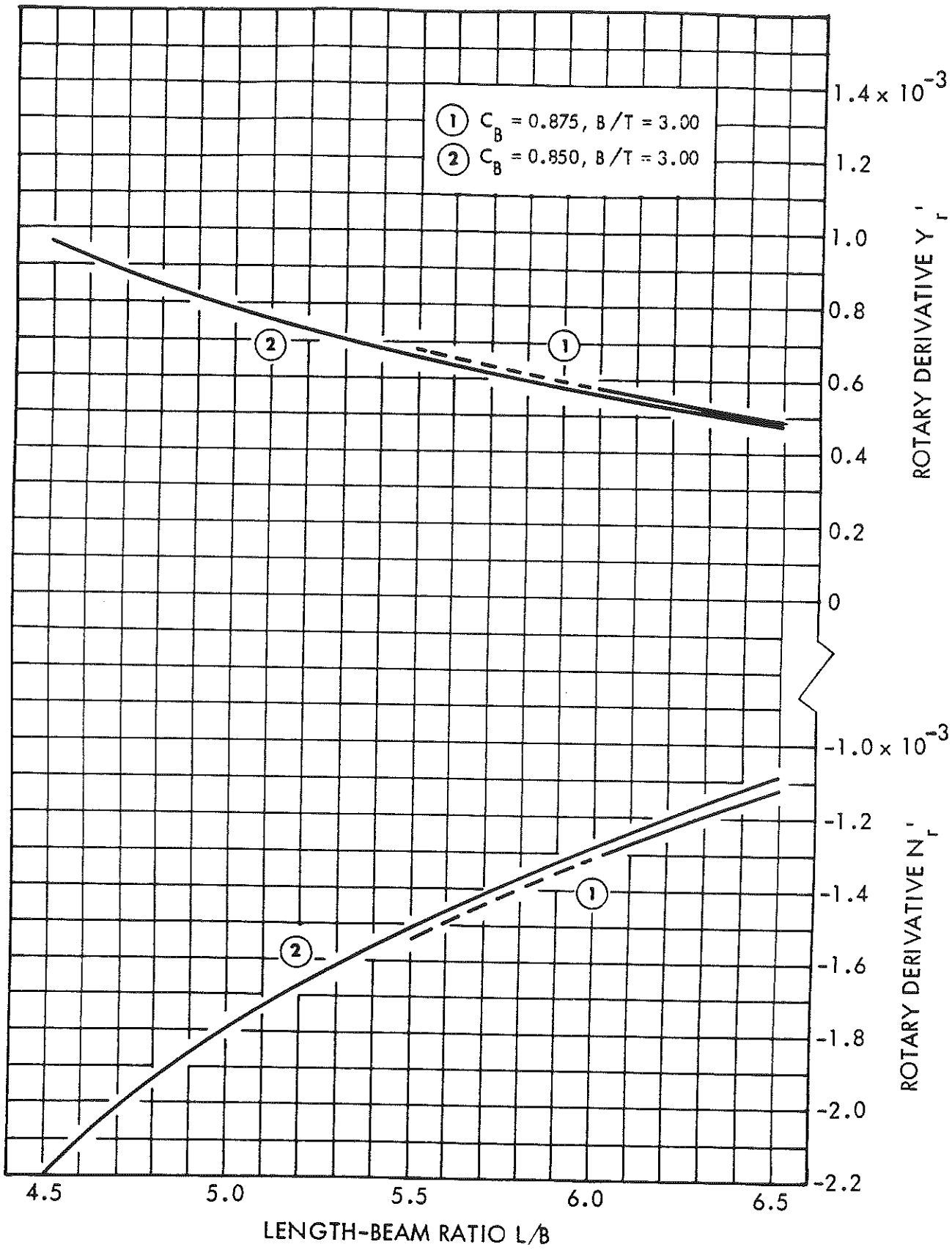

(b) Rotary Derivatives

FIGURE 6-1 - CONTINUED

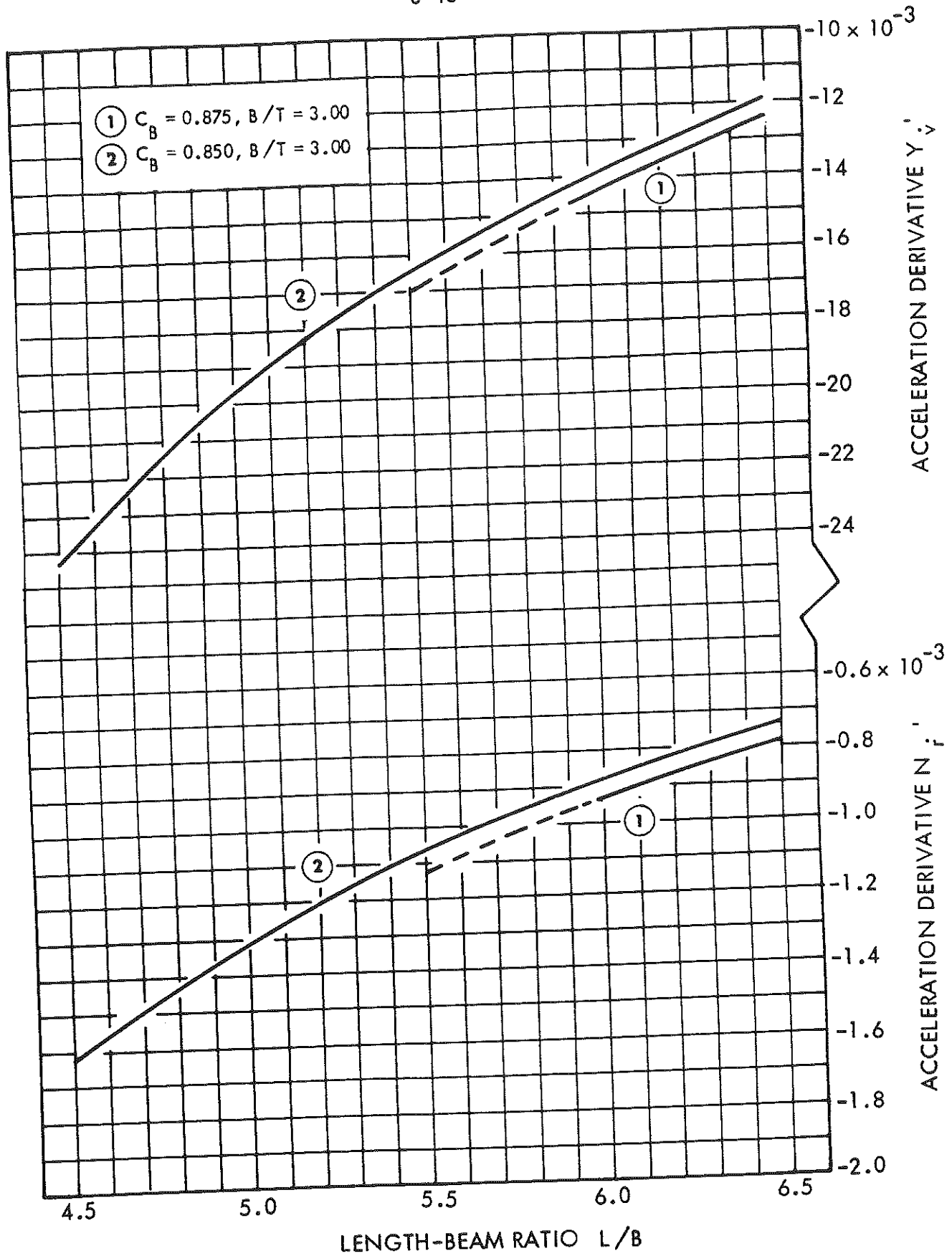

(c) Acceleration Derivatives

FIGURE 6-1 - CONCLUDED

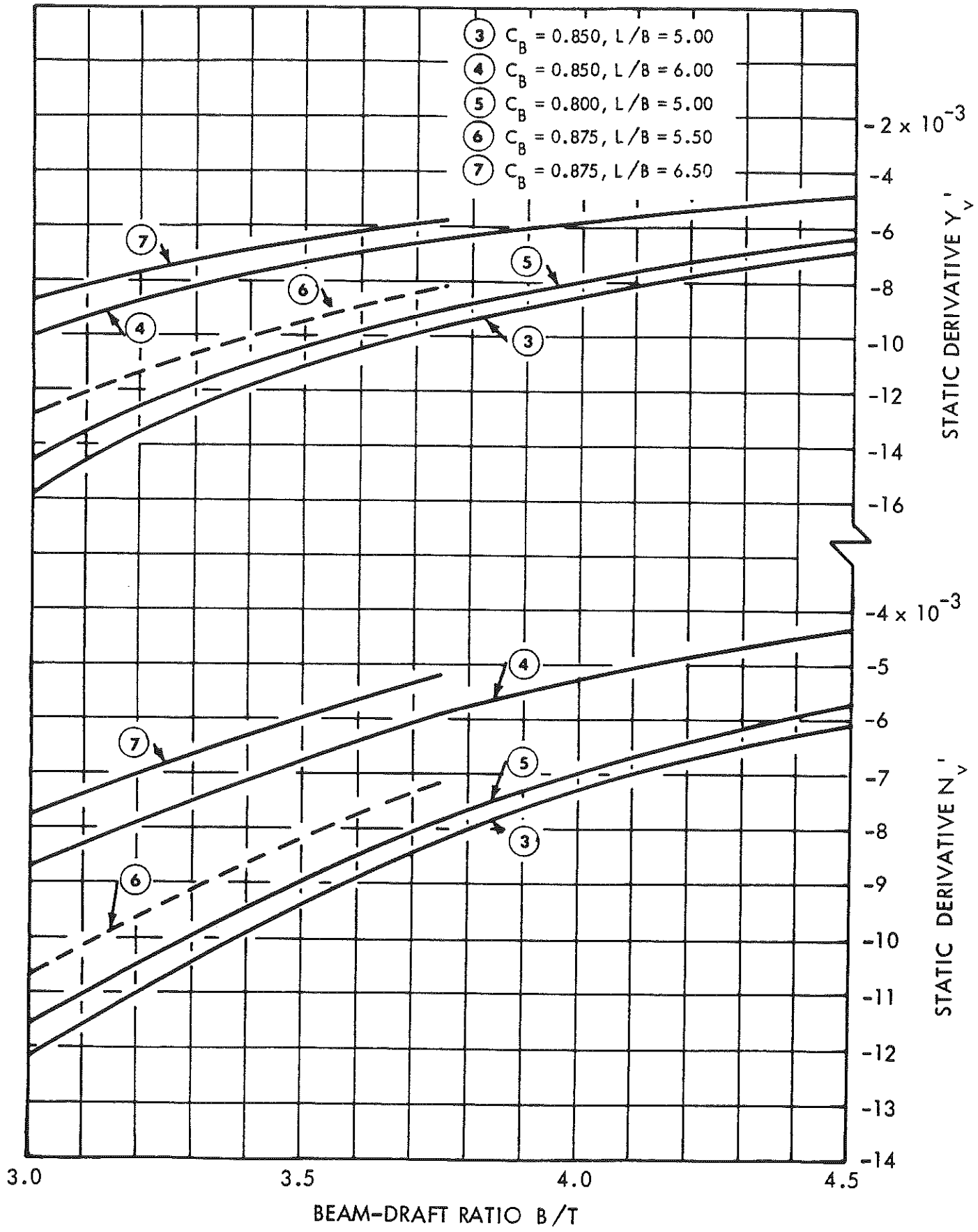

(a) Static Derivatives

FIGURE 6-2 - EFFECT OF B/T VARIATION ON STATIC, ROTARY AND ACCELERATION DERIVATIVES - BARE HULL

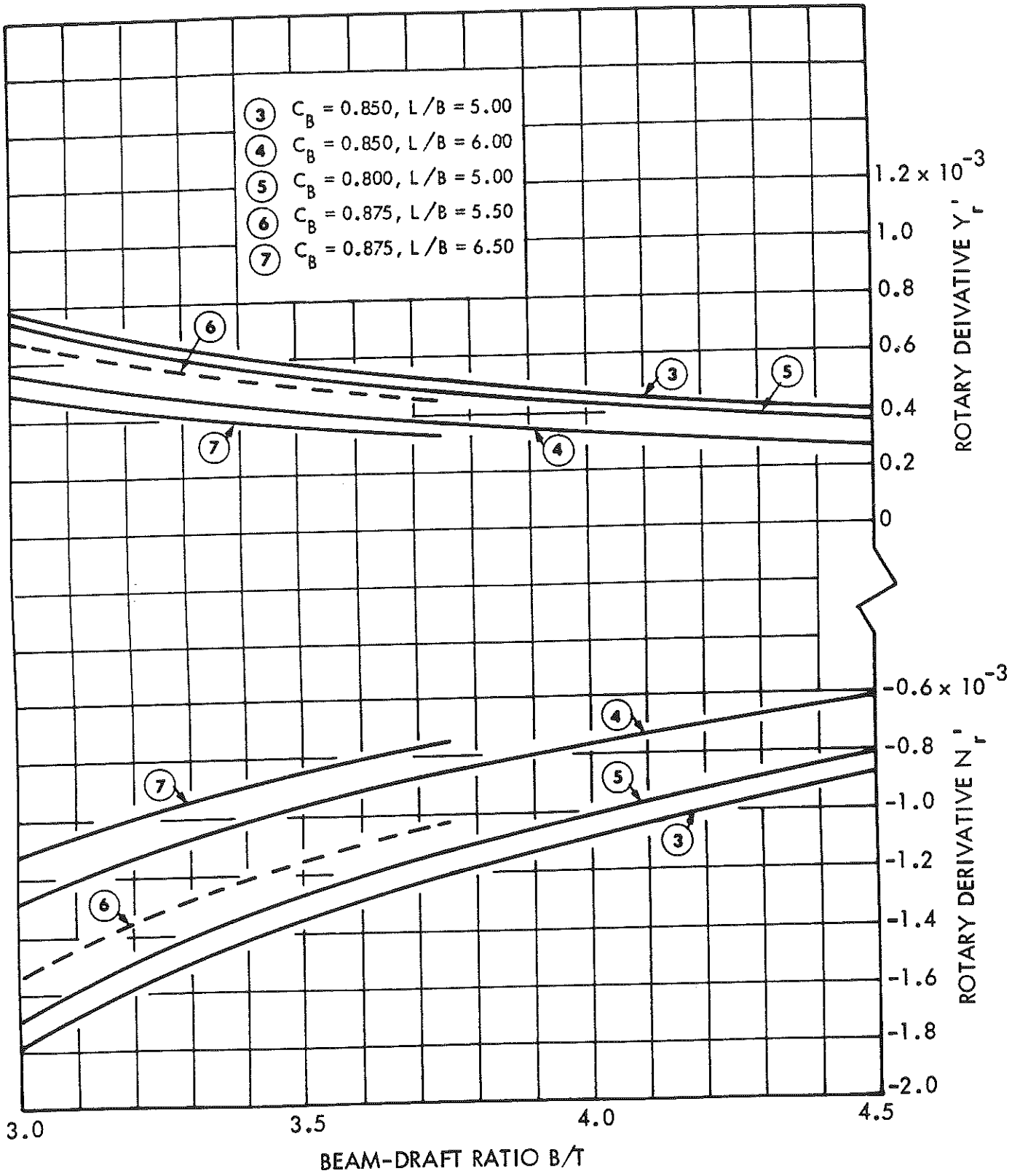

(b) Rotary Derivatives

FIGURE 6-2 - CONTINUED

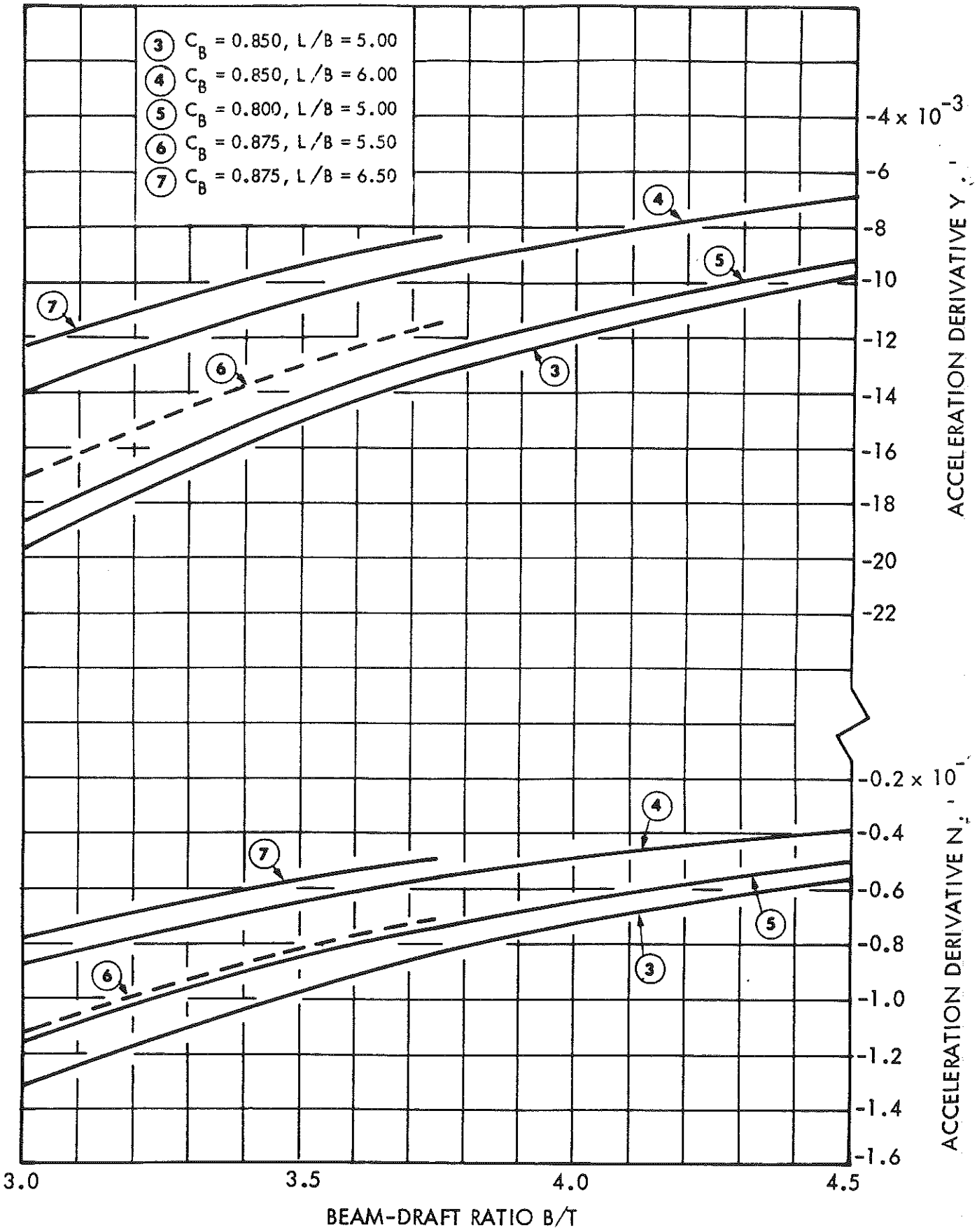

(c) Acceleration Derivatives

FIGURE 6-2 - CONCLUDED

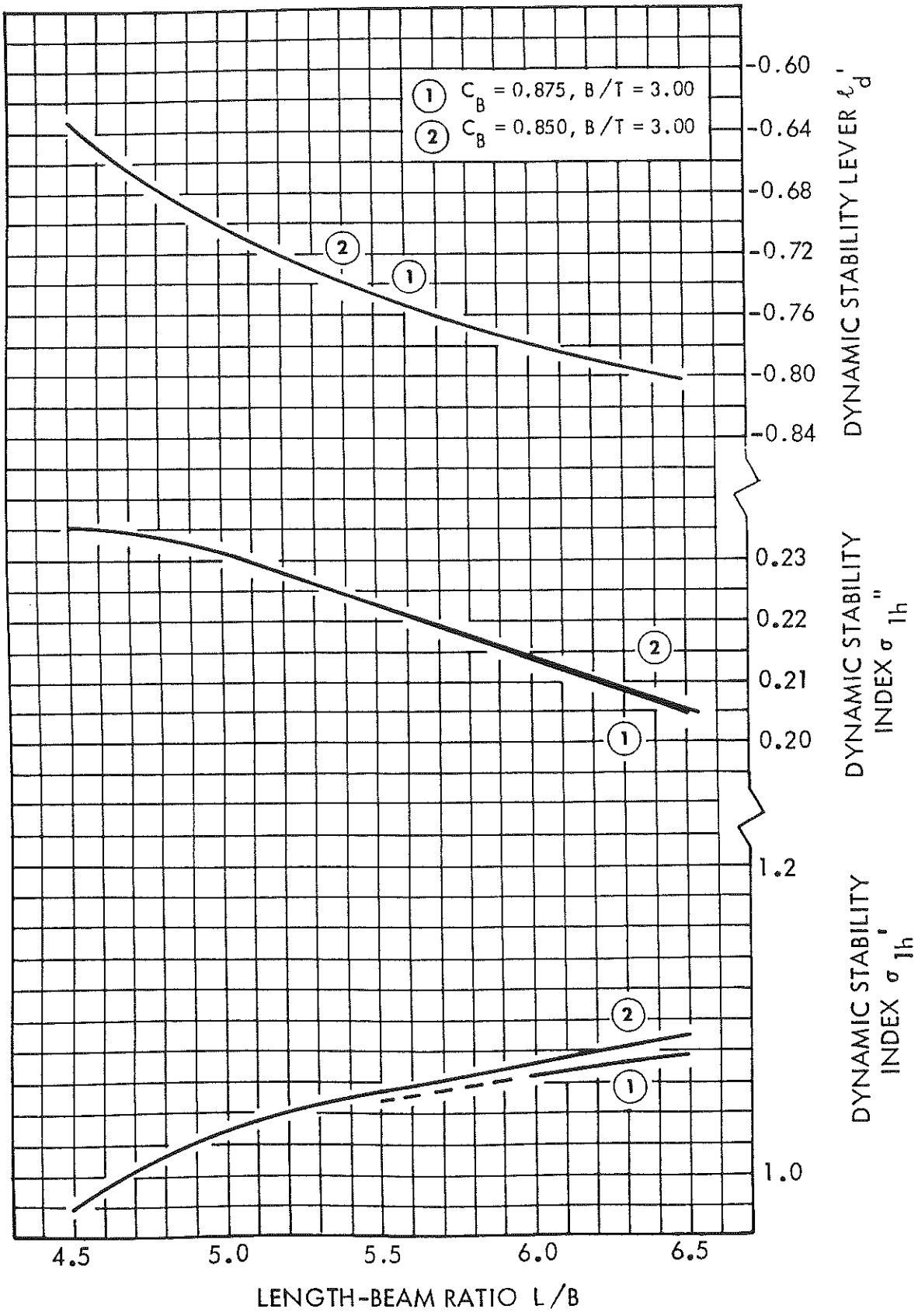

FIGURE 6-3 - EFFECT OF L/B VARIATION ON DYNAMIC STABILITY INDICES - BARE HULL

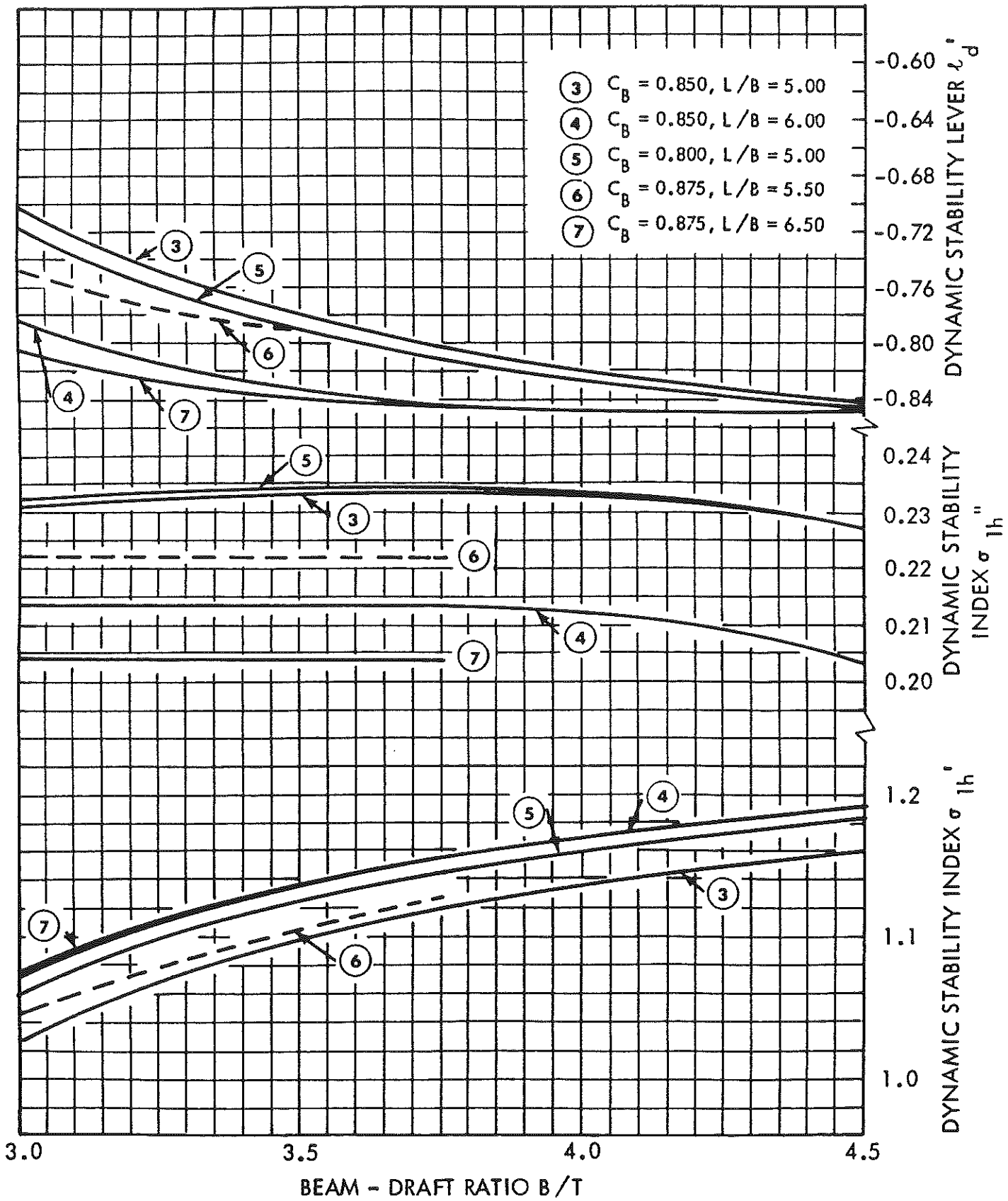

FIGURE 6-4 - EFFECT OF B/T VARIATION ON DYNAMIC STABILITY INDICES - BARE HULL

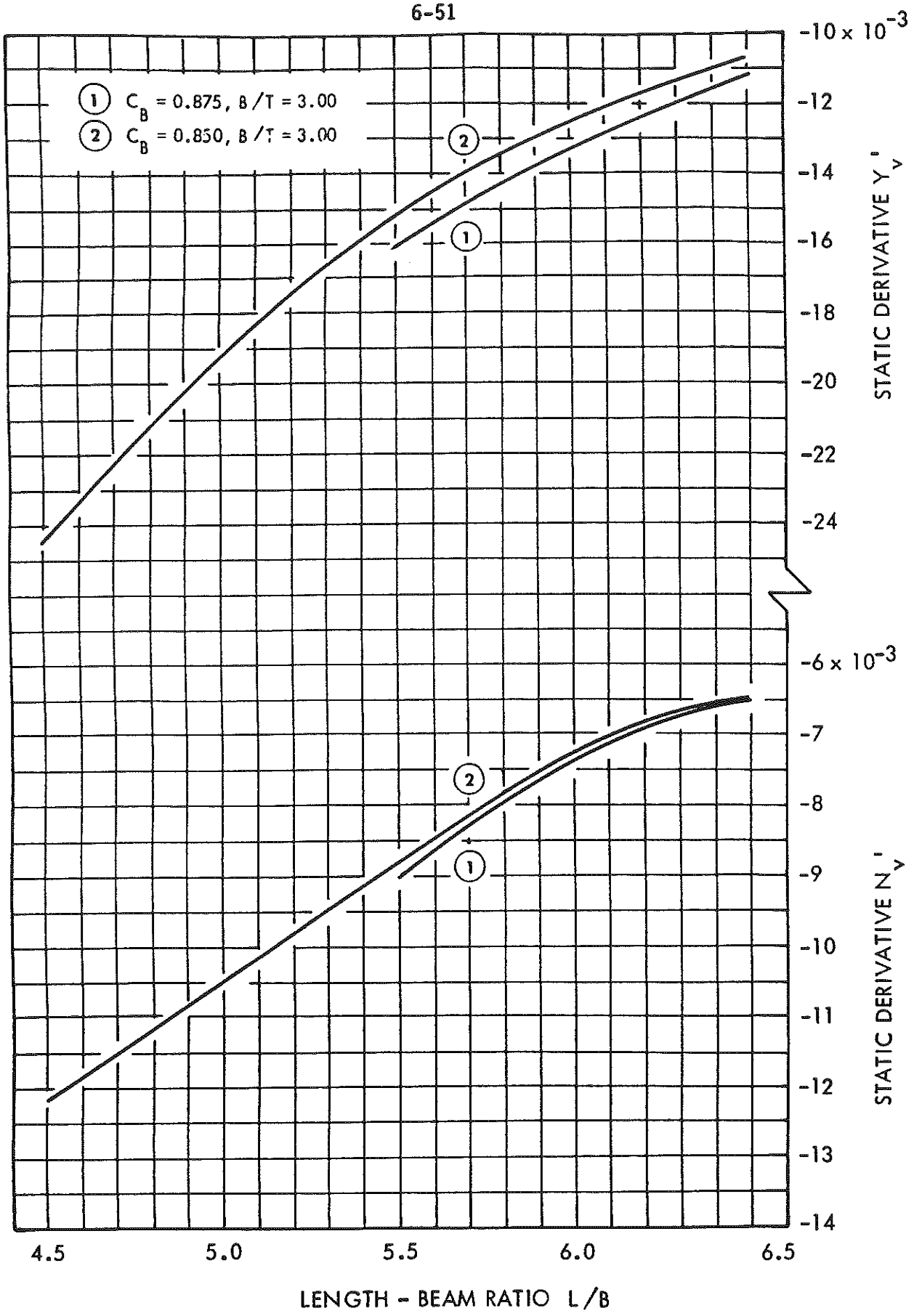

(a) Static Derivatives

FIGURE 6-5 - EFFECT OF L/B VARIATION ON STATIC, ROTARY, AND ACCELERATION DERIVATIVES - WITH STANDARD RUDDER - PROPELLER COMBINATION

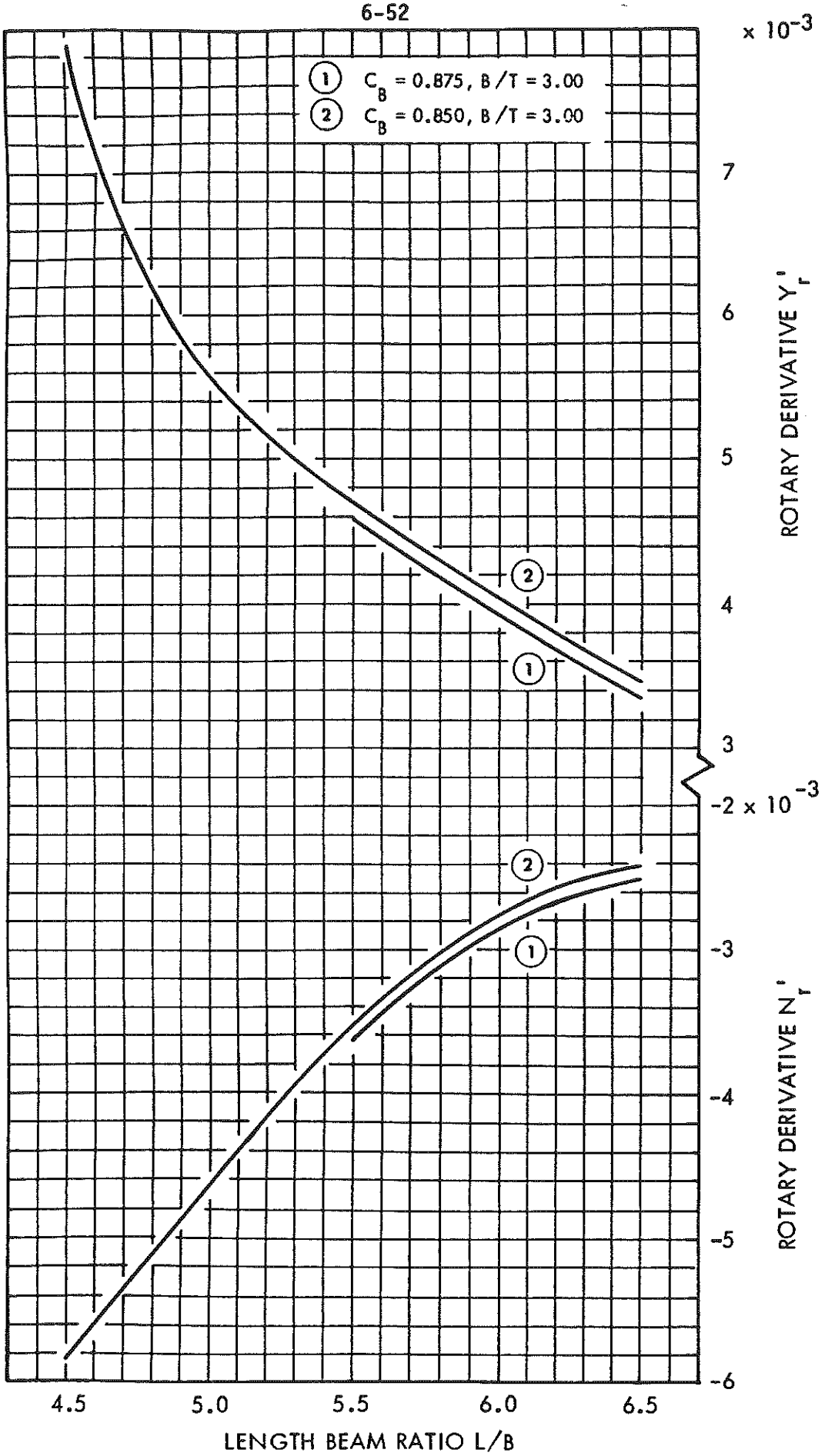

(b) Rotary Derivatives

FIGURE 6-5 - CONTINUED

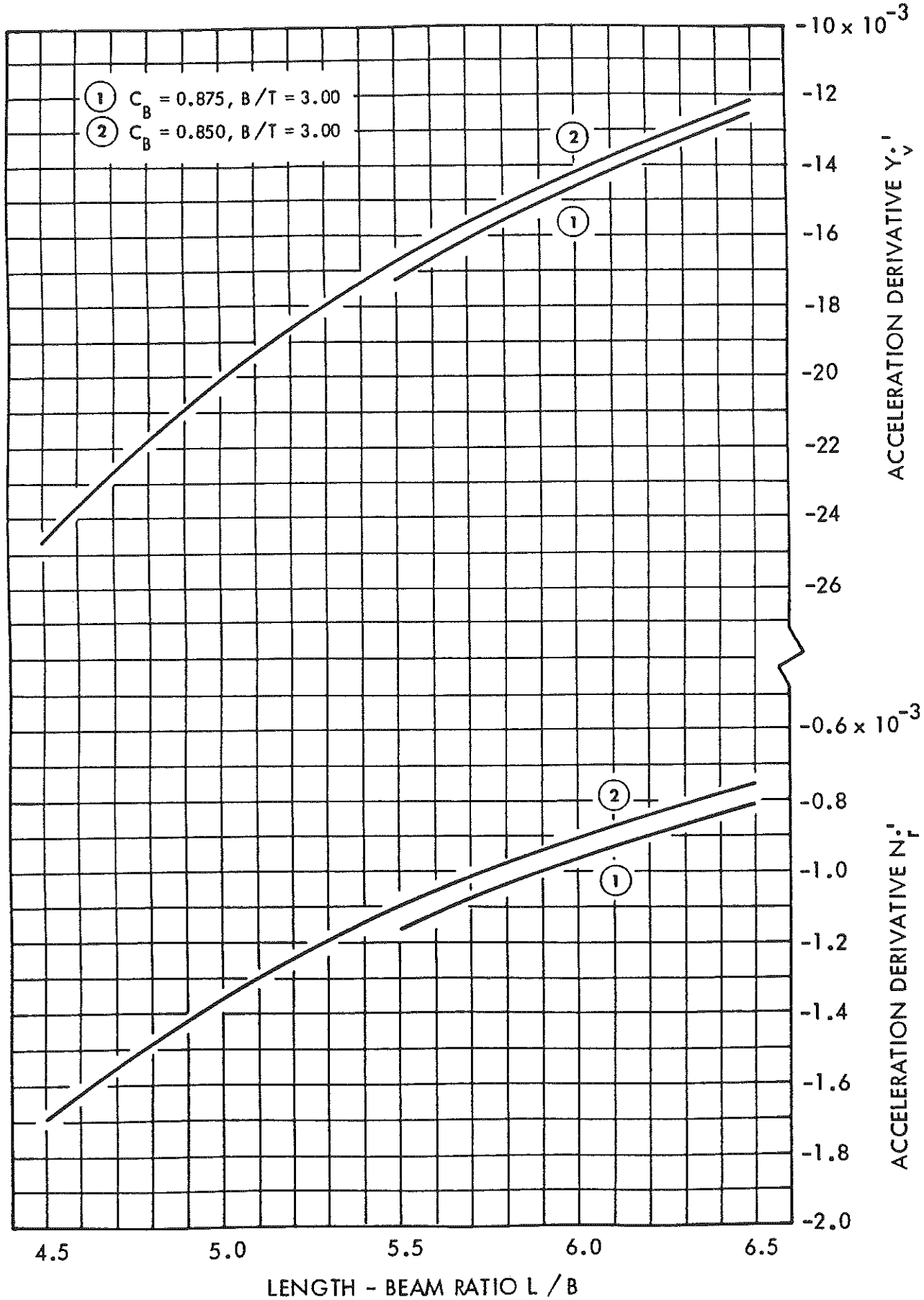

(c) Acceleration Derivatives

FIGURE 6-5 - CONCLUDED

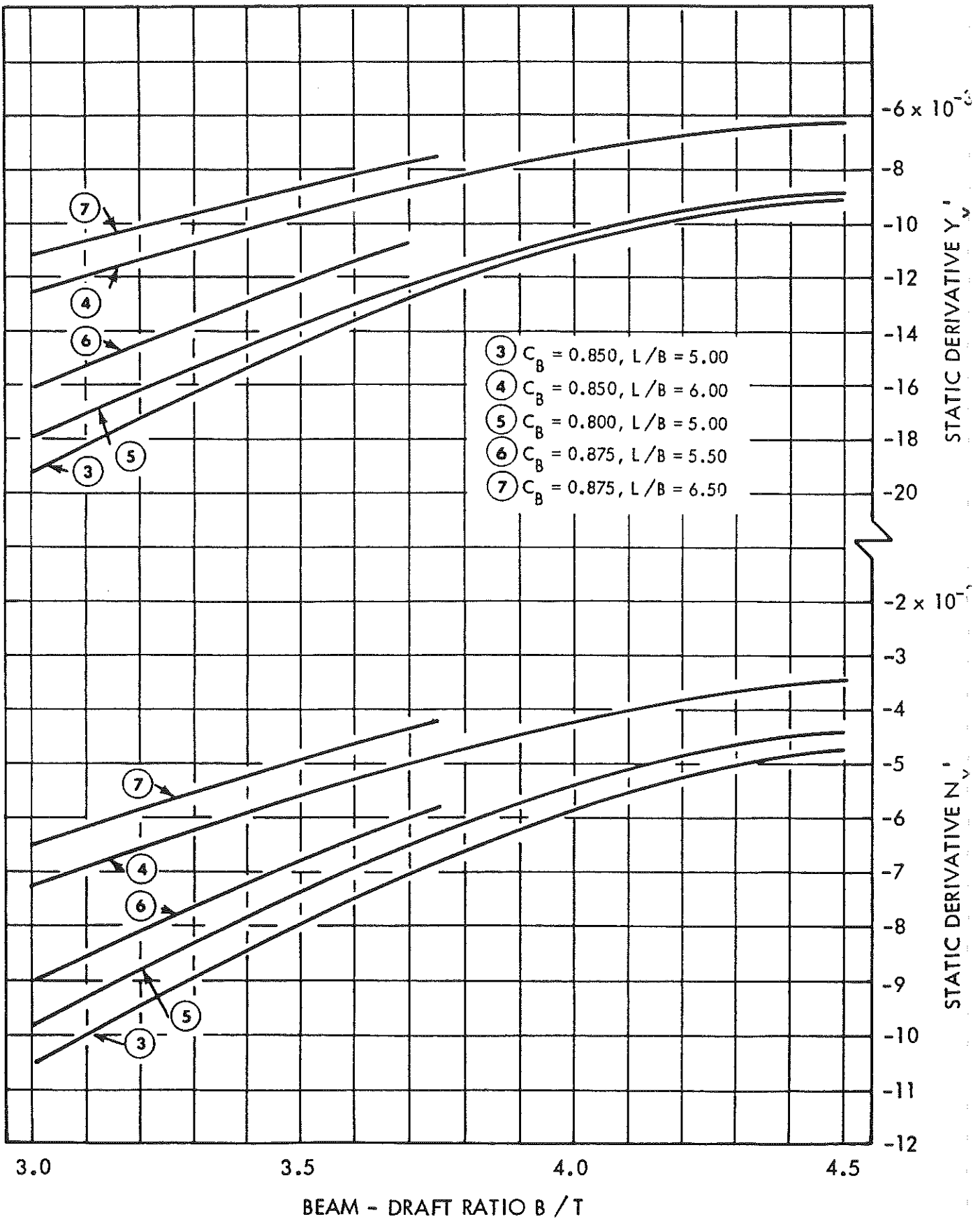

(a) Static Derivatives

FIGURE 6-6 - EFFECT OF B/T VARIATION ON STATIC, ROTARY AND ACCELERATION DERIVATIVES - WITH STANDARD RUDDER - PROPELLER COMBINATION

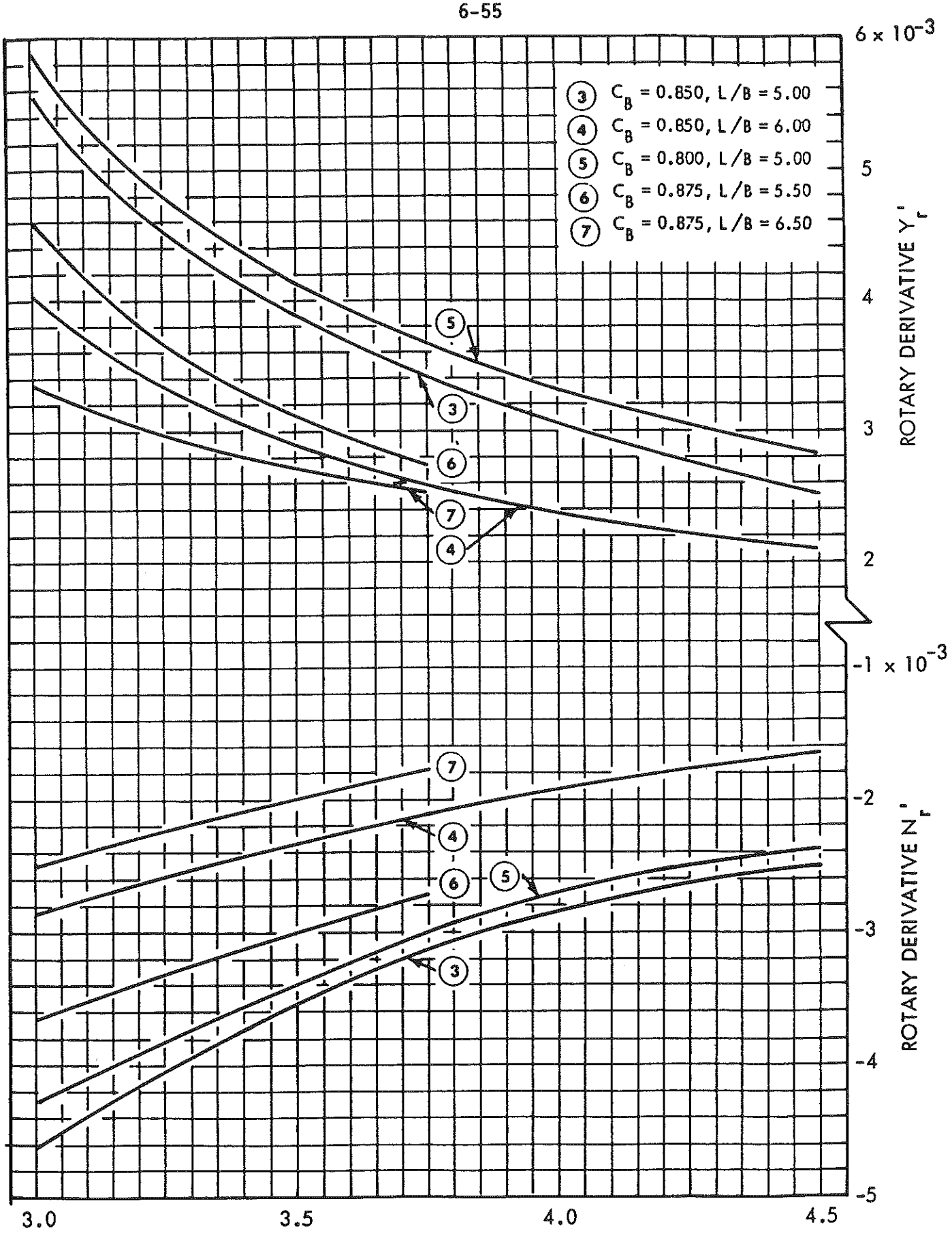

(b) Rotary Derivatives

FIGURE 6-6 - CONTINUED

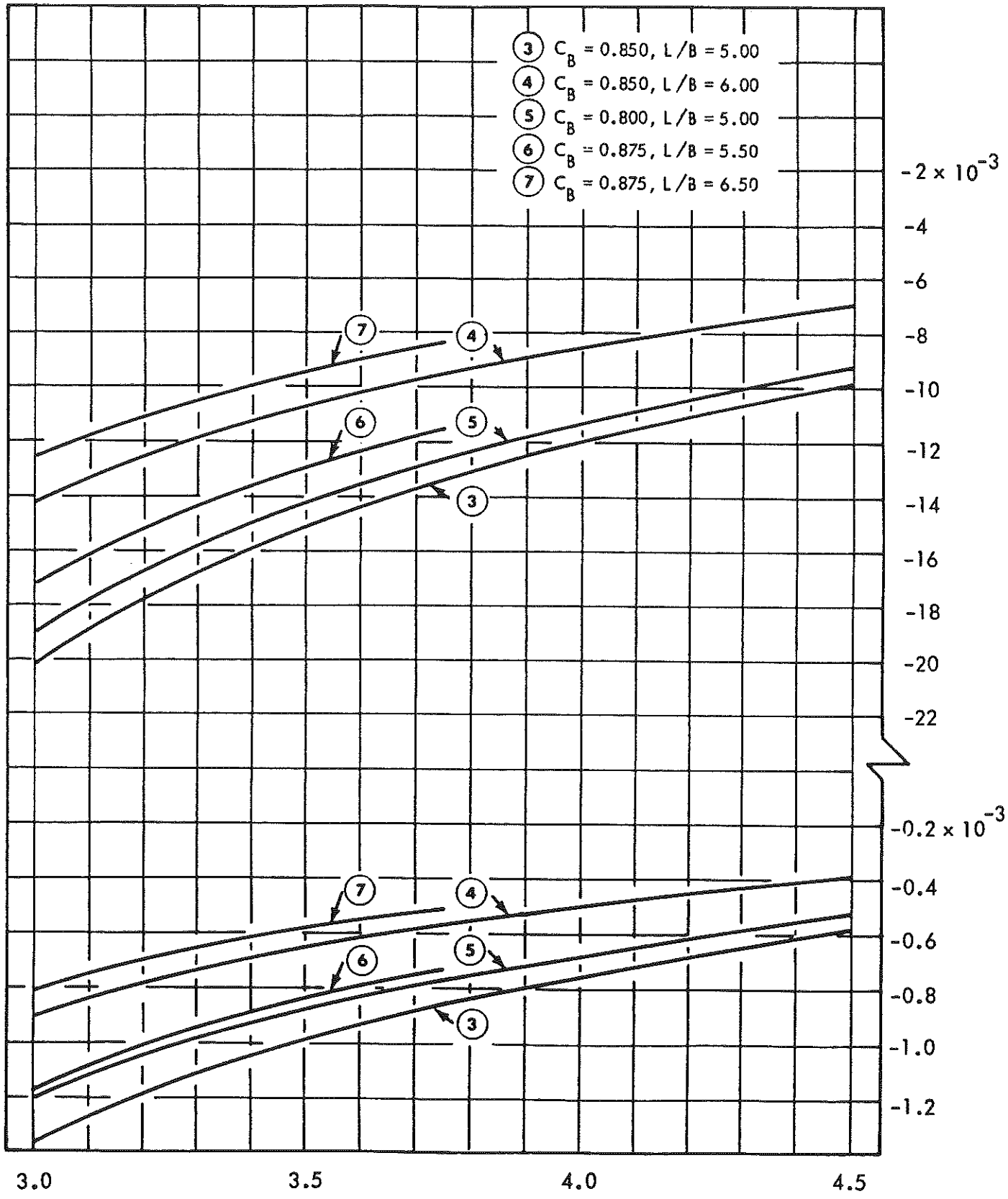

(c) Acceleration Derivatives

FIGURE 6-6 - CONCLUDED

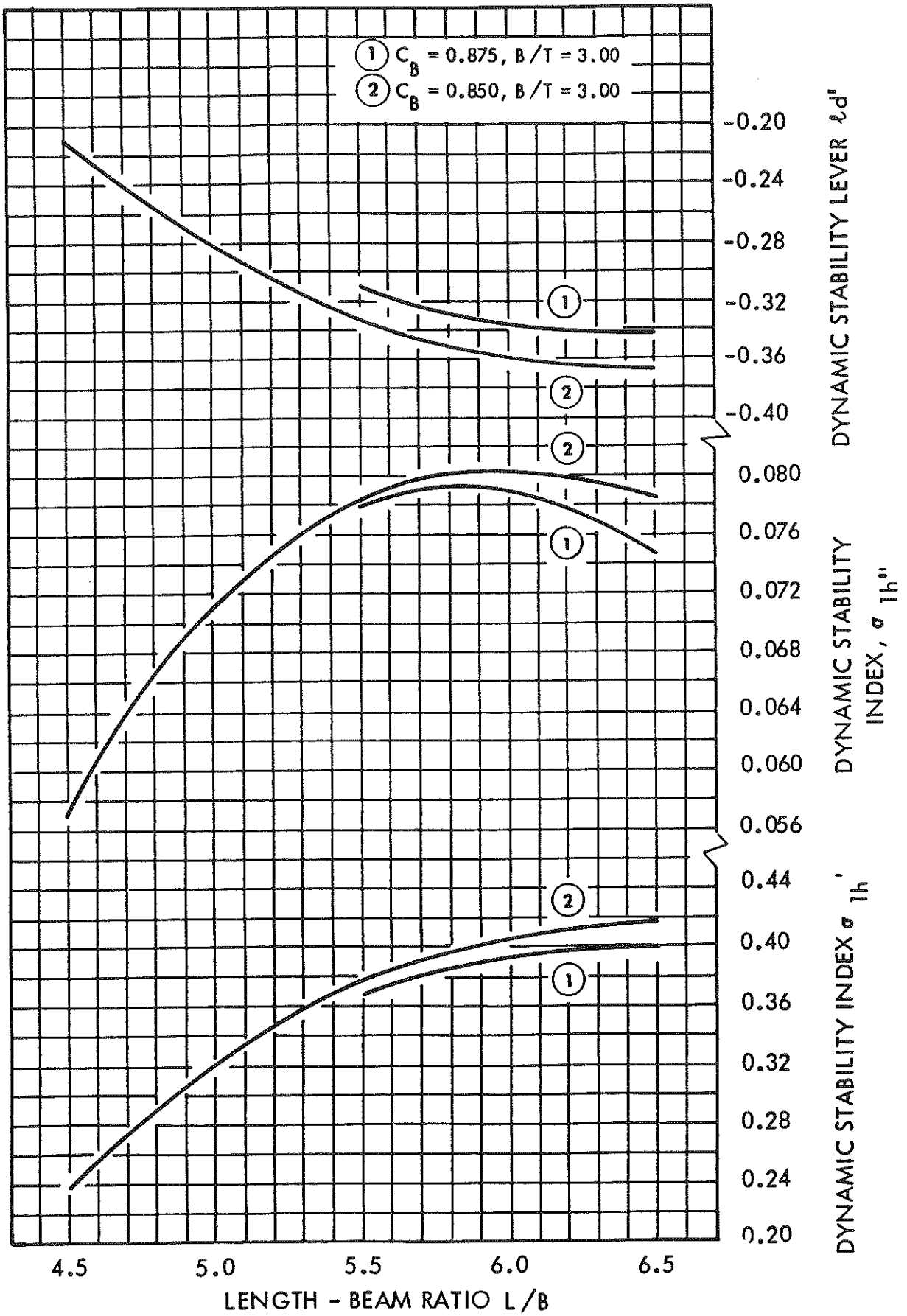

FIGURE 6-7 - EFFECT OF L/B VARIATION ON DYNAMIC STABILITY INDICES - WITH STANDARD RUDDER - PROPELLER COMBINATION

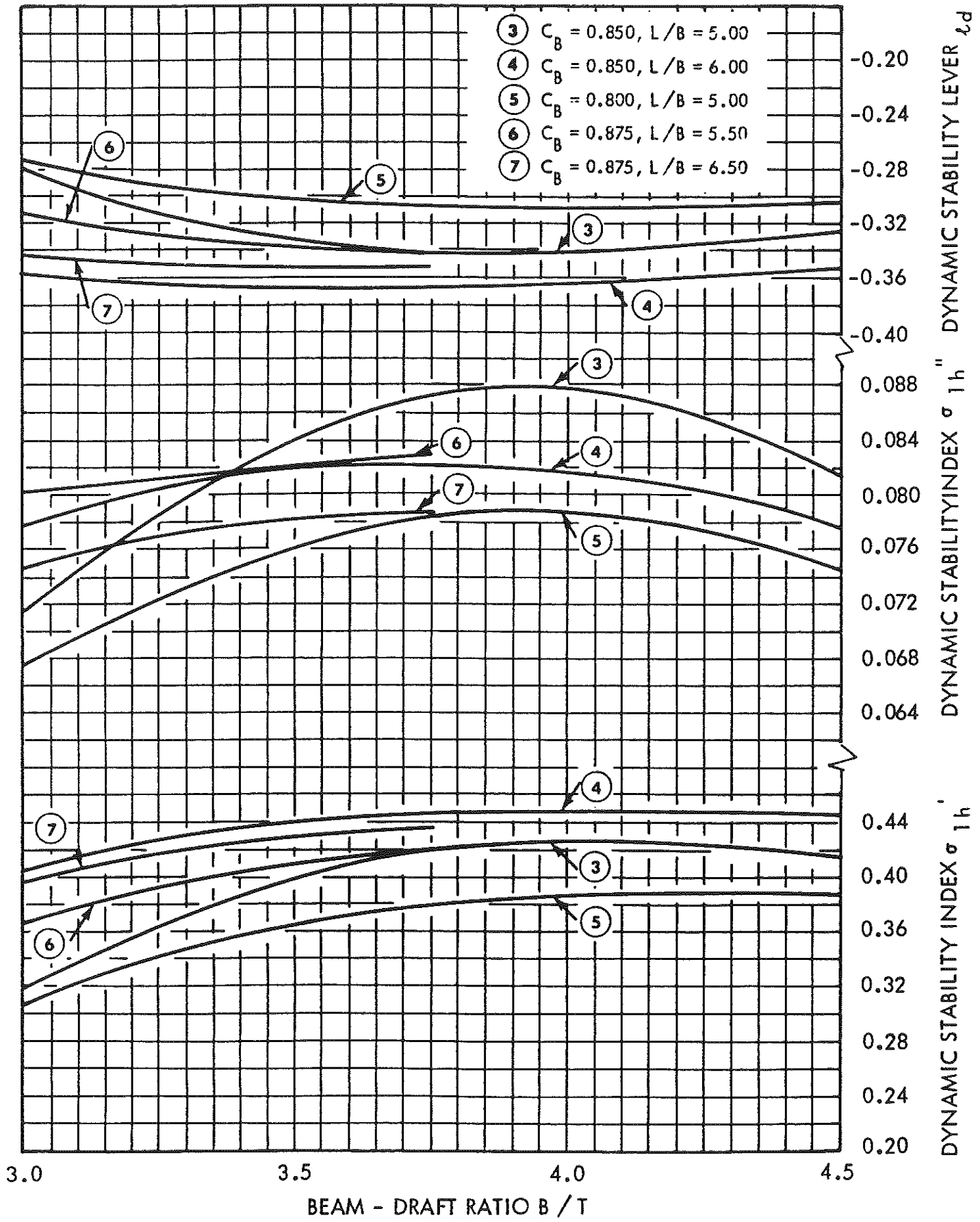

FIGURE 6-8 - EFFECT OF B/T VARIATION ON DYNAMIC STABILITY INDICES - WITH STANDARD RUDDER - PROPELLER COMBINATION

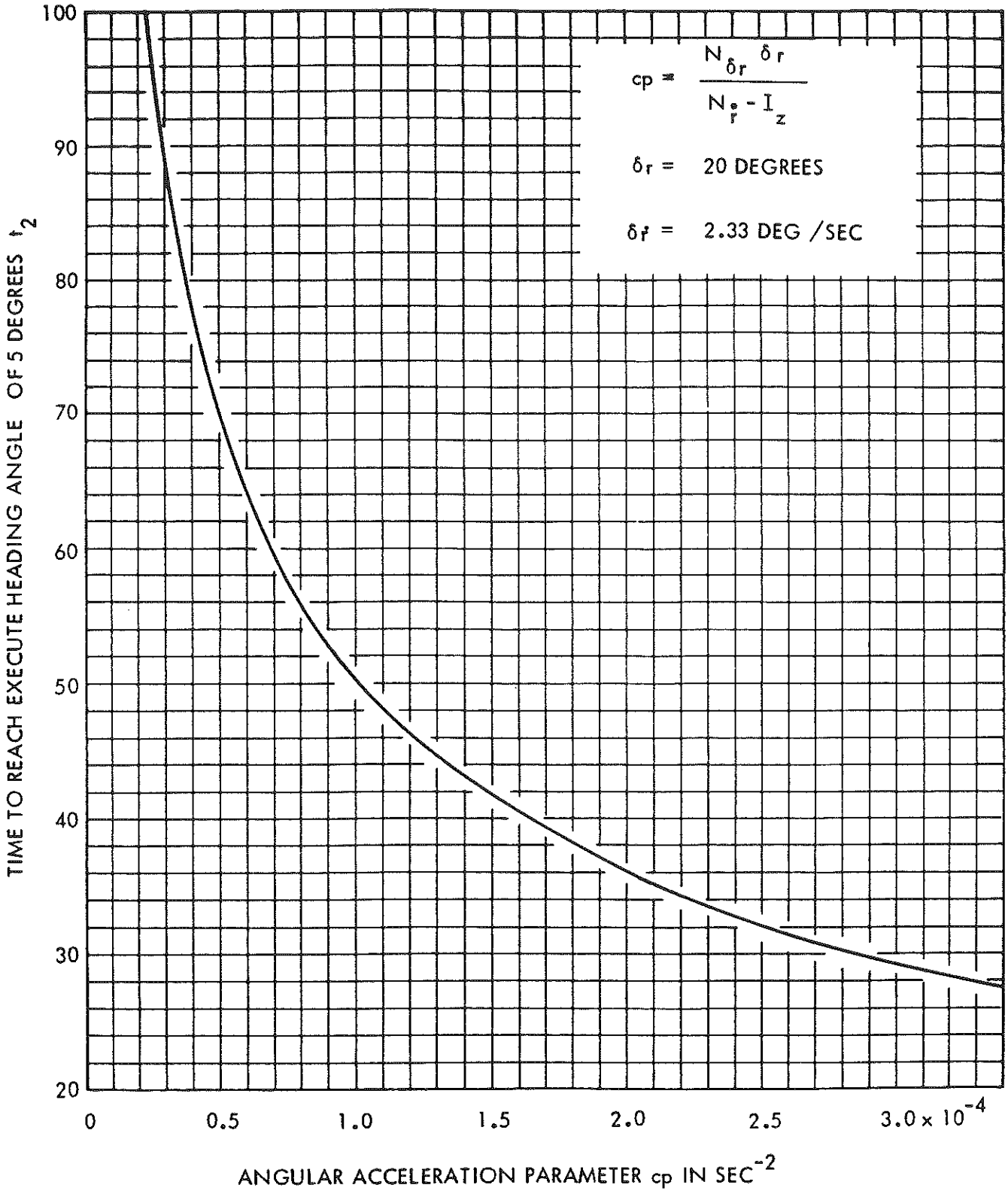

FIGURE 6-9 - EFFECT OF DIMENSIONAL ANGULAR ACCELERATION PARAMETER ON TIME TO REACH EXECUTE HEADING CHANGE OF 5 DEGREES

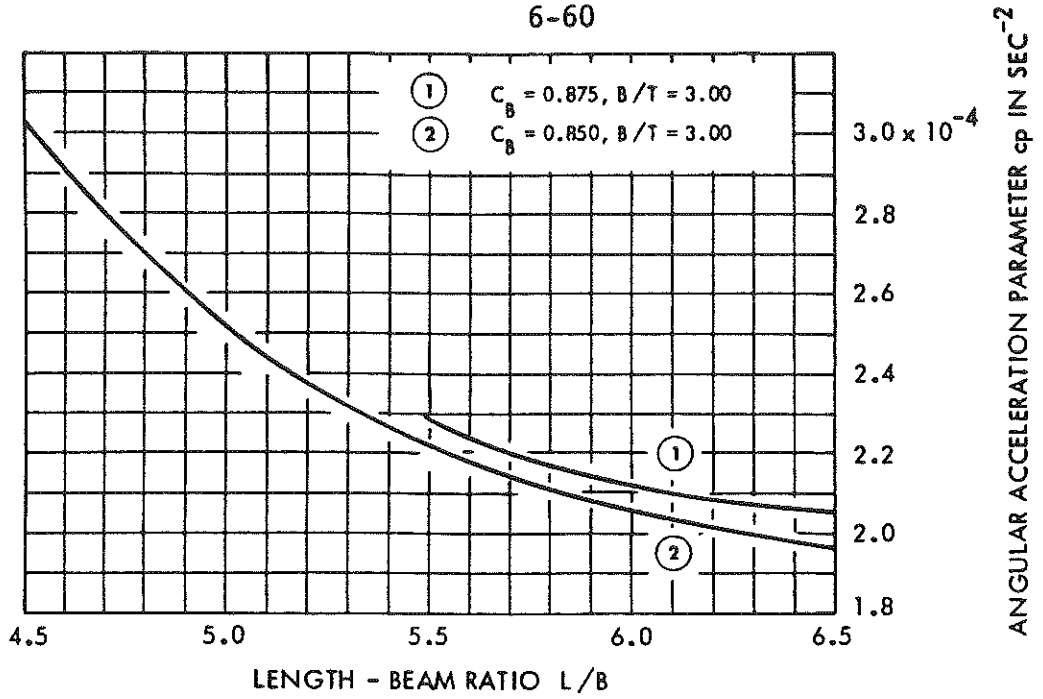

FIGURE 6-10 - EFFECT OF L/B VARIATION ON DIMENSIONAL ANGULAR ACCELERATION PARAMETER - 350,000 TONS DISPLACEMENT

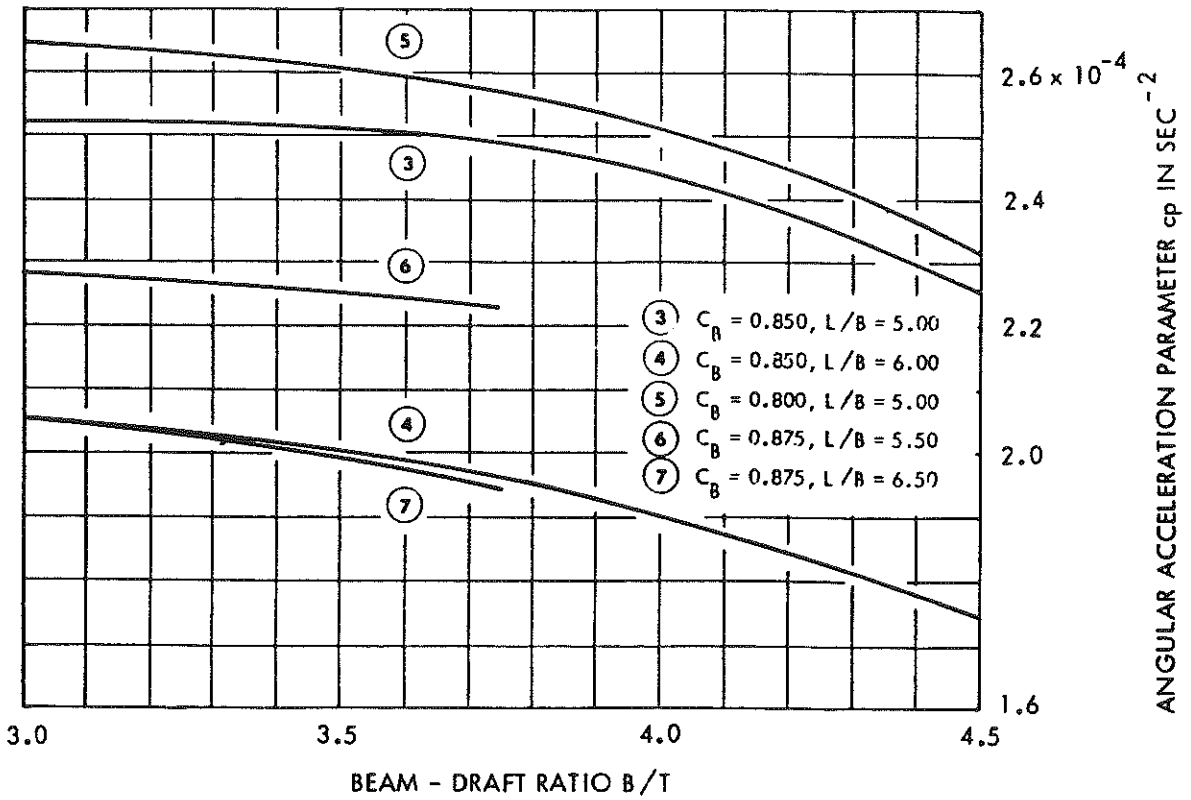

FIGURE 6-11 - EFFECT OF B/T VARIATION ON DIMENSIONAL ANGULAR ACCELERATION PARAMETER - 350,000 TONS DISPLACEMENT

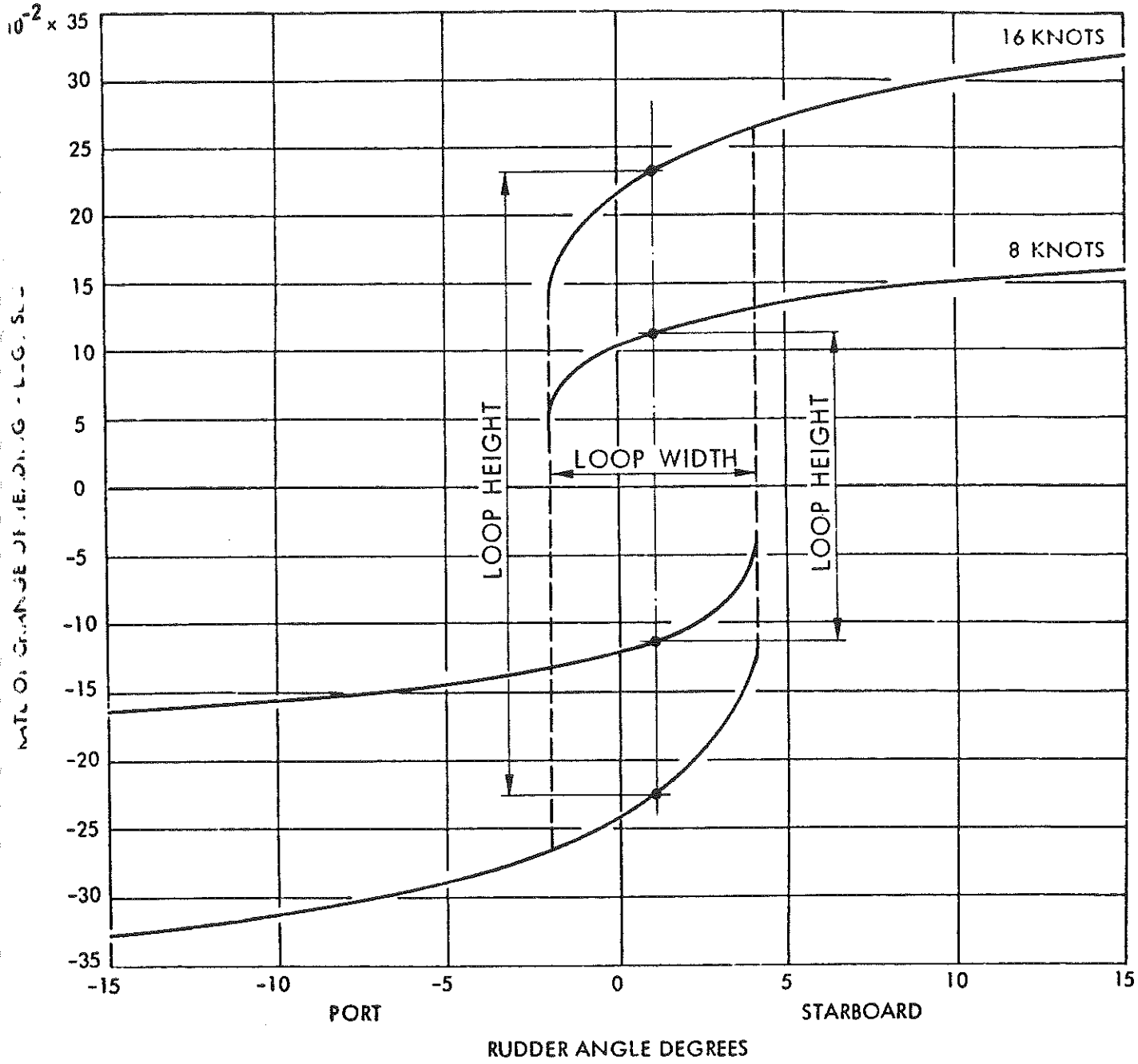

FIGURE 6-12 - RESULTS OF A SPIRAL MANEUVER FOR SHIP E - 350,000 TONS DISPLACEMENT

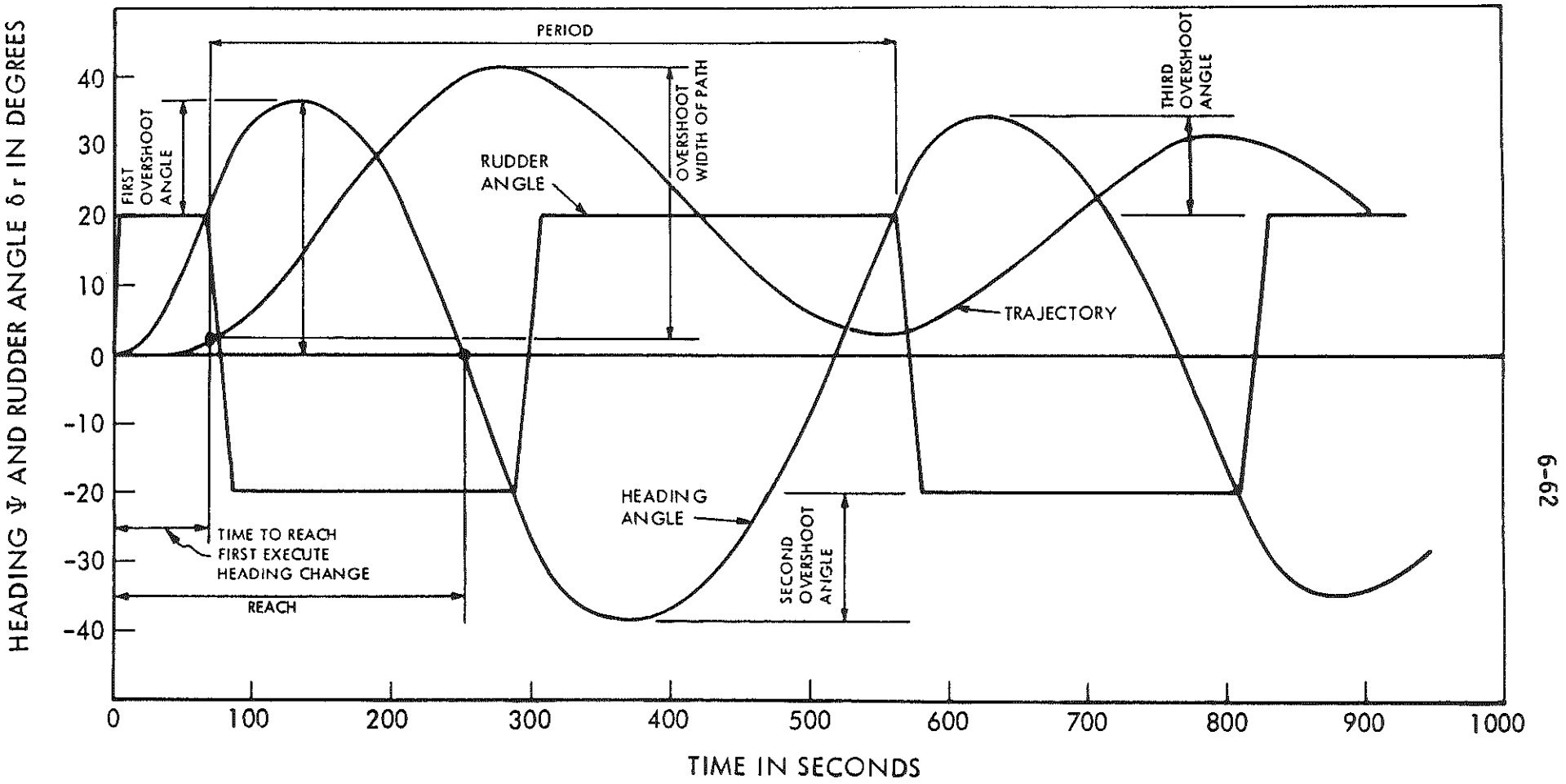

FIGURE 6-13 - TIME HISTORY OF 20-20 ZIGZAG MANEUVER FOR SHIP E - 350,000 TONS DISPLACEMENT, APPROACH SPEED 16 KNOTS

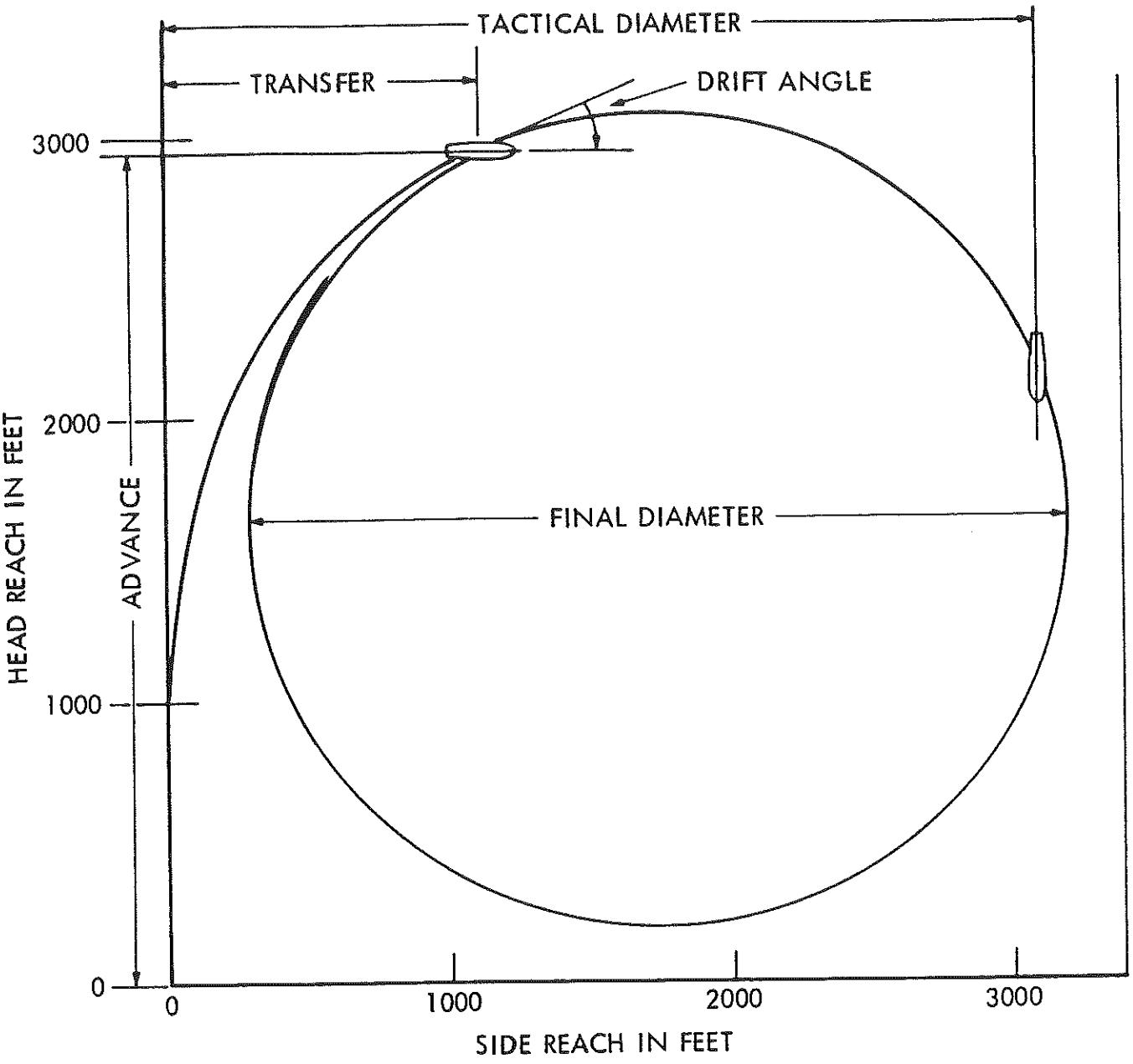

FIGURE 6-14 - PATH DURING A 35 DEGREE STARBOARD STEADY - TURNING MANEUVER FOR SHIP E - 350,000 TONS DISPLACEMENT, APPROACH SPEED 16 KNOTS

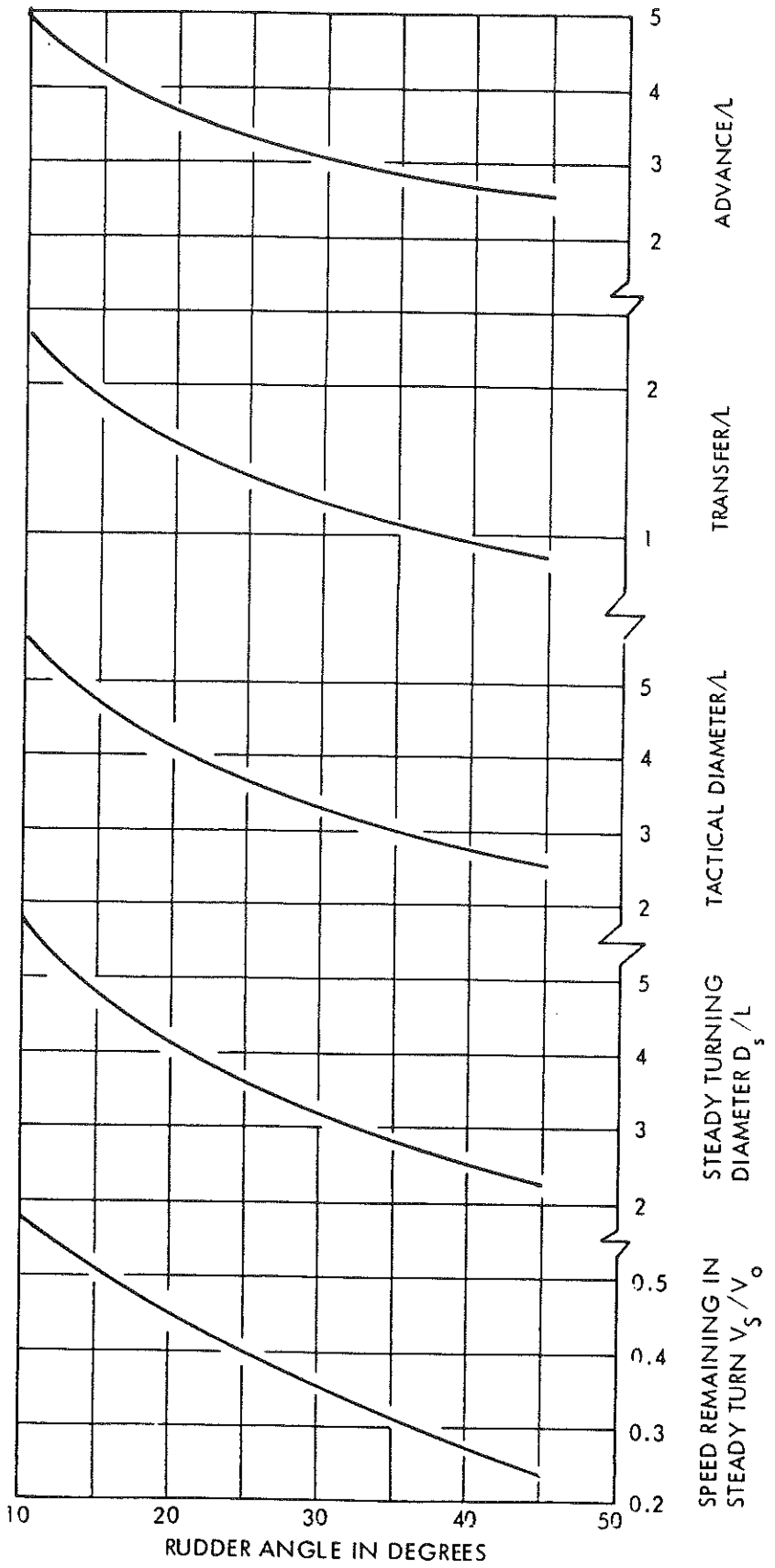

FIGURE 6-15 - VARIATION OF NONDIMENSIONAL MEASURE WITH RUDDER ANGLE FOR SHIP E, 350,000 TONS DISPLACEMENT

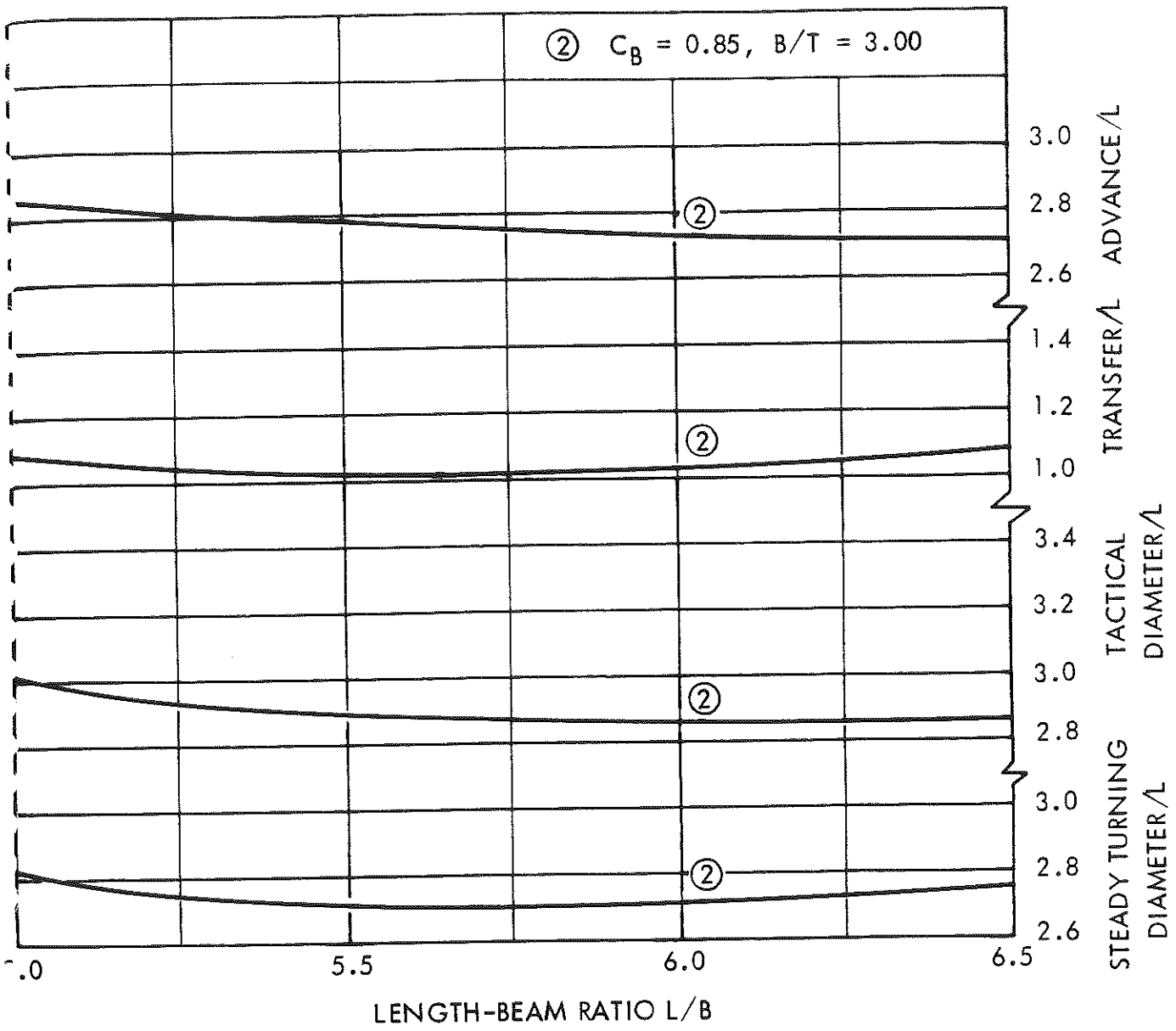

FIGURE 6-16 - EFFECT OF L/B VARIATION ON NONDIMENSIONAL MEASURES ASSOCIATED WITH A 35 DEGREE RUDDER STARBOARD TURN

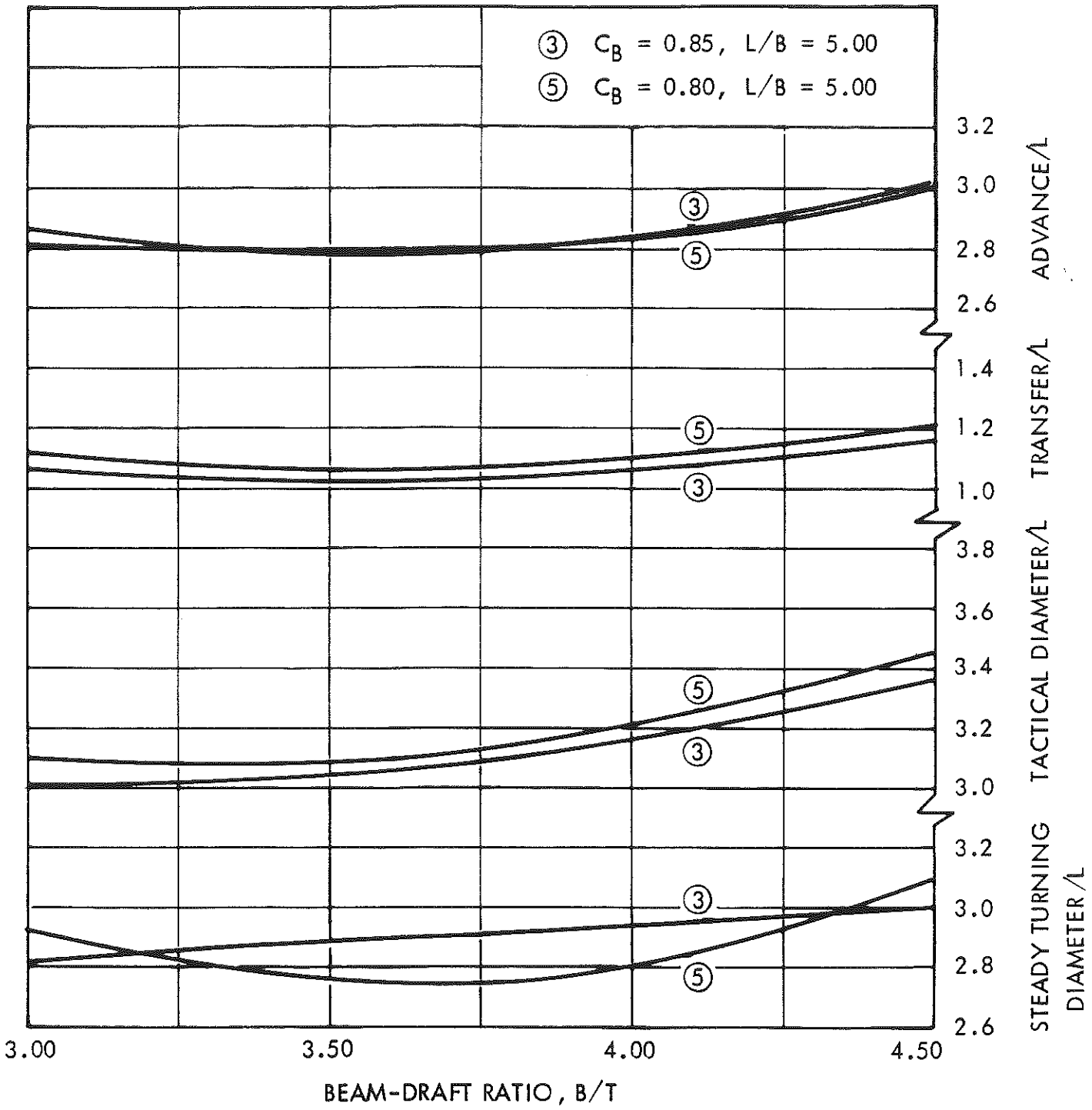

FIGURE 6-17 - EFFECT OF B/T VARIATION ON NONDIMENSIONAL MEASURES ASSOCIATED WITH A 35 DEGREE RUDDER STARBOARD TURN

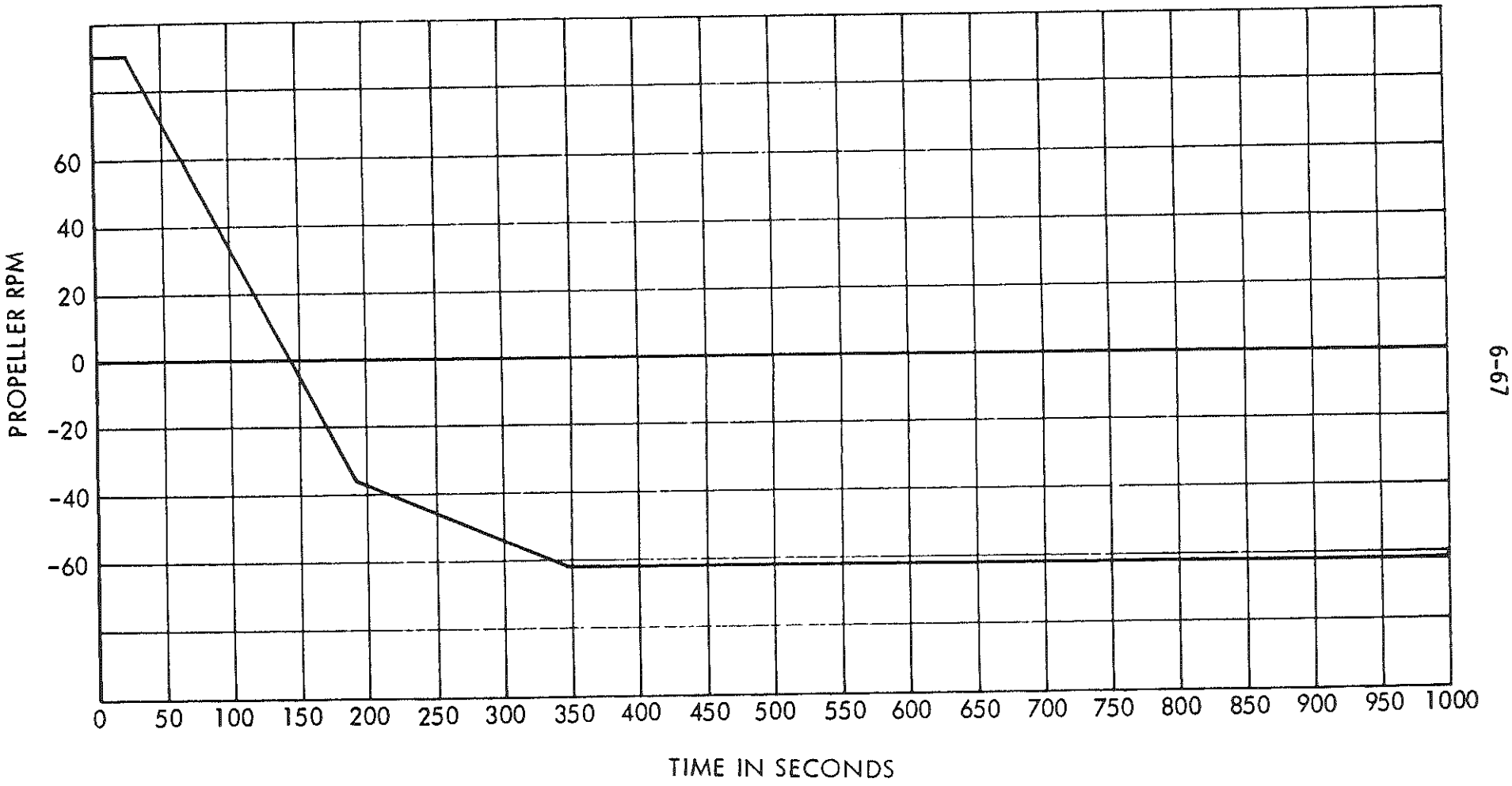

FIGURE 6-18 - TIME HISTORY OF CHANGE IN PROPELLER RPM USED IN SIMULATED STOPPING MANEUVERS

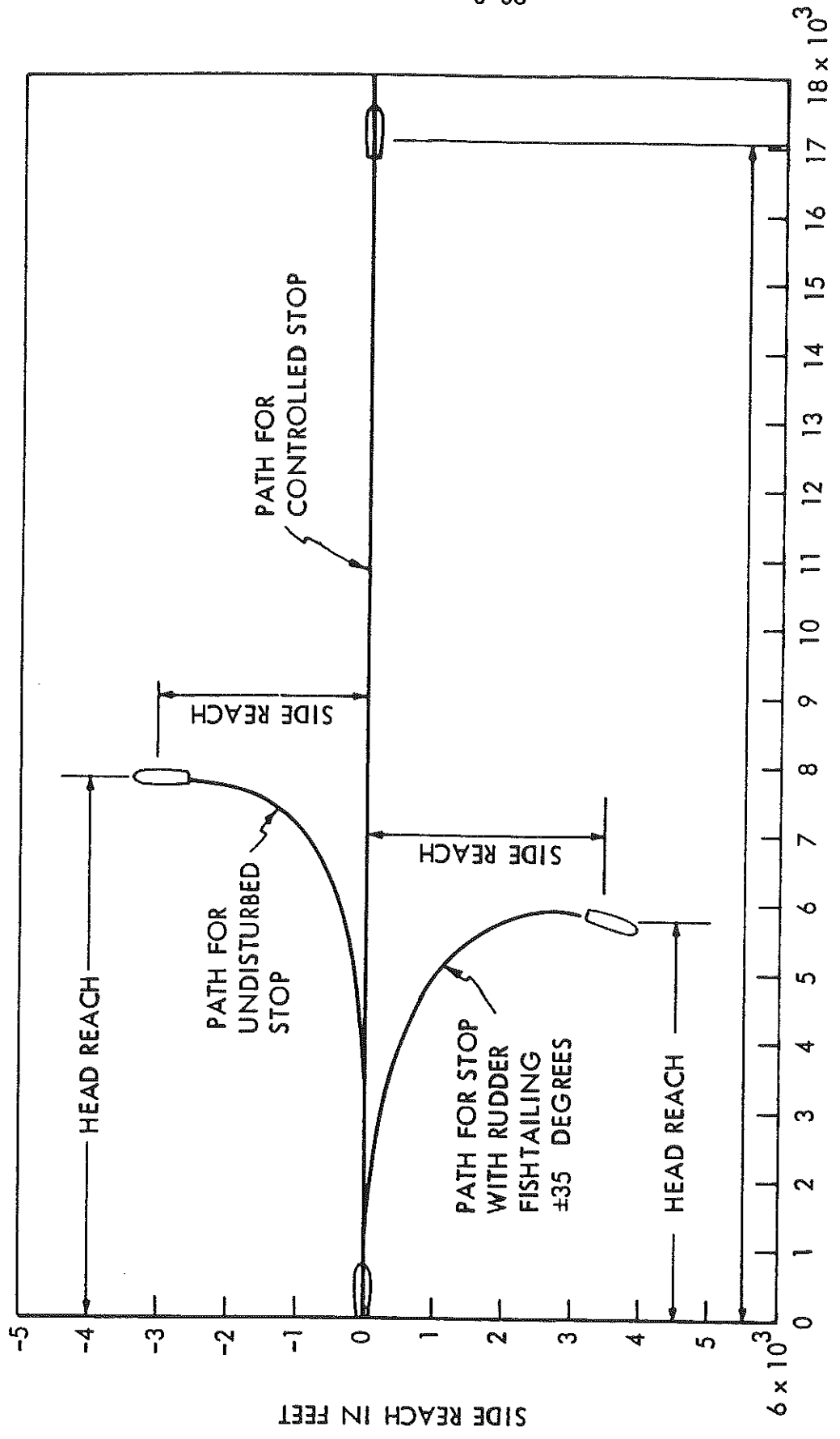

FIGURE 6-19 - PATH DURING STOPPING MANEUVERS FOR SHIP E - 350,000 TONS DISPLACEMENT, 16 KNOT APPROACH SPEED

Table 6-1

Nondimensional Stability Derivatives, Hull Constants, and Stability Indices for 350,000 Tons Displacement - Bare Hull

	Designation							
	A	B	C	D	E	F	G	H
Y_v'	-0.01513	-0.01268	-0.01141	-0.0235	-0.0192	-0.01553	-0.01852	-0.01165
N_v'	-0.00855	-0.0072	-0.00649	-0.01273	-0.01069	-0.00878	-0.010	-0.00665
Y_r'	0.00458	0.00394	0.00335	0.00788	0.00557	0.00473	0.00583	0.00346
N_r'	-0.00365	-0.00294	-0.0025	-0.00582	-0.00462	-0.00351	-0.00428	-0.0024
$Y_{\dot{v}}'$	-0.01726	-0.0146	-0.012?4	-0.02473	-0.02017	-0.01677	-0.01899	-0.01218
$N_{\dot{v}}'$	-0.00003	-0.00005	-0.00005	0.0001	0.00002	-0.00002	0.00004	-0.00004
$Y_{\dot{r}}'$	-0.00025	-0.00025	-0.00025	-0.00035	-0.00035	-0.00035	-0.00051	-0.00035
$N_{\dot{r}}'$	-0.001167	-0.000964	-0.00081	-0.001685	-0.00136	-0.001099	-0.001196	-0.000761
$Y_{\delta r}'$	0.00479	0.00416	0.00381	0.00716	0.00555	0.0045	0.00548	0.00335
$N_{\delta r}'$	-0.00249	-0.00216	-0.00198	-0.00373	-0.00289	-0.00235	-0.00288	-0.00174
m'	0.01928	0.0162	0.01381	0.02798	0.02267	0.01873	0.02133	0.01341
I_z'	0.001205	0.001013	0.000863	0.001749	0.001417	0.001171	0.001333	0.000838
$-Y_{\dot{v}}'/m'$	0.8952	0.9010	0.9080	0.8840	0.8900	0.8950	0.8900	0.9080
σ_{1h}'	0.3566	0.3749	0.3931	0.2740	0.3280	0.3676	0.3075	.0.4067
σ_{2h}'	-2.2799	-2.234	-2.272	-2.401	-2.411	-2.309	-2.415	-2.297
σ_{1h}''	0.07589	0.07529	0.07486	0.0660	0.07368	0.07748	0.06769	0.07669
ℓ_v'	0.5651	0.5678	0.5688	0.5417	0.5568	0.5654	0.5400	0.5708
ℓ_r'	0.2483	0.2400	0.2390	0.2896	0.2702	0.2507	0.2761	0.2412
ℓ_d'	-0.3168	-0.3278	-0.3298	-0.2521	-0.2866	-0.3147	-0.2639	-0.3296

Table 6-1 (Concluded)

	Designation							
	I	J	K	L	M	N	O	P
Y_v'	-0.00895	-0.00666	-0.01294	-0.00935	-0.00795	-0.012	-0.01022	-0.00874
N_v'	-0.00485	-0.0033	-0.00687	-0.00448	-0.00435	-0.00617	-0.00556	-0.00402
Y_r'	0.00259	0.00209	0.00342	0.00251	0.00255	0.00367	0.00273	0.00282
N_r'	-0.00212	-0.00165	-0.00314	-0.0025	-0.00178	-0.00303	-0.00272	-0.00235
$Y_{\dot{v}}'$	-0.00951	-0.00691	-0.01349	-0.00981	-0.00841	-0.01268	-0.01157	-0.00923
$N_{\dot{v}}'$	-0.0002	-0.0002	-0.00016	-0.00016	-0.0002	-0.00014	-0.00019	-0.00014
$Y_{\dot{r}}'$	-0.00024	-0.00011	-0.00024	-0.00011	-0.00012	-0.0004	-0.00012	-0.00029
$N_{\dot{r}}'$	-0.000576	-0.000391	-0.000857	-0.000586	-0.000512	-0.000756	-0.000735	-0.000518
$Y_{\delta r}'$	0.00313	0.00243	0.00456	0.00359	0.003	0.00449	0.00388	0.00352
$N_{\delta r}'$	-0.00163	-0.00126	-0.00238	-0.001865	-0.00156	-0.00234	-0.00202	-0.00184
m'	0.01259	0.01049	0.01813	0.01511	0.01105	0.01707	0.01543	0.01422
I_z'	0.000787	0.000656	0.001133	0.000944	0.00069	0.001067	0.000964	0.000889
$-Y_{\dot{v}}'/m'$	0.7560	0.6580	0.7440	0.6490	0.7610	0.7440	0.7500	0.6490
σ_{1h}'	0.4292	0.4075	0.4113	0.3743	0.4373	0.3756	0.4031	0.3343
σ_{2h}'	-2.287	-2.256	-2.336	-2.319	-2.234	-2.362	-2.316	-2.296
σ_{1h}''	0.07925	0.07080	0.08576	0.07345	0.07731	0.07676	0.07965	0.06428
ℓ_v'	0.5419	0.4955	0.5309	0.4791	0.5472	0.5142	0.5440	0.4600
ℓ_r'	0.2120	0.1964	0.2135	0.1984	0.2094	0.2261	0.2142	0.2061
ℓ_d'	-0.3299	-0.2991	-0.3174	-0.2807	-0.3378	-0.2881	-0.3298	-0.2539

Table 6-2

Nondimensional Stability and Control Derivatives, Hull Constants, and Stability Indices for 350,000 Tons Displacement - With Standard Rudder-Propeller Combination

	Designation							
	A	B	C	D	E	F	G	H
Y_v'	-0.01513	-0.01268	-0.01141	-0.0235	-0.0192	-0.01553	-0.01852	-0.01165
N_v'	-0.00855	-0.0072	-0.00649	-0.01273	-0.01069	-0.00878	-0.010	-0.00665
Y_r'	0.00458	0.00394	0.00335	0.00788	0.00557	0.00473	0.00583	0.00346
N_r'	-0.00365	-0.00294	-0.0025	-0.00582	-0.00462	-0.00351	-0.00428	-0.0024
$Y_{\dot{v}}'$	-0.01726	-0.0146	-0.01254	-0.02473	-0.02017	-0.01677	-0.01899	-0.01218
$N_{\dot{v}}'$	-0.00003	-0.00005	-0.00005	0.0001	0.00002	-0.00002	0.00004	-0.00004
$Y_{\dot{r}}'$	-0.00025	-0.00025	-0.00025	-0.00035	-0.00035	-0.00035	-0.00051	-0.00035
$N_{\dot{r}}'$	-0.001167	-0.000964	-0.00081	-0.001685	-0.00136	-0.001099	-0.001196	-0.000761
$Y_{\delta r}'$	0.00479	0.00416	0.00381	0.00716	0.00555	0.0045	0.00548	0.00335
$N_{\delta r}'$	-0.00249	-0.00216	-0.00198	-0.00373	-0.00289	-0.00235	-0.00288	-0.00174
m'	0.01928	0.0162	0.01381	0.02798	0.02267	0.01873	0.02133	0.01341
I_z'	0.001205	0.001013	0.000863	0.001749	0.001417	0.001171	0.001333	0.000838
$-Y_{\dot{v}}'/m'$	0.8952	0.9010	0.9080	0.8840	0.8900	0.8950	0.8900	0.9080
σ_{1h}'	0.3566	0.3749	0.3931	0.2740	0.3280	0.3676	0.3075	0.4067
σ_{2h}'	-2.2799	-2.234	-2.272	-2.401	-2.411	-2.309	-2.415	-2.297
σ_{1h}''	0.07589	0.07529	0.07486	0.0660	0.07368	0.07748	0.06769	0.07669
ℓ_v'	0.5651	0.5678	0.5688	0.5417	0.5568	0.5654	0.5400	0.5708
ℓ_r'	0.2483	0.2400	0.2390	0.2896	0.2702	0.2507	0.2761	0.2412
ℓ_d'	-0.3168	-0.3278	-0.3298	-0.2521	-0.2866	-0.3147	-0.2639	-0.3296

Table 6-2 (Concluded)

	Designation							
	I	J	K	L	M	N	O	P
Y_v'	-0.00895	-0.00666	-0.01294	-0.00935	-0.00795	-0.012	-0.01022	-0.00874
N_v'	-0.00485	-0.0033	-0.00687	-0.00448	-0.00435	-0.00617	-0.00556	-0.00402
Y_r'	0.00259	0.00209	0.00342	0.00251	0.00255	0.00367	0.00273	0.00282
N_r'	-0.00212	-0.00165	-0.00314	-0.0025	-0.00178	-0.00303	-0.00272	-0.00235
$Y_{\dot{v}}'$	-0.00951	-0.00691	-0.01349	-0.00981	-0.00841	-0.01268	-0.01157	-0.00923
$N_{\dot{v}}'$	-0.0002	-0.0002	-0.00016	-0.00016	-0.0002	-0.00014	-0.00019	-0.00014
$Y_{\dot{r}}'$	-0.00024	-0.00011	-0.00024	-0.00011	-0.00012	-0.0004	-0.00012	-0.00029
$N_{\dot{r}}'$	-0.000576	-0.000391	-0.000857	-0.000586	-0.000512	-0.000756	-0.000735	-0.000518
$Y_{\delta r}'$	0.00313	0.00243	0.00456	0.00359	0.003	0.00449	0.00388	0.00352
$N_{\delta r}'$	-0.00163	-0.00126	-0.00238	-0.001865	-0.00156	-0.00234	-0.00202	-0.00184
m'	0.01259	0.01049	0.01813	0.01511	0.01105	0.01707	0.01543	0.01422
I_z'	0.000787	0.000656	0.001133	0.000944	0.00069	0.001067	0.000964	0.000889
$-Y_{\dot{v}}'/m'$	0.7560	0.6580	0.7440	0.6490	0.7610	0.7440	0.7500	0.6490
σ_{1h}'	0.4292	0.4075	0.4113	0.3743	0.4373	0.3756	0.4031	0.3343
σ_{2h}'	-2.287	-2.256	-2.336	-2.319	-2.234	-2.362	-2.316	-2.296
σ_{1h}''	0.07925	0.07080	0.08576	0.07345	0.07731	0.07676	0.07965	0.06428
ℓ_v'	0.5419	0.4955	0.5309	0.4791	0.5472	0.5142	0.5440	0.4600
ℓ_r'	0.2120	0.1964	0.2135	0.1984	0.2094	0.2261	0.2142	0.2061
ℓ_d'	-0.3299	-0.2991	-0.3174	-0.2807	-0.3378	-0.2881	-0.3298	-0.2539

Table 6-3

Incremental Contribution to Nondimensional Stability and Control Derivatives Due to Standard Rudder-Propeller Combinations - 350,000 Tons Displacement

Ship I.D.	$\Delta Y_v'$	$\Delta N_v'$	$\Delta Y_r'$	$\Delta N_r'$	$Y_{\delta r}'$	$N_{\delta r}'$	$\frac{\Delta N_v'}{\Delta Y_v'}$	$\frac{\Delta Y_v'}{Y_{\delta r}'}$	$\frac{\Delta N_v'}{N_{\delta r}'}$	$\frac{\Delta N_r'}{\Delta Y_r'}$
A	-0.00326	0.00169	0.00390	-0.00211	0.00479	-0.00249	-0.518	-0.681	-0.679	-0.541
B	-0.00282	0.00147	0.00336	-0.00163	0.00416	-0.00216	-0.521	-0.678	-0.681	-0.485
C	-0.00246	0.00128	0.00286	-0.00138	0.00381	-0.00198	-0.520	-0.672	-0.646	-0.483
D	-0.00430	0.00224	0.00691	-0.00362	0.00716	-0.00373	-0.521	-0.601	-0.600	-0.524
E	-0.00345	0.00179	0.00478	-0.00284	0.00555	-0.00289	-0.520	-0.622	-0.619	-0.594
F	-0.00285	0.00148	0.00407	-0.00201	0.00450	-0.00235	-0.519	-0.633	-0.630	-0.494
G	-0.00343	0.00179	0.00508	-0.00259	0.00548	-0.00288	-0.522	-0.626	-0.622	-0.509
H	-0.00213	0.00111	0.00298	-0.00131	0.00355	-0.00185	-0.521	-0.600	-0.600	-0.439
I	-0.00198	0.00103	0.00222	-0.00127	0.00313	-0.00163	-0.520	-0.632	-0.632	-0.573
J	-0.00158	0.00082	0.00182	-0.00104	0.00243	-0.00126	-0.518	-0.650	-0.650	-0.569
K	-0.00284	0.00148	0.00289	-0.00194	0.00456	-0.00238	-0.521	-0.623	-0.622	-0.671
L	-0.00244	0.00122	0.00213	-0.00163	0.00359	-0.00187	-0.520	-0.680	-0.681	-0.765
M	-0.00186	0.00097	0.00222	-0.00103	0.00300	-0.00156	-0.520	-0.620	-0.620	-0.464
N	-0.00293	0.00152	0.00317	-0.0019	0.00449	-0.00234	-0.519	-0.653	-0.650	-0.599
O	-0.00253	0.00131	0.00228	-0.00169	0.00388	-0.00202	-0.518	-0.652	-0.649	-0.741
P	-0.00241	0.00125	0.00246	-0.00153	0.00352	-0.00184	-0.519	-0.685	-0.679	-0.622

Table 6-4

Incremental Contribution to Stability and Control Derivatives Due to Change in Propeller Loading Coefficient - 350,000 Tons Displacement

Ship I.D.	$Y_{v\eta}'$	$N_{v\eta}'$	$Y_{r\eta}'$	$N_{r\eta}'$	$Y_{\delta r\eta}'$	$N_{\delta r\eta}'$	$Y_{v\eta}'/Y_{\delta r\eta}'$
A	-0.00292	0.00152	0.00152	-0.00079	0.00479	-0.00249	0.610
B	-0.00266	0.00138	0.00138	-0.00072	0.00416	-0.00216	0.639
C	-0.00255	0.00133	0.00133	-0.00069	0.00381	-0.00198	0.669
D	-0.00394	0.00205	0.00205	-0.00107	0.00716	-0.00373	0.550
E	-0.00322	0.00167	0.00167	-0.00087	0.00555	-0.00289	0.580
F	-0.00275	0.00143	0.00143	-0.00074	0.00450	-0.00235	0.611
G	-0.00318	0.00165	0.00165	-0.00086	0.00548	-0.00288	0.580
H	-0.00238	0.00124	0.00124	-0.00064	0.00355	-0.00185	0.670
I	-0.00175	0.00091	0.00091	-0.00047	0.00313	-0.00163	0.559
J	-0.00119	0.00062	0.00062	-0.00032	0.00243	-0.00126	0.490
K	-0.00228	0.00119	0.00119	-0.00062	0.00456	-0.00238	0.500
L	-0.00154	0.00080	0.00080	-0.00042	0.00359	-0.00187	0.429
M	-0.00177	0.00092	0.00092	-0.00048	0.00300	-0.00156	0.590
N	-0.00225	0.00117	0.00117	-0.00061	0.00449	-0.00234	0.501
O	-0.00206	0.00107	0.00107	-0.00056	0.00388	-0.00202	0.531
P	-0.00151	0.00079	0.00079	-0.00041	0.00352	-0.00184	0.429

Table 6-5

Dimensional Angular Acceleration Parameters for 350,000 Tons Displacement

Ship I.D.	8 Knots		16 Knots	
	cp sec^{-2}	t_2 sec	cp sec^{-2}	t_2 sec
A	0.570×10^{-4}	66	2.28×10^{-4}	34
B	0.529	68	2.11	35
C	0.515	69	2.06	36
D	0.756	57	3.03	29
E	0.630	63	2.52	32
F	0.552	67	2.21	35
G	0.662	61	2.65	31
H	0.493	70	1.97	36
I	0.489	70	1.96	35
J	0.436	75	1.74	39
K	0.624	63	2.49	32
L	0.563	67	2.25	35
M	0.486	71	1.95	36
N	0.643	62	2.57	32
O	0.556	67	2.23	35
P	0.580	66	2.32	33

Note: Values are for a rudder angle of 20 degrees and a rudder deflection rate of 2.33 deg/sec.

Table 6-6

Equations of Motion for Surface Ship Maneuvering Simulation

AXIAL FORCE

$$m[\dot{u} - vr - x_G r^2] =$$

$$+ \tfrac{1}{2} \rho L^4 \left[X_{rr}' r^2\right]$$

$$+ \tfrac{1}{2} \rho L^3 \left[X_{\dot{u}}' \dot{u} + X_{vr}' vr\right]$$

$$+ \tfrac{1}{2} \rho L^2 \left[X_{vv}' v^2\right] + \tfrac{1}{2} \rho L^2 \left[X_{vv\eta}' v^2\right] (\eta - 1)$$

$$+ \tfrac{1}{2} \rho L^2 u^2 \left[a_1 + b_1 \eta + c_1 \eta^2\right]$$

$$+ \tfrac{1}{2} \rho L^2 u_R^2 \left[X_{\delta r \delta r}' \delta r^2 + X_{\delta r \delta r \eta \eta}' \delta r^2 \eta^2\right]$$

LATERAL FORCE

$$m\left[\dot{v} + ur + x_G \dot{r}\right] =$$

$$+ \tfrac{1}{2} \rho L^4 \left[Y_{\dot{r}}' \dot{r} + Y_{r|r|}' r|r|\right]$$

$$+ \tfrac{1}{2} \rho L^3 \left[Y_{\dot{v}}' \dot{v}\right]$$

$$+ \tfrac{1}{2} \rho L^3 \left[Y_r' ur + Y_{v|r|}' v|r|\right]$$

$$+ \tfrac{1}{2} \rho L^2 \left[Y_*' u_*^2 + Y_v' uv + Y_{v|v|}' v|v|\right]$$

$$+ \tfrac{1}{2} \rho L^2 \left[Y_{\delta r}' u_R^2 \delta r\right]$$

$$+ \tfrac{1}{2} \rho L^3 \left[Y_{r\eta}' ur\right] (\eta - 1) + \tfrac{1}{2} \rho L^2 \left[Y_{v\eta}' uv\right] (\eta - 1)$$

YAWING MOMENT

$$I_z \dot{r} + mx_G (\dot{v} + ur) =$$

$$+ \tfrac{1}{2} \rho L^5 \left[N_{\dot{r}}' \dot{r} + N_{r|r|}' r|r|\right]$$

$$+ \tfrac{1}{2} \rho L^4 \left[N_{\dot{v}}' \dot{v}\right]$$

$$+ \tfrac{1}{2} \rho L^4 \left[N_r' ur + N_{r|v|}' r|v|\right]$$

$$+ \tfrac{1}{2} \rho L^3 \left[N_*' u_*^2 + N_v' uv + N_{v|v|}' v|v|\right]$$

$$+ \tfrac{1}{2} \rho L^3 \left[N_{\delta r}' u_R^2 \delta r\right]$$

$$+ \tfrac{1}{2} \rho L^4 \left[N_{r\eta}' ur\right] (\eta - 1) + \tfrac{1}{2} \rho L^3 \left[N_{v\eta}' uv\right] (\eta - 1)$$

where

$$u_R^2 = du^2 + eun D_p + f n^2 D_p^2$$

$$u_*^2 = d_* u^2 + e_* un D_p + f_* n^2 D_p^2$$

D_p = Propeller diameter

n = Propeller rotational speed

Table 6-7a

Nondimensional Hydrodynamic Coefficients and Constants for Equations of Motion for Use in Computer Simulation Studies
350,000 Tons Displacement

	Ship Designation			
	A	B	C	D
$X_{\dot{u}}'$	-0.00108	-0.000859	-0.00069	-0.00172
X_{vr}'	0.01295	0.01095	0.00941	0.01855
X_{vv}'	0.00186	0.00287	0.001345	0.00164
$X_{\delta r\delta r}'$	-0.00269	-0.00248	-0.00255	-0.00278
X_{rr}'	0.0	0.0	0.0	0.0
$X_{vv\eta}'$	0.00091	0.0 0082	0.0 0082	0.0 0110
$Y_{\dot{v}}'$	-0.01726	-0.01460	-0.01254	-0.02473
Y_{*}'	0.000071	0.000063	0.00006	0.00011
Y_{v}'	-0.01365	-0.0110	-0.00959	-0.01674
$Y_{v\|v\|}'$	-0.03109	-0.0398	-0.0327	-0.05857
Y_{r}'	0.00458	0.00394	0.00335	0.00788
$Y_{r\|r\|}'$	0.0 0215	0.0 0205	0.0 0205	0.0 0225
$Y_{v\|r\|}'$	-0.0158	-0.0152	-0.0144	-0.0168
$Y_{\dot{r}}'$	-0.00025	-0.00025	-0.00025	-0.00035
$Y_{\delta r}'$	0.00479	0.00416	0.00381	0.00716
$Y_{r\eta}'$	0.00152	0.00138	0.00133	0.00205
$Y_{v\eta}'$	-0.00292	-0.00266	-0.00255	-0.00394
$N_{\dot{r}}'$	-0.001167	-0.000964	-0.00081	-0.001685
N_{*}'	-0.000037	-0.000033	-0.000031	-0.000057
N_{v}'	-0.00824	-0.00798	-0.00993	-0.01314
$N_{v\|v\|}'$	0.00299	0.00754	0.03944	0.01441
N_{r}'	-0.00365	-0.00294	-0.0025	-0.00582
$N_{r\|r\|}'$	-0.0 0043	-0.00042	-0.00045	-0.0 0049
$N_{\|v\|r}'$	-0.00505	-0.00495	-0.00483	-0.00525
$N_{\dot{v}}'$	-0.00003	-0.00005	-0.00005	0.0001
$N_{\delta r}'$	-0.00249	-0.00216	-0.00198	-0.00373
$N_{v\eta}'$	0.00152	0.00138	0.00133	0.00205
$N_{r\eta}'$	-0.00079	-0.00072	-0.00069	-0.001065
a_1	-0.000860	-0.000688	-0.000605	-0.000308
b_1	-0.000850	-0.000700	-0.000550	-0.002000
c_1	0.00155	0.001246	0.001050	0.002100
a_2	-0.000840	-0.000768	-0.000695	-0.000892
b_2	-0.000560	-0.000332	-0.000205	-0.000708
c_2	0.00140	0.001100	0.000900	0.001610
a_3	-0.000840	-0.000768	-0.000695	-0.000892
b_3	0.000400	0.000300	0.000300	0.000600
c_3	-0.000300	-0.000200	-0.000200	-0.000400
a_4	-0.000840	-0.000768	-0.000695	-0.000892
b_4	0.0000	-0.000900	0.0	0.0
c_4	-0.000700	-0.000590	-0.000500	-0.00100
m'	0.01928	0.01620	0.01381	0.02798
I_x'	0.000071	0.000050	0.000036	0.000153
I_z'	0.001205	0.001013	0.000863	0.001749

Notes: Subscripts 1, 2, 3, and 4 refer to segments 1, 2, 3, and 4, for X' as a function of η corresponding to $2 < \eta < \infty$, $0 < \eta < 0$, and $-\infty < \eta < -1.0$, respectively. Value of I_z' is based on $k_z' = 0.25$ and value of I_x' is based on $k_x' = 0.333$ B/L.

Table 6-7a (Continued)

	Ship Designation			
	E	F	G	H
$X_{\dot{u}}'$	-0.00133	-0.001045	-0.00125	-0.000671
X_{vr}'	0.01608	0.01513	0.01424	0.00914
X_{vv}'	0.00248	0.00174	0.00160	0.00197
$X_{\delta r\delta r}'$	-0.00290	-0.00240	-0.00255	-0.00235
X_{rr}'	0.0	0.0	0.0	0.0
$X_{vv\eta}'$	0.00100	0.000925	0.00093	0.00103
$Y_{\dot{v}}'$	-0.02017	-0.01677	-0.01899	-0.01218
Y_{*}'	0.000086	0.000071	0.000086	0.00006
Y_{v}'	-0.01512	-0.01295	-0.01161	-0.00924
$Y_{v\|v\|}'$	-0.0534	-0.04123	-0.0606	-0.03702
Y_{r}'	0.00557	0.00473	0.00583	0.00346
$Y_{r\|r\|}'$	0.0023	0.00245	0.00205	0.00230
$Y_{v\|r\|}'$	-0.0163	-0.0158	-0.0163	-0.0144
$Y_{\dot{r}}'$	-0.00035	-0.00035	-0.00051	-0.00035
$Y_{\delta r}'$	0.00555	0.00450	0.00548	0.00335
$Y_{r\eta}'$	0.00167	0.00143	0.00165	0.00093
$Y_{v\eta}'$	-0.00322	-0.00275	-0.00318	-0.00178
$N_{\dot{r}}'$	-0.00136	-0.001099	-0.001196	-0.000761
N_{*}'	-0.000045	-0.000037	-0.000045	-0.000031
N_{v}'	-0.01095	-0.00876	-0.01117	-0.00515
$N_{v\|v\|}'$	0.01327	0.00899	0.01687	0.0020
N_{r}'	-0.00462	-0.00351	-0.00428	-0.00240
$N_{r\|r\|}'$	-0.00038	-0.000492	-0.00043	-0.00044
$N_{\|v\|r}'$	-0.00515	-0.00505	-0.00515	-0.00483
$N_{\dot{v}}'$	0.00002	-0.00002	0.00004	-0.00004
$N_{\delta r}'$	-0.00289	-0.00235	-0.00288	-0.00174
$N_{v\eta}'$	0.00167	0.00143	0.00165	0.000923
$N_{r\eta}'$	-0.00087	-0.00074	-0.00086	-0.00048
a_1	-0.000021	-0.000403	-0.003593	0.0
b_1	-0.002054	-0.001326	-0.000017	-0.001169
c_1	0.002086	0.001624	-0.002056	0.001304
a_2	-0.000838	-0.000717	-0.001025	-0.000641
b_2	-0.000849	-0.000645	-0.000765	-0.000438
c_2	0.001687	0.001362	0.001791	0.001080
a_3	-0.000838	-0.000717	-0.001025	-0.000641
b_3	0.001201	0.000887	0.000683	0.000883
c_3	-0.000054	-0.000199	-0.000362	-0.000285
a_4	-0.001291	-0.001158	-0.001705	-0.001189
b_4	-0.000114	-0.000075	-0.000551	-0.000272
c_4	-0.000916	-0.000721	-0.000921	-0.000892
m'	0.02267	0.01873	0.02133	0.01341
I_x'	0.000101	0.000069	0.000095	0.000035
I_z'	0.001417	0.001171	0.001333	0.000838

Table 6-7a (Continued)

	Ship Designation			
	I	J	K	L
$X_{\dot{u}}'$	-0.000667	-0.000556	-0.00107	-0.000888
X_{vr}'	0.00713	0.00518	0.01012	0.00736
X_{vv}'	0.000739	0.000263	0.00188	0.000657
$X_{\delta r\delta r}'$	-0.00255	-0.00235	-0.00258	-0.002692
X_{rr}'	0.0	0.0	0.0	0.0
$X_{vv\eta}'$	0.00083	0.00065	0.000984	0.00092
$Y_{\dot{v}}'$	-0.00951	-0.00691	-0.01349	-0.00981
Y_{*}'	0.000063	0.000063	0.000086	0.000086
Y_{v}'	-0.00736	-0.00594	-0.01031	-0.00751
$Y_{v\|v\|}'$	-0.02688	-0.01778	-0.03718	-0.02622
Y_{r}'	0.00259	0.00209	0.00342	0.00251
$Y_{r\|r\|}'$	0.00191	0.00162	0.00147	0.00145
$Y_{v\|r\|}'$	-0.0152	-0.0152	-0.0163	-0.0163
$Y_{\dot{r}}'$	-0.00024	-0.00011	-0.00024	-0.00011
$Y_{\delta r}'$	0.00313	0.00243	0.00456	0.00359
$Y_{r\eta}'$	0.00091	0.00062	0.00119	0.00080
$Y_{v\eta}'$	-0.00175	-0.00119	-0.00228	-0.00154
$N_{\dot{r}}'$	-0.000576	-0.000391	-0.000857	-0.000586
N_{*}'	-0.000033	-0.000033	-0.000045	-0.000045
N_{v}'	-0.00506	-0.00359	-0.00728	-0.00475
$N_{v\|v\|}'$	0.00602	0.00324	0.00895	0.00423
N_{r}'	-0.00212	-0.00165	-0.00314	-0.0025
$N_{r\|r\|}'$	-0.000421	-0.00037	-0.00069	-0.00038
$N_{\|v\|r}'$	-0.00495	-0.00495	-0.00515	-0.00515
$N_{\dot{v}}'$	-0.0002	-0.0002	-0.00016	-0.00016
$N_{\delta r}'$	-0.00163	-0.00126	-0.00238	-0.001865
$N_{v\eta}'$	0.000911	0.000619	0.00119	0.000803
$N_{r\eta}'$	-0.00047	-0.00032	-0.00062	-0.00042
a_1	-0.000639	-0.000812	0.0	0.0
b_1	-0.000770	-0.000484	-0.001448	-0.001381
c_1	0.001139	0.001019	0.001658	0.001515
a_2	-0.000680	-0.000515	-0.000906	-0.000649
b_2	-0.000168	-0.000375	-0.000513	-0.000674
c_2	0.000847	0.000890	0.001419	0.001324
a_3	-0.000680	-0.000515	-0.000906	-0.000649
b_3	0.000139	0.000247	0.000474	0.000578
c_3	-0.000316	-0.000274	-0.000445	-0.000189
a_4	-0.000503	-0.000287	-0.000741	-0.000537
b_4	-0.000191	0.000017	-0.000112	-0.000164
c_4	-0.000822	-0.000732	-0.001196	-0.001042
m'	0.01259	0.01049	0.01813	0.01511
I_x'	0.000039	0.000032	0.000080	0.000067
I_z'	0.000787	0.000656	0.001133	0.000944

Table 6-7a (Concluded)

	Ship Designation			
	M	N	O	P
$X_{\dot{u}}'$	-0.000553	-0.0010	-0.00086	-0.00084
X_{vr}'	0.00631	0.00951	0.00868	0.00692
X_{vv}'	0.00149	0.00192	0.00176	0.00140
$X_{\delta r\delta r}'$	-0.00275	-0.00270	-0.00245	-0.00262
X_{rr}'	0.0	0.0	0.0	0.0
$X_{vv\eta}'$	0.00092	0.000935	0.00096	0.00095
$Y_{\dot{v}}'$	-0.00841	-0.01268	-0.01157	-0.00923
Y_{*}'	0.00006	0.000086	0.000071	0.000086
Y_{v}'	-0.00662	-0.01013	-0.00781	-0.00800
$Y_{v\|v\|}'$	-0.02561	-0.03229	-0.0336	-0.0222
Y_{r}'	0.00255	0.00367	0.00273	0.00282
$Y_{r\|r\|}'$	0.00182	0.00212	0.00205	0.00205
$Y_{v\|r\|}'$	-0.0144	-0.0163	-0.0158	-0.0163
$Y_{\dot{r}}'$	-0.00012	-0.0004	-0.00012	-0.00029
$Y_{\delta r}'$	0.0030	0.00449	0.00388	0.00352
$Y_{r\eta}'$	0.00092	0.00117	0.00107	0.00079
$Y_{v\eta}'$	-0.00177	-0.00225	-0.00206	-0.00151
$N_{\dot{r}}'$	-0.000512	-0.000756	-0.000735	-0.000518
N_{*}'	-0.000031	-0.000045	-0.000037	-0.000045
N_{v}'	-0.00432	-0.00638	-0.00575	-0.00431
$N_{v\|v\|}'$	0.00390	0.00692	0.00512	0.00414
N_{r}'	-0.00178	-0.00303	-0.00272	-0.00235
$N_{r\|r\|}'$	-0.00037	-0.000560	-0.000525	-0.00043
$N_{\|v\|r}'$	-0.00483	-0.00515	-0.00505	-0.00515
$N_{\dot{v}}'$	-0.0002	-0.00014	-0.00019	-0.00014
$N_{\delta r}'$	-0.00156	-0.00234	-0.00202	-0.00184
$N_{v\eta}'$	0.00092	0.00117	0.00107	0.000787
$N_{r\eta}'$	-0.00048	-0.00061	-0.00056	-0.00041
a_1	-0.000391	0.0	-0.001113	-0.001643
b_1	-0.000805	-0.001529	-0.000776	-0.000273
c_1	0.001085	0.001503	0.001522	0.001361
a_2	-0.000611	-0.000739	-0.000694	-0.000757
b_2	-0.000253	-0.000371	-0.000669	-0.000491
c_2	0.000864	0.001110	0.001364	0.001248
a_3	-0.000611	-0.000739	-0.000694	-0.000757
b_3	0.000306	0.000648	0.000596	0.000319
c_3	-0.000208	-0.000202	0.000203	-0.000197
a_4	-0.000478	-0.000504	-0.000546	-0.000563
b_4	-0.000136	-0.000012	-0.000138	-0.000272
c_4	-0.000782	-0.001097	-0.001085	-0.000982
m'	0.01105	0.01707	0.01543	0.01422
I_x'	0.000029	0.000076	0.000057	0.000063
I_z'	0.00069	0.001067	0.000964	0.000889

Table 6-7b

Nondimensional Hydrodynamic Coefficients and Constants for Equations of Motion for Use in Computer Simulation Studies-350,000 Tons Displacement

(Rudder/Propeller and Hull/Propeller Velocity Coefficients)

Ship Designation	Rudder/Propeller Velocity Coefficients						Hull/Propeller Velocity Coefficients					
	d		e		f		d_*		e_*		f_*	
	$n \geq 0$	$n < 0$	$n \geq 0$	$n < 0$	$n \geq 0$	$n < 0$	$n \geq 0$	$n < 0$	$n \geq 0$	$n < 0$	$n \geq 0$	$n < 0$
A	0.260	0.260	0.385	0.220	0.068	-0.001	0.0	0.0	0.500	-0.168	0.120	-0.299
B	0.260	0.260	0.392	0.220	0.067	-0.001	0.0	0.0	0.500	-0.168	0.177	-0.283
C	0.280	0.280	0.384	0.200	0.066	-0.001	0.0	0.0	0.440	-0.148	0.118	-0.295
D	0.220	0.220	0.430	0.220	0.070	-0.001	0.0	0.0	0.500	-0.165	0.121	-0.300
E	0.280	0.280	0.345	0.200	0.076	-0.001	0.0	0.0	0.450	-0.149	0.117	-0.282
F	0.280	0.280	0.350	0.200	0.066	-0.001	0.0	0.0	0.450	-0.148	0.115	-0.280
G	0.290	0.290	0.370	0.220	0.066	-0.001	0.0	0.0	0.400	-0.133	0.116	-0.285
H	0.290	0.290	0.341	0.210	0.063	-0.001	0.0	0.0	0.470	-0.149	0.112	-0.280
I	0.285	0.285	0.389	0.250	0.069	-0.001	0.0	0.0	0.440	-0.144	0.118	-0.290
J	0.290	0.290	0.360	0.220	0.067	-0.001	0.0	0.0	0.400	-0.133	0.111	-0.270

Table 6-8

Comparison of Numerical Measures from Spiral Maneuvers

Ship I.D.	8 Knots			16 Knots		
	Height of Loop deg/sec	Width of Loop degrees	Neutral Rudder Angle degrees	Height of Loop deg/sec	Width of Loop degrees	Neutral Rudder Angle degrees
A						
B	0.2462	7.0	1.0 R	0.4925	7.0	1.0 R
C						
D						
E	0.229	5.0	1.0 R	0.458	5.0	1.0 R
F	0.217	5.1	1.1 R	0.433	5.1	1.1 R
G	0.245	7.0	1.0 R	0.489	7.0	1.0 R
H	0.166	3.0	1.0 R	0.332	3.0	1.0 R
I	0.176	5.9	1.6 R	0.353	5.9	1.6 R
J	0.161	5.6	1.6 R	0.321	5.6	1.6 R
K	0.220	6.0	1.0 R	0.440	6.0	1.0 R
L	0.182	5.6	1.2 R	0.364	5.6	1.2 R
M	0.174	4.6	0.9 R	0.347	4.6	0.9 R
N	0.188	4.6	1.1 R	0.375	4.6	1.1 R
O	0.201	6.4	1.0 R	0.402	6.4	1.0 R
P	0.163	4.5	1.3 R	0.325	4.5	1.3 R

Table 6-9

Comparison of Numerical Measures from Zigzag Maneuvers at an Approach Speed of 8 Knots

(a) 5-5 Zigzag

Ship I.D.	First Overshoot						Reach	Second Overshoot Heading Angle	Third Overshoot Heading	Period
	Time to reach execute heading change seconds	Overshoot Angle degrees	Total Heading Change degrees	Width of Path at Execute feet	Overshoot Width of Path feet	Total Width of Path feet	seconds	degrees	degrees	seconds
A										
B	140	5.4	10.4	23	710	733	530			
C										
D										
E	133	4.6	9.6	22	586	608	479			
F	140	4.8	9.8	24	639	663	510			
G	128	5.3	10.3	21	664	685	493			
H	153	2.9	7.9	27	441	468	470			
I	152	3.9	8.9	23	554	577	508			
J	170	2.9	7.9	26	462	488	505			
K	134	4.3	9.3	19	546	565	469			
L	152	2.8	7.8	21	412	433	457			
M	151	3.4	8.4	24	482	506	479			
N	137	3.4	8.4	20	436	456	435			
O	143	4.0	9.0	20	555	575	500			
P	153	2.3	7.3	23	347	370	417			

Table 6-9 (Continued)

(b) 10-10 Zigzag (8 knots)

Ship I.D.	First Overshoot						Reach	Second Overshoot Heading Angle	Third Overshoot Heading	Period
	Time to Reach Execute Heading Change seconds	Overshoot Angle degrees	Total Heading Change degrees	Width of Path at Execute feet	Overshoot Width of Path feet	Total Width of Path feet	seconds	degrees	degrees	seconds
A										
B	136	10.0	20.0	42	1334	1376	530	31.3	23.4	1242
C										
D										
E	130	8.8	18.8	44	1145	1189	488	27	20.3	1128
F	136	9.4	19.4	46	1256	1302	519	27.9	20.2	1204
G	124	10.0	20.0	40	1262	1302	496	18.9	10.8	1153
H	148	6.4	16.4	51	953	1004	490	16.6	12.8	1048
I	147	7.3	17.3	43	1079	1122	514	20.2	13.0	1172
J	160	6.0	16.0	48	985	1033	524	17.6	10.6	1213
K	130	8.3	18.3	36	1076	1112	483	23.5	15.8	1121
L	144	6.0	16.0	39	902	941	478	18.8	12.0	1121
M	146	6.6	16.6	44	951	995	493	16.4	10.9	1089
N	131	6.6	16.6	38	888	926	448	18.1	12.4	1005
O	139	7.8	17.8	38	1109	1147	510	22.0	15.4	1166
P	144	4.9	14.9	40	753	793	443	13.9	9.0	991

Table 6-9 (Concluded)

(c) 20-20 Zigzag (8 knots)

Ship I.D.	First Overshoot						Reach	Second Overshoot Heading Angle	Third Overshoot Heading	Period
	Time to Reach Execute Heading Change seconds	Overshoot Angle degrees	Total Heading Change degrees	Width of Path at Execute feet	Overshoot Width of Path feet	Total Width of Path feet	seconds	degrees	degrees	seconds
A										
B	140	14.7	34.7		1933	2027	508	18.7	13.8	997
C										
D										
E	134	13.7	33.7	93	1744	1837	477	16.5	12.1	940
F	140	13.8	33.8	96	1829	1925	501	17.0	12.2	997
G	128	14.1	34.1	86	1768	1854	466	15.8	11.9	902
H	153	10.6	30.6	110	1569	1679	489	13.9	10.0	953
I	151	10.7	30.7	95	1635	1730	498	11.7	8.5	973
J	165	8.7	28.7	106	1540	1646	514	10.1	7.3	1017
K	134	11.8	31.8	75	1517	1592	466	12.7	9.7	915
L	146	9.6	29.6	77	1473	1550	473	11.6	8.3	939
M	153	9.7	29.7	97	1422	1519	493	10.4	7.4	975
N	134	10.7	30.7	81	1427	1508	444	12.2	8.9	879
O	142	11.5	31.5	82	1640	1722	488	12.9	9.8	951
P	148	8.3	28.3	87	1302	1389	447	10.1	7.5	884

Table 6-10

Comparison of Numerical Measures from Zigzag Maneuvers at an Approach Speed of 16 Knots

(a) 5-5 Zigzag

Ship I.D.	First Overshoot						Reach	Second Overshoot Heading Angle	Third Overshoot Heading	Period
	Time to Reach Execute Heading Change seconds	Overshoot Angle degrees	Total Heading Change degrees	Width of Path at Execute feet	Overshoot Width of Path feet	Total Width of Path feet	seconds	degrees	degrees	seconds
A										
B	69	5.9	10.9	22	773	795	272	104.8		
C										
D										
E	67	5.4	10.4	23	675	698	393	71.8		
F	69	4.9	9.9	23	653	676	257	73.4	35.3	1156
G	63	5.9	10.9	20	729	749	255	116.6		1495
H	76	3.4	8.4	26	493	519	244	23.1	19.6	708
I	75	4.2	9.2	22	596	618	260	61.9	23.7	1216
J	85	3.2	8.2	26	491	517	257	55.3	19.0	1275
K	68	5.1	10.1	18	633	651	248	90.9	26.4	1360
L	76	3.1	8.1	20	443	463	233	60.9	21.7	1220
M	76	3.7	8.7	23	518	541	247	37.6	21.0	910
N	67	3.4	8.4	19	446	465	220	38.0	23.5	823
O	69	4.4	9.4	21	599	620	257	75.0	27.5	1304
P	76	2.4	7.4	21	355	376	214	26.6	35.6	768

Table 6-10 (Continued)

(b) 10-10 Zigzag (16 knots)

Ship I.D.	First Overshoot						Reach	Second Overshoot Heading Angle	Third Overshoot Heading	Period
	Time to Reach Execute Heading Change seconds	Overshoot Angle degrees	Total Heading Change degrees	Width of Path at Execute feet	Overshoot Width of Path feet	Total Width of Path feet	seconds	degrees	degrees	seconds
A										
B	68	12.3	22.3	43	1596	1639	283	33.5	24.4	651
C										
D										
E	66	10.5	20.5	23	1338	1361	267	28.6	21.3	586
F	68	11.0	21.0	45	1433	1478	273	29.9	21.3	627
G	62	11.8	21.8	39	1456	1495	258	30.4	20.8	598
H	74	7.5	17.5	50	1069	1119	255	18.0	13.9	545
I	73	8.4	18.4	43	1213	1256	267	21.3	14.0	606
J	80	7.0	17.0	47	1094	1141	272	18.6	11.1	625
K	65	9.8	19.8	35	1234	1269	253	25.4	16.4	584
L	72	6.7	16.7	38	944	1016	246	20.0	13.0	577
M	73	7.7	17.7	43	1067	1110	257	17.4	11.4	563
N	66	7.5	17.5	34	972	1006	230	19.3	13.1	517
O	69	8.7	18.7	36	1208	1244	258	23.4	16.1	601
P	72	5.5	15.5	41	812	853	227	15.3	10.0	513

Table 6-10 (Concluded)

(c) 20-20 Zigzag (16 knots)

Ship I.D.	First Overshoot						Reach	Second Overshoot Heading Angle	Third Overshoot Heading	Period
	Time to Reach Execute Heading Change seconds	Overshoot Angle degrees	Total Heading Change degrees	Width of Path at Execute feet	Overshoot Width of Path feet	Total Width of Path feet	seconds	degrees	degrees	seconds
A										
B	72	18.2	38.2	92	2247	2339	271	20.1	15.6	595
C										
D										
E	68	16.4	36.4	90	1983	2073	253	18.2	13.9	493
F	71	17.2	37.2	93	2128	2221	268	18.7	13.3	527
G	65	16.9	36.9	141	1949	2090	246	18.1	13.9	476
H	77	13.3	33.3	104	1817	1921	260	15.4	12.0	502
I	76	13.2	33.2	93	1868	1961	264	13.3	9.8	513
J	84	10.4	30.4	105	1704	1809	269	11.8	8.7	531
K	68	14.2	34.2	73	1717	1790	246	14.6	11.4	481
L	74	12.1	32.1	80	1691	1771	251	13.4	9.6	495
M	77	12.1	32.1	92	1631	1723	261	11.6	9.1	512
N	68	13.5	33.5	79	1663	1742	237	14.0	10.2	466
O	74	14.3	34.3	76	1899	1975	259	14.4	11.6	499
P	74	10.6	30.6	86	1502	1588	237	11.9	8.9	468

Comparison of Numerical Measures from Steady Turning Maneuvers at an Approach Speed of 8 Knots

(a) 10-Degree Right Rudder Angle Turn

Ship I.D.	Time to Change Heading 90 Degrees seconds	Time to Change Heading 180 Degrees seconds	Speed Remaining in Steady Turn knots	Advance feet	Transfer feet	Tactical Diameter feet	Steady Turning Diameter feet
A							
B	513	1013	4.99	5186	2467	5853	6074
C							
D							
E	502	1016	4.62	5030	2409	5726	5922
F	525	1074	4.50	5232	2493	5917	6177
G	492	996	4.90	4918	2414	5809	5965
H	610	1217	5.16	6024	3131	7365	7566
I	634	1313	5.05	6190	3264	7938	8078
J	730	1485	5.44	7095	3880	9337	9401
K	538	1114	4.82	5300	2602	6439	6570
L	630	1290	5.11	6239	3143	7790	7788
M	646	1336	5.10	6180	3310	8009	8158
N	563	1175	4.72	5550	2801	6880	7027
O	579	1186	5.01	5764	2835	7018	7130
P	661	1339	5.41	6488	3459	8423	8377

Table 6-11 (Continued)

(b) 20-Degree Right Rudder Angle Turn (8 knots)

Ship I.D.	Time to Change Heading 90 Degrees seconds	Time to Change Heading 180 Degrees seconds	Speed Remaining in Steady Turn knots	Advance feet	Transfer feet	Tactical Diameter feet	Steady Turning Diameter feet
A							
B	392	842	3.97	3847	1722	4353	4441
C							
D							
E	382	848	3.59	3709	1656	4214	4211
F	400	903	3.44	3854	1712	4339	4409
G	376	824	3.96	3670	1702	4355	4330
H	447	962	3.92	4293	2053	5050	5126
I	483	1083	3.90	4568	2265	5827	5718
J	551	1207	4.22	5174	2661	6755	6534
K	371	949	3.73	3745	1400	4746	4688
L	473	1051	3.92	4541	2115	5610	5419
M	502	1140	3.74	4463	2216	5698	5700
N	424	974	3.47	4039	1874	4935	4832
O	439	977	3.9	4240	1940	5114	5066
P	488	1068	4.14	4650	2278	5922	5723

Table 6-11 (Continued)

(c) 35 Degree Right Rudder Angle Turn (8 knots)

Ship I.D.	Time to Change Heading 90 Degrees seconds	Time to Change Heading 180 Degrees seconds	Speed Remaining in Steady Turn knots	Advance feet	Transfer feet	Tactical Diameter feet	Steady Turning Diameter feet
A							
B	317	761	2.84	2974	1166	3192	3123
C							
D							
E	308	777	2.48	2859	1105	3080	2892
F	322	850	2.23	2967	1137	3150	2956
G	301	722	3.01	2857	1172	3240	3050
H	350	839	2.61	3226	1330	3470	3390
I	388	975	2.64	3500	1500	4236	3871
J	442	1084	2.78	3941	1786	4824	4339
K	347	877	2.66	2986	1150	3412	3218
L	377	952	2.51	3456	1380	3960	3520
M	426	1120	2.28	3334	1397	3920	3708
N	339	927	2.05	3075	1210	3520	3099
O	352	890	2.54	3249	1282	3663	3414
P	385	945	2.74	3504	1470	4145	3708

Table 6-11 (Concluded)

(d) 45 Degree Right Rudder Angle Turn (8 knots)

Ship I.D.	Time to Change Heading 90 Degrees seconds	Time to Change Heading 180 Degrees seconds	Speed Remaining in Steady Turn knots	Advance feet	Transfer feet	Tactical Diameter feet	Steady Turning Diameter feet
A							
B	290	771	2.12	2640	931	2700	2549
C							
D							
E	281	797	1.86	2536	876	2620	2323
F	295	926	1.49	2629	898	2692	2307
G	273	704	2.42	2545	952	2774	2505
H	316	843	1.83	2828	1043	2840	2643
I	354	997	1.86	3112	1232	3579	3051
J	407	1124	1.81	3470	1422	4011	3305
K	324	879	2.14	2628	887	2853	2621
L	344	1014	1.54	3015	1077	3290	2638
M	411	1286	1.40	2896	1046	3170	2823
N	311	1090	1.13	2717	941	3012	2377
O	322	946	1.61	2869	1007	3064	2619
P	350	969	1.82	3075	1144	3427	2796

Table 6-12

Comparison of Numerical Measures from Steady-Turning Maneuvers at an Approach Speed of 16 Knots

(a) 10-Degree Right Rudder Angle Turn

Ship I.D.	Time to Change Heading 90 Degrees seconds	Time to Change Heading 180 Degrees seconds	Speed Remaining in Steady Turn knots	Advance feet	Transfer feet	Tactical Diameter feet	Steady Turning Diameter feet
A							
B	256	507	9.99	5201	2454	5846	6061
C							
D							
E	251	508	9.25	5046	2396	5721	5928
F	263	572	9.02	5248	2482	5977	6191
G	246	498	9.79	4930	2401	5804	5959
H	305	599	10.30	6036	3117	7297	7609
I	317	657	9.99	6205	3252	7933	8124
J	365	743	10.73	7109	3867	9333	9397
K	269	557	9.62	5316	2574	6434	6579
L	283	646	10.17	6034	2510	7785	7873
M	323	668	10.12	6195	3300	8004	8230
N	282	588	9.37	5564	2788	6875	7056
O	290	593	10.01	5780	2822	7012	7176
P	331	670	10.74	6503	3446	8419	8416

Table 6-12 (Continued)

(b) 20 Degree Right Rudder Angle Turn (16 knots)

Ship I.D.	Time to Change Heading 90 Degrees seconds	Time to Change Heading 180 Degrees seconds	Speed Remaining in Steady Turn knots	Advance feet	Transfer feet	Tactical Diameter feet	Steady Turning Diameter feet
A							
B	197	422	7.94	3889	1710	4343	4441
C							
D							
E	192	425	7.18	3752	1646	4213	4213
F	201	453	6.90	3898	1702	4338	4393
G	189	413	7.92	3708	1689	4354	4333
H	225	482	7.84	4334	2043	5048	5726
I	243	543	7.74	4611	2256	5826	5740
J	277	605	8.31	5218	2652	6369	6565
K	187	475	7.46	3788	1391	4740	4688
L	211	517	7.83	4391	1665	5590	5412
M	253	571	7.46	4508	2208	5698	5684
N	213	488	6.91	4082	1866	4935	4811
O	221	500	7.79	4284	1930	5113	5094
P	245	536	8.24	4694	2269	5921	5716

Table 6-12 (Continued)

(c) 35 Degree Right Rudder Angle Turn (16 knots)

Ship I.D.	Time to Change Heading 90 Degrees seconds	Time to Change Heading 180 Degrees seconds	Speed Remaining in Steady Turn knots	Advance feet	Transfer feet	Tactical Diameter feet	Steady Turning Diameter feet
A							
B	161	384	5.68	3062	1159	3196	3130
C							
D							
E	157	392	4.97	2947	1101	3087	2889
F	164	428	4.47	3054	1134	3160	2973
G	153	365	6.02	2939	1166	3245	3060
H	178	423	5.22	3312	1324	3481	3379
I	197	491	5.26	3603	1531	4245	3871
J	224	546	5.49	4032	1783	4831	4337
K	177	448	5.32	3080	1148	3420	3217
L	191	479	5.00	3547	1376	3960	3519
M	216	564	4.54	3429	1397	3928	3692
N	173	467	4.08	3170	1211	3534	3097
O	179	448	5.07	3335	1285	3668	3395
P	195	476	5.47	3595	1467	4152	3702

Table 6-12 (Concluded)

(d) 45 Degree Right Rudder Angle Turn (16 knots)

Ship I.D.	Time to Change Heading 90 Degrees seconds	Time to Change Heading 180 Degrees seconds	Speed Remaining in Steady Turn knots	Advance feet	Transfer feet	Tactical Diameter feet	Steady Turning Diameter feet
A							
B	149	390	4.24	2757	929	2712	2541
C							
D							
E	144	403	3.72	2655	875	2635	2326
F	151	468	2.99	2748	898	2708	2343
G	140	357	4.83	2661	949	2788	2505
H	162	426	3.66	2946	1041	2852	2643
I	181	504	3.68	3232	1232	3595	3005
J	207	567	3.55	3593	1423	4026	3241
K	166	444	4.28	2756	891	2867	2613
L	153	513	3.06	2997	833	3306	2598
M	210	649	2.78	3029	1052	3188	2788
N	160	551	2.22	2841	943	3034	2273
O	165	478	3.21	2989	1008	3080	2589
P	179	490	3.60	3200	1146	3444	2765

Table 6-13

Comparison of Numerical Measures from Stopping Maneuvers Initiated from a Speed of 16 Knots

Ship I.D.	Undisturbed				Controlled				±35 deg Fishtailing			
	Head Reach feet	Side Reach feet	Time to Reach Zero Speed seconds	Heading Change degrees	Head Reach feet	Side Reach feet	Time to Reach Zero Speed seconds	Heading Change degrees	Head Reach feet	Side Reach feet	Time to Reach Zero Speed seconds	Heading Change degrees
E	7833	-3065	611	-181	17070	0	1450	0	5800	3460	550	214
H	8466	-2880	596	-200	20206	0	1746	0	6810	3287	556	216
L	8827	-3862	759	-172	16613	0	1267	0	7551	4160	748	184

CHAPTER 7
SHALLOW WATER EFFECTS

The primary objectives of the shallow water investigations were to provide systematic resistance, propulsion, and maneuvering data for large full-form ships, using the MARAD Series models as a basis. Another objective of the program was to provide complete sets of shallow water hydrodynamic coefficients for mathematical models suitable for use with simulator facilities.

The program was initiated with the selection of four MARAD Series models. Three of these models, with C_B of 0.85 and L/B of 5.00 in common, represent variations in B/T = 3.00, 3.75, and 4.00. The fourth, with C_B = 0.85, B/T = 3.00,and L/B = 6.50, provided some indication of the effect of L/B variation on shallow water characteristics. The shallow water tests of the four selected models were conducted with the LAHPMM system, described in Appendix A.

A substantial portion of the shallow water program was devoted to computer simulation studies using the mathematical models derived from the PMM tests. These studies consisted principally of definitive maneuvers of the open loop type, such as spirals, zigzags, and turns, to obtain numerical measures of inherent directional stability and response to controls of the ship involved. A full load displacement of 200,000 tons was chosen for these studies in lieu of the 350,000 ton displacement used for the deep water investigation on the assumption that such ships are more representative of the bulk type vessels that would use U.S. ports. Simulation studies were conducted for three values of water depth/draft, H/T = 2.5, 1.5, and 1.2. Simulation studies were also performed to compare stopping characteristics in deep water and in shallow water of H/T = 1.2.

The data derived from the shallow water tests and computer simulation studies are presented herein in a format similar to that used for the deep water investigations. Corresponding deep

water data previously obtained for the four configurations, which were reworked for the 200,000 ton displacement, are also included to serve both as a reference condition and a basis for comparison.

Special Considerations and Problem Areas

The term "shallow water" is defined in this text as the depth below which the maneuvering characteristics of a given ship differ significantly from these characteristics in water of unlimited depth. For most ships, shallow water is defined as depth-to-draft ratios, H/T, of about 3.5 or less, with the most pronounced changes taking place at H/T values below 1.5. Therefore, depending on ship size and hull proportions, serious problems associated with maneuverability can extend to harbors and shallow water approaches as well as deep water ports where the water depth varies from about 100 to 120 feet. Unless mentioned otherwise, the term "shallow water" is taken throughout this chapter to apply to the case of unrestricted width, i.e., where the effects of the presence of banks, such as in a channel or canal, are considered to be negligible.

The greatest concern is the case of the modern bulk carrier or tanker of large size and hull proportions which may cause difficulty in operating safely in areas of restricted water depth. Of particular interest in the U.S. are the vessels intended for restricted draft service where the emphasis is on full-form, wide beam, ships with B/T values above 3.00.

At the time of the initial presentation of these results in 1977, Reference 3, full scale trial shallow water data were relatively sparse. Since then a significant number of test results and analytical studies of shallow water effects have been published, including the model tests and full scale trials of the large tanker ESSO OSAKA, Reference 29. For complete references on this subject, publications of the Ship Maneuvering Committee of the International Towing Tank Conference (ITTC) should be consulted.

As in the deep water investigation, the computer simulation approach was selected as the best, and perhaps the only feasible means for providing systematic data on shallow water maneuvering characteristics. This approach was described in detail in Chapter 6.

The requirement for sufficiently large models as a means for producing reliable predictions of resistance, propulsion, and maneuvering characteristics, especially for large full-form merchant ship types, was discussed earlier in connection with the deep water investigations. This requirement is even more important for shallow water model tests for a variety of both hydrodynamic and practical reasons including the following:

1) The Reynolds number, R_N, of the model is much lower in the range of interest than in the deep water case due to the low speeds being simulated. This, in itself, can lead to more pronounced scale effects with small models and may have a noticable effect even on the large series models 20 feet to 27.5 feet in length.

2) Tests with small models are likely to suffer from strong viscous scale effects associated with small underkeel clearances particularly at H/T values of less than 1.4. These scale effects tend to exaggerate the rate at which the various hydrodynamic force and moment coefficients increase with further reduction of clearance, as shown in Reference 30. This is due mainly to the fact that the ratio of boundary layer thickness to underkeel clearance becomes much higher for any given H/T and reaches a critical value of unity sooner in the case of the smaller models.

3) The facilities used for shallow water testing of small models must be built and maintained with relatively greater precision to achieve uniformity of the scaled water depth, particularly to satisfy the requirements of the lowest values of H/T of interest. Much closer tolerances on level and smoothness of the tank bottom as well as on the means for regulating and monitoring water depth are required.

4) The measurement problem is relatively more difficult for small models due to the smaller forces involved in any given condition combined with the increased sensitivity of these forces to the problems listed under Items 1, 2, and 3.

The requirement for simulating ship propulsion point is especially important in the case of large single screw vessels where the propeller loading coefficient for even a relatively large model can be at least twice that of the corresponding full scale ship. It has been amply demonstrated in this connection that both the inherent (controls fixed) directional stability and the control effectiveness of single screw full-form ships in deep water are influenced by the velocity of the slipstream acting over the rudder, as shown in Chapter 6. It is reasonable to conclude, therefore, that these characteristics would be affected at least to an equal extent in the shallow water case. The PMM test technique affords the opportunity to satisfy the ship propulsion point requirement.

Resistance and propulsion tests were conducted as a necessary prerequisite to the deep water PMM tests, to establish the reference ship propulsion point. For the shallow water cases, such tests, at least of limited scope, were considered even more essential in support of PMM tests since experimental data pertaining to the effects of shallow water on the resistance, and especially the propulsion characteristics of single screw full-form ships, are rare. In conducting the resistance tests, it becomes necessary to contend with the problem of restricted basin width which exists in nearly all major facilities where captive model tests are conducted. Even where the effects of the basin walls on resistance in deep water are negligible, they can become progressively more pronounced, especially at H/T values decreasing from 2.5. This is demonstrated in Reference 31 which contains the results from tests of each of a number of small models in which basin width was systematically varied for each of several depths, including shallow water depths in the range of interest.

In view of the foregoing, a procedure was devised for correcting the model resistance measured in a basin of finite width to that which would be obtained in unrestricted shallow water of the same depth. The procedure involves the use of two existing methods: that due to Schlichting's method, Reference 32, for the unrestricted shallow water case and Landweber's method, Reference 33, for the restricted channel case. These methods and their application are further described in References 34 and 35. Both methods use measured model deep water resistance as a means for estimating resistance or loss of speed for the confined case, and are based on the following two assumptions:

1) The theoretical assumption that the wavemaking resistance at "Schlichting's intermediate speed", v_I, is equal to the wavemaking resistance at a corresponding speed in deep water, v_∞. The relationship between v_I and v_∞ is given from wave theory by the formula

$$\frac{v_I}{v_\infty} = \left(\tanh \frac{gh}{v_\infty^2} \right)^{1/2} \qquad [24]$$

where H is the water depth.

2) The empirical assumption that the change in displacement flow around the model or ship hull necessitates a correction to v_I to give the speed, v_H, relative to shallow water or channel. The relationship is derived from systematic model tests and is given as an empirical curve in the form

$$\frac{v_H}{v_I} = \phi \frac{\sqrt{A_X}}{H} \quad \text{(shallow water)} \qquad [25]$$

$$\frac{v_H}{v_I} = \phi \frac{\sqrt{A_X}}{R_H} \quad \text{(restricted channel)} \qquad [26]$$

where the hydraulic radius is defined as

$$R_H = (W \cdot H - A_X)(W+2H+p)$$

and A_X is the maximum cross-sectional area of the hull,
W is the width of the basin or channel, and
p is the wetted perimeter of the hull at maximum section.

For Froude numbers based on depth, $F_H = v/\sqrt{gH}$, of less than 0.5, which exceeds the range of interest in the subject PMM tests, the ratio of v_I/v_∞ is about equal to unity. Therefore, only the empirical relationships of Item 2 have to be taken into account and can be restated as follows:

$$\frac{v_H}{v_\infty} = \phi \frac{\sqrt{A_X}}{H} \quad \text{(shallow water)} \qquad [25a]$$

or

$$\frac{v_H}{v_\infty} = \phi \frac{\sqrt{A_X}}{H} \quad \text{(restricted channel)} \qquad [26a]$$

This also means the added resistance due to the bottom and walls at F_N less than 0.5 is essentially caused by an increase in viscous resistance (frictional and form resistance) as opposed to wavemaking resistance.

The correction procedure is based on the premise that the total measured model resistance at any given shallow water depth in a basin of rectangular cross-section includes an incremental increase in resistance due separately to the presence of walls. The magnitude of this incremental increase depends on the proximity of the walls and is assumed to be equal to the difference between restricted channel resistance and shallow water resistance calculated from the relationships of Equations [26a] and [25a], respectively, using the corresponding measured deep water resistance for the same model as a base. In terms of

the resistance coefficients, the correction is applied as follows:

$$C_{R1} = C_{T1} - C_{Fm} \qquad [27a]$$

$$\Delta C_R = C_{T3} - C_{T2} \qquad [27b]$$

$$\text{net } C_R = C_{R1} - \Delta C_R \qquad [27c]$$

where the subscripts 1, 2, and 3 denote measured, calculated shallow water, and calculated restricted channel values, respectively, and net C_R is the desired value for the case of unrestricted shallow water. The values of C_{T3} and C_{T2} are derived using the faired deep water C_R values given earlier for each series model. Over the range of F_N of interest to the shallow water PMM tests, the deep water C_R is constant. Thus, deep water C_{Tm} is obtained by adding the constant deep water C_R to the same values of C_{Fm} used in Equation [27a] which are based on the water temperatures in the basin at the time of shallow water tests. The net C_R is also treated as a constant. The value is determined by giving most weight to the net C_R data closest to the F_N corresponding to a design speed of 8.0 knots for the 200,000 ton full scale ship.

Once the net C_R has been determined, the procedure for obtaining full scale values of total resistance coefficient, C_{Ts}, and effective horsepower is the same as that given for the deep water case in Chapter 5, namely

$$C_{Ts} = C_{Ti} = \text{net } C_R + C_{Fs} + C_A = \frac{R_{Ts}}{\frac{\rho}{2} Sv^2} \qquad [28a]$$

$$EHP = \frac{R_{Ts}\, v}{550} = \frac{\frac{\rho}{2} SV_K^3}{550} (1.689)^3 \qquad [28b]$$

where C_{Ti} corresponding to 8.0 knots for the 200,000 ton displacement is used for the reference ship propulsion point in

the propulsion and PMM tests representing the case of unrestricted shallow water.

Taking the case of model E as an example, the correction due to restricted width of the basin at the shallowest depth (H/T = 1.2), amounts to about 45 and 60 percent in terms of the corrected, infinite width, values of model C_{Tm} and full scale C_{Ts}, respectively. The impact of this correction on the results of the PMM tests conducted at ship propulsion point is discussed further in the following paragraphs.

The shallow water captive model tests were designed with a view toward producing complete, systematic sets of hydrodynamic coefficients sufficiently comprehensive to simulate ahead maneuvers that the ship would perform in shallow water of a given depth. This includes all of the nonlinear and coupling coefficients not previously obtained in shallow water PMM tests by other investigators. See References 36 and 37. It also includes a class of PMM tests described in Reference 38, i.e., the overload and underload PMM tests discussed in Chapter 5. These tests are especially important for turning and stopping maneuvers, which involve large losses or changes in speed. In the case of the shallow water PMM tests, η is equal to 1.0 at the ship propulsion point for steady speed in unrestricted shallow water, with correction applied to compensate for the effect of basin walls.

In performing the shallow water PMM tests, all of the standard deep water test procedures described earlier were rigorously followed. As in the deep water case, strict attention was paid to the oscillatory modes of the PMM tests, to use frequencies low enough to avoid problems of tank resonance and other free surface effects related principally to test technique. For the shallow water case, special care was exercised to stay well within the range in which the lateral added mass and damping coefficients were sensibly constant or independent of frequency. Above this range, the values may vary drastically with frequency, especially at H/T values as low as

1.2, as indicated by theoretical calculations and the sparse experimental data available, as discussed in Reference 30. Fortunately, the frequency range associated with the shallow water maneuvers of interest is low enough to justify the use of these constant coefficients in computer simulation predictions.

These restrictions on frequency range can raise several problems when conducting shallow water tests with a conventional, low amplitude system. For example, at the very low frequency end where linear coefficients are determined, the model forces are small and difficult to measure accurately even with a relatively large model. However, toward the high frequency end where it is desired to obtain nonlinear damping coefficients, the measurements are complicated by spurious effects such as those due to tank resonance and the frequency dependence previously mentioned. The use of the large amplitude PMM circumvents these problems because the entire test can be conducted at one or more very low frequencies and accurate force measurements can be obtained in both the linear and nonlinear range by varying amplitude.

Another potential problem encountered in shallow water PMM testing is concerned with the effect of restricted basin width on the lateral forces and moments associated with the various modes of motion. These effects can be divided into two categories: direct effects caused by changes to the flow about the model hull and indirect effects due to increased propeller loading, and, consequently, increased velocity of flow over the rudder. The indirect effects on the lateral forces and moments are due to increases in resistance, attributed to the presence of the walls, which must be overcome by the delivered propeller force during the test, whether conducted at model or ship propulsion point. These indirect forces and moments, as well as the longitudinal forces, can be more accurately represented by conducting the PMM test with a reference $\eta = 1.0$ corrected to correspond to the unrestricted shallow water case, as discussed earlier.

At the time of the tests the only available systematic PMM test data on the effects of finite channel width on the major dynamic stability derivatives were those given in Reference 36 for the C4-S-1a "Mariner" type ship and a tanker. The data were presented in the form of tables and graphs showing the variation of pertinent derivatives with width-to-model beam ratio, W/B, for each of three H/T values. The data showed that the absolute values of the various derivatives always tend to increase over the unrestricted shallow water values with decrease in W/B. The rate of increase becomes quite pronounced in the range of W/B of 4.0 down to 3.0, particularly at H/T = 1.2. In general, however, the increases due to restricted wall width become relatively small at W/B above about 5.5 to 6.0, even at H/T = 1.2. For example, the ratio of "added mass" derivative $Y_{\dot{v}}'$ at W/B = 6.0 to that at W/B = ∞ is shown to be less than 1.05, or less than 5 percent higher than the unrestricted case, for both the "Mariner" and tanker models. Similarly, the "added mass moment of inertia" deriviative, $N_{\dot{r}}'$, increases by less than 5 percent for both models at H/T values of 1.9 and 1.5.

For the static derivative Y_v' at W/B = 6.0, the increase due to restricted width shown for the "Mariner" model is about 2 to 5 percent, and about 15 percent for the tanker, over a range of H/T values of 1.9 to 1.3. For the static derivative N_v' at W/B = 6.0, the increases due to restricted width are between +5 and -1 percent for both models over a range of H/T values between 1.9 and 1.2.

For the rotary derivative Y_r' at W/B = 6.0, the increase due to restricted width is shown to be between 10 and 25 percent for the "Mariner" model and between 15 and 50 percent for the tanker model over ranges of 1.9 to 1.3 and 1.9 to 1.2, respectively. For the corresponding rotary derivative, N_r', at W/B = 6.0, the increase due to restricted width is shown to be between 5 and 11 percent for the "Mariner" and between 2 and 18 percent for the tanker. In interpreting these trends it should be noted that the pure rotary forces are relatively small and

difficult to determine accurately since they are measured in conjunction with the mass.

In addition to the direct forces due to restricted width, the static and rotary derivatives are further influenced by the indirect forces due to increased model propeller loading coefficient, as indicated previously. Based on the results of the shallow water PMM tests of a typical MARAD Series model, the indirect effects at W/B = 6.3 and H/T = 1.2, due solely to the presence of the wall, would result in an increase in Y_v', Y_r', and N_r' of about 3, 7, and 5 percent, respectively, and a decrease in N_v' of about 6 percent. The PMM tests of Reference 36 were all conducted at model propulsion point corresponding to each case of combined depth and width. Consequently, the values of the static and rotary derivatives would include the contribution of the indirect effects due naturally to the increased propeller loading caused by proximity to both bottom and wall, at model scale. Thus, the above percentages for increase or decrease in the values of the static and rotary derivative due to indirect effects appear to be reasonable, at least insofar as direction is concerned. For example, by applying these percentages to the case of the tanker model at W/B = 6.0 and H/T = 1.2, the values for percentage increase in N_v' and N_r', assumed to be due to direct wall effects, would become about 5 and 13 percent instead of -1 and 18 percent, respectively. However, the magnitudes of the direct wall effects on Y_v' and Y_r', as well as on N_v' and N_r' derived from Reference 36 must still remain in question due to inability to account for other uncertainties such as scale effects and testing technique problems associated with the use of small models.

In view of the foregoing, no corrections were made to the lateral force and moment coefficients to account for possible direct wall effects due to the restricted width of the HSMB. For the size of the models used in the HSMB PMM tests, W/B was equal to about 6.3 for three of the models and about 5.5 for the

fourth. It is believed, therefore, that if such corrections were made to the acceleration coefficients they would amount to a maximum of 5 percent for H/T = 1.2 and would probably be negligible at H/T larger than 1.5. Furthermore, based on the use of large models and associated techniques, the direct wall effects on the static and rotary coefficients are also believed to be relatively small even at H/T = 1.2.

Considerable emphasis was placed on making allowances for indirect wall effects both in the conduct of PMM tests and analysis of data. Although the indirect wall effects on the static and rotary coefficients cited previously do not appear to be very large, they can become very significant when combined with the corresponding indirect effects due to the difference between model and ship propulsion point, particularly for the case of large single screw full-form ships. Furthermore, the indirect wall effects on the control coefficients $Y_{\delta r}'$ and $N_{\delta r}'$ are relatively large whereas the direct wall affects on these control coefficients can be assumed to be negligible. For example, on the typical MARAD Series model at H/T = 1.2, the indirect wall effects increased $Y_{\delta r}'$ and $N_{\delta r}'$ more than 50 percent, compared with the values for ship propulsion point in unrestricted shallow water. Finally, the indirect wall effects at η = 1.0 on the aforementioned lateral force and moment coefficients, as well as on the axial force coefficients, directly affect the results of the overload and underload PMM tests. Failure to compensate for these indirect wall effects during the course of the tests or in subsequent data analysis would result also in the η-dependent coefficients becoming too large. As a consequence, the resulting mathematical model would be less representative of the unrestricted shallow water case, particularly in maneuvers such as tight turns where large losses of speed are involved.

Test Program and Procedures

The shallow water test program was summarized in Table 3-7. The program was based on the use of four existing series models providing three values of B/T and two values of L/B, for one value of C_B = 0.85. In the interests of economy, shallow water tests were carried out at three water depths for one model (model E) and two water depths for three models (models K, L, and H). With the availability of the corresponding deep water test data, it was expected that the desired mathematical models could be developed for the entire depth range with reasonable accuracy for all four models.

The program consisted primarily of the PMM tests necessary to produce complete mathematical models for computer simulation studies of shallow water maneuvering characteristics of the full scale, 200,000 ton displacement ship configurations. The resistance and propulsion tests were of limited scope, sufficient to establish ship propulsion point and otherwise augment the mathematical model. Included were measurements of hull sinkage and trim as a function of F_N or ship speed, which is critical to shallow water operation, particularly at H/T values of 1.2 and below.

Table 7-1 is a summary of the specific shallow water test conditions and other pertinent data for each of the four MARAD Series models. The information in the table is presented in terms of model and full scale dimensions as well as in nondimensional form. Included in the table are values of the loading coefficient $C_{Ti} = C_{Ts}$ and reciprocal of apparent advance coefficient, $1/J_a$, which correspond to ship propulsion point η = 1.0 of the 200,000 ton full scale ships at a speed of 8.0 knots in unrestricted water of the specified depth. These values were derived from the resistance and propulsion tests and were used for the reference PMM tests. The values of $1/J_a$ are those obtained for the stock propeller and, therefore, may differ from those given later for the optimum propeller. In the interest of completeness, the values corresponding to H/T = 2.5 are also included for the three models that were not tested at

this condition. Also given are the corresponding values of $C_{Ti} = C_{Ts}$ and $1/J_a$ for the deep water case of all four models, for the 200,000 ton ship at a speed of 8.0 knots.

Model Characteristics

MARAD Series models E, K, L, and H, were used in the subject shallow water experiments. The principal geometric characteristics of the four models, corresponding to the full load condition, are repeated in Table 7-2 at both model scale and 200,000 ton displacement full scale. Models E, K, and L represent B/T variations of 3.00, 3.75, and 4.50 with L/B = 5.00 and C_B = 0.85 held constant. Model L represents hull proportions more nearly in the range of existing ships for which at least some shallow water data are available. Combined with model E, two values of L/B = 5.00 and 6.50, with C_B = 0.85 and B/T = 3.00 held constant, were investigated.

Each of the models was equipped with the same standard rudder and propeller used in the corresponding deep water test. The same standard rudder-propeller combination was used for models E and H (with B/T constant), but the combination differed among models E, K, and L (with B/T varied), as indicated by the designations and geometric characteristics given in Table 7-2.

All of the models were relatively large, ranging form 20 to 26 feet in length. Models E, H, and K all had breadths of 4.00 feet and the model L breadth was 4.58 feet.

The test apparatus and procedures used for the shallow water tests are described in Appendix A.

Resistance and Propulsion Data

The shallow water resistance and propulsion tests were conducted primarily to support the LAHPMM tests, to establish the ship propulsion point for the case of unrestricted shallow water. The data were reduced in accordance with the standard deep water procedures. The ITTC 1957 Line and a correlation allowance C_A = 0.00015 were used for extrapolation from model

to ship size. The resistance data were corrected to compensate for the effect of the basin walls. No corrections were made in the propulsion data to account for possible wall effects on wake fraction, w, and thrust deduction, t, which are believed to be small.

Figure 7-1 presents typical curves of nondimensional residuary resistance coefficient, C_R, versus Froude number, F_N, for depth-to-draft ratio H/T values of ∞, 2.5, 1.5, and 1.2 obtained for Model E. At each water depth, C_R remains constant up to an F_N value of at least 0.10, which exceeds the F_N value corresponding to a speed of 8 knots for the 200,000 ton displacement ships. The constant C_R was used in each case to obtain the total resistance coefficient, C_{TS}, for the corresponding full scale ship at a speed of 8 knots, the ship propulsion point.

Figure 7-2 presents curves showing typical variation of hull efficiency factors with propeller loading coefficient, C_{Ti}', at various H/T values, obtained from the overload and underload propulsion tests for model E. Within the limits of test accuracy, all of the curves are straight lines, i.e., are independent of H/T. Accordingly, all of the hull efficiency factors 1-t, 1-w, e_h and e_{rr} for each full scale ship at each water depth were treated as constants.

The constant C_R values for full scale versions of the four individual series models tested are summarized in Table 7-3. The resistance and propulsion characteristics corresponding to the 200,000 ton displacement ship at a speed of 8 knots are summarized in Table 7-4. The values in Table 7-3, including the values obtained from Chapter 5, were used to prepare the curves showing the variation of constant C_R with H/T for each of the four ships presented in Figures 7-3 through 7-6. The values for H/T = 2.5 given in Table 7-3 for ship versions of models K, L, and H are interpolated from these curves. Similarly, the values from Table 7-4 were used to prepare the curves showing the variation of hull efficiency factors with H/T, presented for each

200,000 ton displacement ship in Figures 7-7 through 7-10. Again, the values for H/T = 2.5 given in Table 7-4 for full scale ships K, L, and H are based on interpolations. The values in Tables 7-3 and 7-4 were also used to prepare curves showing the variation of C_R and hull efficiency factors with B/T given in Figures 7-11 and 7-12, respectively.

Effect of Water Depth Variation

Figure 7-3 shows that, for the 200,000 ton displacement ship E, C_R increases gradually with decrease in H/T down to an H/T of about 3.0, but then increases at a progressively more rapid rate until the increase becomes fairly pronounced between H/T = 1.5 and 1.2. The C_R curves for the other three models in Figures 7-4, 7-5, and 7-6 show similar trends. However, the rate of increase begins earlier with the higher B/T ships, as seen by comparing Figure 7-3 (ship E) with Figure 7-5 (ship L), due to the fact that, for a given H/T, the B/T = 4.5 ship is closer to the bottom than the B/T = 3.00 ship.

Figure 7-7 shows that for a typical full scale ship, the wake fraction, w, increases with decrease in H/T, gradually at first, but then with pronounced changes in the vicinity of H/T = 1.5. However, the thrust deduction, t, does not change much over the entire range of H/T values. The net effect is that the hull efficiency, e_h, increases substantially with H/T. The relative rotative efficiency, e_{rr}, is fairly constant over the H/T range. The same general trends are exhibited for the other three ships, as seen in Figures 7-8, 7-9, and 7-10.

Effect of B/T Variation

Figure 7-11 shows the effect of B/T variation on C_R in shallow water at H/T = 1.2 for 200,000 tons displacement, for L/B = 5.00 and C_B = 0.85. C_R at this water depth increases substantially with increase in B/T. This is expected since the full scale ships having higher B/T values are closer to the bottom at the same H/T. At a speed of 8 knots in shallow water

at H/T = 1.2, ship L (B/T = 4.50) will have about a 40 percent higher EHP than ship E (B/T = 3.00).

Figure 7-12 shows the effect of B/T variation on the hull efficiency factors in shallow water at H/T = 1.2. The values of 1-w and 1-t are quite close at B/T values of 3.00 and 4.50, but are somewhat higher at B/T = 3.75. A similar trend is shown for the deep water case in Chapter 5.

Effect of L/B Variation

The effect of L/B variation on C_R in shallow water at H/T = 1.2 for 200,000 tons displacement, with B/T = 3.00 and C_B = 0.85, is indicated by comparing the data given for ships E and H in Table 7-3. C_R tends to decrease quite substantially with increase in L/B between 5.00 and 6.50. At a speed of 8 knots in shallow water, ship H (L/B = 6.50) will have about a 17 percent lower EHP than ship E (L/B = 5.00).

The effect of L/B variation on the hull efficiency factors in shallow water at H/T = 1.2 can be seen by comparing the values for ships E and H given in Table 7-4. Within the limits of experimental accuracy, there does not seem to be any definite trend in 1-w and 1-t with variation in L/B. In the deep water case, 1-w tends to increase and 1-t tends to decrease, resulting in a much lower e_h value between L/B = 5.00 (ship E) to L/B = 6.50 (ship H).

Sinkage and Trim Characteristics

The sinkage and trim of large full-form vessels are very important in the shallow water condition, particularly at H/T below 1.5, resulting in significant effect on the hydrodynamic coefficients which govern the maneuverability characteristics and can set a practical limit on the safe operating speed. Accordingly, trim and sinkage measurements were taken during the shallow water tests and the data are presented for each of the four MARAD Series 200,000 ton ships in Figures 7-13 through 7-13.

In parts (a) and (b) of each figure, the sinkage and trim are plotted in nondimensional coefficient form for estimating the characteristics of geometrically similar vessels of any size and for comparisons with theory. The coefficients, defined on the figure, are based on depth Froude number, F_H, which tends to collapse the data for the various shallow water depths. Parts (c) and (d) are dimensional plots of sinkage at bow and stern, respectively, for the case of the 200,000 ton displacement. The dimensional sinkage data can be used in conjunction with the corresponding water depth data in Table 7-1 to determine clearance to the bottom for the practical range of speeds of the full scale ship.

Directional Stability and Control

The systematic data derived from the shallow water PMM tests are presented and analyzed here on the basis of linearized equations of motion, in a manner similar to that performed for the deep water case in Chapter 6. The nondimensional data presented apply to the full scale 200,000 ton displacement ship operating at 8 knots in full load condition. However, these data can also be used in conjunction with other data presented to closely estimate corresponding values for geometrically similar ships of different size or speed. The data have been corrected to correspond to ship propulsion point in shallow water of unrestricted expanse.

The applicable linearized differential equations of motion for the yaw-sway degrees of freedom were presented in Chapter 6. The value of the nondimensional stability and control derivatives derived from the shallow water PMM tests of Models E, K, L, and H are presented separately for each water depth condition in Tables 7-5 through 7-8, respectively. The value of $1/J_a$ for ship propulsion point corresponding to $\eta = 1.0$ can be obtained for each depth condition from Table 7-1. Included in the tables are the values of the deep water derivatives taken from Chapter 6. These derivatives have been adjusted to correspond to the case of

200,000 tons displacement and 8.0 knots speed. In most cases, the adjustment required was negligible and was not made. For model E, which is used as a reference throughout this chapter, the derivative values for all three shallow water depth conditions were obtained directly from separate PMM tests. For models K, L, and H, the values corresponding to H/T = 2.5 were interpolated from cross-plots (for H/T = 1.2, 1.5, and the deep water values) using the case of model E as the guide.

Tables 7-5 through 7-8 also include the values of the dynamic stability indices and other pertinent parameters resulting from the analyses discussed in the following sections. For ease of comparison, all of the data as well as the derivative values for each shallow water depth condition are expressed in separate columns as ratios to the corresponding deep water values.

The principal stability and control derivatives and dynamic stability indices are summarized in Table 7-9 to provide a direct comparison for deep water and shallow water at H/T = 1.2. Table 7-10 presents the incremental contributions to the nondimensional stability and control derivatives of the 200,000 ton displacement ships due to change in propeller loading coefficient resulting in a change in $1/J_a$. It should be noted that for a given ship the $1/J_a$ value corresponding to a reference $\eta = 1.0$ differs for each of the shallow water depths, as shown in Table 7-1. The data in Table 7-10 can be used directly to estimate the stability derivatives and, in turn, the dynamic stability indices, for full scale vessels of sizes significantly different from 200,000 tons displacement, using procedures similar to those given for the deep water case in Chapter 6.

Effect of Water Depth Variation

The data in Tables 7-5 through 7-8 have been used to prepare graphs which show the variation with H/T of the dynamic stability derivatives and indices for a given configuration. The graphs showing the variation of the nondimensional static, rotary, and

acceleration derivatives with H/T are presented individually for 200,000 ton displacement ships E, K, L, and H in Figures 7-17 through 7-20, respectively. Similarly, graphs showing the variation of the dynamic stability indices with H/T are presented in Figures 7-21 through 7-24, respectively. These graphs can be used to determine the values of the derivatives and stability indices for intermediate water depths within the range of discrete values shown in the tables. As noted previously, the graphs have been used to supply the H/T = 2.5 values for models K, L, and H, which were not obtained directly from the test program. In general, the graphs show that the values of the various derivatives and indices do not begin to change significantly until H/T is decreased to about 3.0. This suggests that the tabulated deep water values can be used with reasonably good accuracy when the water depth is such as to exceed H/T = 3.0. This also appears to be true of the mathematical models used for computer simulation, as discussed later. The specific effects of H/T variation on the stability derivatives and dynamic stability indices, respectively, are discussed in order in the following paragraphs.

Insofar as all of the nondimensional stability derivatives are concerned, the most dramatic effects of H/T variation take place at H/T values below about 2.0 for the cases of the four models investigated. The characteristic trend in this region, shown by Figures 7-17 through 7-20, is for the absolute values of all major derivatives to increase at a progressively greater rate until a relatively high value is reached at H/T = 1.2.

The static derivatives Y_v' and N_v' show the most pronounced increases between deep water and shallow water of H/T = 1.2. For example, the Y_v' values at H/T = 1.2 range from about 5.6 (model H) to 10.5 (model L) times larger than the comparative deep water values. The increases in N_v' are somewhat smaller than those for Y_v' and range from about 4.0 to 8.3 times the deep water values for the same two models, respectively. The relatively smaller rate of increase in the

N_v' values can be attributed to the shift in static force center from deep to shallow water of H/T = 1.2, as indicated by the static lever, ℓ_v', values in Table 7-6. For example, ℓ_v' changes from about 0.57 to 0.41 ship lengths (model H) and from about 0.48 to 0.38 ship lengths (model L) forward of the LCG from deep to shallow water of H/T = 1.2. In both cases, the value of ℓ_v' becomes smaller, i.e., the static force center moves closer to the LCG, which accounts for the increase in N_v' being relatively smaller than that of Y_v'.

The rotary derivatives Y_r' and N_r' show rates of increase with H/T which are considerably smaller than those for the static derivatives. For example, the Y_r' values at H/T = 1.2 range from about 2.3 (model E) to 4.8 (model L) times larger than the comparative deep water values. As for the statics, the increases in N_r' are also somewhat smaller than the values for Y_r' and range from about 2.0 to 2.5 times the deep water values for the same two models, respectively. Since Y_r' is always positive, an increase in Y_r' means a decrease in the negative value of $(Y_r'-m)$. Together with the increased negative value of N_r', this results in a substantial increase, or movement of the rotary force center forward, between the cases of deep water and H/T = 1.2. For example, the rotary force center moves from about 0.27 to 0.90 ship lengths forward of LCG on model E and from about 0.2 to 2.2 ship lengths forward of LCG on model L. This is further discussed later in connection with the use of the dynamic stability lever.

The values of the acceleration, or added mass, derivative, $Y_{\dot{v}}'$, show rate of increase with H/T which are also quite substantial. For example, the $Y_{\dot{v}}'$ values at H/T = 1.2 range from about 4.7 (model E) to 5.1 (model L) times larger than the comparative deep water values. However, the increases in the acceleration, or added moment of inertia derivative, $N_{\dot{r}}'$, are relatively much smaller. The values of $N_{\dot{r}}'$ at H/T = 1.2 range from about 1.9 (model E) to 2.4 (model L) times the deep water values. The relationship between $N_{\dot{r}}'$ and $Y_{\dot{v}}'$ at any given

water depth can be expressed as follows:

$$k_{zH}' = \sqrt{\frac{N_{\dot{r}}'}{Y_{\dot{v}}'}} \qquad [29]$$

where k_{zH} is considered effectively as a "hydrodynamic radius of gyration" about the z-axis analogous to the gyradius k_z'. It is interesting to note that, for the deep water case, the value of k_{zH}' is about 0.25 for all four of the series models and is equal to the constant value of k_z' used to establish full scale I_z' in Chapter 6. At H/T = 1.2, the k_{zH}' values are 0.163, 0.160, 0.169, and 0.155 for models E, K, L, and H, respectively, for an average of about 0.16. Thus, it appears that the relationship of Equation [29] can be very useful both in analyzing the data from shallow water PMM tests and in making estimates of acceleration derivatives for other configurations.

The acceleration derivatives $N_{\dot{v}}'$ and $Y_{\dot{r}}'$ are very small in magnitude and, therefore, the ratios to the deep water values given in the tables are not meaningful. For example, since the deep water value for $N_{\dot{v}}'$ (model E) is only 0.00002, the ratio at 1.2 becomes 100.5. Although the values themselves are small, they show a consistent trend with variation in H/T. This can be seen from the quantity $N_{\dot{v}}'/Y_{\dot{v}}'$ which can be considered as a measure of the location of the center of hydrodynamic added mass. For all of the models, the center of added mass tends to move aft with decrease in H/T with the greatest changes taking place at H/T between 1.5 and 1.2. For the case of model E, this center moves from about 0.001 ship lengths forward of the LCG to 0.002, 0.01, and 0.02 ship lengths aft the LCG, for H/T values of 2.5, 1.5, and 1.2, respectively.

The inherent directional stability characteristics, as manifested by the dynamic stability indices σ_{1h}', σ_{1h}'', and ℓ_d', also change significantly with H/T variation. Here again, the most pronounced changes occur at H/T values below about 2.0, as is clearly shown for the four 200,000 ton displacement ships

in Figures 7-21 through 7-24. Below H/T = 2.0, the trend in all cases is for the ship to become less inherently directionally unstable, or more stable, at a progressively increased rate as it approaches the shallowest depth at H/T = 1.2. Taking the case of ship E in Figure 7-21 as an example, the curves of the dynamic stability indices σ_{1h}' and σ_{1h}'' remain fairly flat at their deep water unstable (positive) values as H/T is decreased down to about 2.0. Then the positive values of the indices start to gradually decrease, indicating that the ship is becoming less inherently directionally unstable, until about H/T = 1.5. Beyond this point, there is a sharp decrease in the positive values until σ_{1h}' and σ_{1h}'' become equal to zero, indicating neutral stability, at H/T of about 1.33. The values of these two indices then increase negatively at a fairly high rate indicating that the ship is becoming progressively more inherently directionally stable as H/T is further decreased. At H/T = 1.2, the values of σ_{1h}' and σ_{1h}'' are -0.5608 and -0.1259 compared with the deep water values of 0.3331 and 0.07482, respectively. Thus, based on these dynamic stability indices, ship E, which would be inherently unstable to a fairly high degree in deep water, would be stable to even a higher degree in shallow water of H/T = 1.2 by a ratio of about -1.7.

There is some evidence that there is a region of H/T values, usually between 1.8 and 3.0 for the models investigated, where the ship may become more inherently unstable than in deep water, as indicated by the results of the shallow water PMM tests of Reference 36. This trend is also confirmed by results of the ESSO OSAKA trials reported in Reference 29. However, this effect appears to be relatively small as shown by the curves of σ_{1h}' and σ_{1h}'' in Figures 7-21 through 7-24, and probably would have little influence on the maneuvering characteristics of the ship.

The dynamic stability lever ℓ_d' follows the general trends of σ_{1h}' and σ_{1h}''. However, the variations of ℓ_d' with H/T are generally more pronounced than those of the other two dynamic stability indices. For example, the values of ℓ_d' obtained at

H/T = 1.2 for ships L and H seem to be unduly high and result in ratios to the deep water values of about -6.5 and -5.9, respectively, compared with about -2.3 and -1.0 for the other two stability indices. The large values of ℓ_d' are attributed mainly to the large changes in the damping lever, ℓ_d', with H/T since the changes in the static lever ℓ_v' are relatively small. The reason for this is apparent from Equation [10], Chapter 6. When a ship becomes more stable, the value of Y_r', which is always positive, becomes progressively larger and the negative value of $(Y_r'-m')$ becomes smaller. As the value of Y_r' approaches that of m', as in the case of H/T values in the vicinity of 1.2, the value of ℓ_r' becomes very large and at $Y_r'= m'$ is infinite. Thus, for very stable ships, small changes in Y_r', whether real or due to experimental error, result in large changes in ℓ_r', and, consequently, in large changes in ℓ_d'. Thus, it appears that ℓ_d' is not a very satisfactory criterion for quantitatively indicating the degree of stability for the case of highly stable ships, particularly in the shallow water situation. It is also interesting to note that if Y_r' should become greater than m', then ℓ_r', and consequently ℓ_d', would become negative which would indicate that the ship is unstable.

Effect of B/T Variation

Figure 7-25 and Table 7-9 show the effect of B/T variation on the inherent directional stability characteristics of ships E, K, L, and H in shallow water at H/T = 1.2. Based on the dynamic stability indices σ_{1h}' and σ_{1h}'', inherent directional stability at H/T = 1.2 increases uniformly with B/T from 3.00 to 4.50, as indicated by the increases in the negative values of the indices. Based on the dynamic stability lever, there is a relatively small increase in stability between B/T = 3.00 and 3.75, but a fairly sharp increase between 3.75 and 4.50. However, this trend is discounted for reasons given earlier. For the comparable deep water case where the full scale ships are

inherently directionally unstable, there is a relatively small increase in instability from B/T = 3.00 to 3.75, then a slight decrease thereafter to 4.50. The same trend shows in all three indices, as seen in Figure 6-8 and for the deep water case in Table 7-9. The increase in stability with B/T for equal displacement hulls at constant H/T = 1.2 appears to be reasonable since the underkeel clearance decreases with increase in B/T. This can be readily seen from the test conditions given for models E, K, H, and L in Table 7-1.

Effect of L/B Variation

The effect of L/B variation on inherent directional stability characteristics in shallow water at H/T = 1.2 can be seen by comparing the dynamic stability indices for ship E (L/B = 5.00) with those for ship H (L/B = 6.5) given in Table 7-9. Based on the dynamic stability index σ_{1h}', there is a substantial increase in inherent directional stability (-0.5608 compared with -0.7528) from increasing L/B from 5.00 to 6.50 at H/T = 1.2. Based on σ_{1h}'', however, the increase is relatively smaller (-0.1259 compared with -0.1419). In the deep water case where both ships are unstable, there is a decrease in instability which is very small if based on σ_{1h}' (0.7482 compared with 0.07338 for L/B = 5.00 and 6.50, respectively). The increase in stability with L/B at H/T = 1.2 can be attributed, at least partially, to the decrease in underkeel clearance for the constant volume comparison of L/B = 5.00 to 6.50, as indicated in Table 7-1.

Inherent Control Effectiveness

Inherent control effectiveness is of particular importance in shallow water maneuverability where the hydrodynamic characteristics of the hull undergo drastic changes, particularly at H/T values below 1.5. As for the deep water case, the dimensional angular acceleration parameter, cp, defined in

Chapter 6, is used here as a criterion of inherent control effectiveness.

Figure 7-26, derived from Figure 6-9, shows the relationship between the dimensional angular acceleration parameter, cp, and time, t_2, to reach an execute heading change of 5 degrees. The figure is generally applicable to ships of any size, within the tested range of characteristics.

Effect of Water Depth Variation

Table 7-11 is a comparison of the cp values corresponding to a speed of 8.0 knots for the four 200,000 ton displacement ships in deep and shallow water. These cp values were computed as described in Chapter 6 using the appropriate nondimensional derivatives given in Tables 7-5 through 7-8. The cp values in Table 7-11 were also used to prepare the curves of Figure 7-27 which show the effect of variation in H/T for each of the four ships. Included in the table are corresponding t_2 values for a heading change of 5 degrees. The t_2 values in Column 1 were read to the nearest second from Figure 7-26. The t_2 values in Column 2 were derived from the results of computer simulation studies (20-20 zigzag) using the complete, nonlinear, mathematical models derived in Chapter 6 for each H/T listed in the table. The t_2 values read from Figure 7-26 are in close agreement with those obtained from the computer simulation studies for H/T values down through 1.5. However, the t_2 values at H/T = 1.2 are significantly higher than those read from Figure 7-26, as evident from Table 7-11 and the data points superimposed on Figure 7-26. The apparent reasons for this are discussed further in the following paragraphs.

Figure 7-27 shows, for the case of each of the four ships, that cp tends to remain constant down to about H/T = 2.2, but then tends to decrease at a progressively greater rate until a value considerably smaller than for deep water is reached at H/T = 1.2. This suggests that a given ship of the series type will always have much less inherent control effectiveness in very

shallow water than it has at the same speed in deep water. This is due to the fact that, although the control moment derivative, $N_{\delta r}'$, increases with decrease in H/T, the added moment of inertia derivative, $N_{\dot{r}}'$, and consequently $(N_{\dot{r}}'-I_z')$, increases at a greater rate.

Normally, it would be expected that the control force derivative, $Y_{\delta r}'$, and control moment derivative, $N_{\delta r}'$, would both increase substantially in going from deep to shallow water of H/T = 1.2. This results from the large increase in resistance with the attendant increases in propeller loading coefficient ($C_{Ti} = C_{Ts}$) and $1/J_a$ at ship propulsion point in the shallow water condition. As a result, the propeller slipstream velocity over the rudder becomes much higher, tending to increase the nondimensional control derivatives which are based on ship velocity. Some of this increase in propeller slipstream velocity is offset by the increase in wake fraction, w, shown for the shallowest water depths by the propulsion test results. Nevertheless, the value of $Y_{\delta r}'$ at H/T = 1.2 still remains quite large, as much as about 1.62 times that for deep water in the case of model L. However, $N_{\delta r}'$ for the same case increases only by about 1.14 times the corresponding deep water value. In fact, for model E, the increase in $N_{\delta r}'$ at H/T = 1.2 is only about 1.02 times the deep water value. This result is shown more clearly by the following tabular comparison of the quantity $N_{\delta r}'/Y_{\delta r}'$ for each of the 200,000 ton displacement ships at each of the depth conditions.

$N_{\delta r}'/Y_{\delta r}'$

Ship	H/T = ∞	H/T = 2.5	H/T = 1.5	H/T = 1.2
E	-0.521	-0.525	-0.524	-0.451
K	-0.522	-0.527	-0.524	-0.403
L	-0.519	-0.518	-0.500	-0.365
H	-0.519	-0.523	-0.523	-0.451

The value of $N_{\delta r}'/Y_{\delta r}'$ is a measure of the longitudinal distance from the LCG to the center of action of the rudder force. In the case of all of the series models, the centerline of the rudder stock is located at the after perpendicular which is 0.525 ship lengths aft of the LCG. It may be noted that in nearly all cases down to H/T = 1.5, the center of action of the rudder force is close to the centerline of the rudder stock which is in accordance with past experience with results of deep water tests. However, at H/T = 1.2, the center of action of the rudder force moves a substantial distance forward of the rudder stock, the most pronounced effects being on the high B/T models K and L. This phenomenon may be due to a strong interaction effect between the rudder-propeller combination and hull which occurs only when the ship is in very close proximity to the bottom. Because of the large models used and quality of the test data, it is believed that the effects shown in the above table are realistic, and account for much of the loss of inherent control effectiveness in very shallow water.

As noted earlier, the basic chart of cp versus t_2 in Figure 7-26 has wide applicability regardless of ship size, and usually without consideration of degree of inherent dynamic stability or instability. In the case of H/T = 1.2, however, there seems to be a significant departure from the basic curve. This can probably be attributed to the very high degree of inherent stability (δ_{1h}' = -0.56 to -0.85) characteristic of the four models at H/T = 1.2, which apparently has an effect on t_2 even at a heading change angle of only 5.0 degrees. For such cases, therefore, the broken line shown in Figure 7-26 should provide a better estimate of the t_2 values.

Figure 7-28 shows the effect of B/T variation on cp for the 200,000 ton displacement ships at H/T = 1.2 for an approach speed of 8.0 knots. For purposes of comparison, corresponding variation for the deep water case is shown by the broken line. At H/T = 1.2 the value of cp for the ships increases with B/T until a maximum is reached at 3.75, decreasing again until a

value lower than that at 3.00 is reached at 3.75. In the deep water case, there is no change in cp with B/T until about 3.75, but then there is a decrease until the lowest value is reached at B/T = 4.50. In all cases, the cp values are lower than for the deep water case. Coupled with the fact that t_2 for a given cp value at H/T = 1.2 is higher than for deep water, it can be expected that each of these ships will have relatively poor inherent control characteristics from the standpoint of initiating a course change.

Simulated Maneuvering Characteristics

Simulated maneuvers for the four series models E, L, K, and H were developed using the equations of motion derive in Chapter 6.

Tables 7-12 through 7-15 present complete sets of the nondimensional hydrodynamic coefficients and constants necessary to formulate the basic mathematical models for the 200,000 ton displacement ships corresponding to the series models investigated at each of the specified H/T values. The values of the coefficients at H/T = 2.5 for ships K, L, and H were obtained by interpolation from cross-curves in a manner similar to that mentioned earlier for the case of the nondimensional stability and control derivatives. The η-dependent terms for the deep water case have been modified wherever necessary for the 200,000 ton displacement and, therefore, may differ slightly in some cases from the values presented for the 350,000 ton displacement ships in Chapter 6. Included for the deep water case also are values of the nonlinear coefficients $Y_{r|r|}'$ and $N_{r|r|}'$ which have been extrapolated from the results of the shallow water LAHPMM tests. In all cases, the nondimensional hydrodynamic coefficients in Tables 7-12 through 7-15 apply strictly to the case of the 200,000 ton displacement ship having the geometric characteristics listed in in Table 7-2, and where η = 1.0 corresponds to ship propulsion point at 8.0 knots for the specified depth condition. However, the same sets of nondimensional coefficients can be used with reasonably good

accuracy for other geometrically similar ships within ±20 percent of the length of the given standard ship. To accomodate geometrically similar ships of other sizes, the values of those nondimensional coefficients which are influenced by propeller loading coefficients (η-dependent coefficients) can be readily converted using the estimation procedures described in Chapter 6.

The procedures used to arrive at the numerical values for the complete sets of hydrodynamic coefficients given in Tables 7-12 through 7-15 are essentially the same as those described for the deep water case in Chapter 6.

The results of the computer simulation studies for each of the definitive maneuvers are presented and discussed separately in the following sections. Unless stated otherwise, all of the results pertain to the case of 200,000 ton full load displacement in calm water of specified H/T and unrestricted expanse. A rudder deflection rate of 2.33 degrees per second was assumed in all cases. All derived measures are expressed dimensionally in real time and distance. For analyses involving different ship sizes, the dimensional values can be converted readily to nondimensional values by use of appropriate normalizing factors, as indicated in the discussion.

Spirals

Figure 7-29 shows the effect of H/T variation on the curves of steady heading rate change versus rudder angle derived from simulated spiral maneuvers conducted on each of the four series ships. Loop height and width are compared in Table 7-16. Included in Table 7-16 are other relevant data such as values of neutral angles at steady turning rates at rudder angles of -20, -10, 0, 10, and 20 degrees.

It can be readily seen from the curves in Figure 7-29 and the numerical measures in Table 7-16 that the degree of inherent directional instability or stability for each of the four ships changes significantly with H/T variation, as shown by the marked change in their loop characteristics. Taking for example ship E

in Figure 7-29a, at H/T = 2.5 the loop height is slightly greater than for deep water, but then it decreases substantially at H/T = 1.5, until at H/T = 1.2 there is no loop, indicating that the ship has become inherently directionally stable at this water depth. The curves for ships K and L given in Figures 7-29b and 7-29c, respectively, show the same trends except that, at H/T = 2.5, ship K is slightly less unstable than in deep water. The curves for ship H given in Figure 7-29d show a similar trend, but indicate that the ship becomes stable at H/T = 1.5. In general, the trends in degree of inherent instability or stability with H/T variation shown by the spiral data agree quite closely with those resulting from the stability indices based on analysis of the linearized equations of motion.

The effect of B/T and L/B variation on degree of inherent directional stability at H/T = 1.2 is indicated to some extent by the slopes through neutral angle of the appropriate curves in Figure 7-29. Based on the average of the steady turning rates at ±10 degrees rudder angle in Table 7-16, these slopes are approximately 0.128, 0.111, and 0.092 deg/sec/deg rudder for ships E, K, and L, representing B/T values of 3.00, 3.75, and 4.50, respectively. This indicates that the degree of inherent stability at H/T = 1.2 increases with increase in B/T, as shown by the decrease in slope values. Comparable values for δ_{1h}'', the dynamic stability index based on equal displacement ships, are about -0.126, -0.156, and -0.167, respectively. The increasing negative values of δ_{1h}'' also show the same trend in stability increase with increase in B/T. Similarly, the slope values for ships E and H, representing L/B variations of 5.0 and 6.5, are approximately 0.128 and 0.080 deg/sec/deg rudder, compared, respectively, with δ_{1h}'' values from Tables 7-5 and 7-8 of about -0.126 and -0.142. Both the slope and the δ_{1h}'' values indicate an increase in degree of stability with increase in L/B. As stated earlier, the above comparisons must be tempered by the fact that the slope values are a measure of inherent stability as well as rudder effectiveness.

At H/T = 1.2, all four ships are inherently directionally stable to a fairly high degree, as indicated both by the simulated spiral results and the dynamic indices. Therefore, it can be reasonably expected that at this shallow water depth condition they will have excellent coursekeeping characteristics with minimum rudder activity.

Zigzags

Simulated zigzag maneuvers in deep and shallow water of various depths were performed for each of the four 200,000 ton displacement ships. The program included 5-5, 10-10, and 20-20 zigzags, all of which were conducted at an approach speed of 8.0 knots. Figure 7-30 is a comparison of time histories of rudder angle, heading angle, and path for a 20-20 zigzag maneuver conducted on ship E for the cases of deep water and shallow water of H/T = 2.5, 1.5, and 1.2. The primary numerical measures of interest obtained from the overshoot maneuver are the time to reach execute heading change angle, t_2, overshoot heading angle, and overshoot width of path. All three of these numerical measures are important for evaluating maneuvering in confined or congested waterways.

Table 7-17 is a summary and comparison of the numerical measures derived from all of the zigzag maneuvers simulated for each of the four series ships. The effects of H/T variation on the primary numerical measures for each full scale ship are generally as follows:

1) The ship takes a longer time to reach a given heading as H/T is decreased. The most pronounced increases in time occur between H/T = 1.5 and 1.2.

2) The heading angle overshoots become smaller with decrease in H/T. The most pronounced reductions occur between H/T = 1.5 and 1.2.

3) The associated path width overshoots become smaller with decrease in H/T. The most pronounced reductions occur between H/T = 1.5 and 1.2.

The following quantitative trends with H/T variation may be noted using the 20-20 overshoot maneuver of ship E as a specific example: Between deep and shallow water of H/T = 1.5, the time to reach execute increases from about 111 to 119 seconds; the heading angle overshoot decreases from about 1685 to 1250 feet. However, between H/T = 1.5 and 1.2, the time to reach execute increases from about 119 to 151 seconds, the heading angle overshoot decreases from about 12.35 to 4.30 degrees, and the path width overshoot decreases from about 1250 to 804 feet.

These trends with H/T variations may have been anticipated from the analysis of the inherent directional stability and inherent control effectiveness characteristics of each 200,000 ton displacement ship considered earlier. This is due to the fact that in the transient part of a given course changing maneuver the time to reach execute, t_2, is governed predominantly by inherent control effectiveness, as indicated by the directional angular acceleration parameter, cp. However, the magnitudes of the heading angle and path width overshoots are governed predominantly by inherent directional stability, as indicated by stability indices such as δ_{1h}' or δ_{1h}'', although cp can have a secondary effect. For example, in the 20-20 zigzags of ship E, the values of cp correspond to increases in t_2 over the deep water case of 6 and 28 percent compared with those from the zigzag maneuver of 7 and 36 percent at H/T = 1.5 and 1.2, respectively. The percentages obtained from the cp relationship are slightly lower than those obtained from the simulated zigzag. This is reasonable since the cp relationship applies more rigorously to small heading changes. Nevertheless, both cases show a relatively small increase in t_2 between deep water and H/T = 1.5 and a relatively large increase in t_2 between H/T = 1.5 and 1.2. Similarly, the stability indices δ_{1h}' and δ_{1h}'' show relatively small decreases in inherent instability between deep water and H/T = 1.5 which accounts for the relatively small reductions in the overshoots in this range, but indicate that the ship becomes inherently stable to a high degree

at H/T = 1.2. This probably accounts for the relatively large reductions in overshoots between H/T = 1.5 and 1.2.

The effect of B/T variation on shallow water overshoot characteristics is shown in Table 7-17 by comparing the numerical measures for ships E, K, and L at H/T = 1.2. Based on the 20-20 zigzag as an example, there is a small increase in t_2 between B/T = 3.00 and 3.75 (151 to 154 seconds for ships E and K), but a substantial increase in t_2 between B/T = 3.75 and 4.50 (154 to 176 seconds for ships K and L). The heading angle overshoots decrease fairly uniformly between B/T = 3.00 and 4.50 (4.3, 3.57, and 2.94 degrees for ships E, K, and L, respectively). The path width overshoots show the same trend as the heading angle overshoots, but their relative values are influenced somewhat by the differences in length among the full scale ships. The values of the stability index, δ_{1h}", are -0.1259, -0.1579, and -0.1669 for B/T = 3.00, 3.75, and 4.50, respectively, which indicates that the degree of inherent stability increases with increase in B/T and, thus, confirms the trend of decreasing values shown by the overshoots. However, the cp values do not seem to confirm the trend in t_2 values between B/T = 3.00 and 3.75.

The effect of L/B variation on shallow water overshoot characteristics is shown by comparing the numerical measures for ships E and H at H/T = 1.2 in Table 7-17. For the 20-20 zigzag case, the t_2 values are 151 and 204 seconds, the heading angle overshoots are 4.30 and 2.67 degrees, and the path width overshoots are 804 and 855 feet for L/B = 5.00 (ship E) and L/B = 6.50 (ship H), respectively. Thus, both t_2 and heading angle overshoot decrease with increase in L/B over the range between 5.00 and 6.50, but the path width overshoot increases somewhat with increase in L/B over the same range. The increase in the latter is probably due to the large differences between the lengths of the ships (851.64 feet for ship E compared with 1014.42 for ship H). For example, the nondimensional path width overshoots are 0.944 and 0.843 ship lengths for ships E and L, respectively, which agrees with the trend shown by the heading

angle overshoots. For the case of the L/B variation, the trends in the numerical measures are in general agreement with those shown by the values of cp and δ_{1h}' given in Tables 7-11 and 7-17, respectively.

The trends with H/T variation shown by the other numerical measures in Table 7-16 for the 20-20 zigzag maneuver are summarized as follows, with the most pronounced changes between H/T = 1.5 and 1.2:

1) Total heading change decreases with decrease in H/T.

2) Path width at execute increases with decrease in H/T.

3) Total path width decreases with decrease in H/T.

4) Reach decreases with decrease in H/T, but the decrease between H/T = 1.5 and 1.2 is not as pronounced as with the other numerical measures.

5) Period generally decreases with decrease in H/T, except for ships L and H where it increases between H/T = 1.5 and 1.2.

As stated previously, the numerical measures from the 5-5 zigzag maneuvers are more indicative of coursekeeping rather than course changing ability. It is interesting to note from Table 7-16 that for the deep water case the 5-5 zigzag maneuvers could not be completed for ships E, K, and L and for ship H the second and third heading angle overshoots are very large compared with the first. This is characteristic of full-form ships with a relatively high degree of inherent directional instability, indicating that, for acceptable coursekeeping, there must be continuous rudder activity and the heading angle errors must be kept very small. However, in shallow water at H/T = 1.2, the second and third heading overshoot angles are not much larger than the first. Therefore, all other conditions being equal, the same ships should have very good coursekeeping ability with minimal use of rudder.

Turning Circles

Figure 7-31 is a comparison of the path data obtained from simulated 35 degree starboard steady turning maneuvers performed

for ship E in deep water and shallow water at H/T = 1.2. The numerical measures of primary interest are the advance, transfer, tactical diameter, and steady turning (final) diameter, as defined on the figure, the times to change heading 90 and 180 degrees, and speed loss in turning.

Simulated steady turning maneuvers in deep and shallow water of various constant depths (H/T = 2.5, 1.5, and 1.2) were performed for each of the four series ships. The program included turns with 10, 20, 35, and 45 degree rudder angles. All turns were made to starboard using a steady approach speed of 8 knots. The numerical measures derived from these steady turning maneuvers are compared in Table 7-18 for each of the four series ships.

Figure 7-32 shows the effect of H/T variation on the principal numerical measures from a 35 degree starboard steady turning maneuver of ship E. The data in the figure are given in nondimensional form. In general, the changes in the numerical measures are relatively small for water depths down to H/T = 1.4. However, between H/T = 1.5 and 1.2, all of the nondimensional numerical measures shown increase sharply. In the case of ship E, the tactical and steady turning diameters at H/T = 2.5 appear to be somewhat smaller than for deep water. A similar trend is exhibited in the simulated spiral results which indicate that this ship is slightly more inherently directionally unstable at H/T = 2.5 than in deep water. In the cases of the other three ships, the tactical and steady turning diameters, as well as the other numerical measures, tend to increase slightly between deep water and shallow water at H/T = 2.5. As shown in Figure 7-32, the greatest differences between deep and shallow water steady turning characteristics occur at H/T = 1.2. These differences are considered in more detail in the following paragraphs.

The extent to which the numerical measures from steady turning maneuvers of the four full scale ships differ between deep and shallow water at H/T = 1.2 varies substantially with the

rudder angle used. This is shown in Table 7-19 which is a comparison of the nondimensional tactical and steady turning diameters of the four ships in deep and shallow water at H/T = 1.2, corresponding to rudder angles between 10 and 45 degrees. The data given in Table 7-18 for typical ship E are also shown by the curves of Figure 7-33. For ship E, at rudder angles of 10 and 20 degrees, both the tactical and steady turning diameters at H/T = 1.2 are about 3 and 2 times the corresponding deep water values, respectively. For the standard rudder angle of 35 degrees, however, the tactical diameter is about 67 percent higher whereas the steady turning diameter is only 35 percent higher than in the deep water case. For 45 degrees rudder angle, the increases over deep water are only 55 and 19 percent, respectively.

The reasons for the spread between the tactical and steady turning diameter ratios can be deduced from Figure 7-33. The tactical and steady turning diameters for the deep water case are quite close, although the difference between them tends to increase slightly at the higher rudder angles. This can be attributed, at least in part, to the large drift angles in steady turns associated with ships as inherently unstable as ship E in deep water, which can amount to 25 degrees or more in minimum diameter turns. A large drift angle tends to decrease the tactical diameter relative to the steady turning diameter, as can be seen from the definitions on Figure 7-31. However, due to the high degree of stability at H/T = 1.2, the transfer tends to be large and the drift angle tends to be small, both of which tend to increase the magnitude of the tactical diameter relative to the steady turning diameter. It should be noted that the tactical diameter is probably a more important numerical measure than the steady turning diameter for most shallow water maneuvering situations. Therefore, for ship E an increase in tactical diameter of 67 or 55 percent for 35 and 45 degrees rudder, respectively, constitutes a major difference between the handling qualities of the ship in deep and shallow water.

The effect of operation in shallow water at H/T = 1.2 on the other numerical measures such as the times to change heading, advance, transfer, and speed remaining in steady turn, are also of interest. Table 7-18c shows that for ship E with 35 degrees rudder, the time to change heading 90 degrees is about 40 percent higher, whereas the time to change heading 180 degrees is only about 5 percent higher than the corresponding deep water values. Conversely, the advance and transfer are about 31 and 132 percent higher, respectively, than the corresponding deep water values. The speed remaining in the steady turn is about 55 percent of the approach speed compared with 31 percent for the deep water case, i.e., the loss of speed in the turn shown for ship E in shallow water at H/T = 1.2 is 45 percent compared with 69 percent in deep water. The smaller speed loss can be attributed mainly to the small drift angle associated with the high degree of inherent stability of the ship in shallow water in contrast to the very large drift angle associated with the high degree of instability for the same ship in deep water.

Figure 7-34 shows the effect of B/T variation on nondimensional numerical measures associated with a 35 degree starboard turn of the series ships in shallow water at H/T = 1.2. In terms of ship lengths, there is very little difference in tactical diameter for B/T values between 3.00 and 4.50, as also shown in Table 7-19. Similarly, there is very little difference in the advance and transfer. The steady turning diameter varies from about 3.66 to 3.95 ship lengths, which amounts to an increase of about 0.3 ship lengths for B/T increase from 3.00 to 4.50. The speed loss increases from about 45 to 47 percent of the approach speed between B/T = 3.00 and 3.75, but then decreases to about 39 percent between B/T = 3.75 and 4.00.

Based on the dimensional numerical measures shown in Table 7-19, which are of more operational significance, the differences due to B/T variation are much larger since the length of the equal displacement ships increases with increase in B/T. For example, it can be seen by comparing the data for ships E, K, and

L that the tactical diameters at H/T = 1.2 are 4090, 4354, and 4743 feet for B/T = 3.00, 3.75, and 4.50, respectively, which amounts to an increase of about 16 percent between B/T = 3.00 and 4.50. It is also of interest to note from Table 7-18 that the increases in tactical diameter over the deep water case are 67%, 40%, and 40% with 35 degrees rudder and 55%, 28%, and 23% with 45 degrees rudder for B/T = 3.00, 3.75, and 4.50, respectively.

The effect of L/B variation on the numerical measures from steady turning maneuvers in shallow water at H/T = 1.2 can be seen by comparing the values for ship E (L/B = 5.00) with those for ship H (L/B = 6.50) given in Table 7-18. For the 35 degree rudder case, Table 7-18c, the dimensional values of advance, transfer, tactical diameter, and steady turning diameter all increase substantially for L/B increasing from 5.00 to 6.50, due mainly to the increase in length for the equal volume ships. However, even on a nondimensional basis, the tactical diameter becomes larger at the higher L/B. For example, Table 7-19 shows that the nondimensional tactical diameter with 35 degrees rudder angle at H/T = 1.2 increases from 4.80 ship lengths at L/B = 5.00 to 5.64 ship lengths at L/B = 6.50. It is also evident from Table 7-19 that the deep water values of tactical diameter/L for both 35 and 45 degrees rudder are close for ships E and H. Therefore, the increases in tactical diameter with respect to the deep water case are much greater for L/B = 6.50 than for L/B = 5.00.

Stopping Maneuvers

Figure 7-35 is a comparison of typical path trajectories resulting from simulated stopping maneuvers from 8 knots ahead speed, with ship E in deep water and shallow water at H/T = 1.2, for 0 and 35 degrees rudder angles. The principal numerical measures are the head reach and side reach and the time to reach zero speed and heading change. The numerical measures for all four of the ships are summarized and compared in Table 7-20. Figure 7-35 indicates that, for the zero rudder angle case, the ship swings to port both in deep and shallow water, due to the

neutral rudder angle of about 1 degree right which, when the rudder is centered, is equivalent to a rudder angle of 1 degree left. In the full scale case, the ship could swing either to port or starboard depending on the magnitude of external disturbances such as wind, currents, and waves, particularly for the unstable ship in deep water.

Figure 7-35 and Table 7-20 indicate that with the rudder fixed at zero, the head reach of ship E in shallow water at H/T = 1.2 is somewhat greater than in deep water. The side reach and heading change are much smaller, however, indicating that, while stopping with this rudder position, the ship will remain more nearly on its original course at H/T = 1.2. The time it takes for the ship to reach zero speed is also considerably longer at H/T = 1.2.

With the rudder held at 35 degrees right, the head reach of ship E at H/T = 1.2 is substantially greater than in deep water. This is due mainly to the much smaller drift angles and associated smaller losses in speed relative to those obtained in deep water. For similar reasons, the side reach and heading change are much smaller at H/T = 1.2 than in deep water. The time to reach zero speed values for the 35 degree rudder angle stopping maneuver is much greater at H/T = 1.2 than in deep water. As expected, however, both the head reach and time to reach zero speed values for the 35 degree rudder maneuver are much smaller than the corresponding values obtained with the zero degree maneuver for either the shallow or deep water case.

The trends in the numerical measures obtained from the two types of stopping maneuvers conducted for the three other series ships are essentially the same as those shown for ship E. At H/T = 1.2, the head reach for the zero degree rudder maneuver decreases with increase in B/T between 3.00 and 4.50 despite the increase in length of the ship, as seen by comparing the values for ships E, K, and L in Table 7-20. In the same type of maneuver, the head reach does not change significantly with L/B between 5.00 and 6.50 despite the increase in length of the ship,

i.e., ship E compared with ship H. For the 35 degree rudder maneuver at H/T = 1.2, the head reach decreases between B/T = 3.00 and 3.75, but then increases again up to B/T = 4.50. Between L/B = 5.00 and 6.50 the trend is toward an increase in head reach with increase in L/B.

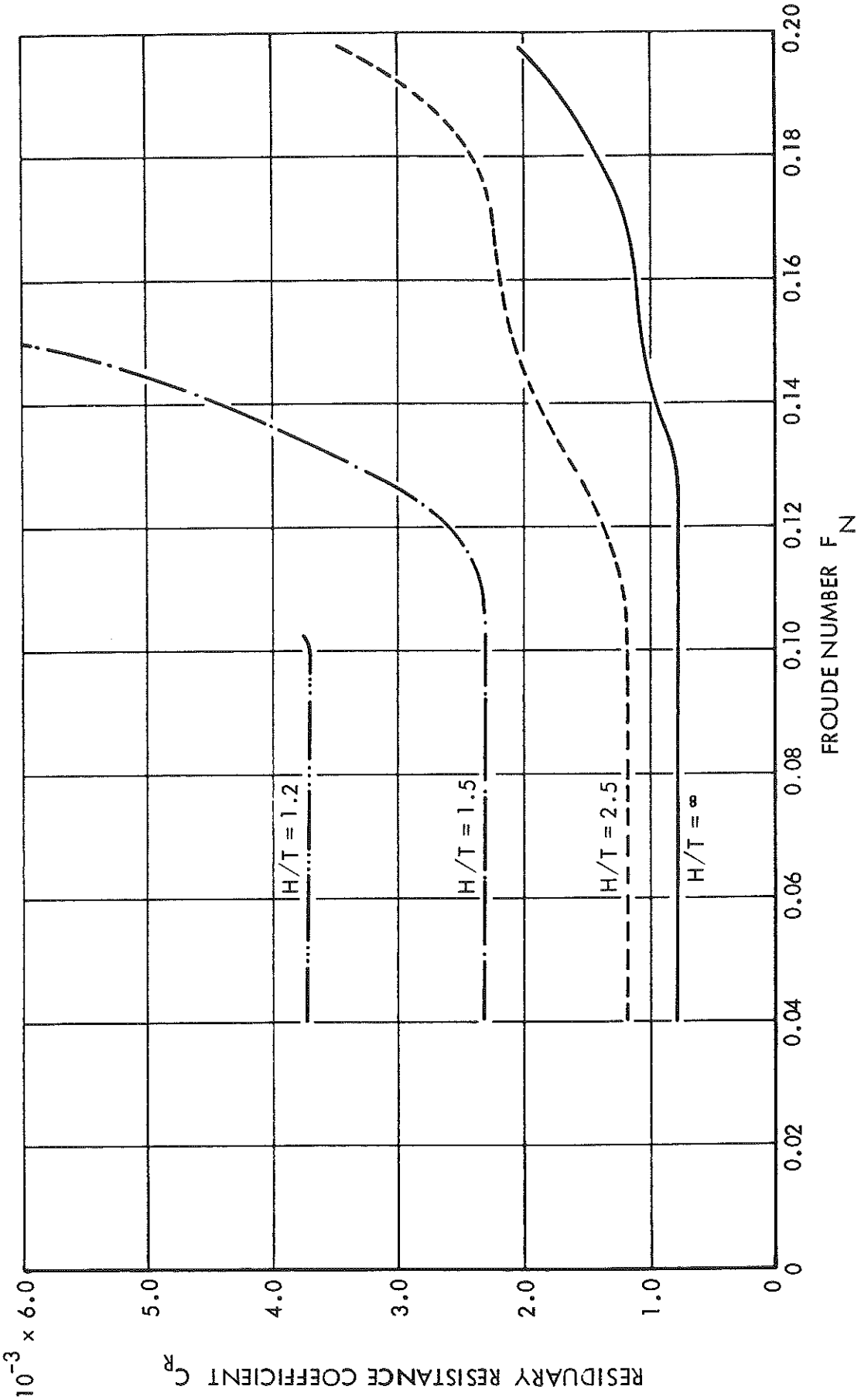

FIGURE 7-1 - TYPICAL CURVES OF RESIDUARY RESISTANCE COEFFICIENT VERSUS FROUDE NUMBER FOR VARIOUS H/T VALUES - SHIP E

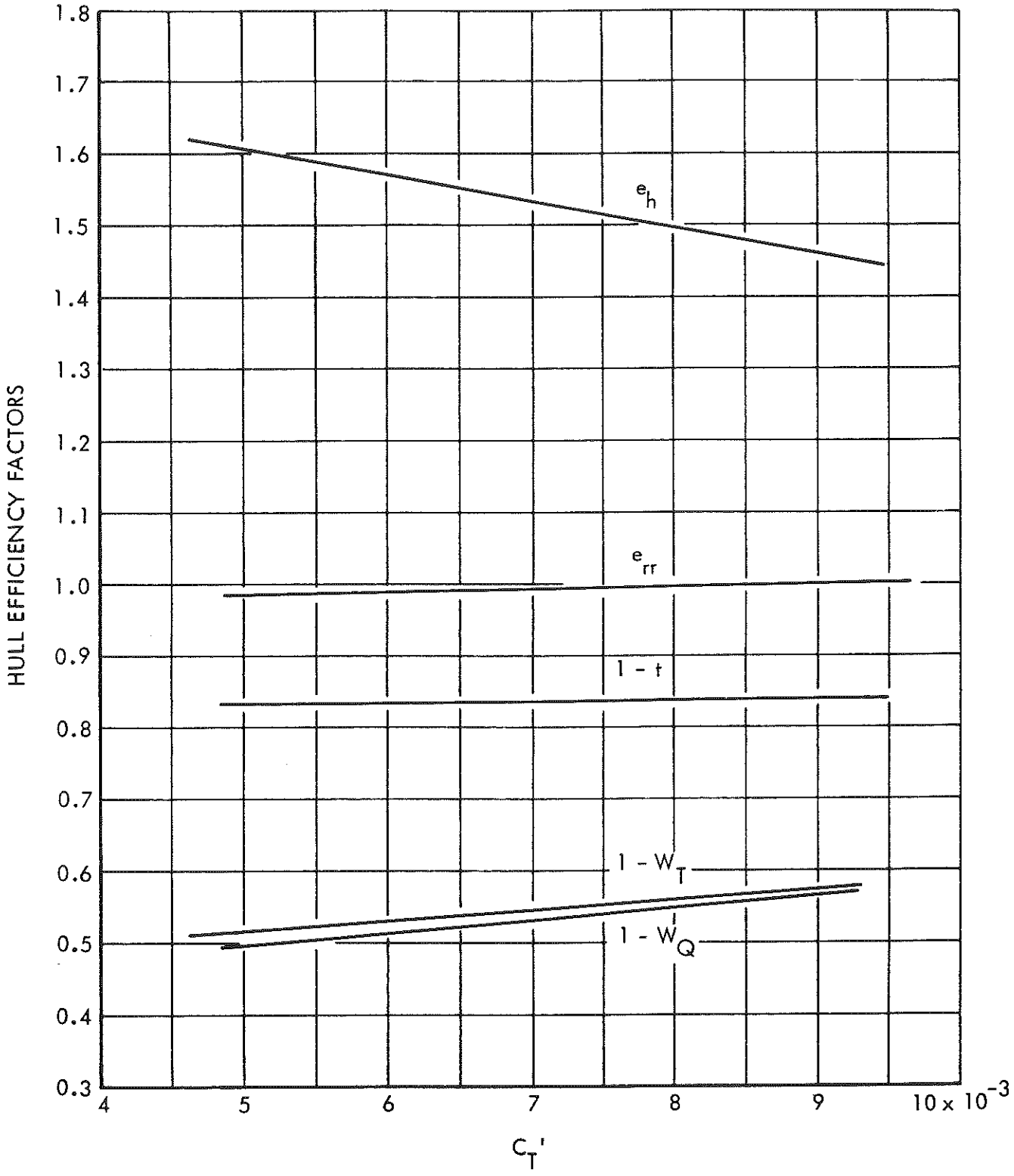

FIGURE 7-2 - VARIATION OF HULL EFFICIENCY FACTORS WITH PROPELLER LOADING COEFFICIENT AT VARIOUS H/T VALUES - Model E

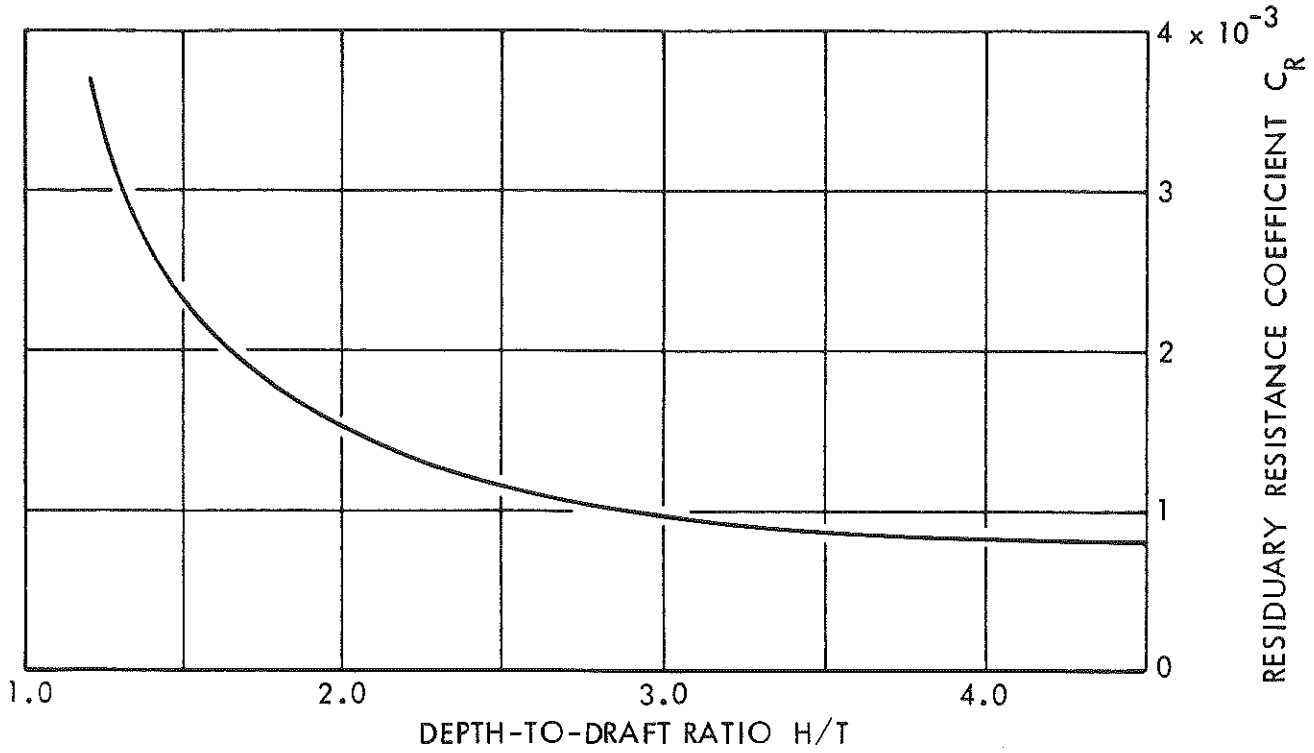

FIGURE 7-3 - SHIP E - VARIATION OF RESIDUARY RESISTANCE COEFFICIENT WITH H/T AT LOW F_N

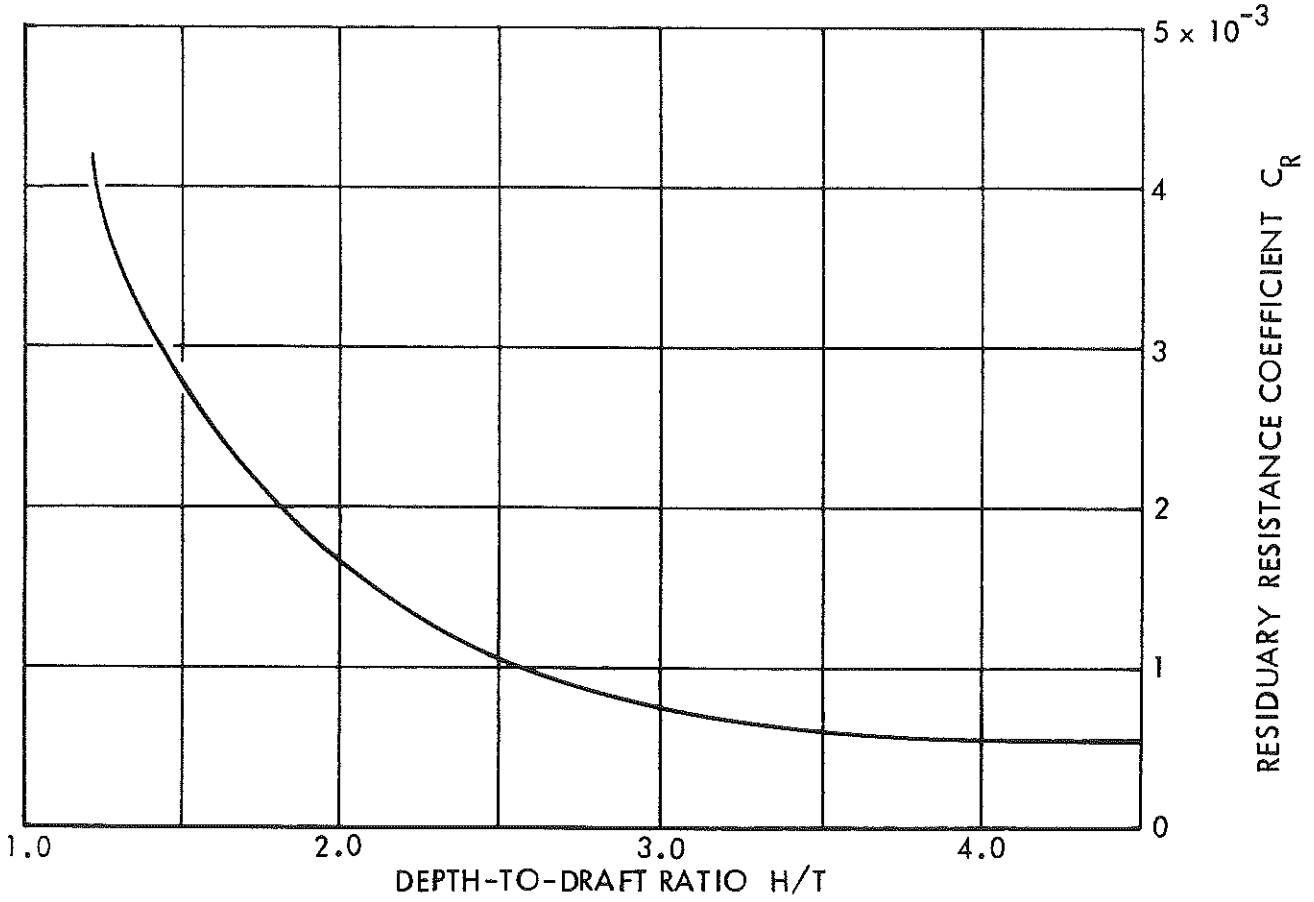

FIGURE 7-4 - SHIP K - VARIATION OF RESIDUARY RESISTANCE COEFFICIENT WITH H/T AT LOW F_N

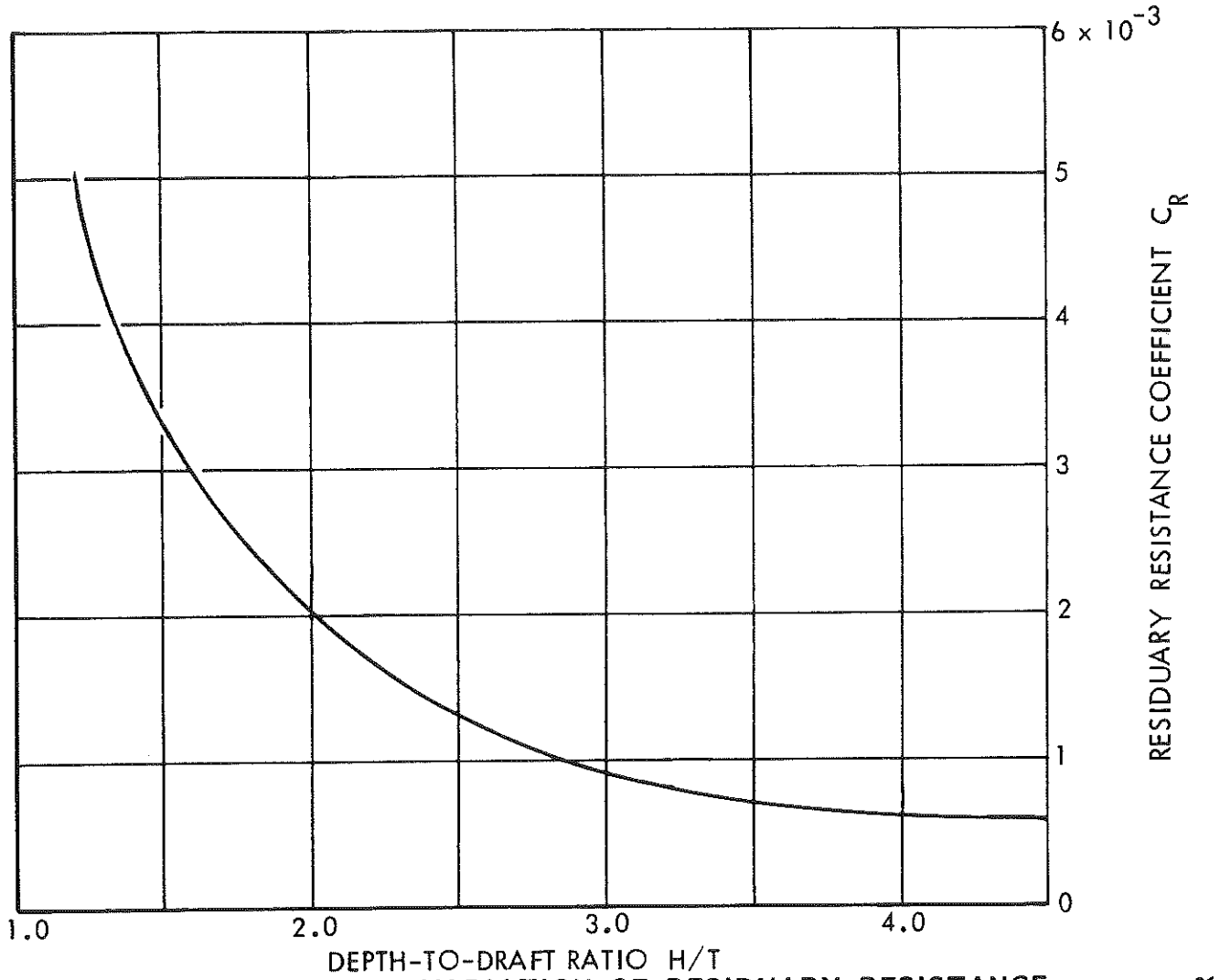

FIGURE 7-5 - SHIP L - VARIATION OF RESIDUARY RESISTANCE COEFFICIENT WITH H/T AT LOW F_N

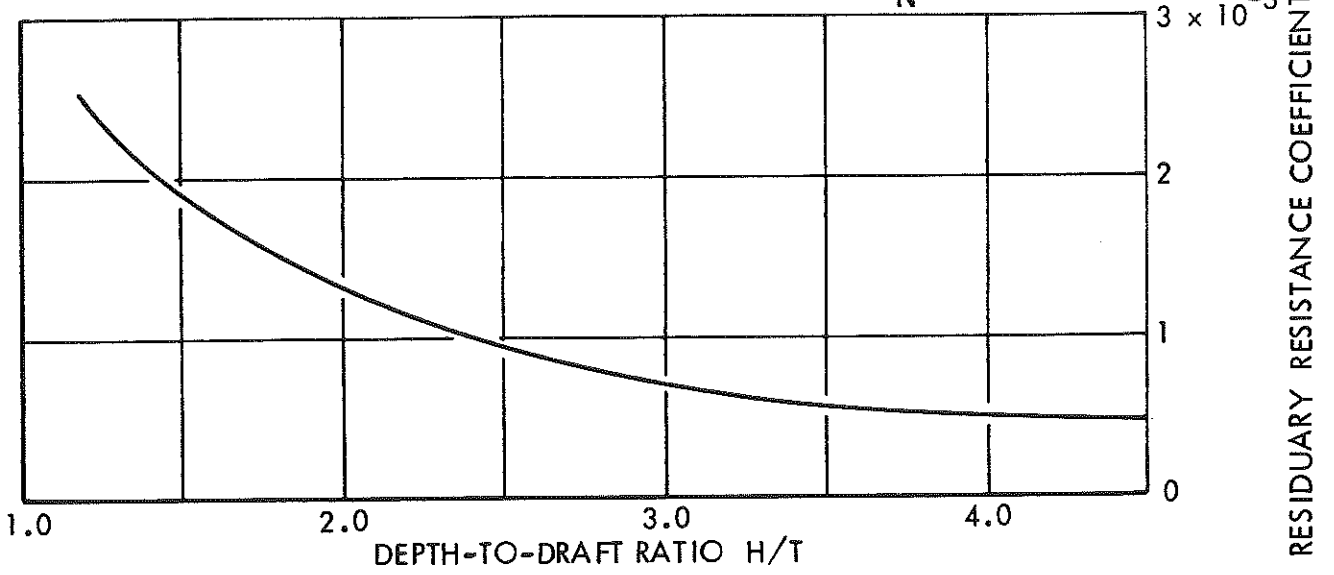

FIGURE 7-6 - SHIP H - VARIATION OF RESIDUARY RESISTANCE COEFFICIENT WITH H/T AT LOW F_N

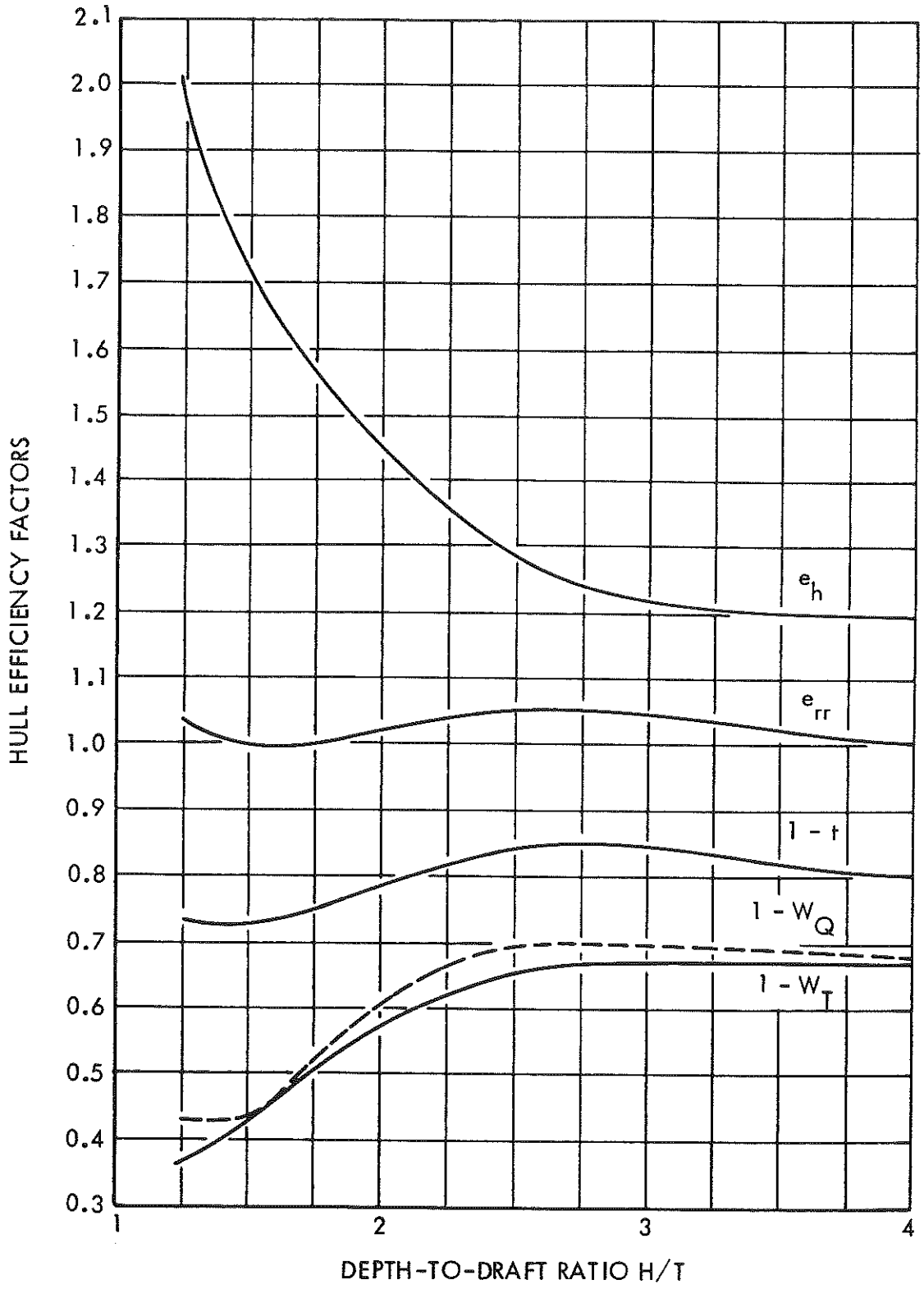

FIGURE 7-7 - SHIP E - VARIATION OF HULL EFFICIENCY FACTORS WITH H/T

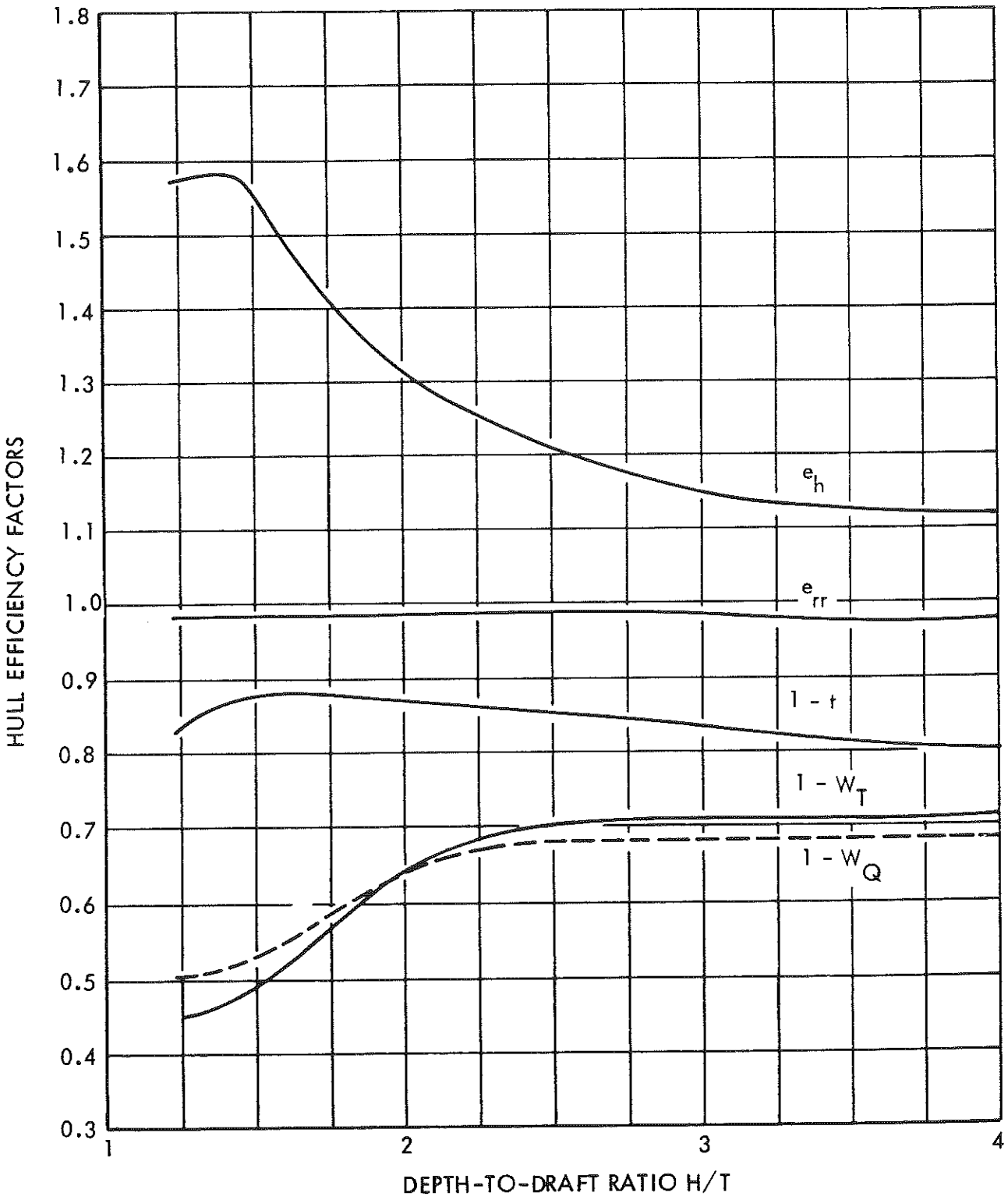

FIGURE 7-8 - SHIP K - VARIATION OF HULL EFFICIENCY FACTORS WITH H/T

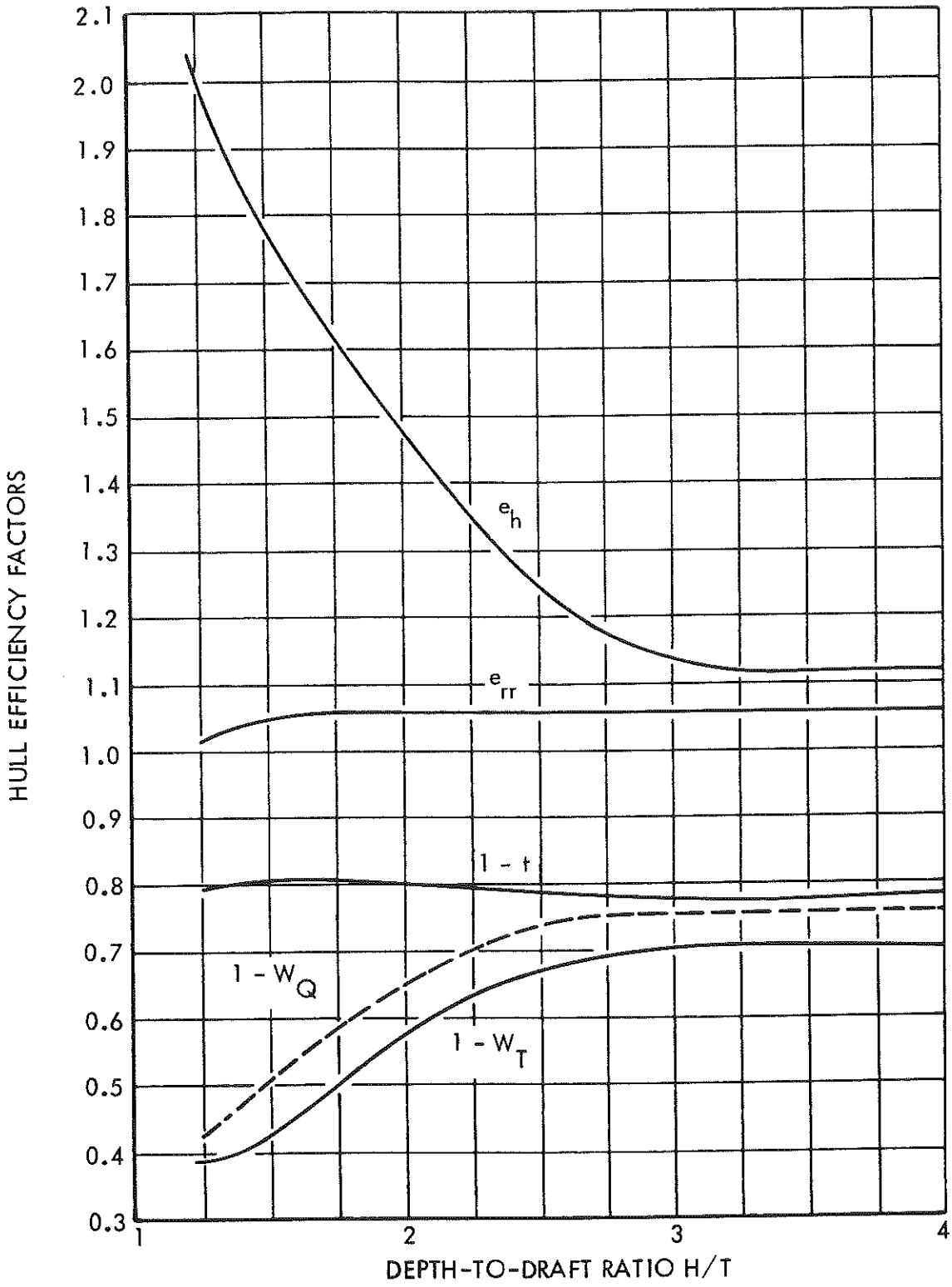

FIGURE 7-9 - SHIP L - VARIATION OF HULL EFFICIENCY FACTORS WITH H/T

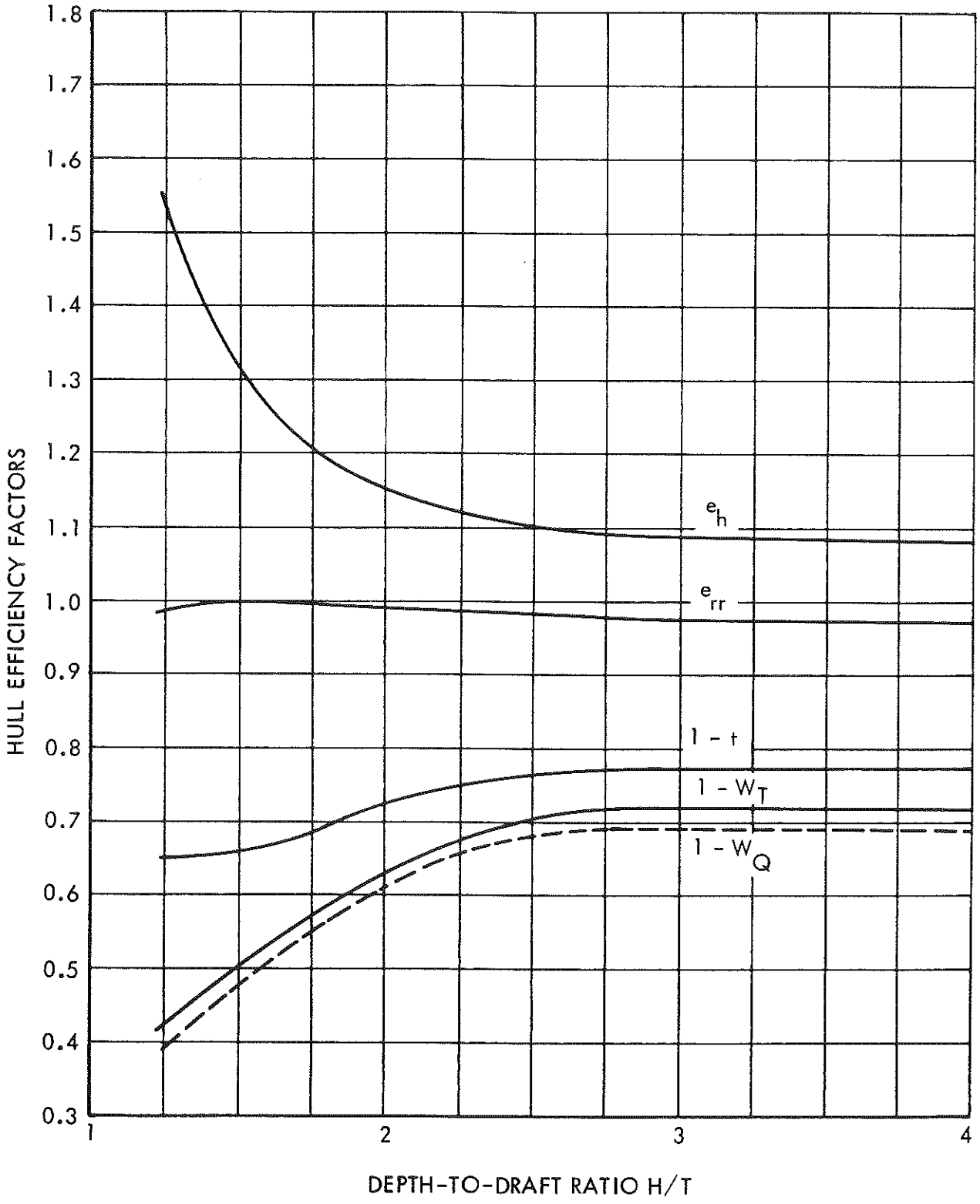

FIGURE 7-10 - SHIP H - VARIATION OF HULL EFFICIENCY FACTORS WITH H/T

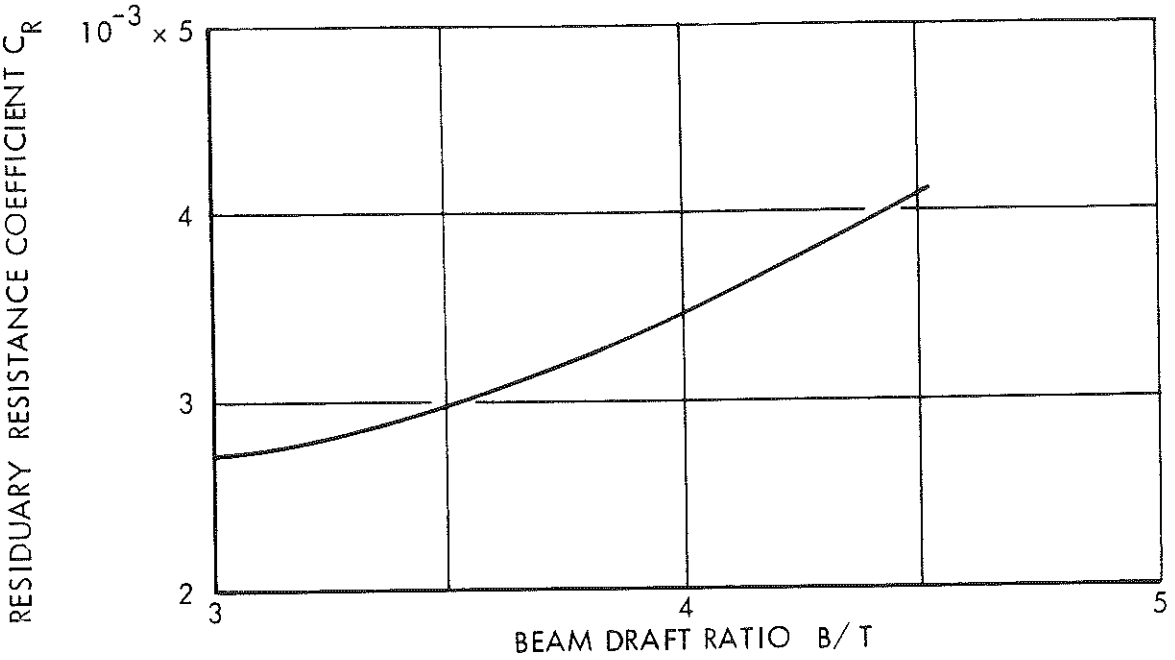

FIGURE 7-11 - VARIATION OF RESIDUARY RESISTANCE COEFFICIENT WITH B/T AT H/T = 1.2

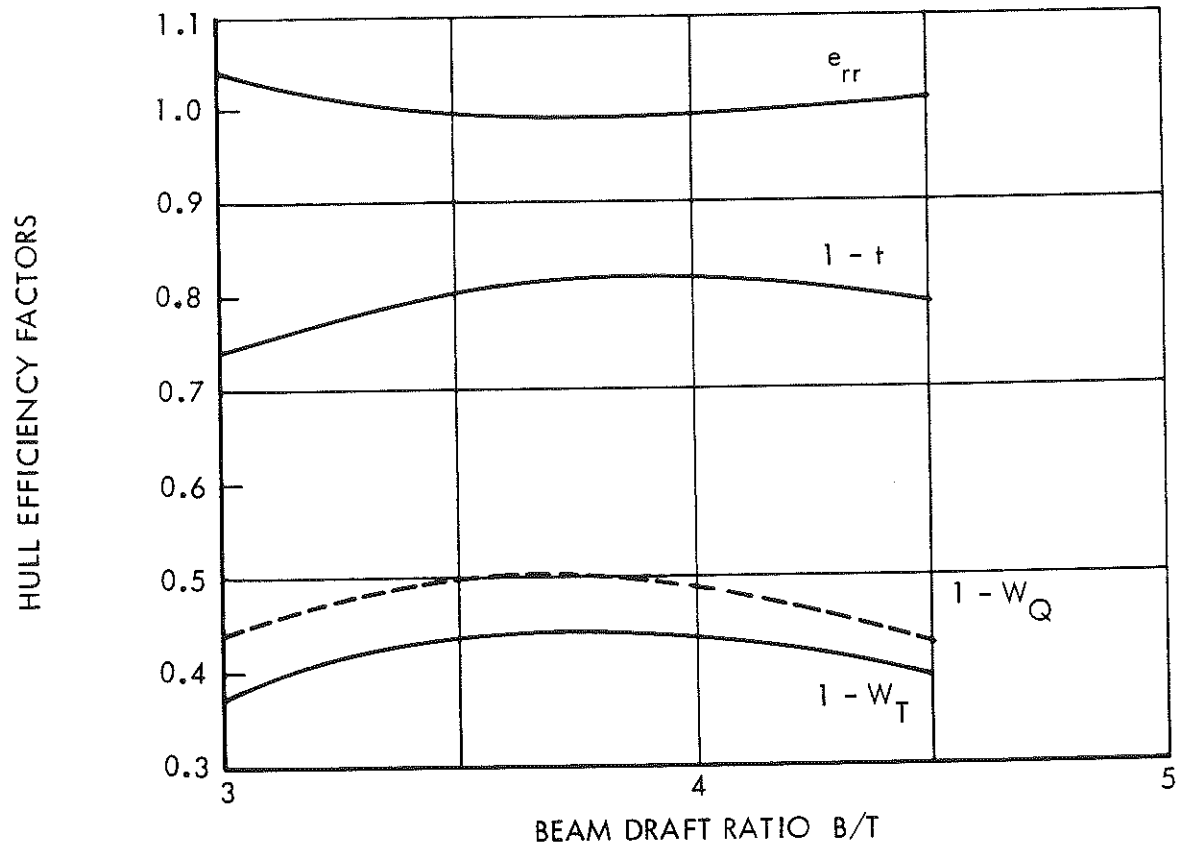

FIGURE 7-12 - VARIATION OF HULL EFFICIENCY FACTORS WITH B/T AT H/T = 1.2

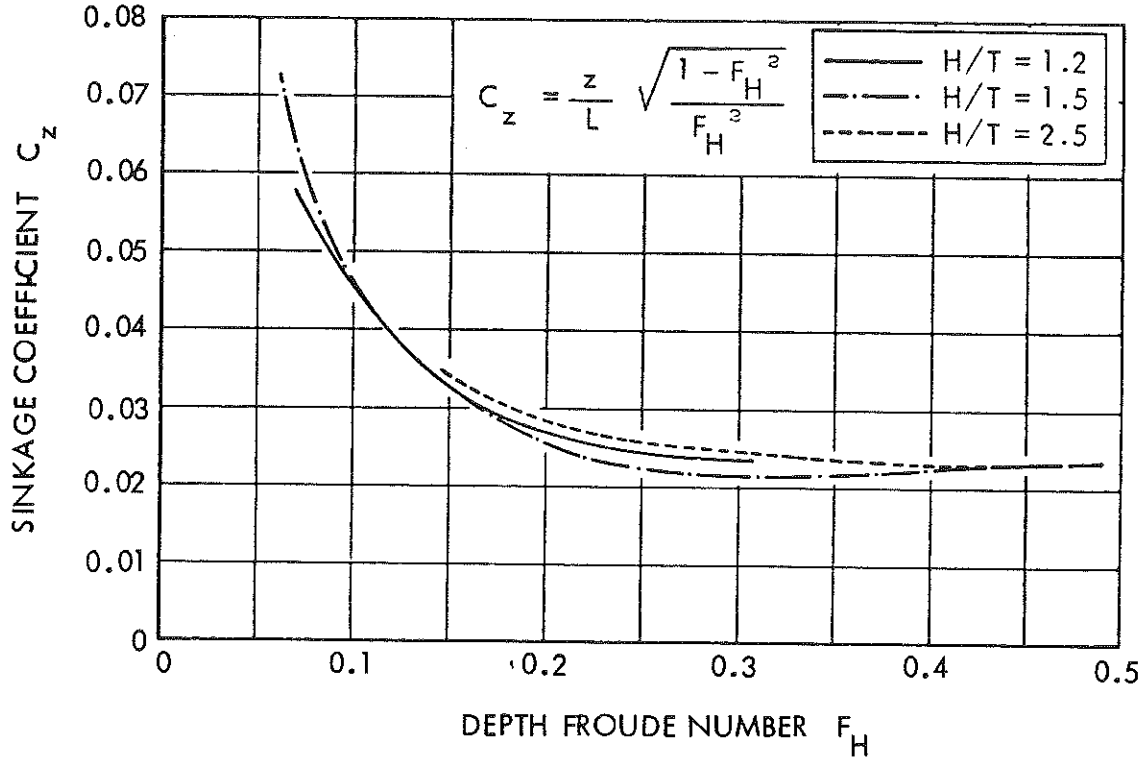

a) Nondimensional Sinkage Coefficient C_z

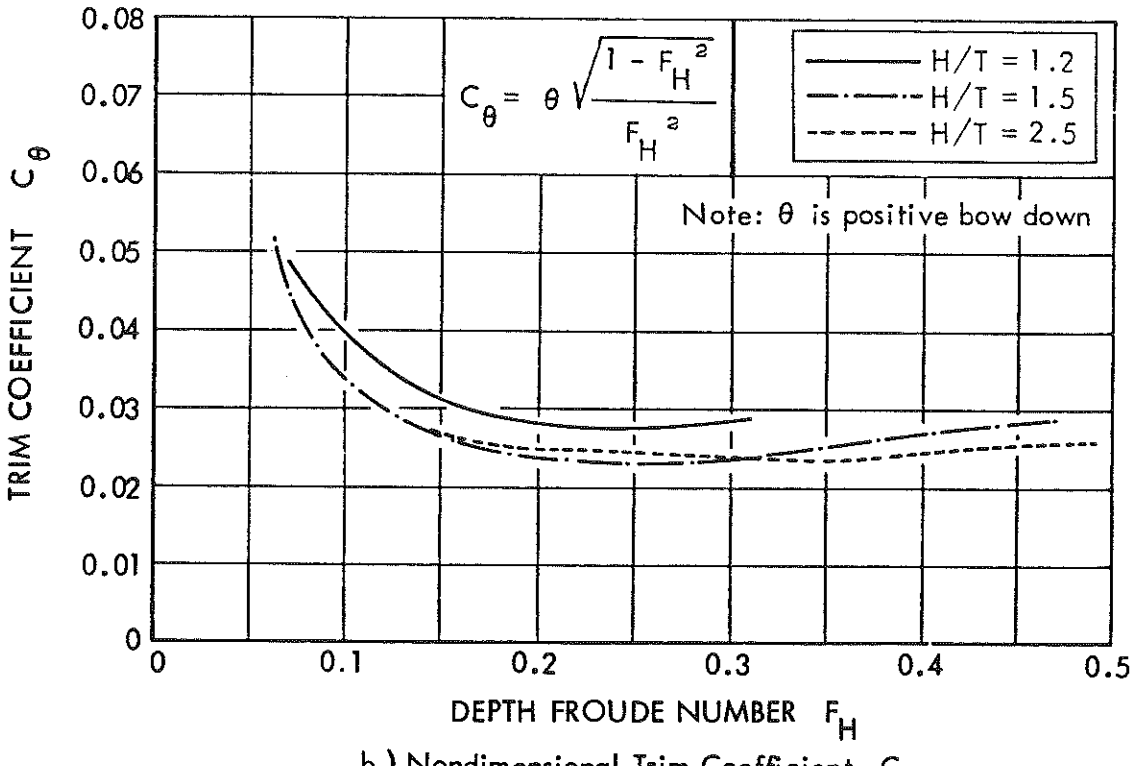

b) Nondimensional Trim Coefficient C_θ

FIGURE 7-13 - SHIP E - SINKAGE AND TRIM CHARACTERISTICS

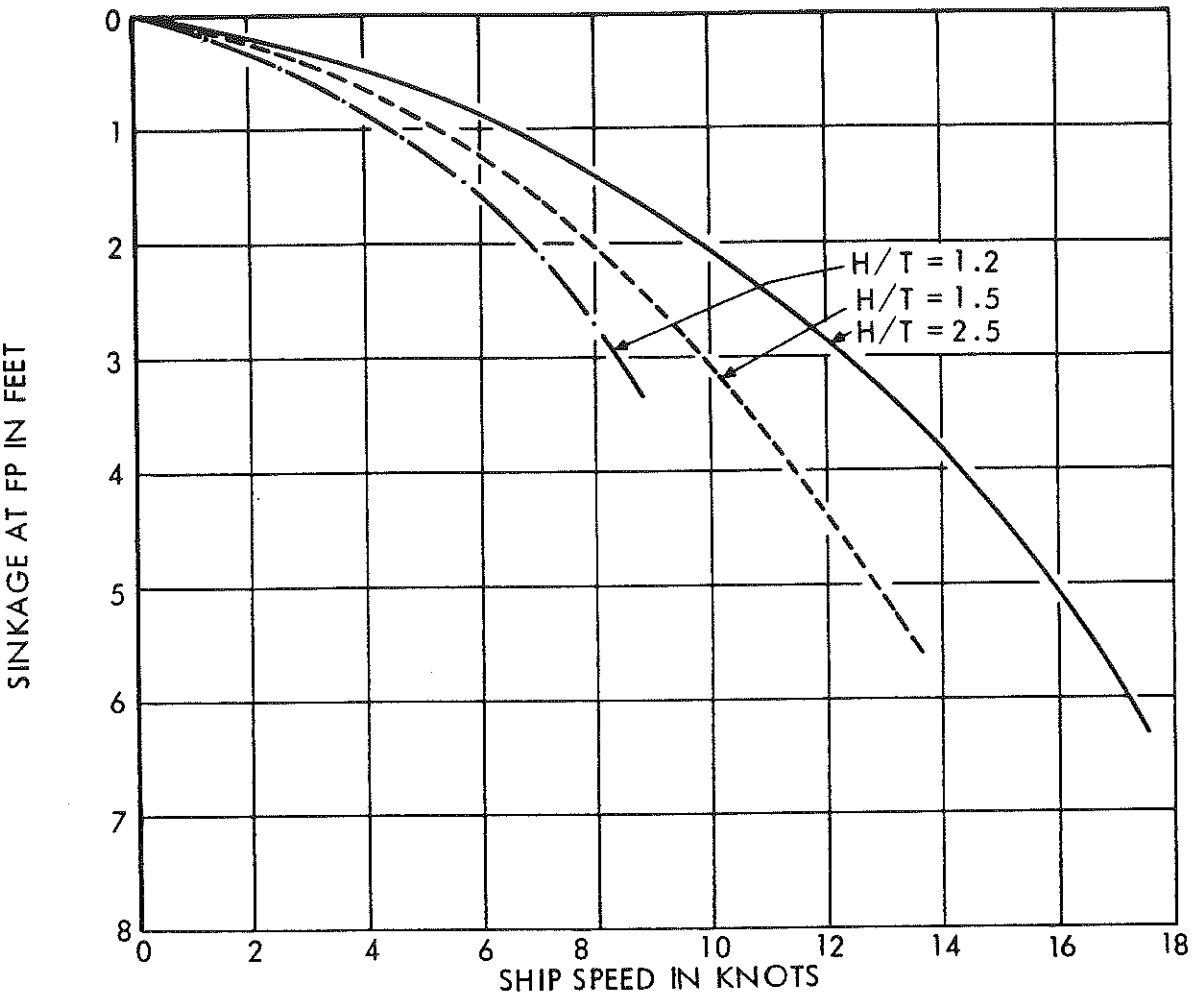

c) Sinkage at Bow

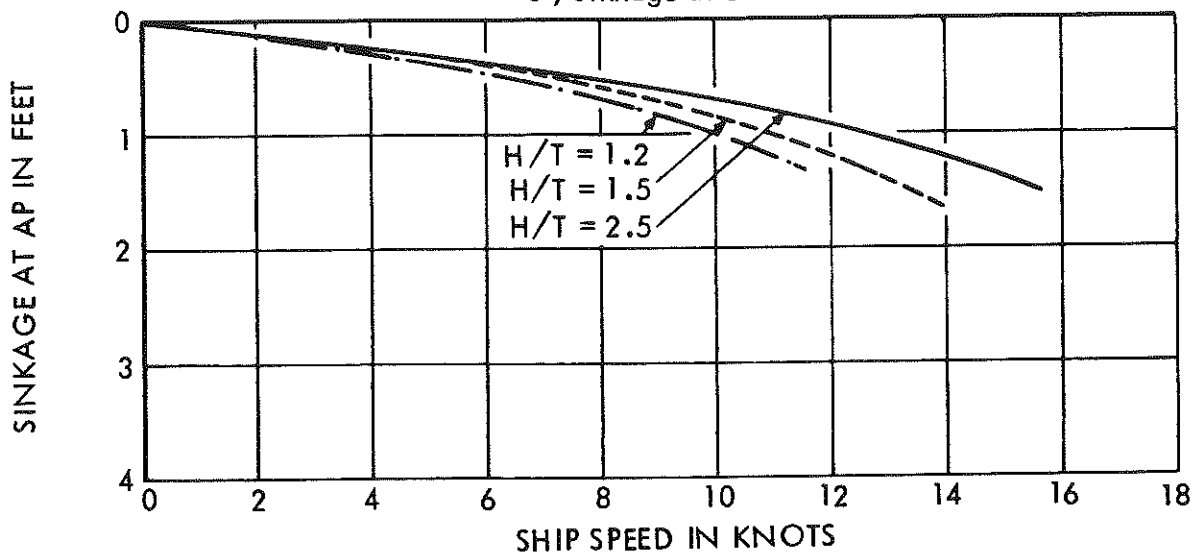

d) Sinkage at Stern

FIGURE 7-13 - CONCLUDED

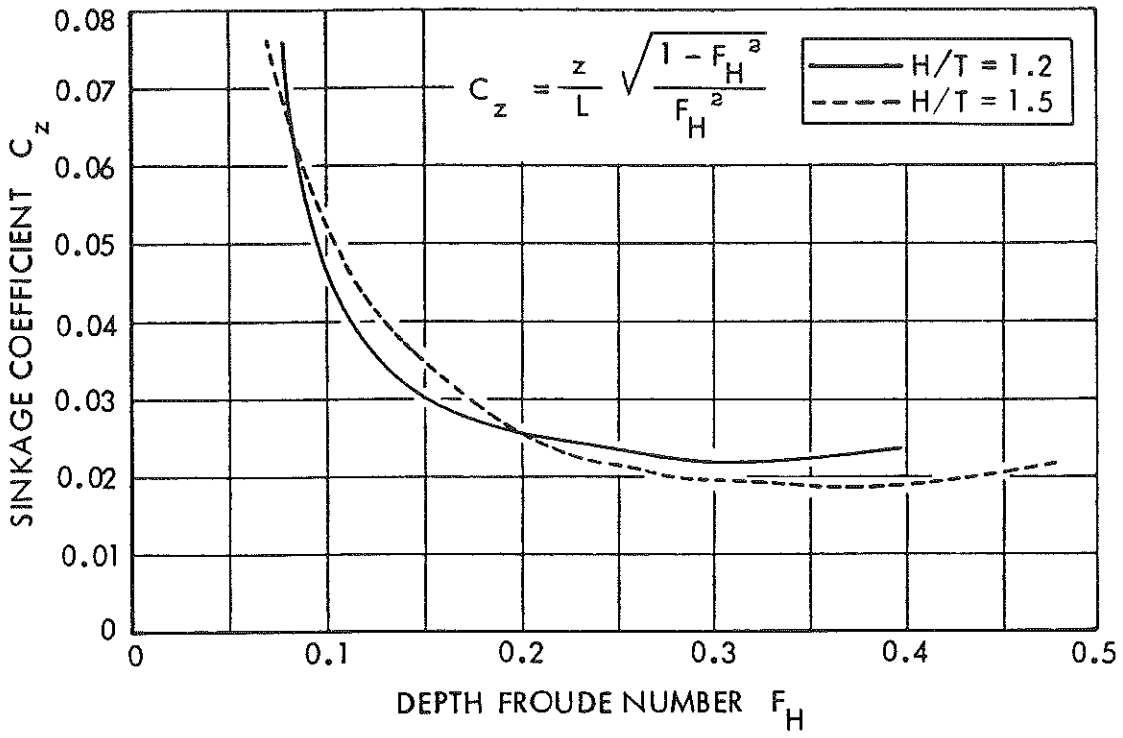

a) Nondimensional Sinkage Coefficient C_z

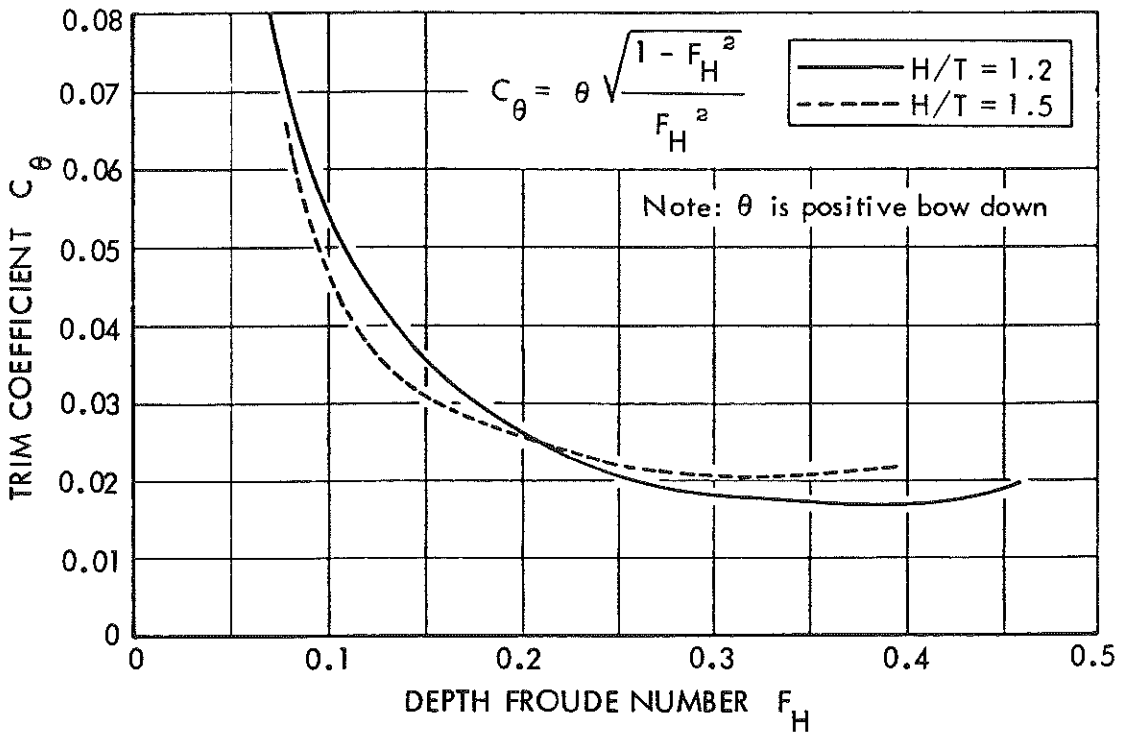

b) Nondimensional Trim Coefficient C_θ

FIGURE 7-14 - SHIP K - SINKAGE AND TRIM CHARACTERISTICS

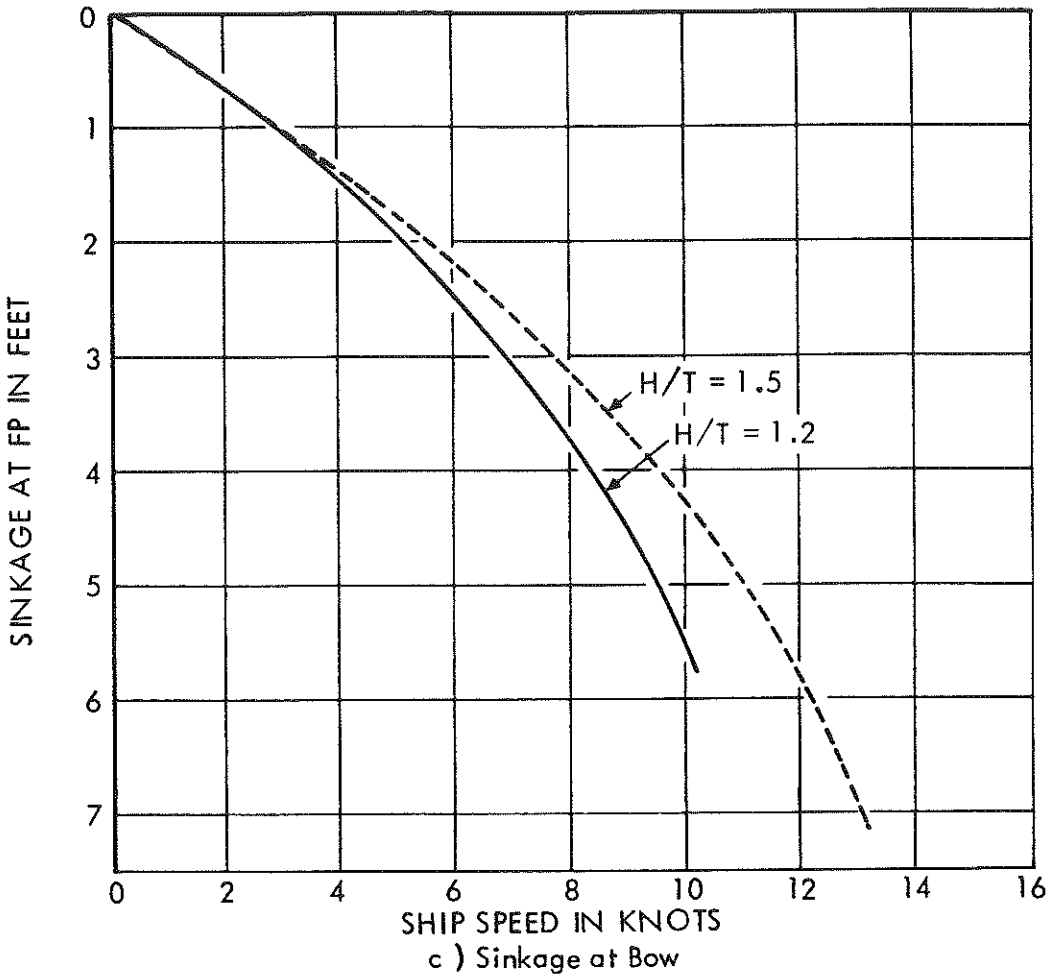

c) Sinkage at Bow

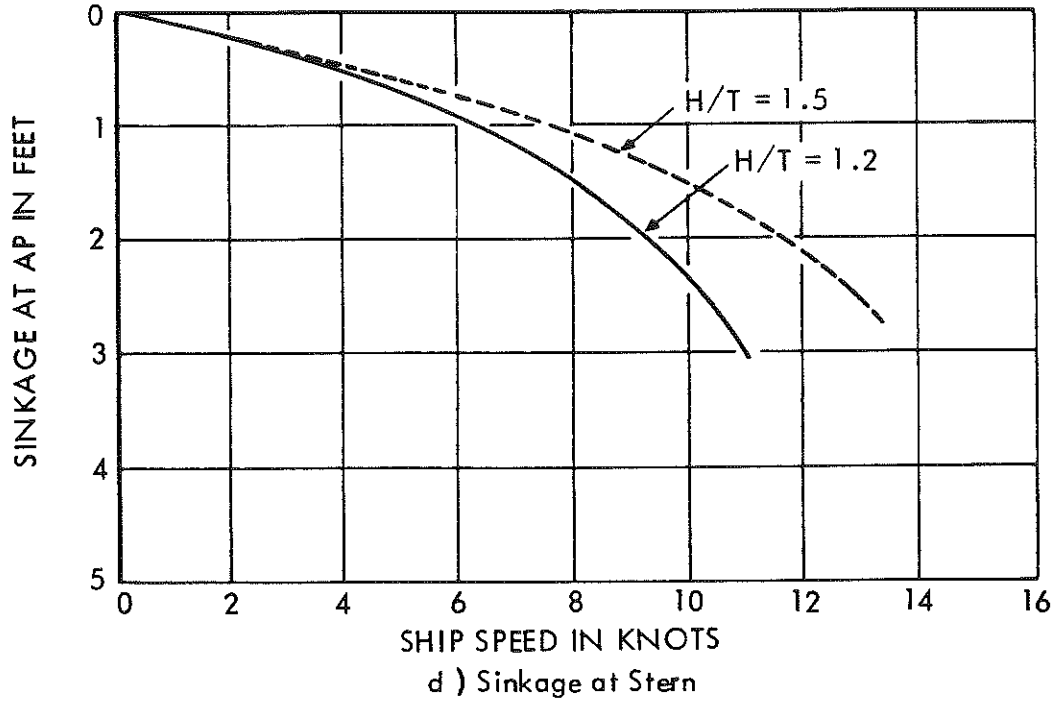

d) Sinkage at Stern

FIGURE 7-14 - CONCLUDED

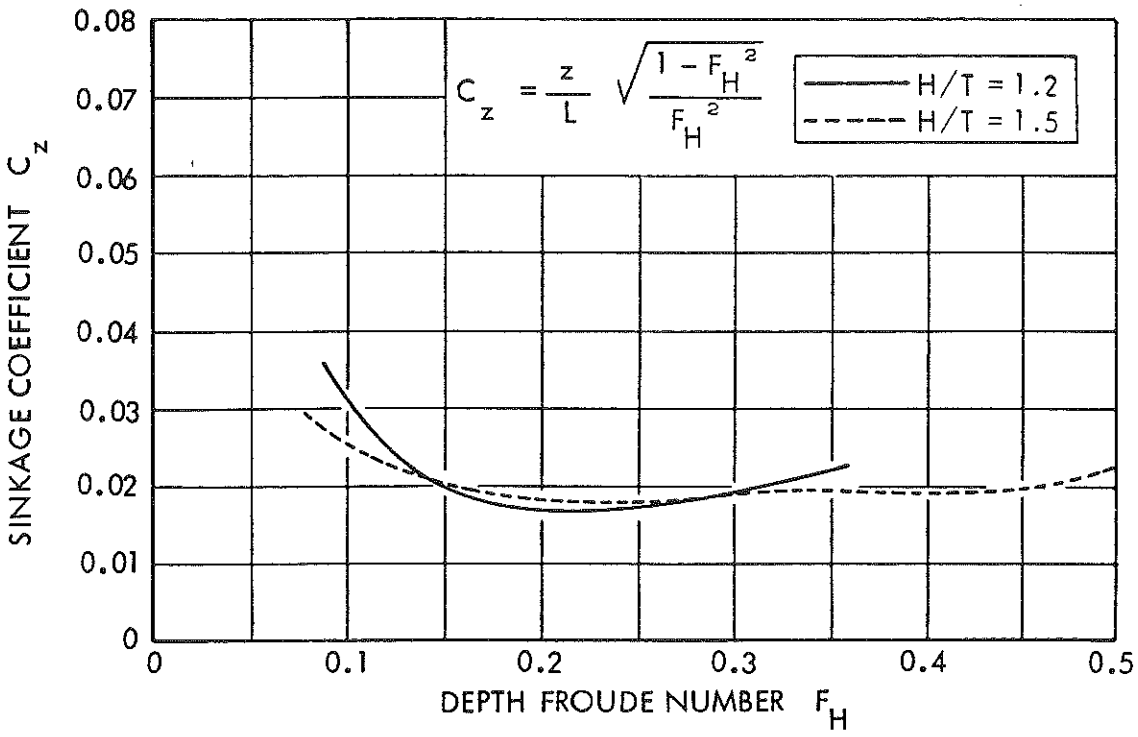

a) Nondimensional Sinkage Coefficient C_z

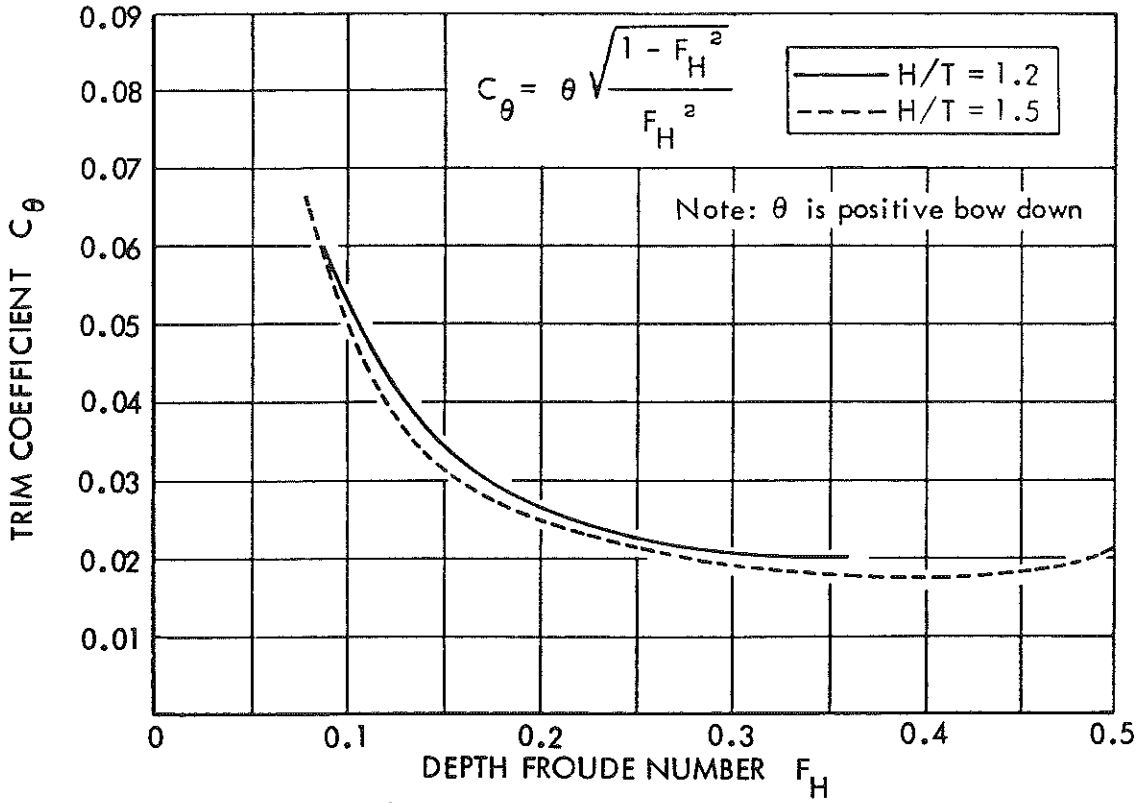

b) Nondimensional Trim Coefficient C_θ

FIGURE 7-15 - SHIP L - SINKAGE AND TRIM CHARACTERISTICS

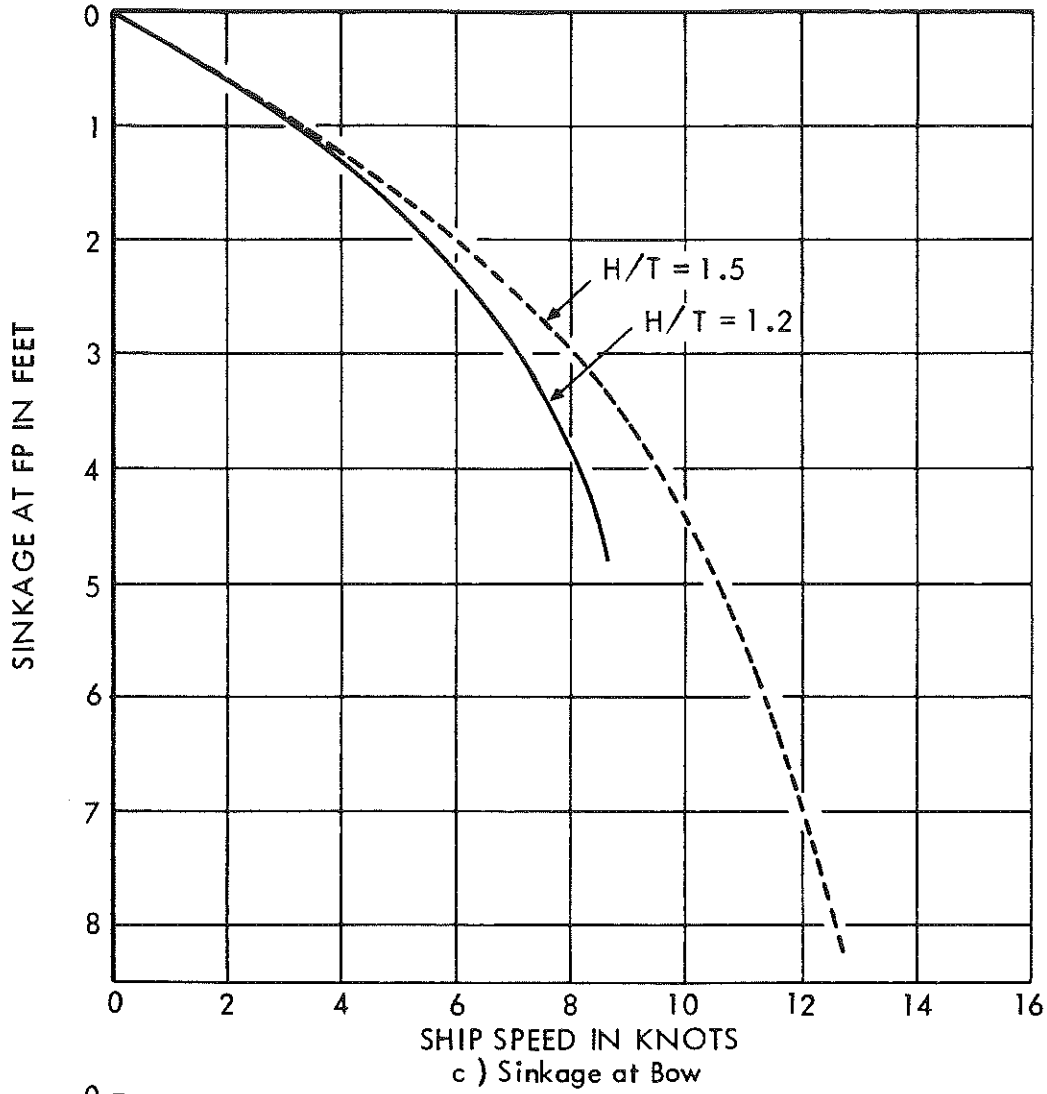

c) Sinkage at Bow

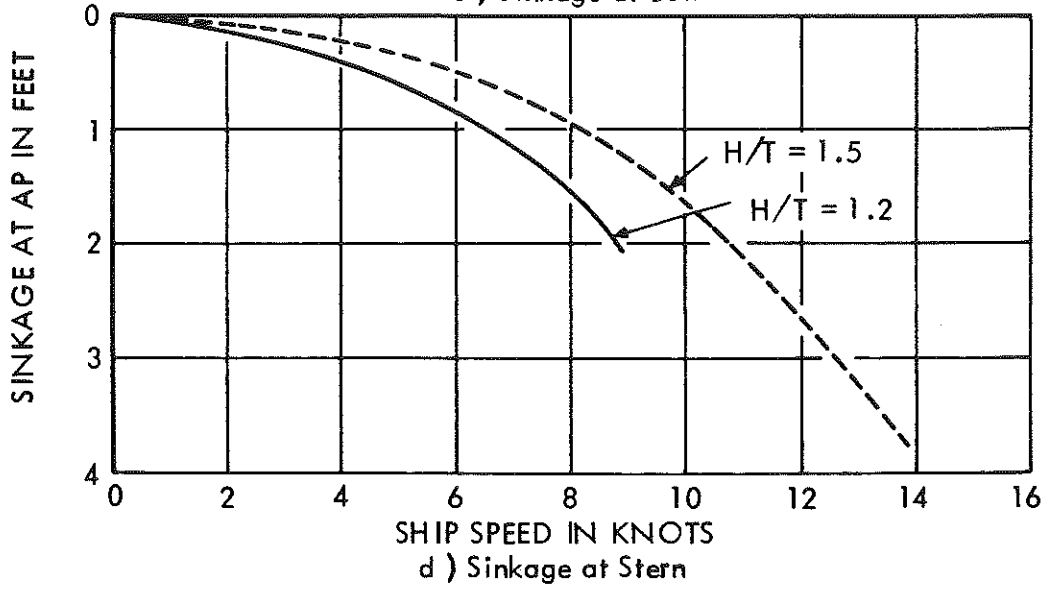

d) Sinkage at Stern

FIGURE 7-15 - CONCLUDED

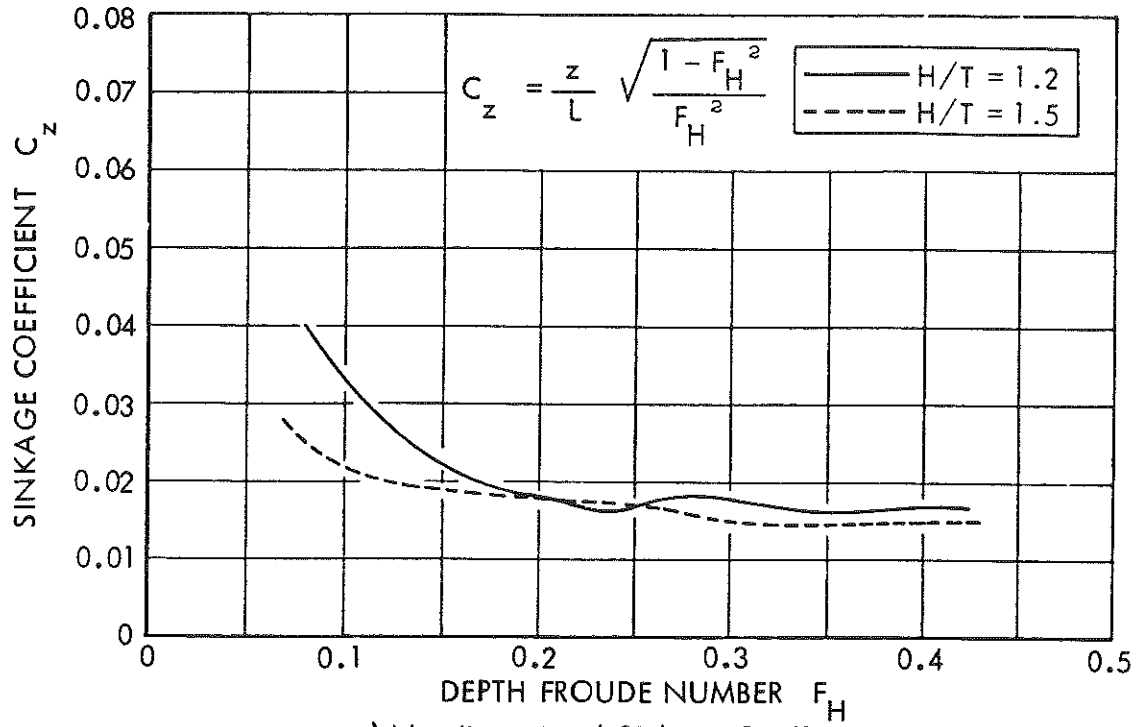

a) Nondimensional Sinkage Coefficient C_θ

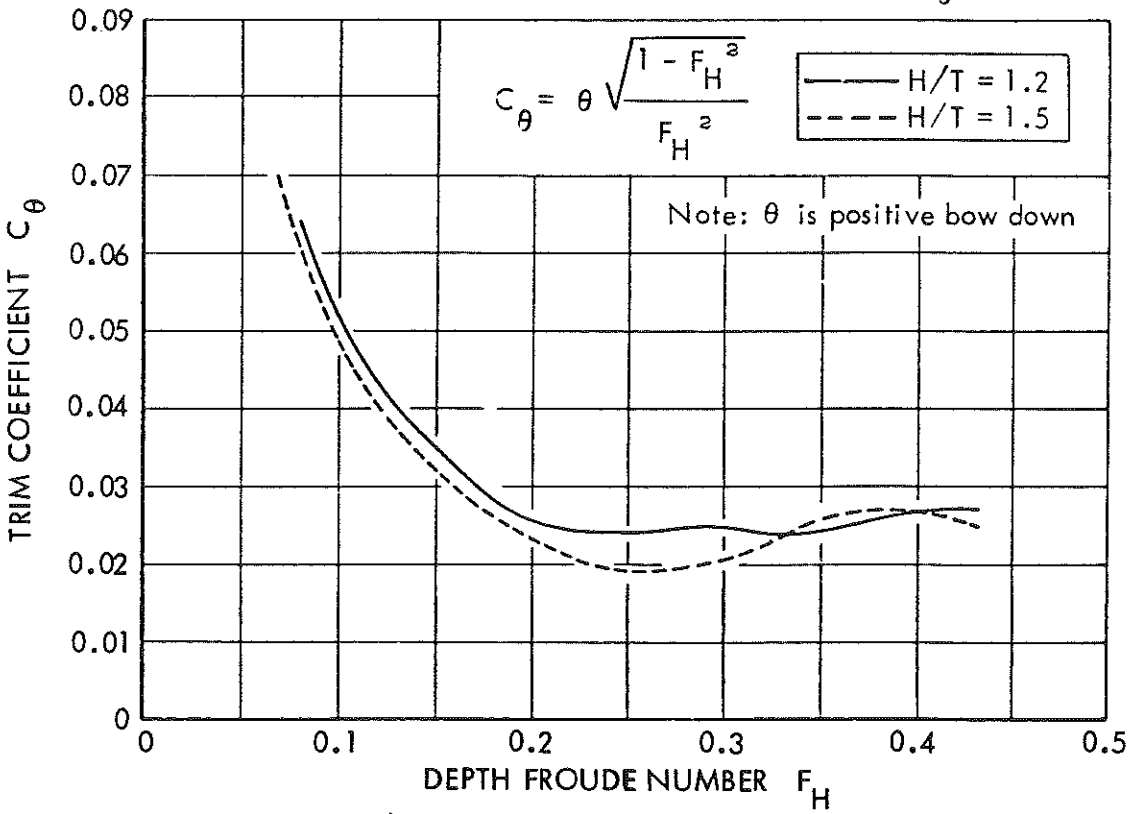

b) Nondimensional Trim Coefficient C_θ

FIGURE 7-16 - SHIP H - SINKAGE AND TRIM CHARACTERISTICS

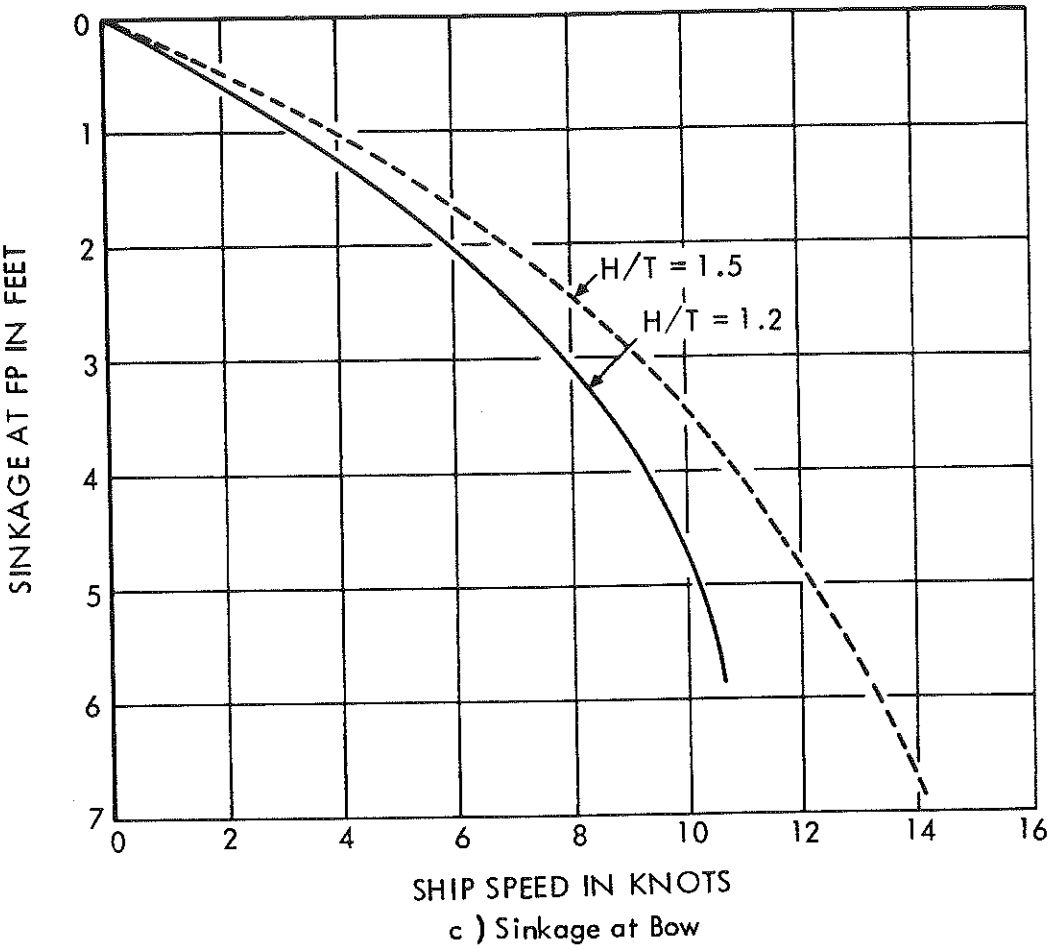

c) Sinkage at Bow

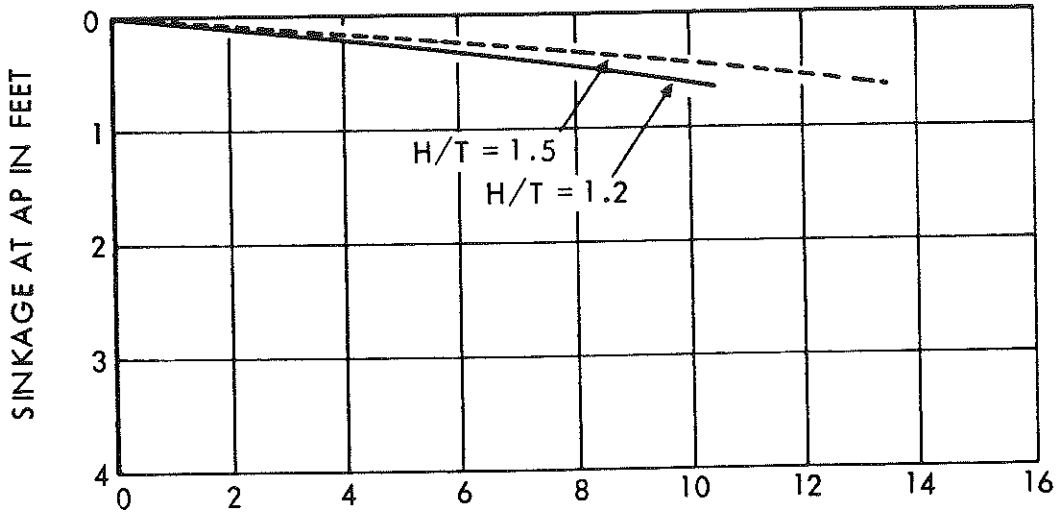

d) Sinkage at Stern

FIGURE 7-16 - CONCLUDED

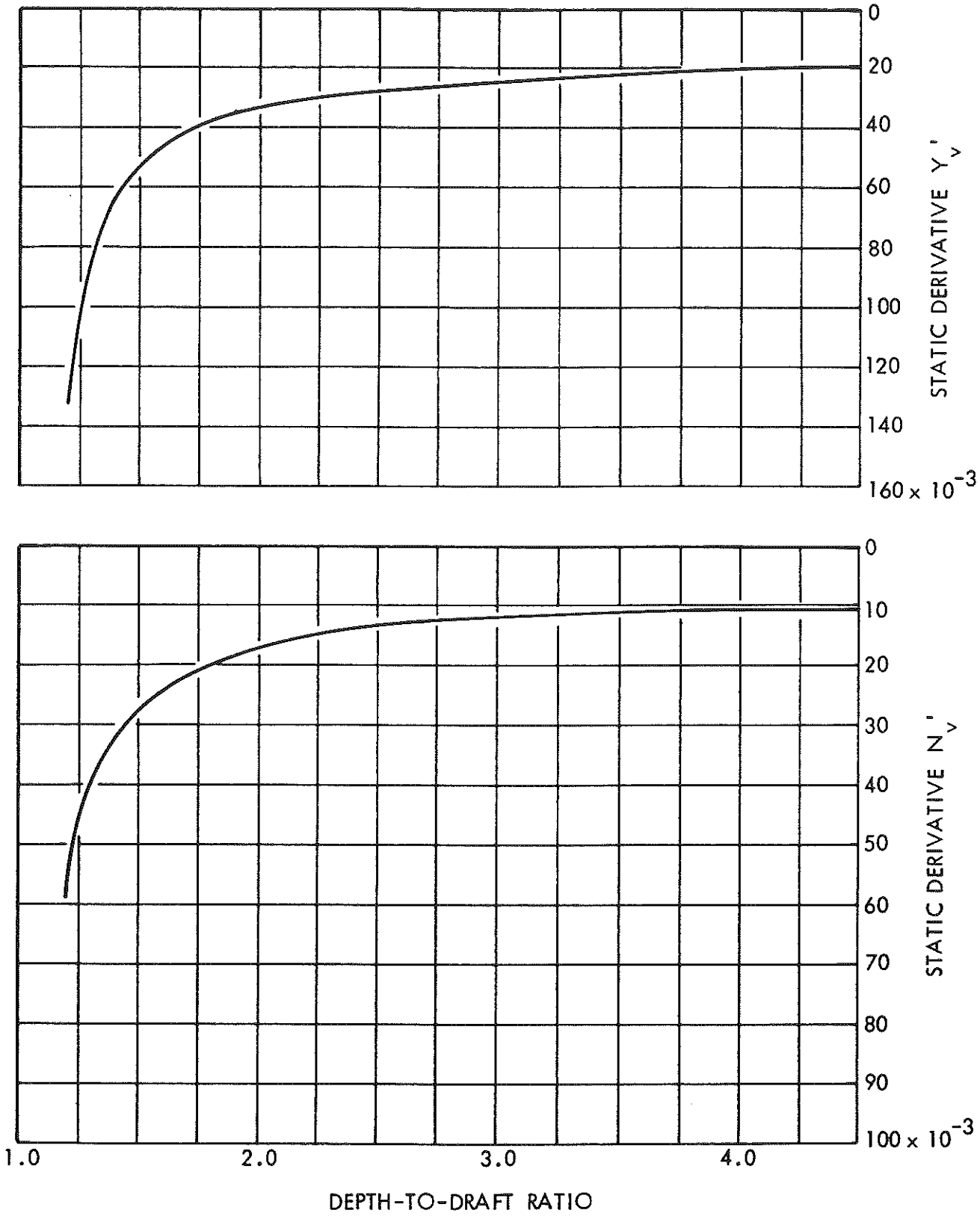

FIGURE 7-17 - SHIP E - EFFECT OF H/T VARIATION ON STATIC, ROTARY, AND ACCELERATION DERIVATIVES

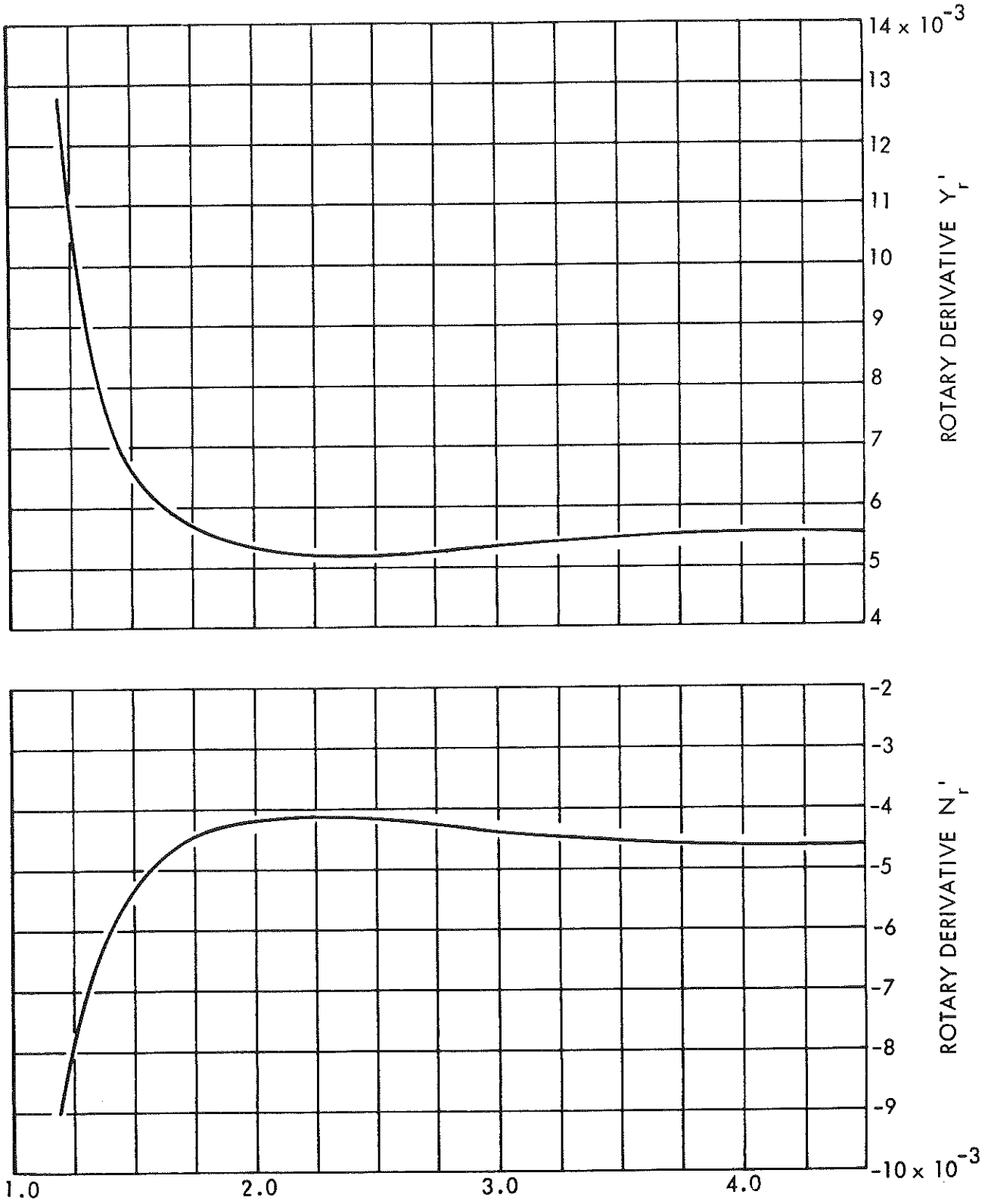

FIGURE 7-17 - CONTINUED

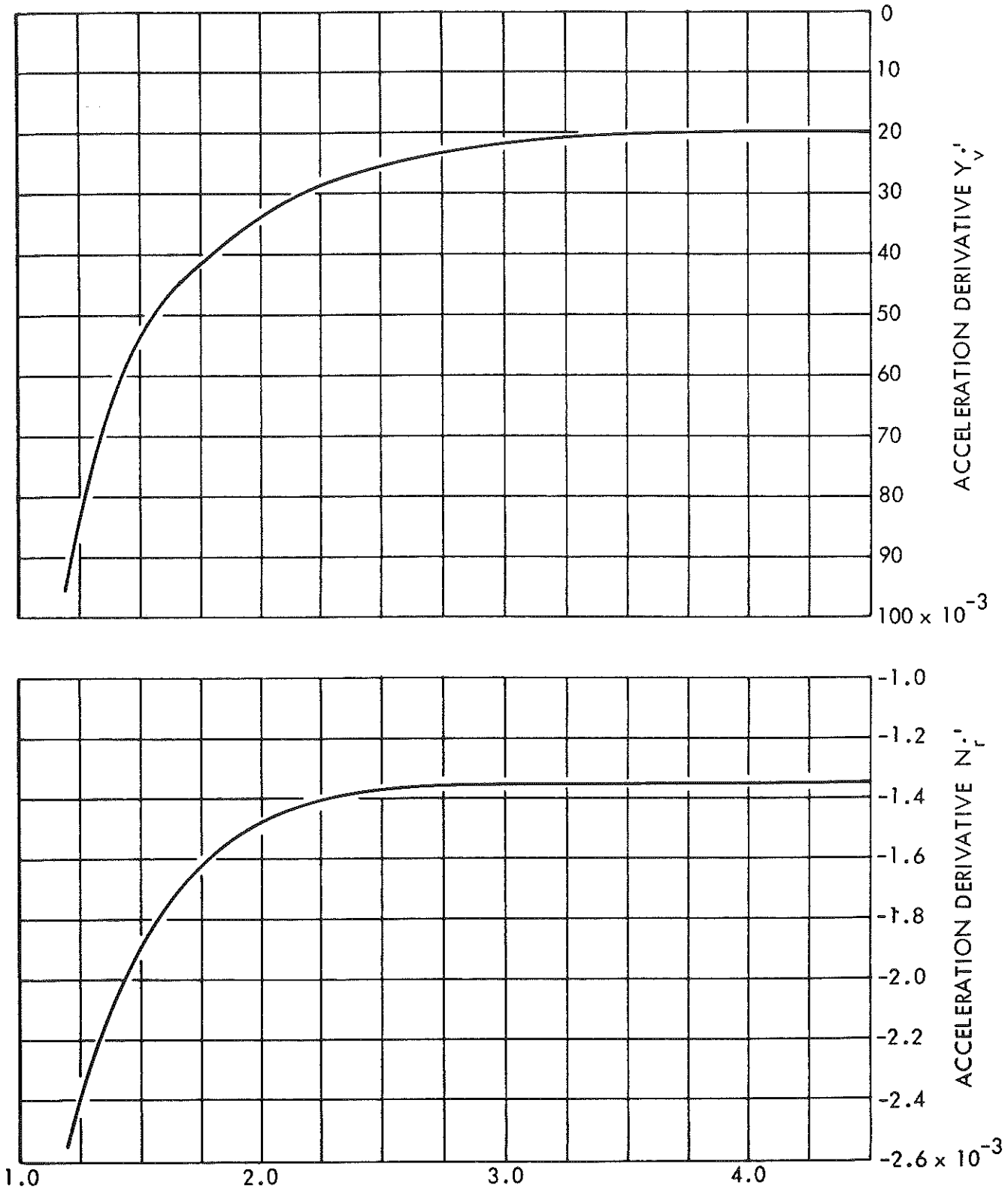

FIGURE 7-17 - CONCLUDED

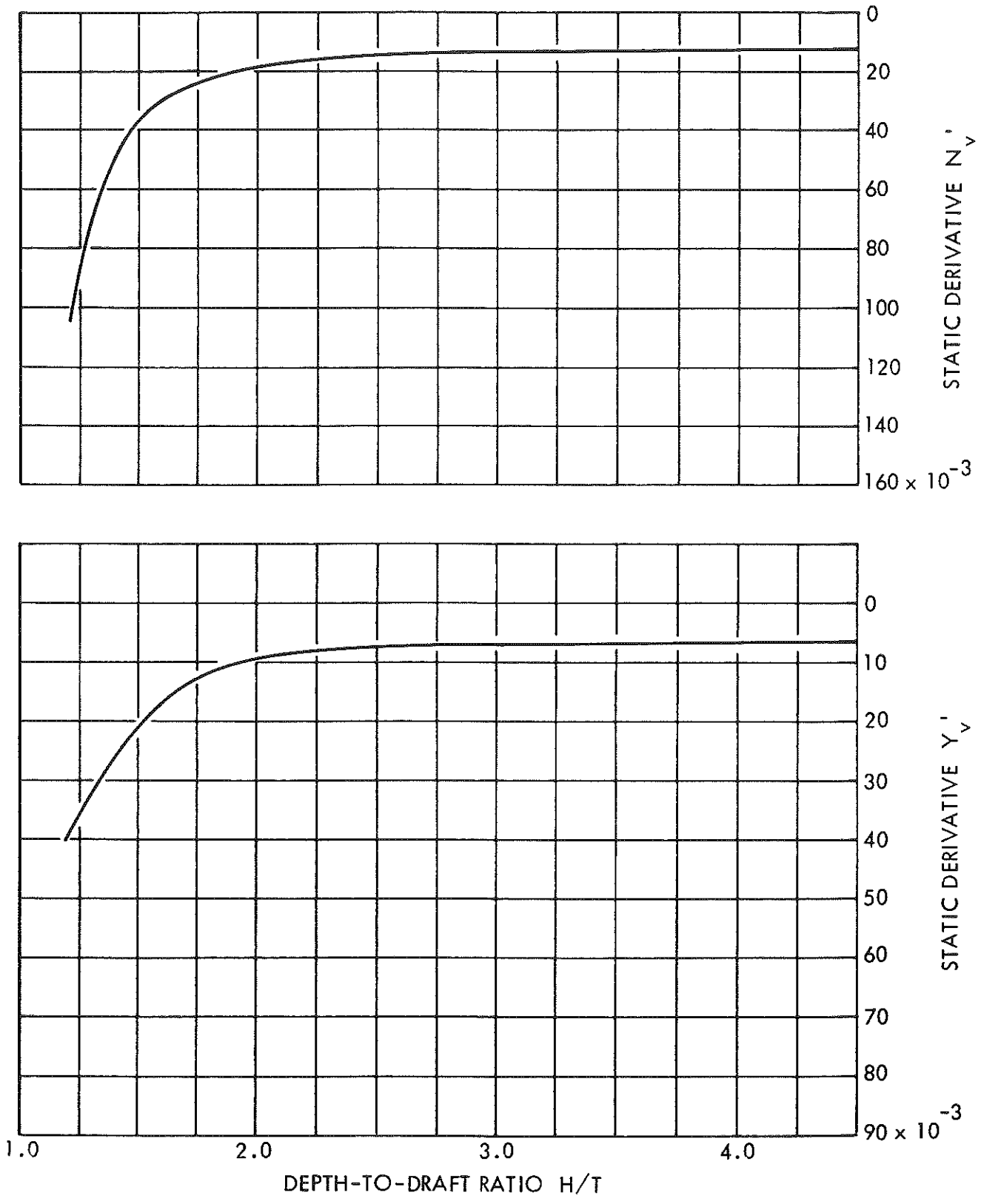

FIGURE 7-18 - SHIP K - EFFECT OF H/T VARIATION ON STATIC, ROTARY, AND ACCELERATION DERIVATIVES

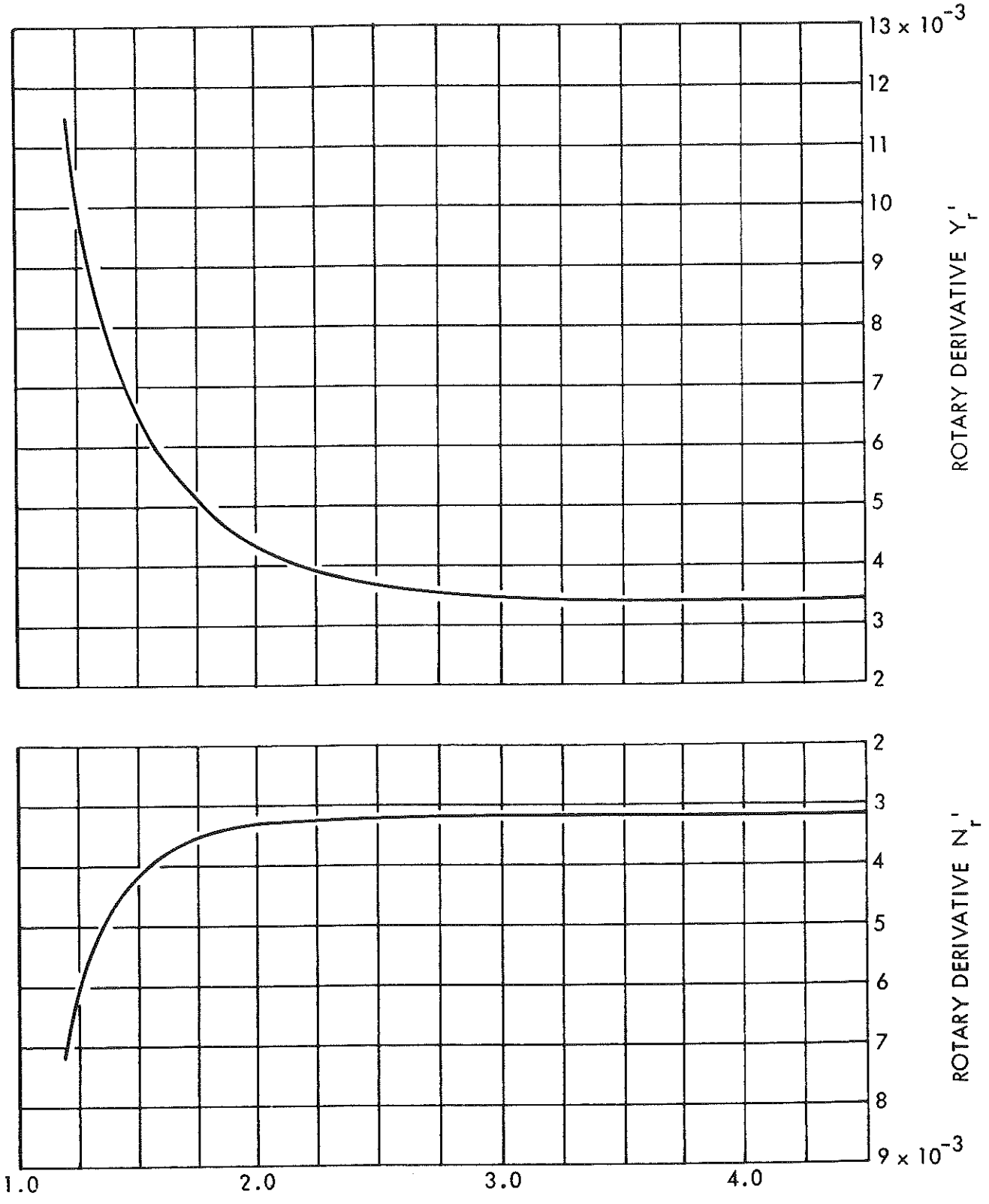

FIGURE 7-18 - CONTINUED

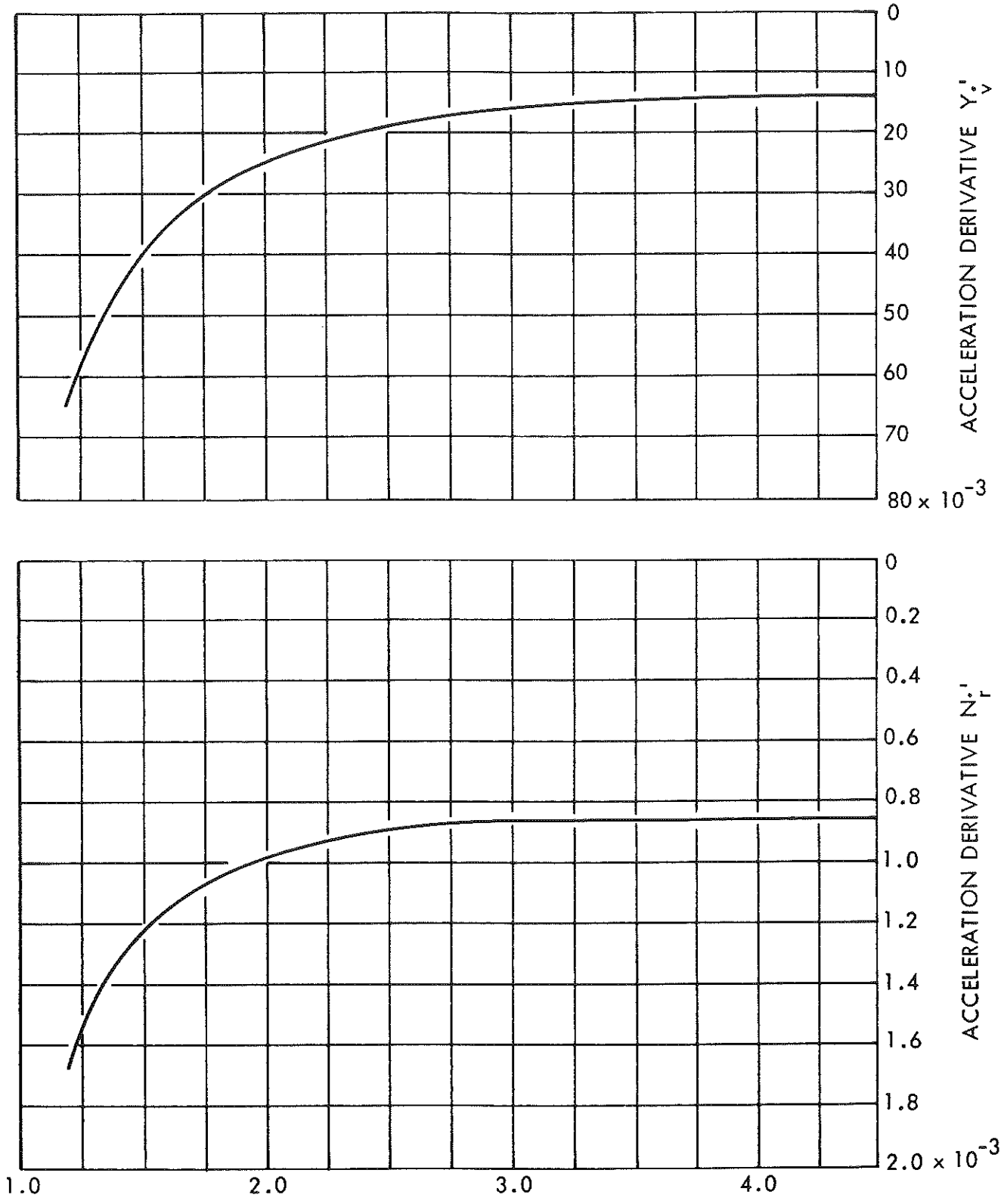

FIGURE 7-18 - CONCLUDED

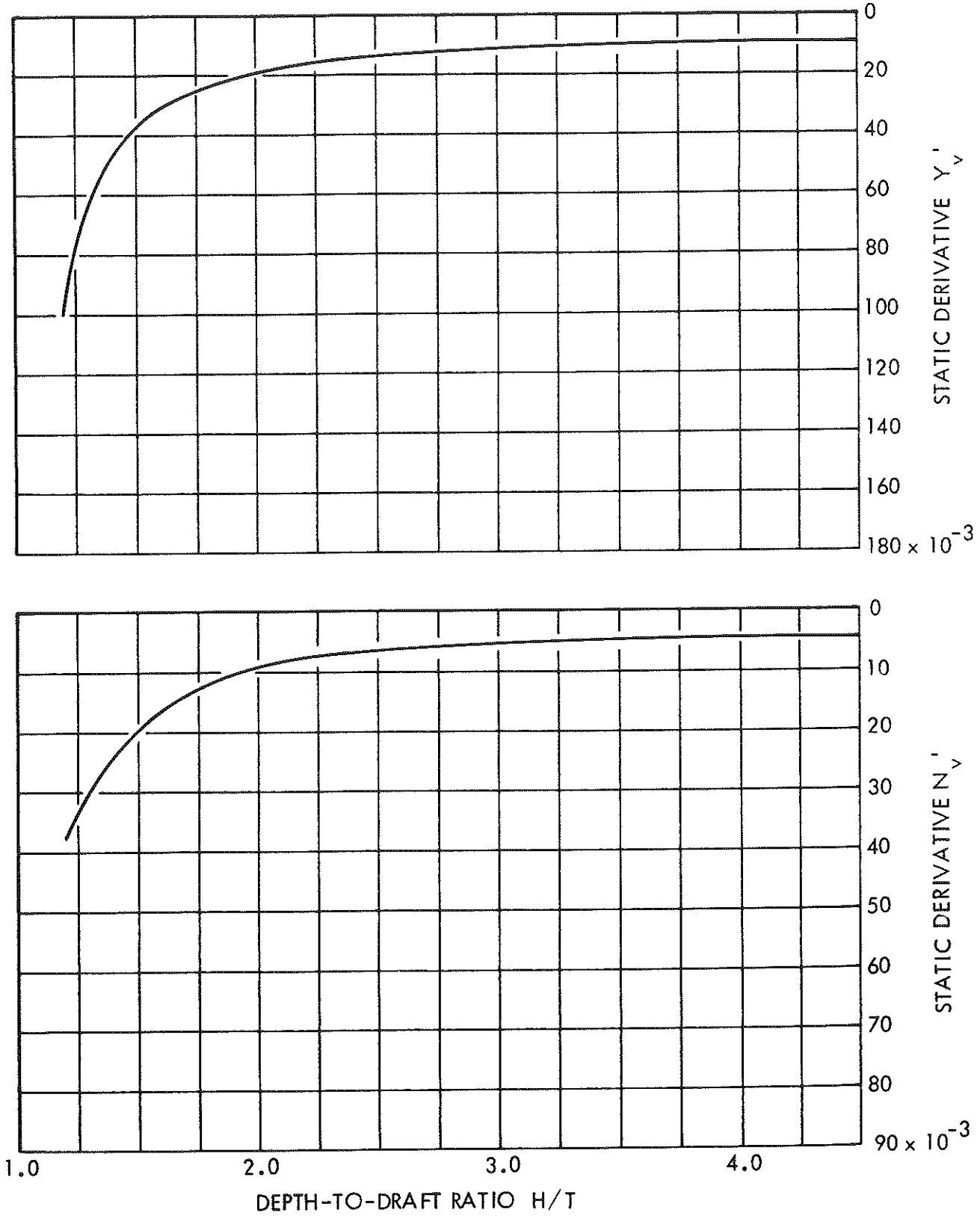

FIGURE 7-19 - SHIP L - EFFECT OF H/T VARIATION ON STATIC, ROTARY, AND ACCELERATION DERIVATIVES

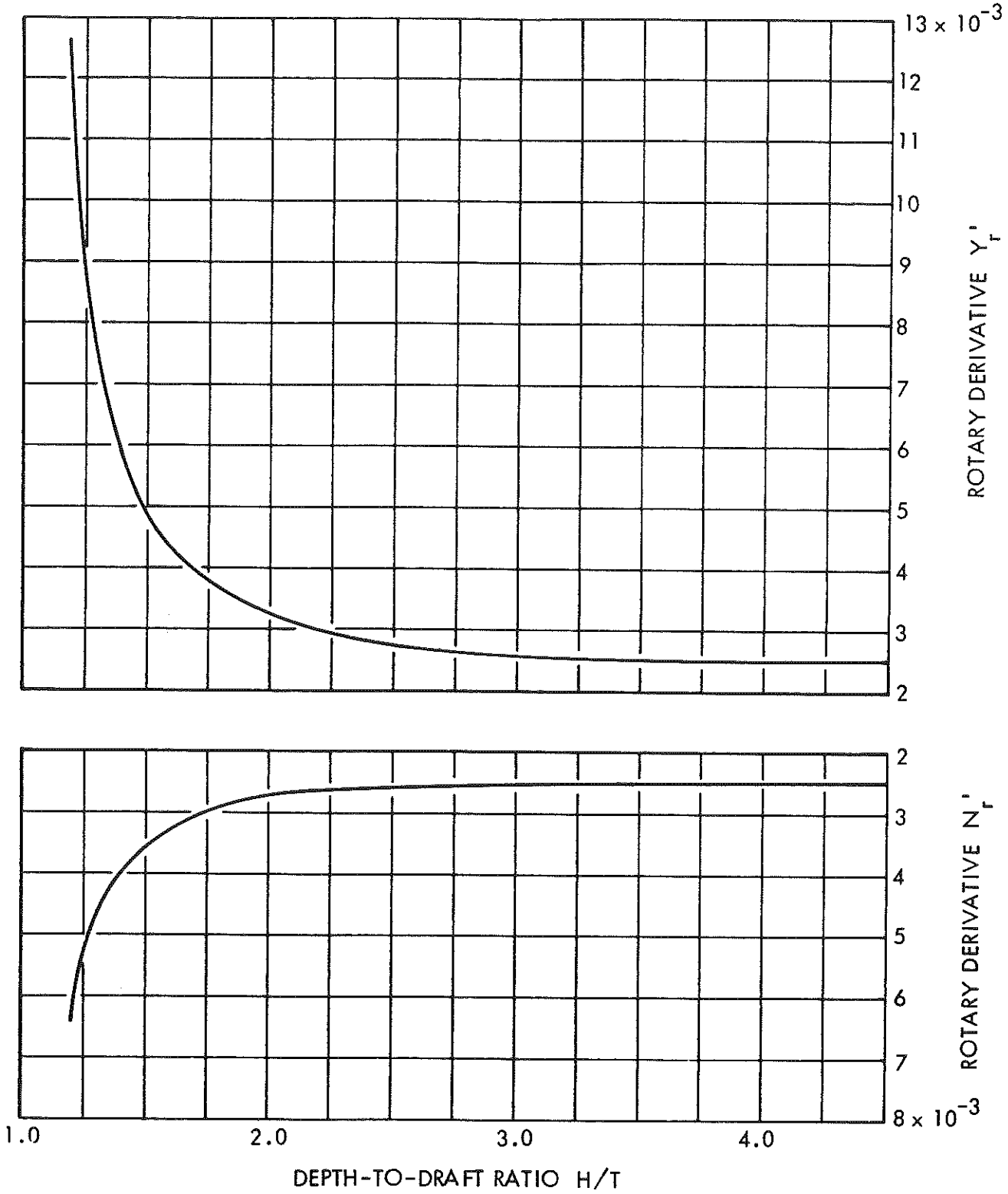

FIGURE 7-19 - CONTINUED

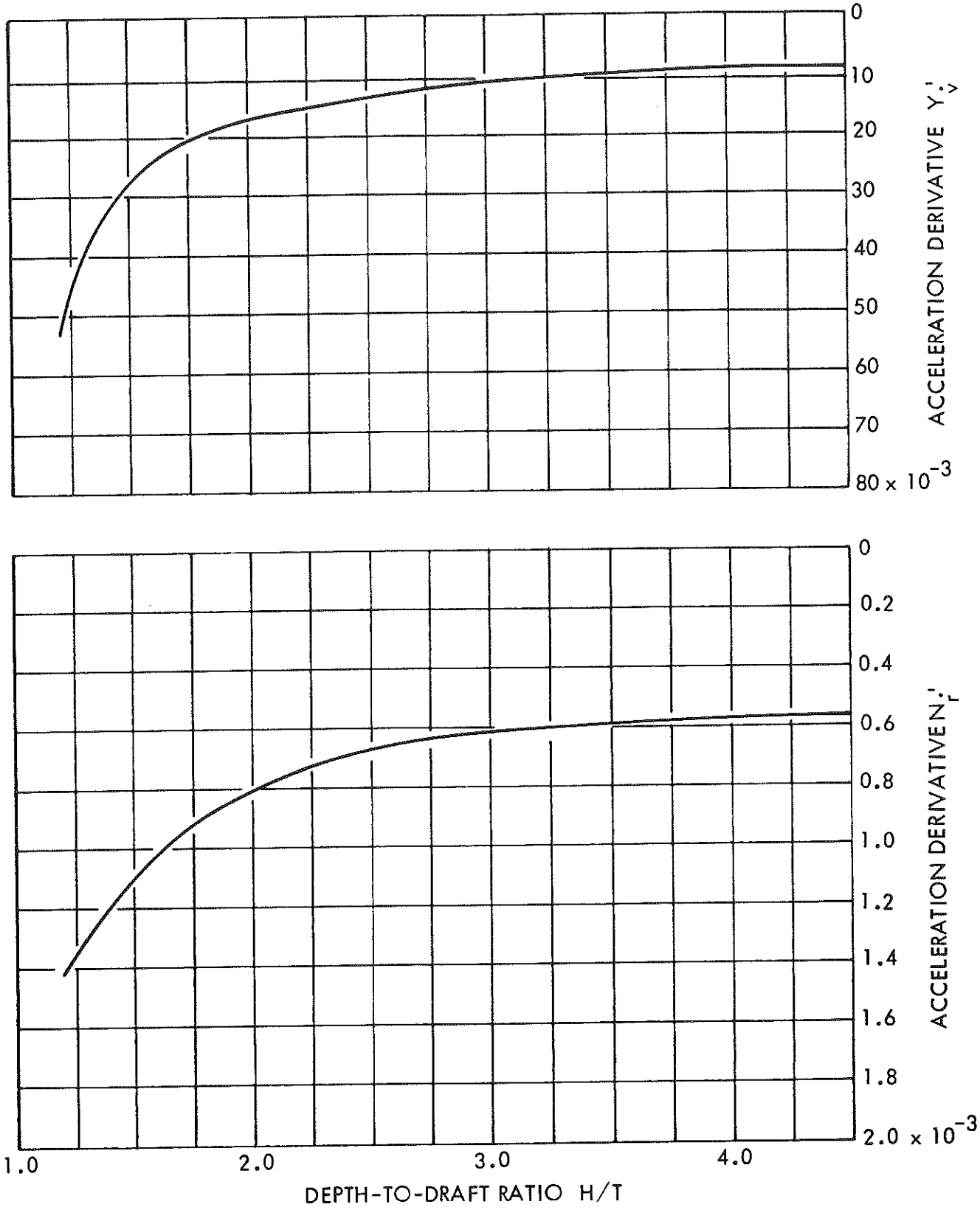

FIGURE 7-19 - CONCLUDED

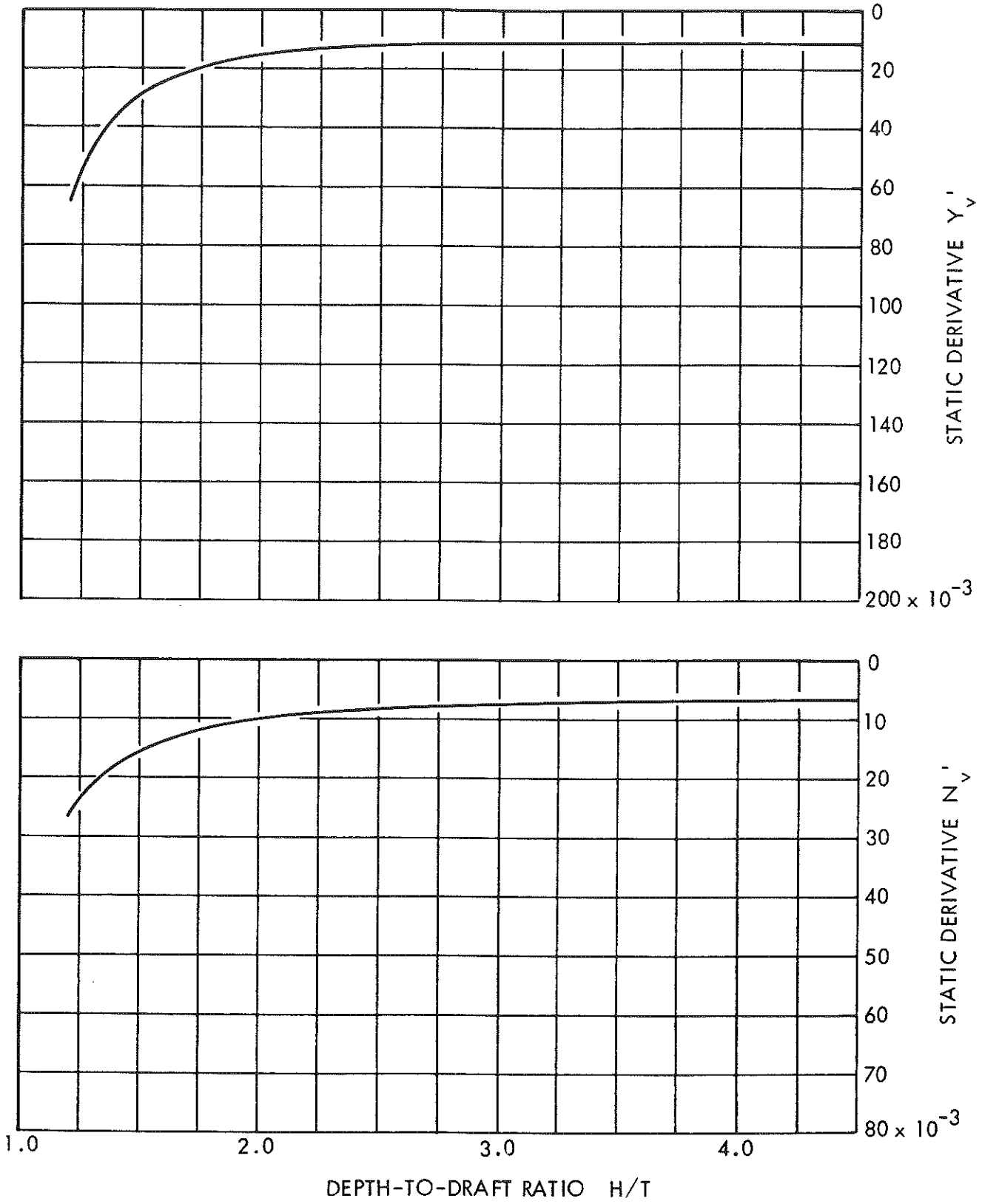

FIGURE 7-20 - SHIP H - EFFECT OF H/T VARIATION ON STATIC, ROTARY, AND ACCELERATION DERIVATIVES

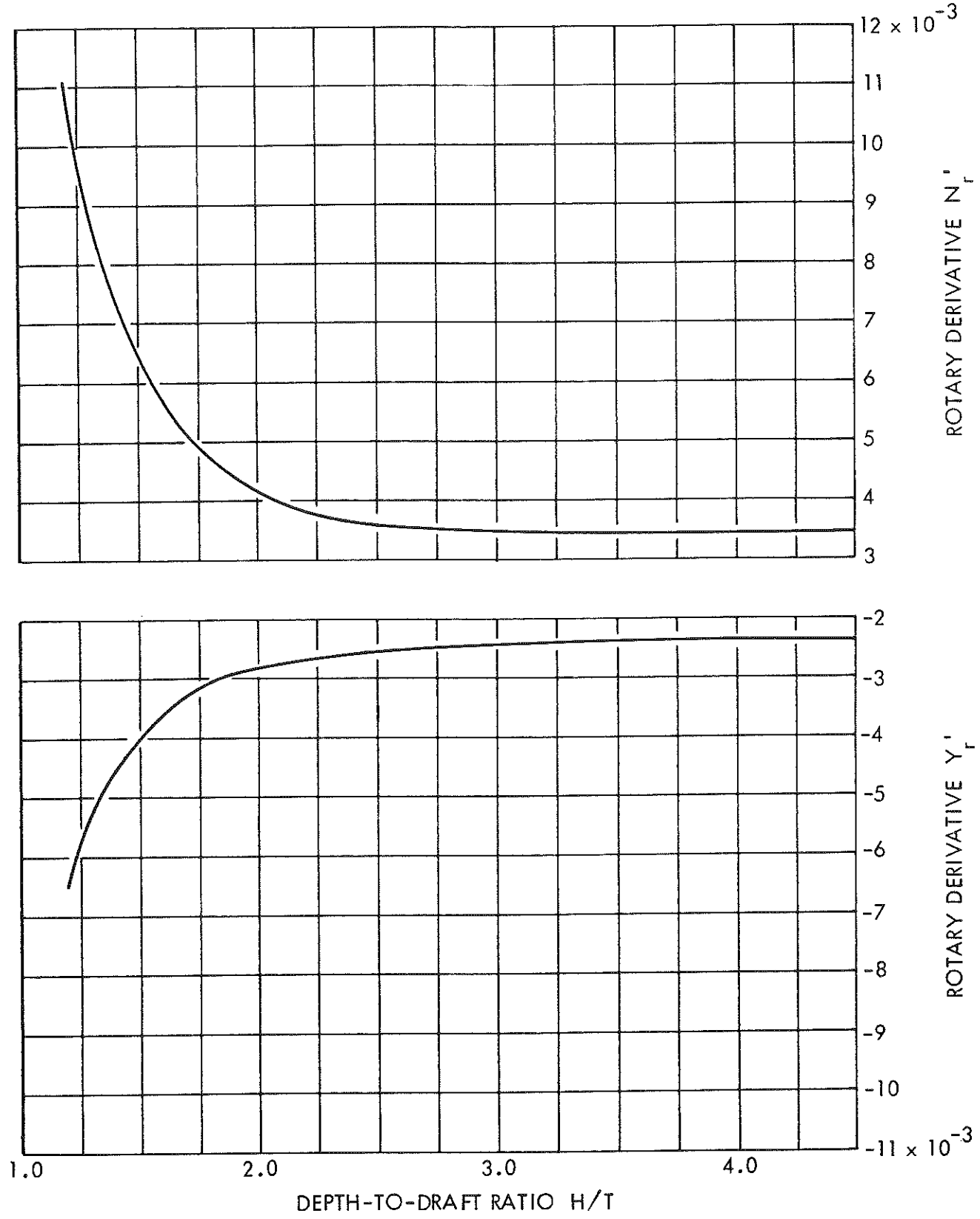

FIGURE 7-20 - CONTINUED

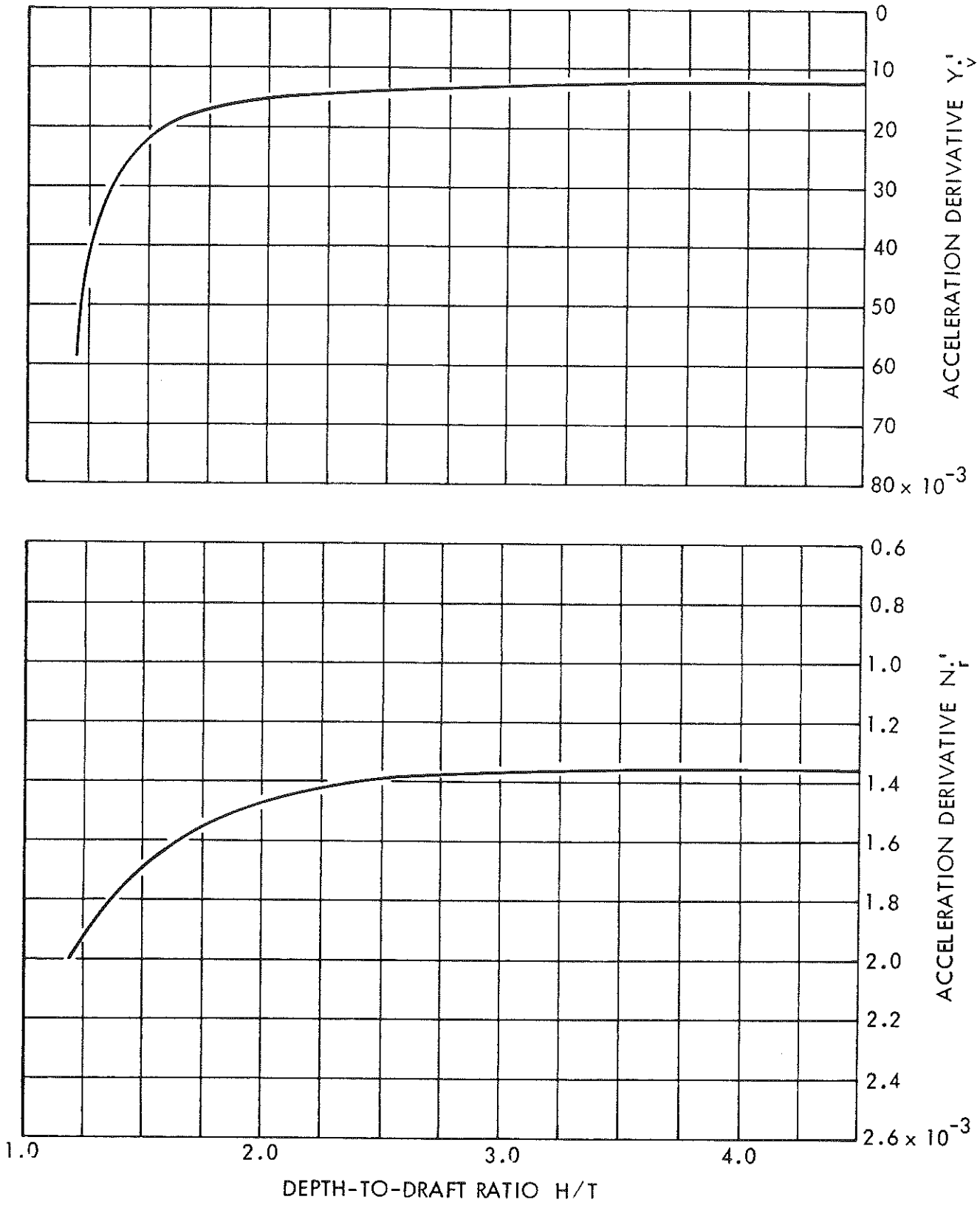

FIGURE 7-20 - CONCLUDED

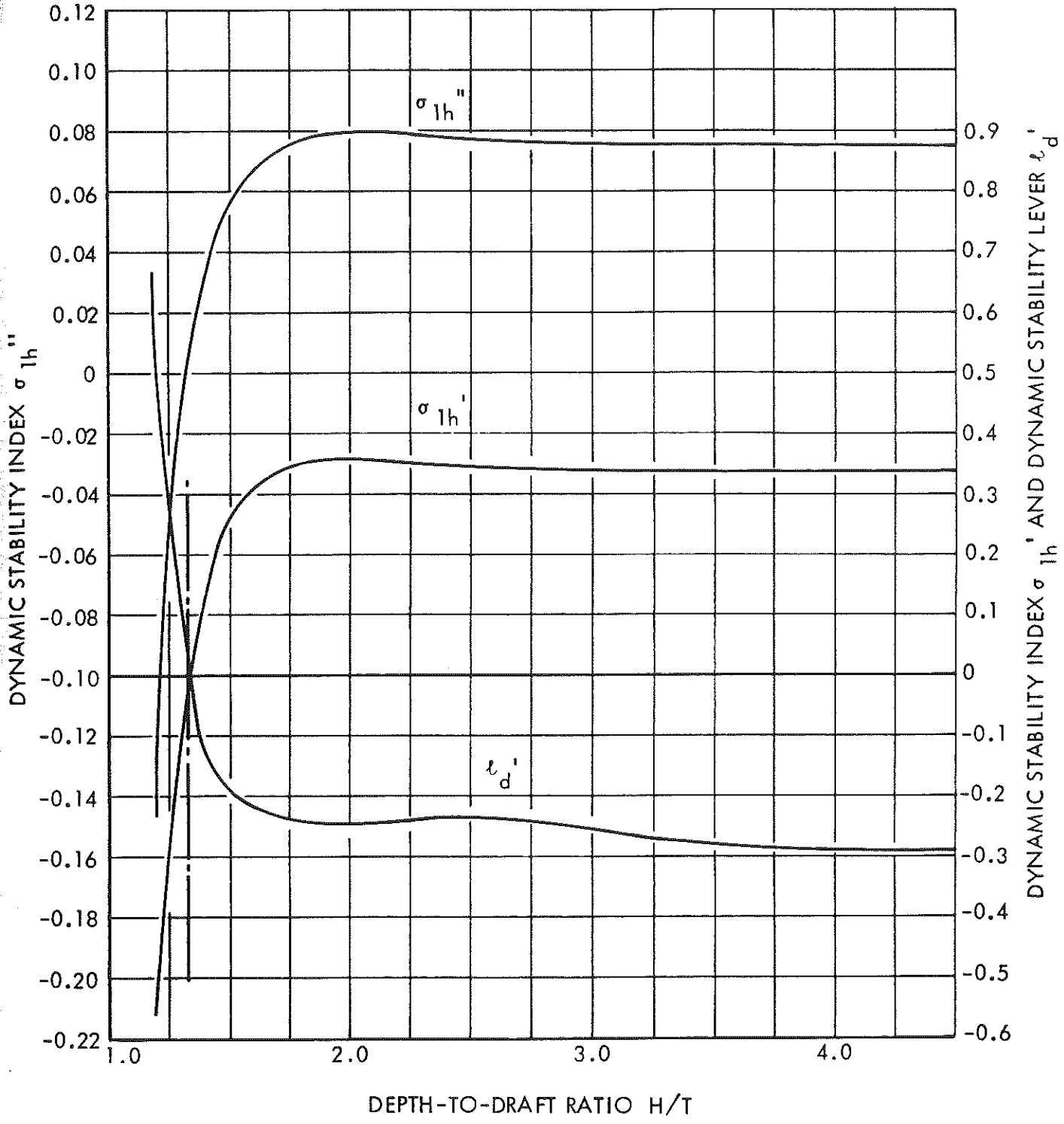

FIGURE 7-21 - SHIP E - EFFECT OF H/T VARIATION ON DYNAMIC STABILITY INDICES

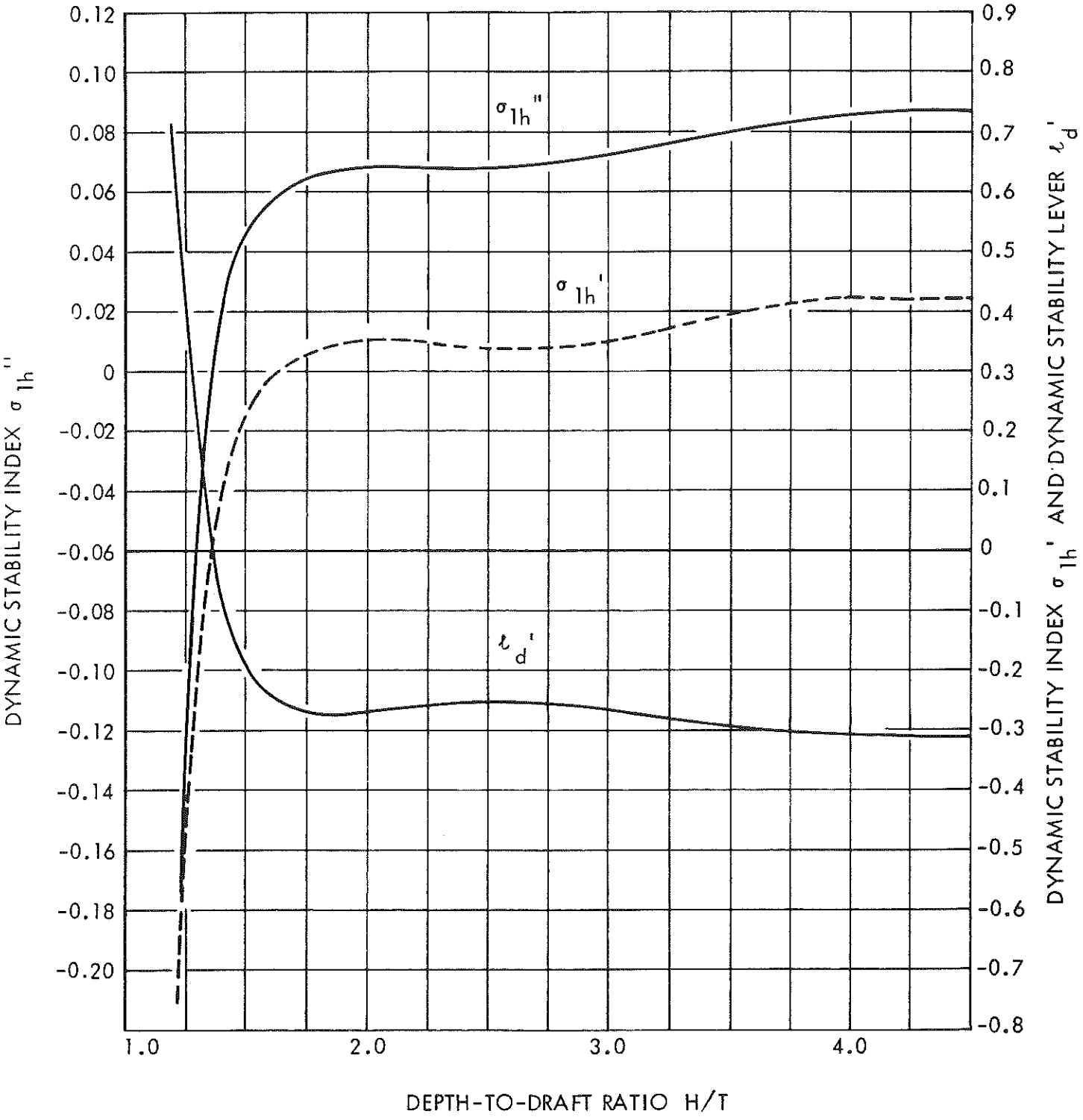

FIGURE 7-22 - SHIP K - EFFECT OF H/T VARIATION ON DYNAMIC STABILITY INDICES

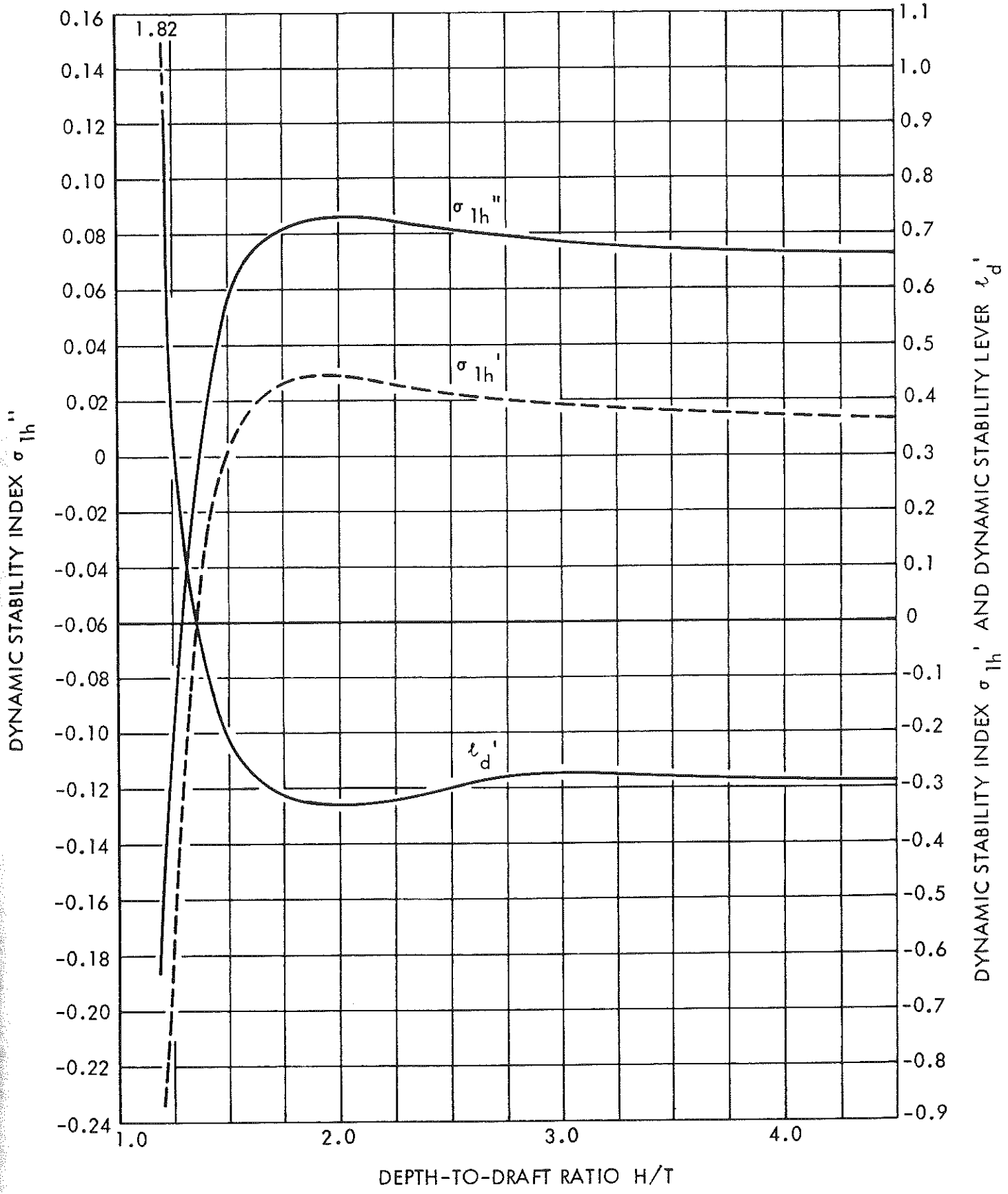

FIGURE 7-23 - SHIP L - EFFECT OF H/T VARIATION ON DYNAMIC STABILITY INDICES

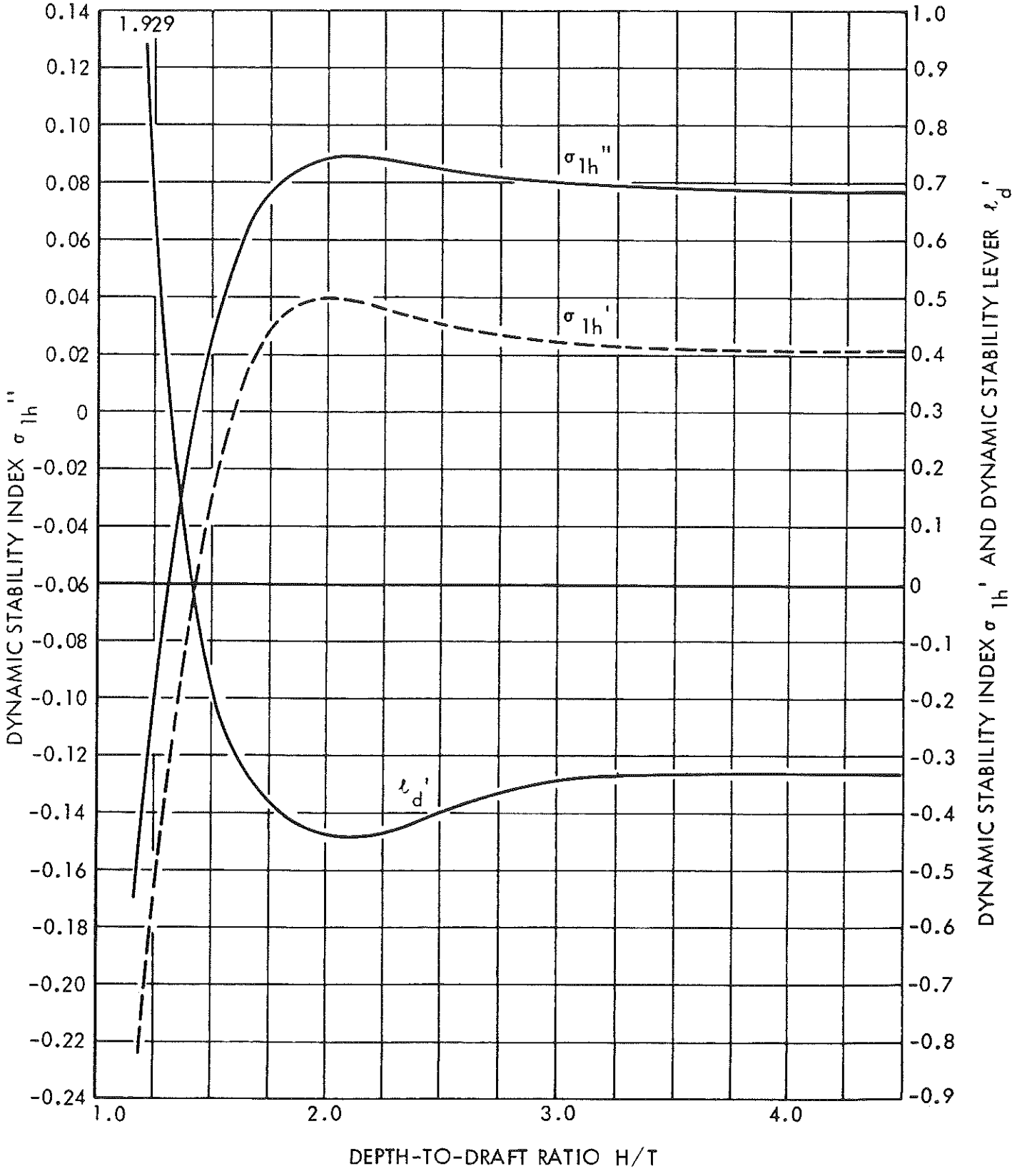

FIGURE 7-24 - SHIP H - EFFECT OF H/T VARIATION ON DYNAMIC STABILITY INDICES

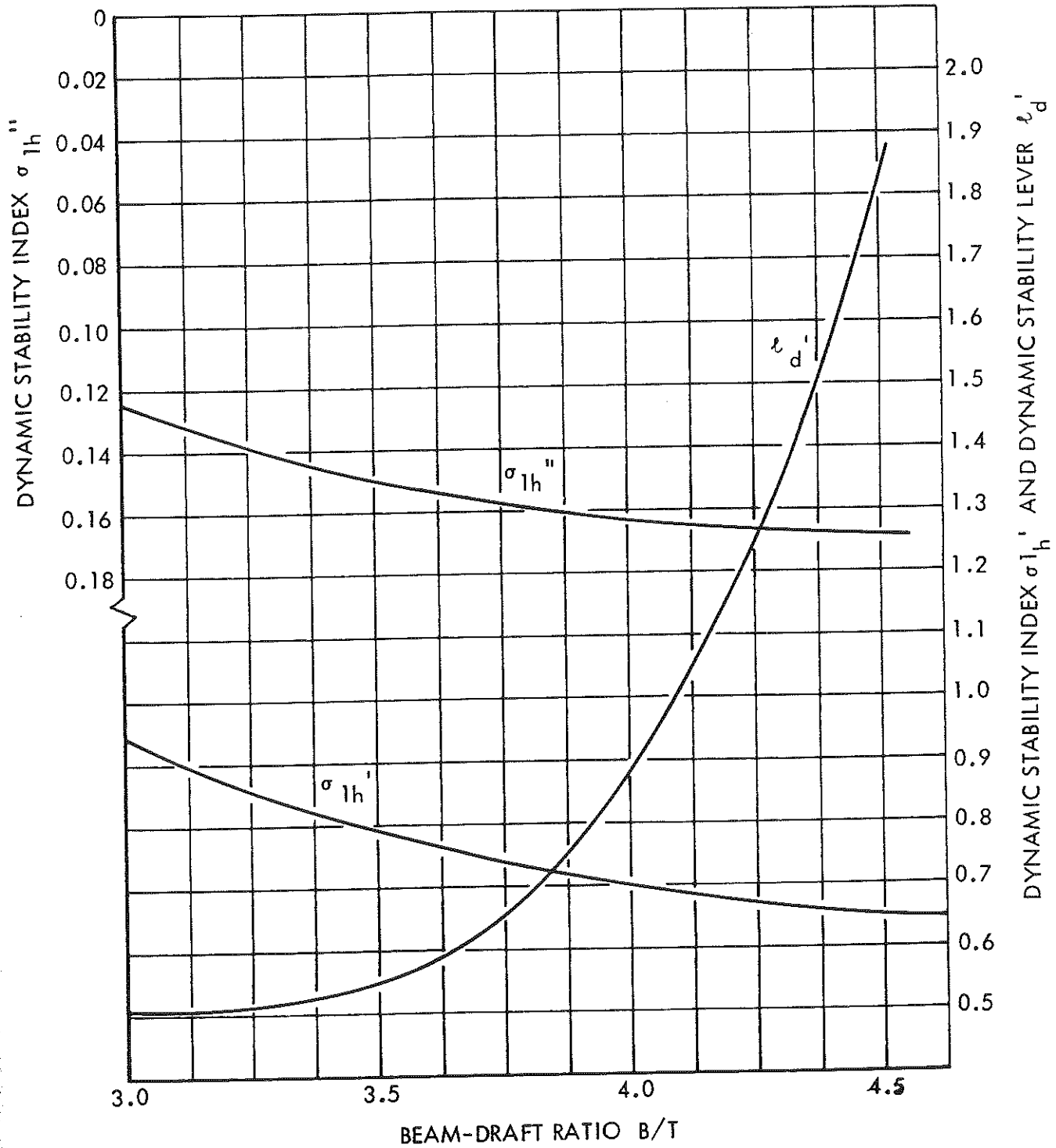

FIGURE 7-25 - EFFECT OF B/T VARIATION ON DYNAMIC STABILITY INDICES AT H/T = 1.2 - 200,000 TONS DISPLACEMENT

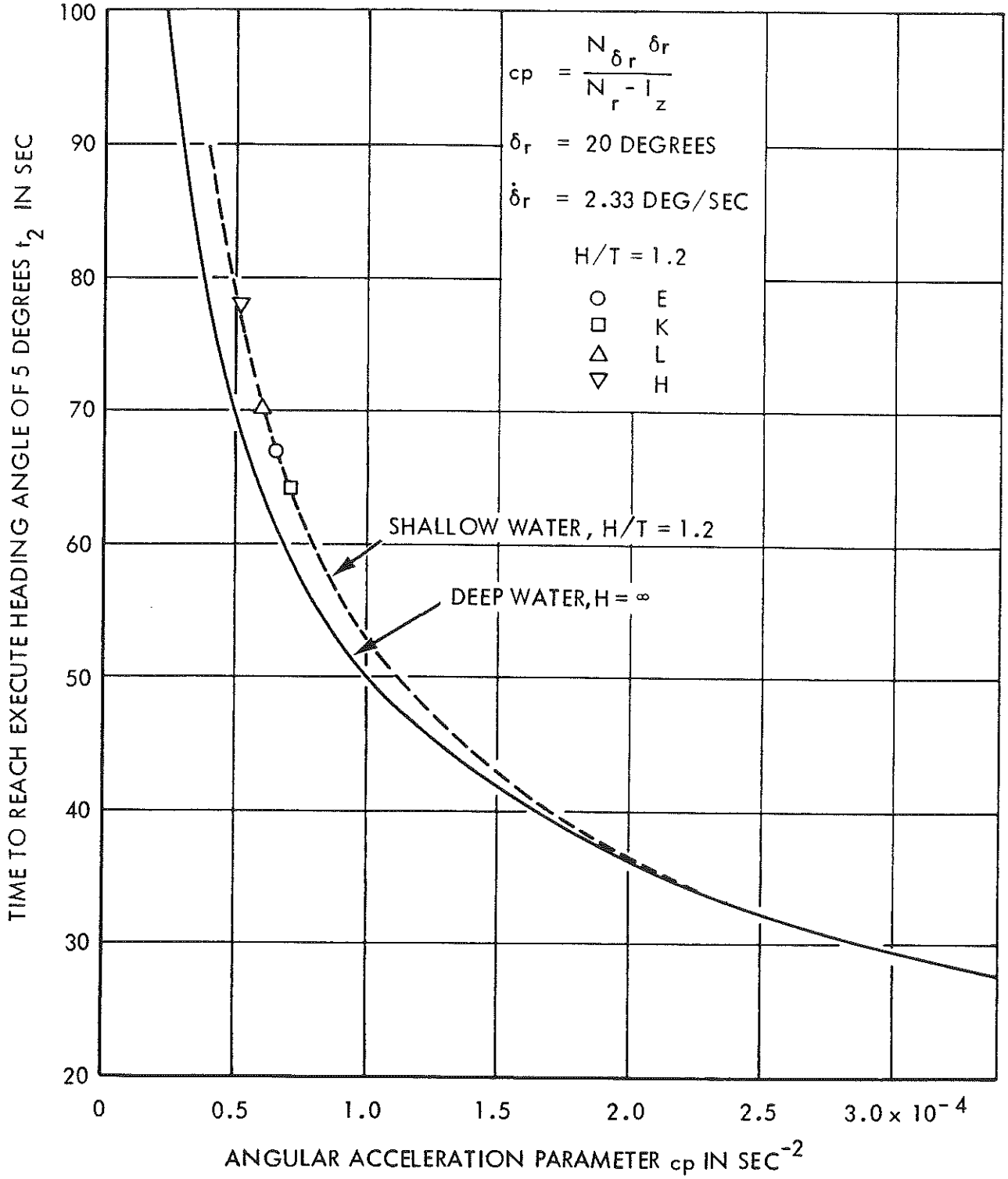

FIGURE 7-26 - TIME TO REACH EXECUTE HEADING CHANGE OF 5 DEGREES AS A FUNCTION OF DIMENSIONAL ANGULAR ACCELERATION PARAMETER

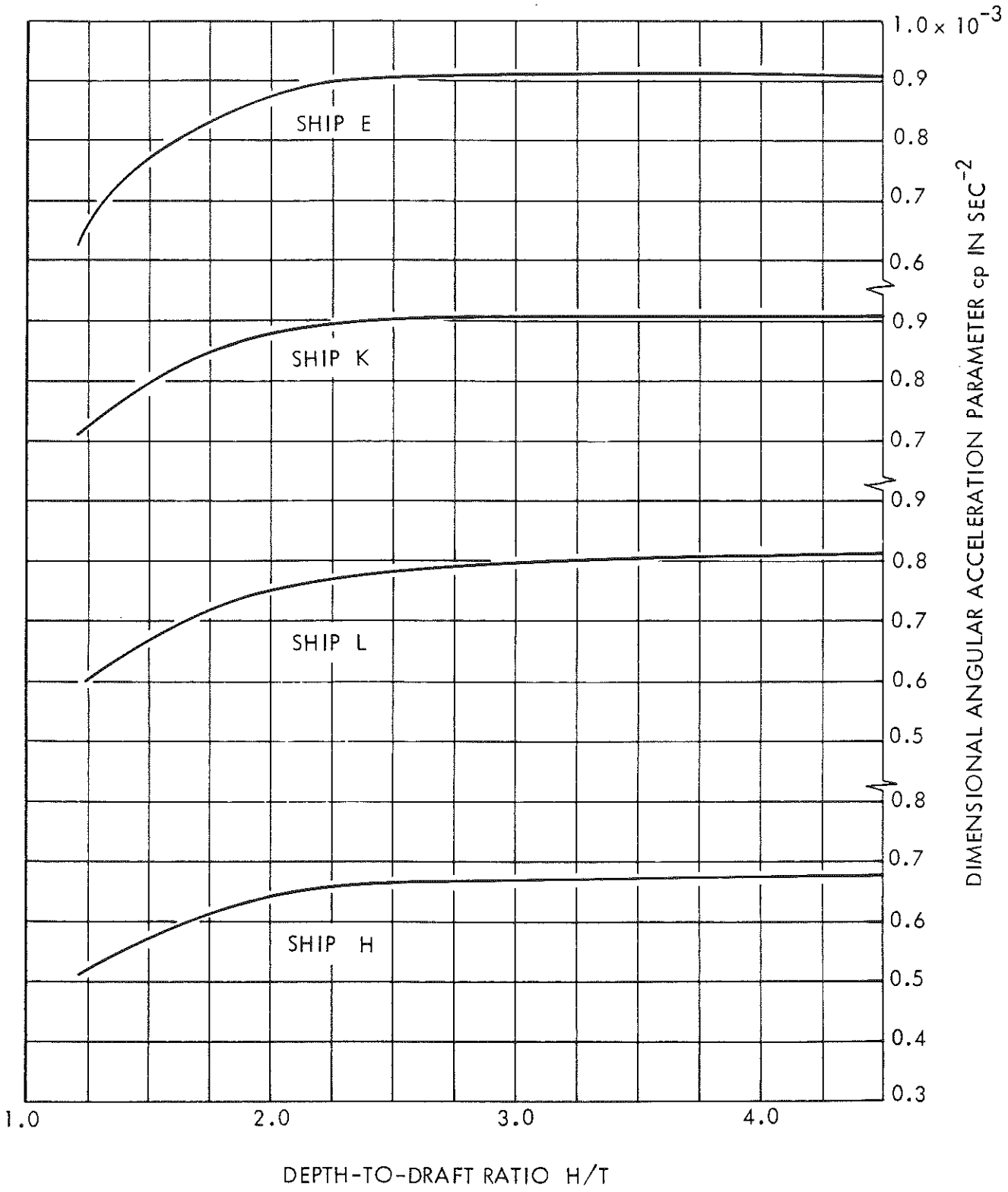

FIGURE 7-27 - EFFECT OF H/T VARIATION ON DIMENSIONAL ANGULAR ACCELERATION - 200,000 TON DISPLACEMENT

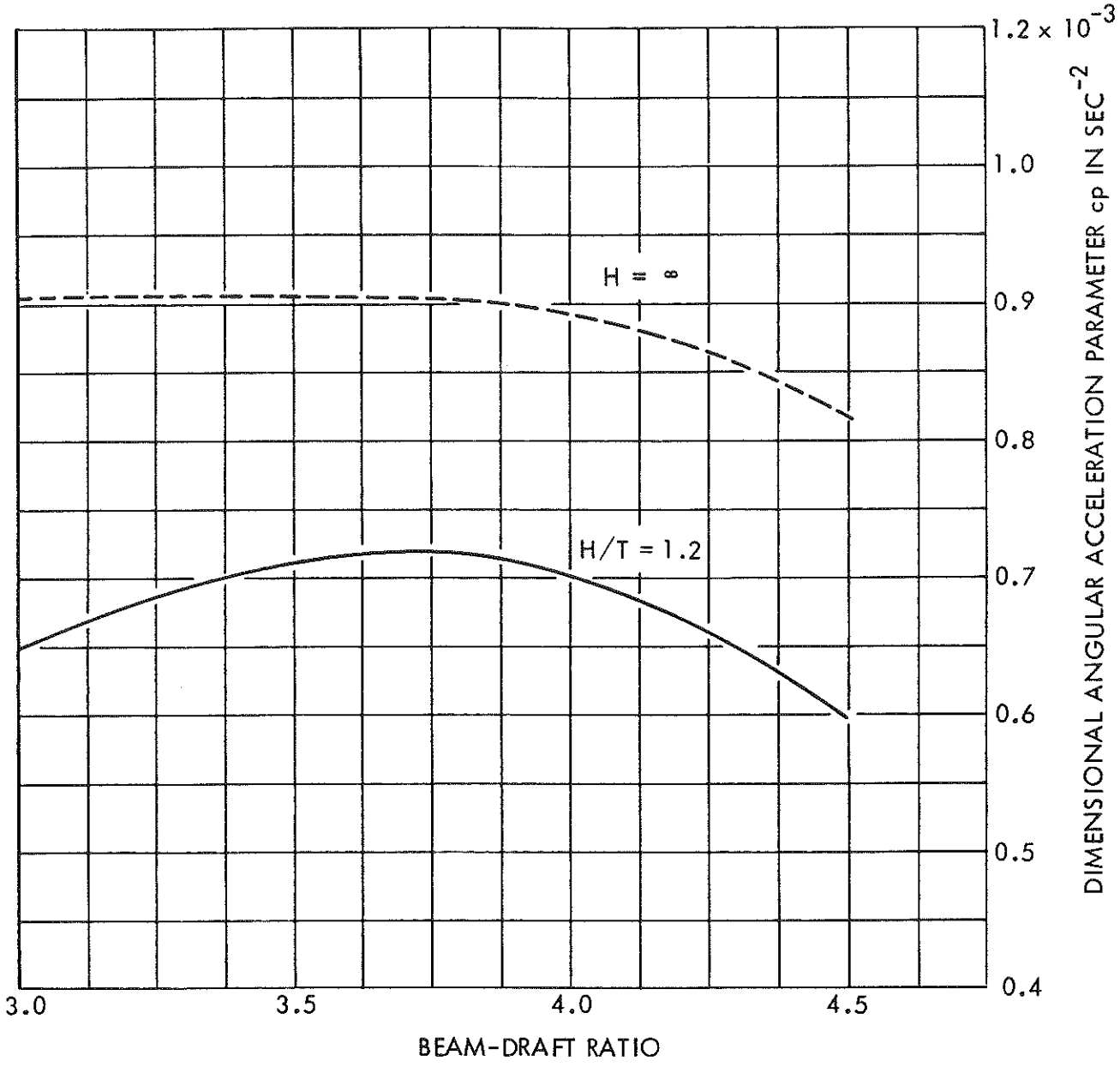

FIGURE 7-28 - EFFECT OF B/T VARIATION ON DIMENSIONAL ANGULAR ACCELERATION PARAMETER AT H/T = 1.2 - 200,000 TONS DISPLACEMENT

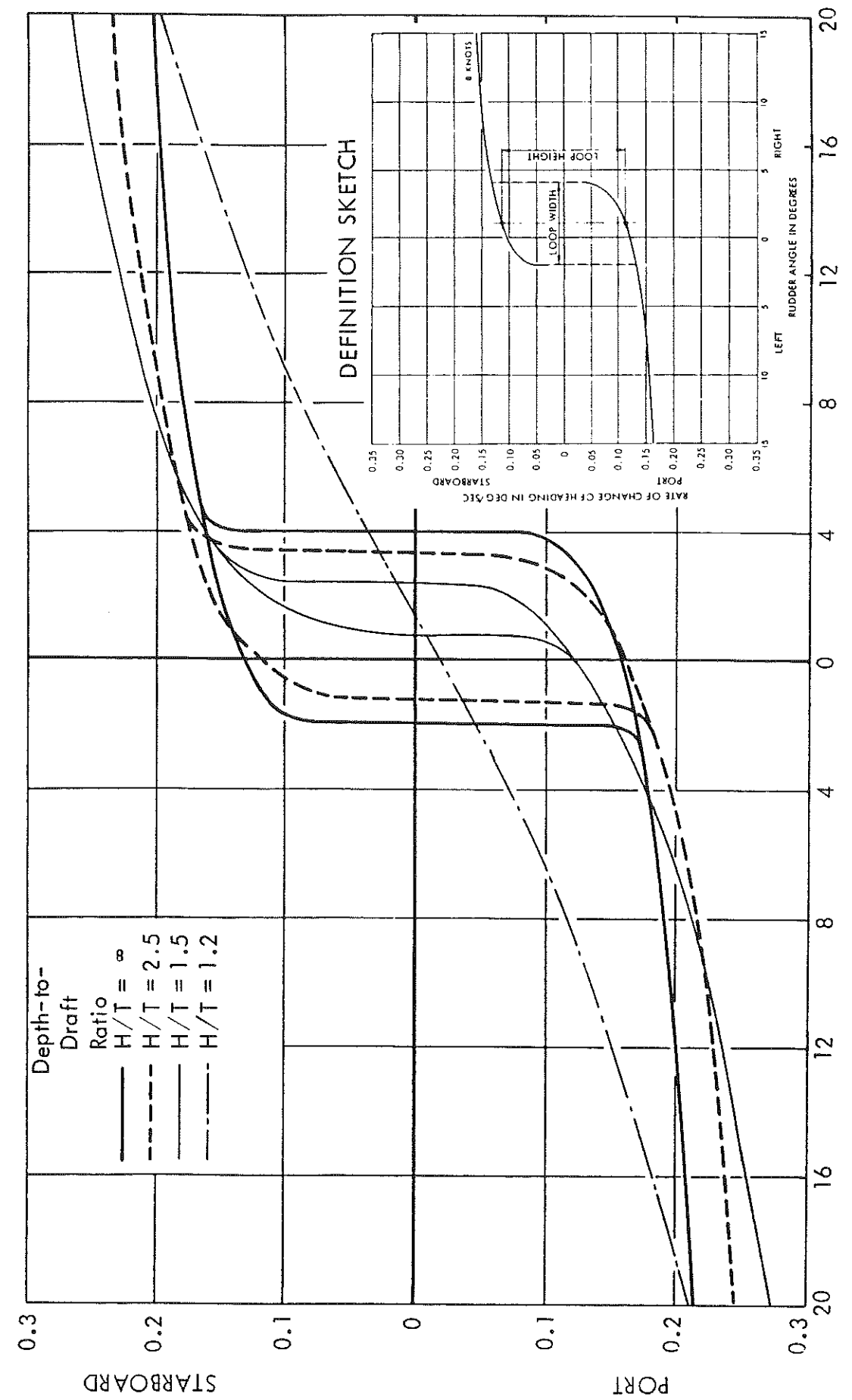

a) SHIP E

FIGURE 7-29 - EFFECT OF H/T VARIATION ON HEADING RATE CHANGE VERSUS RUDDER ANGLE CURVES FOR 200,000 TON DISPLACEMENT

Data shown are for an approach speed of 8 knots

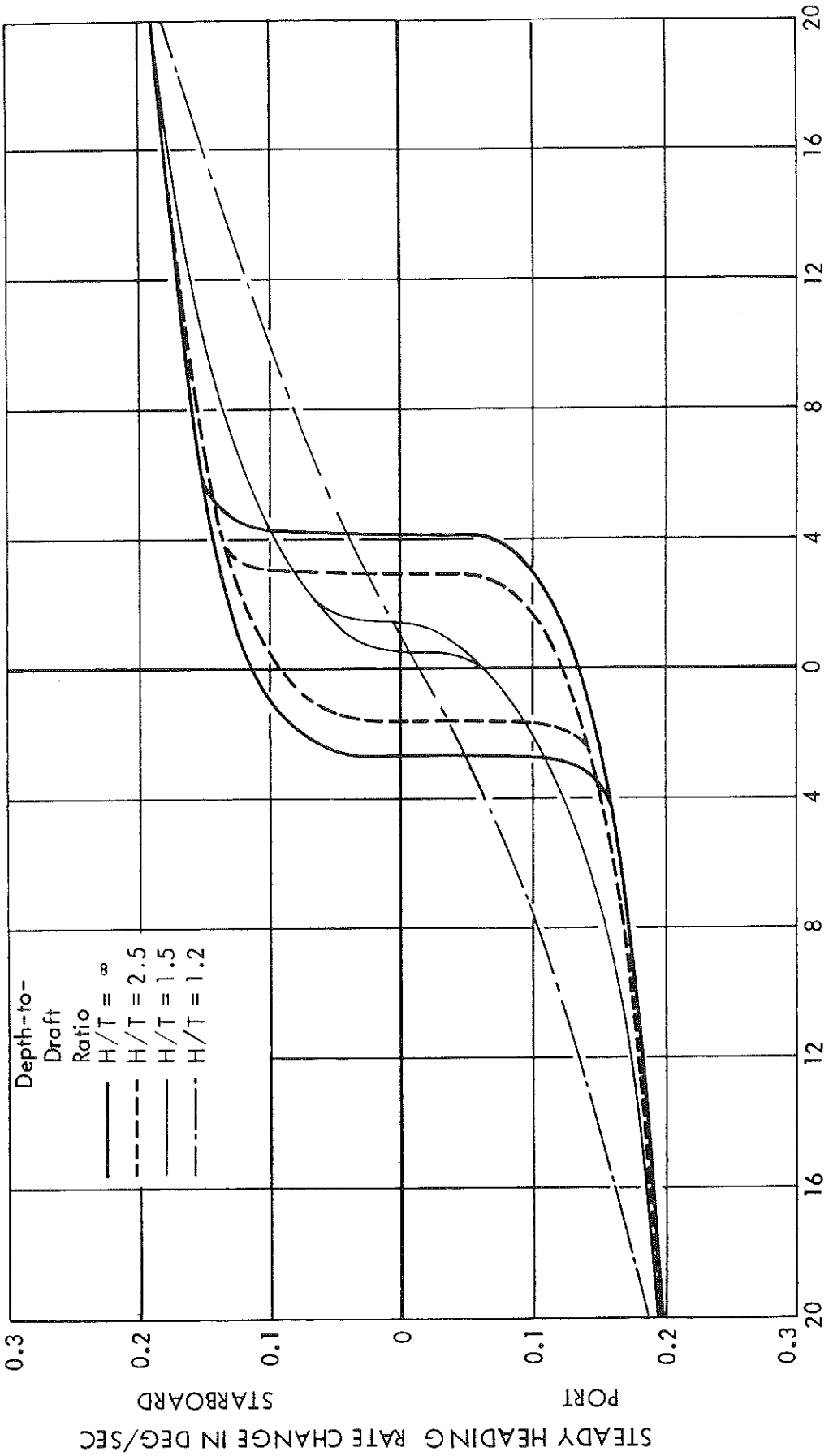

b) SHIP K

FIGURE 7-29 - CONTINUED

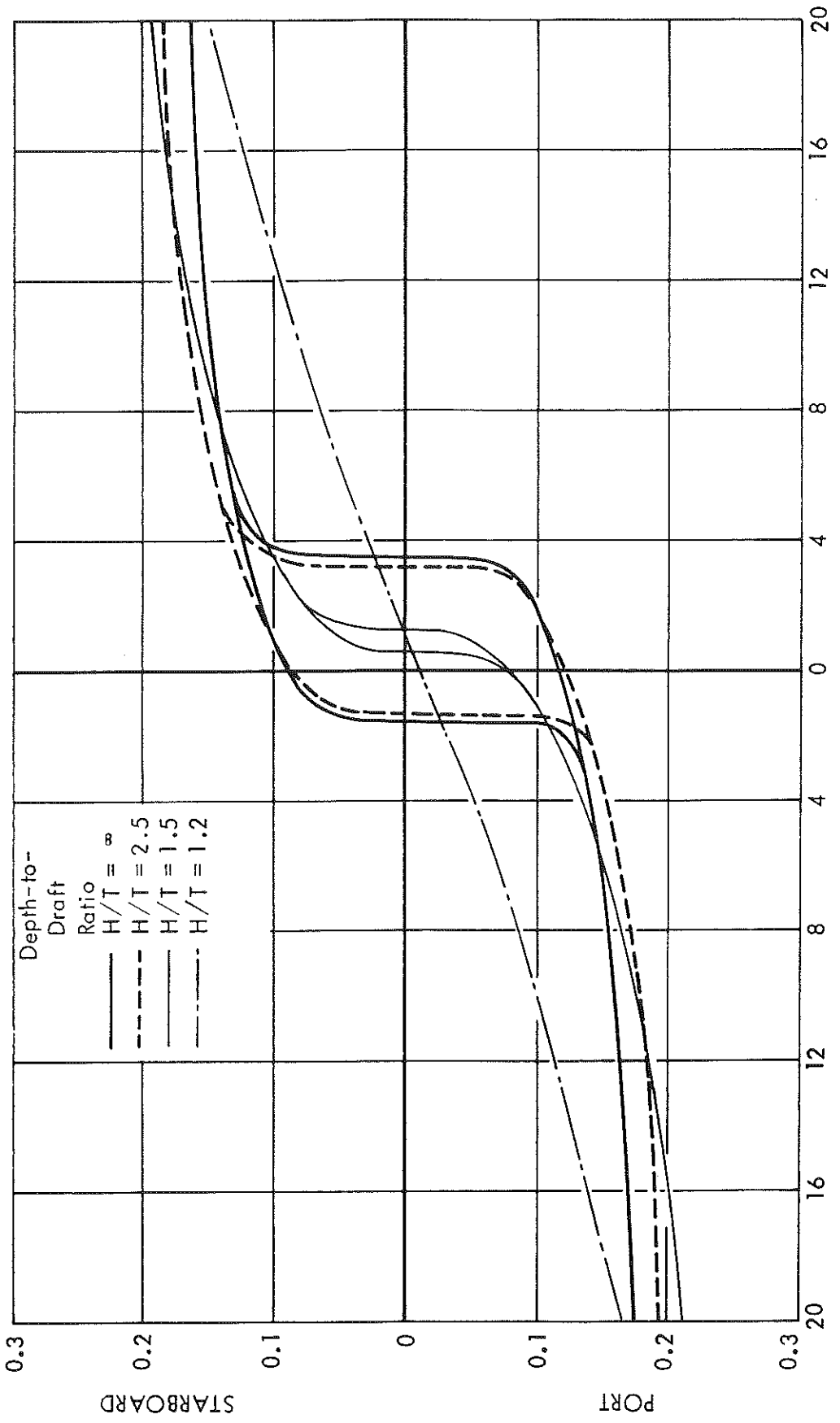

c) Ship L

FIGURE 7-29 - CONTINUED

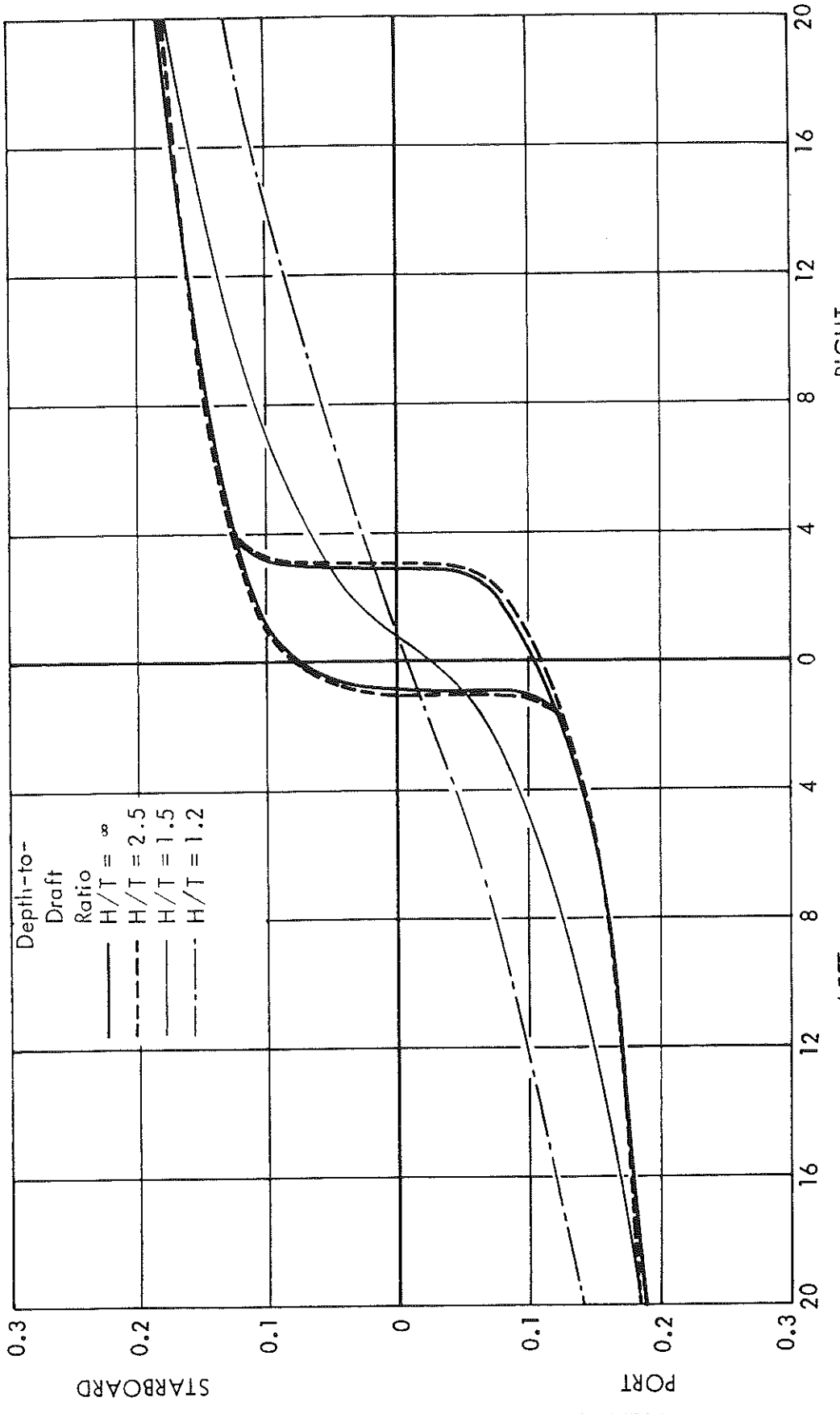

d) Ship H

FIGURE 7-29 - CONCLUDED

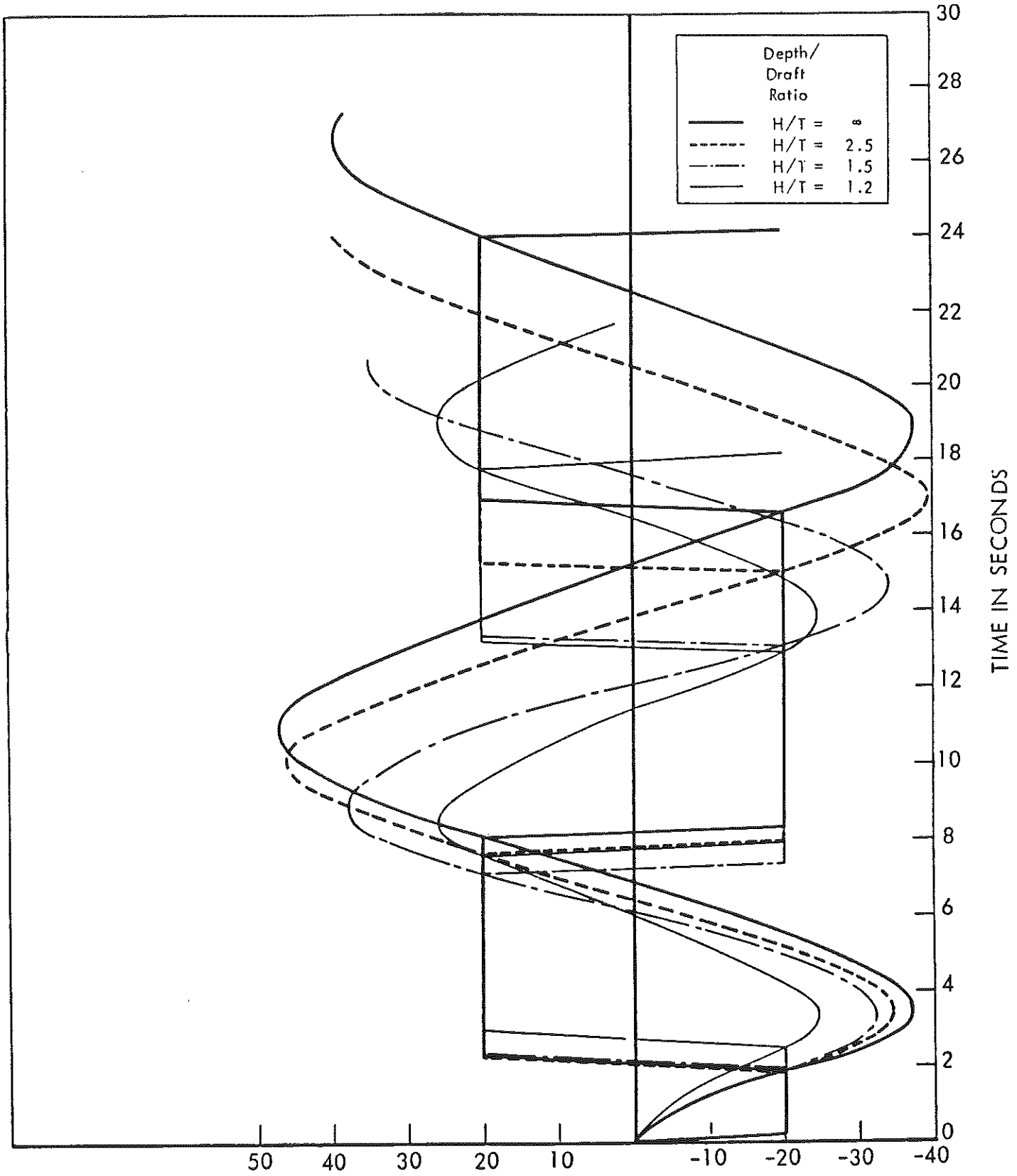

a) Heading Angle Trajectories

FIGURE 7-30 - COMPARISON OF TIME HISTORIES OF A 20-20 ZIGZAG MANEUVER FOR 200,000 TONS DISPLACEMENT IN DEEP AND SHALLOW WATER - SHIP E AT AN APPROACH SPEED OF 8 KNOTS

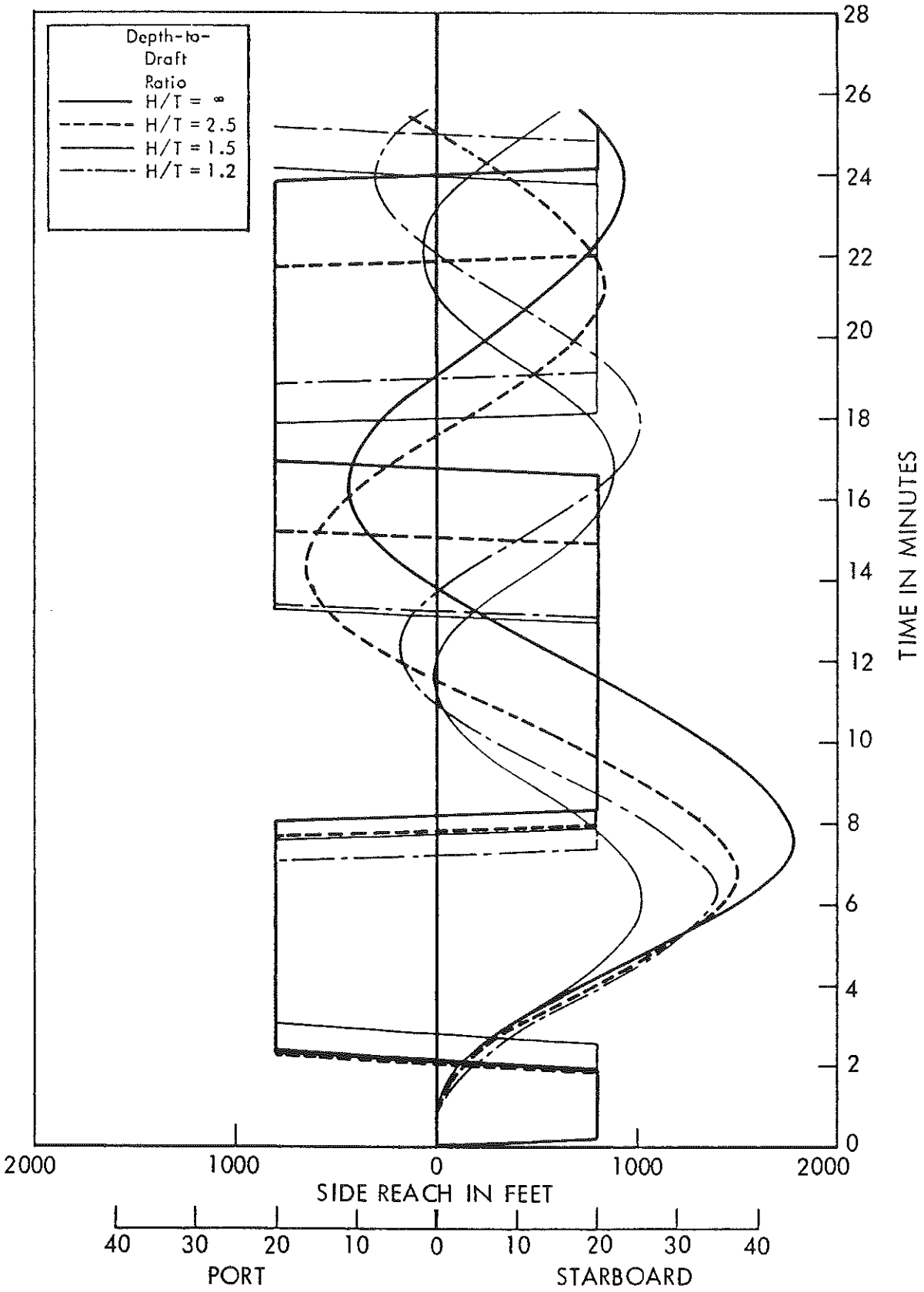

b) Path Trajectories

FIGURE 7-30 - CONCLUDED

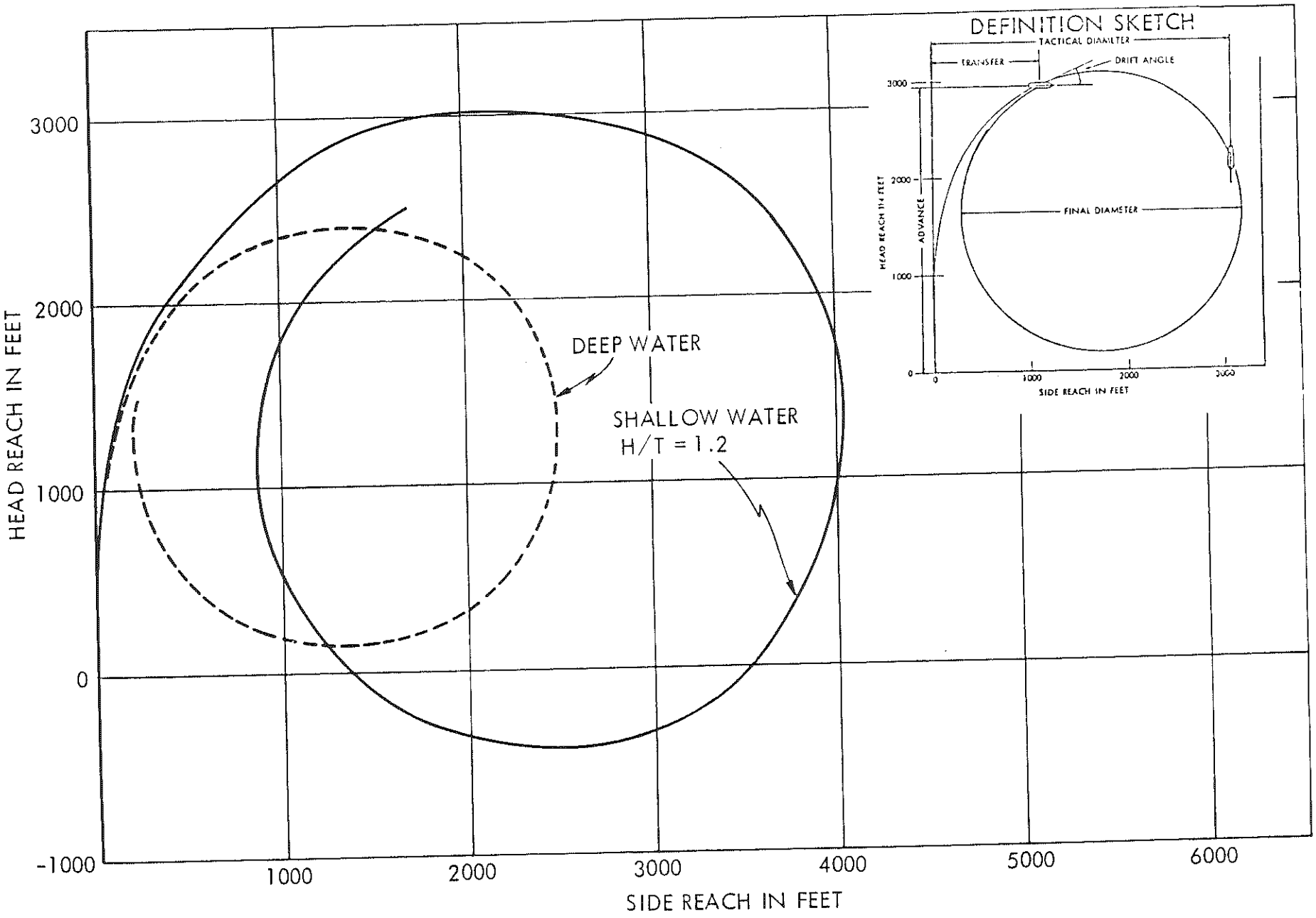

FIGURE 7-31 - COMPARISON OF PATH DURING A 35 DEGREE STARBOARD STEADY TURNING MANEUVER IN DEEP AND SHALLOW WATER AT H/T = 1.2, FOR 200,000 TON DISPLACEMENT SHIP E AT AN APPROACH SPEED

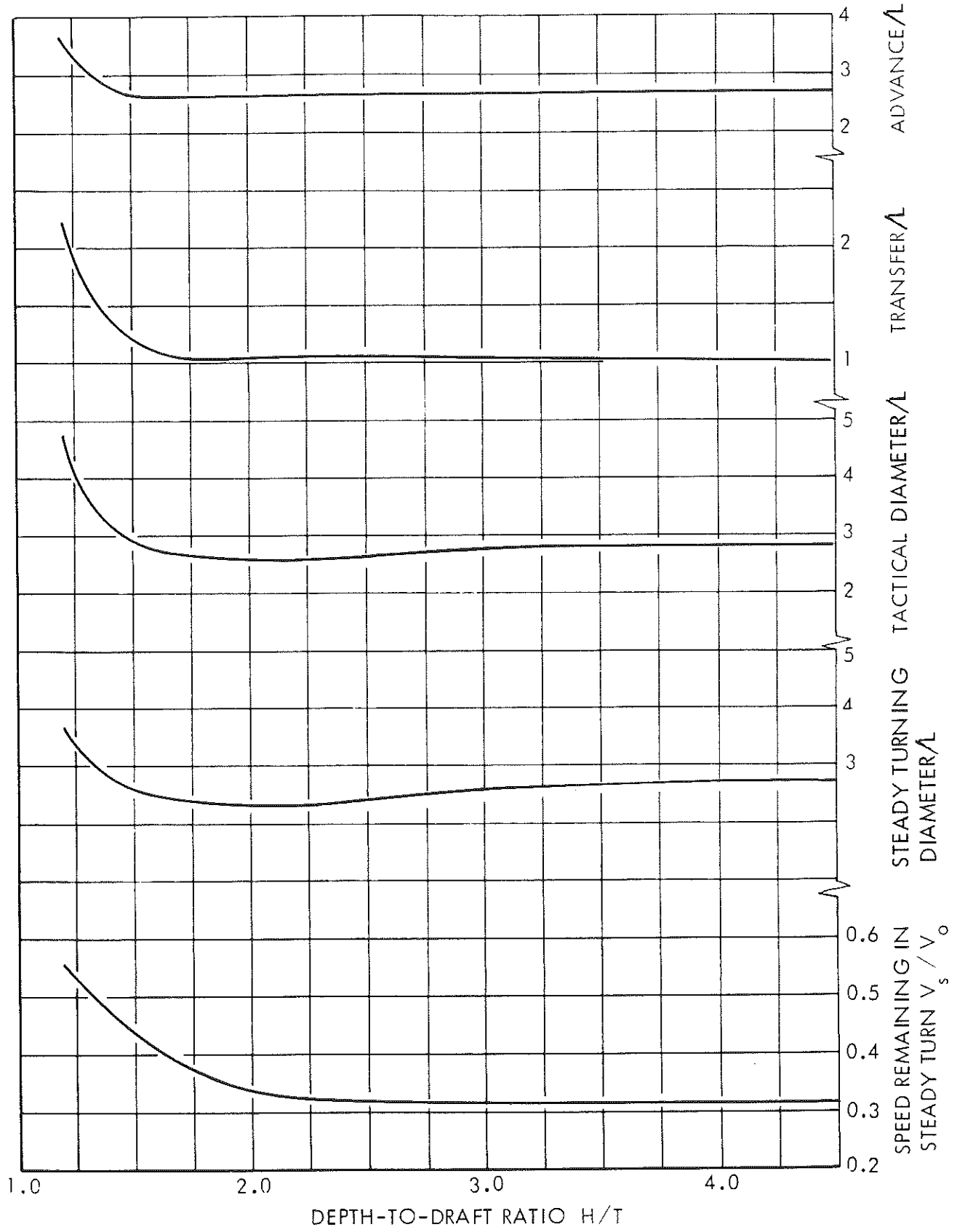

FIGURE 7-32 - EFFECT OF H/T VARIATION ON NONDIMENSIONAL NUMERICAL MEASURES FROM A 35 DEGREE STARBOARD STEADY TURNING MANEUVER OF 200,000 TON DISPLACEMENT SHIP E AT AN APPROACH SPEED OF 8 KNOTS

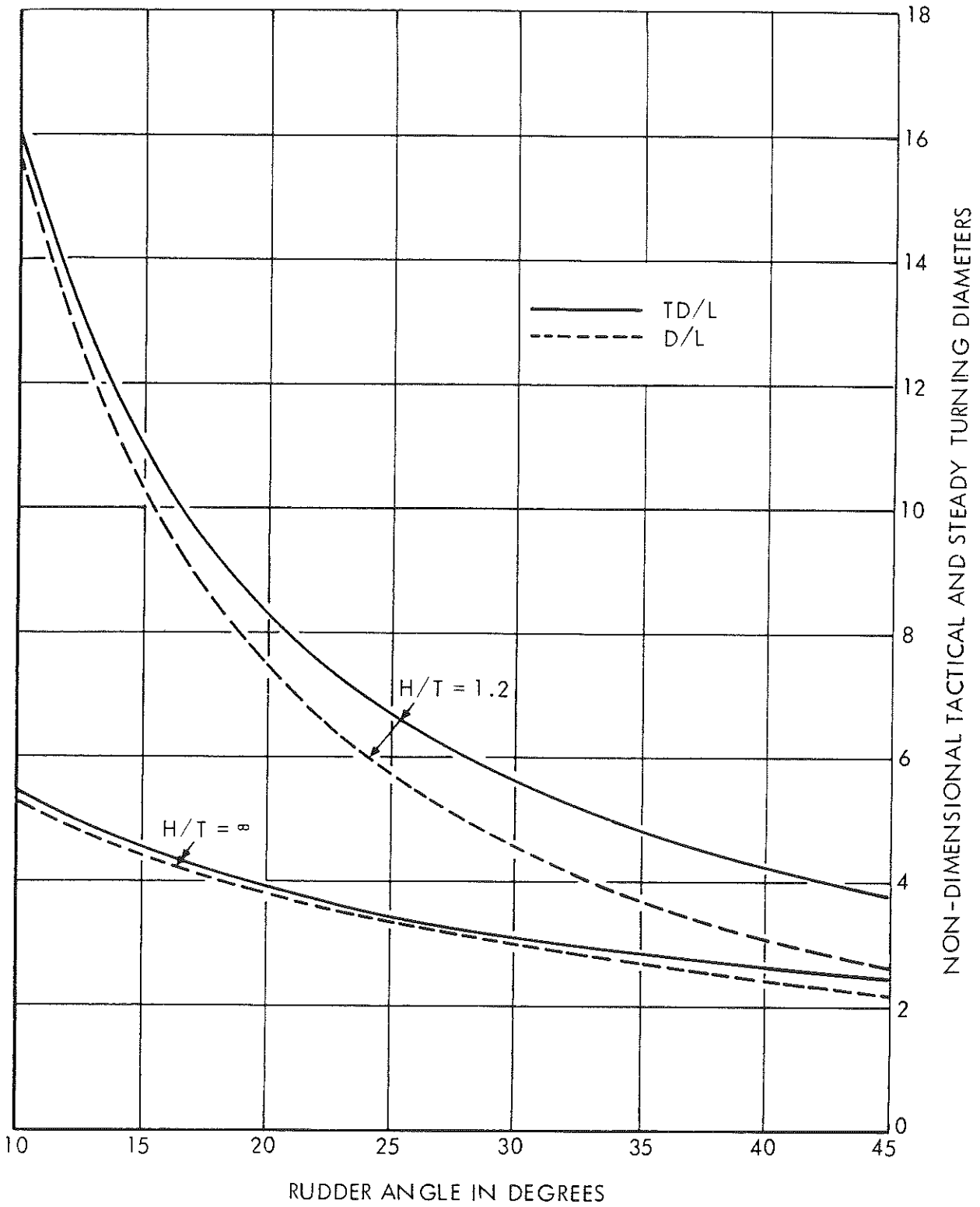

FIGURE 7-33 - VARIATION OF NONDIMENSIONAL TACTICAL AND STEADY TURNING DIAMETER WITH RUDDER ANGLE FOR 200,000 TON DISPLACEMENT SHIP E IN DEEP AND SHALLOW WATER AT H/T = 1.2

Data shown are for an approach speed of 8 knots

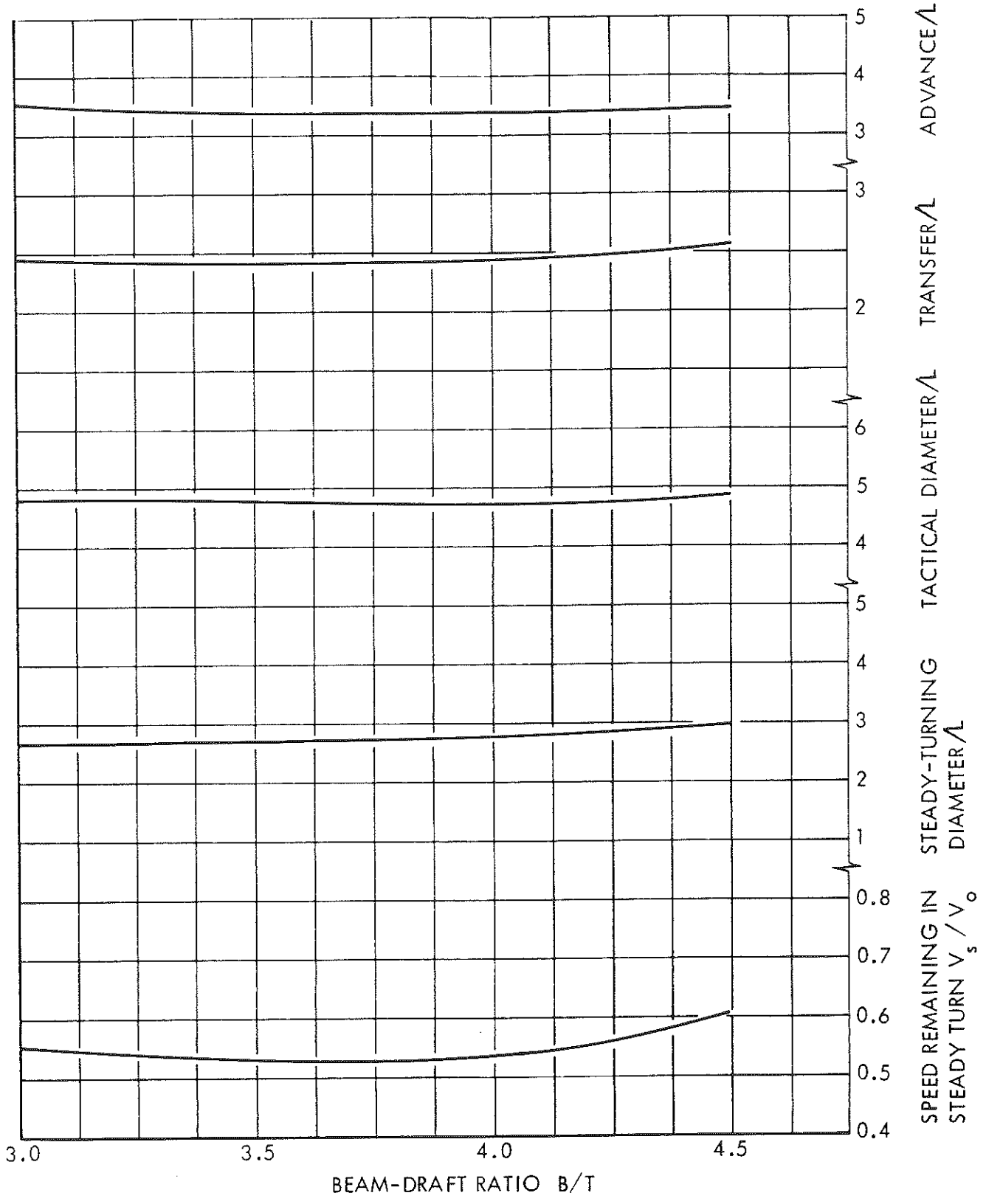

FIGURE 7-34 - EFFECT OF B/T VARIATION ON NONDIMENSIONAL NUMERICAL MEASURES ASSOCIATED WITH A 35 DEGREE STARBOARD TURN AT H/T = 1.2

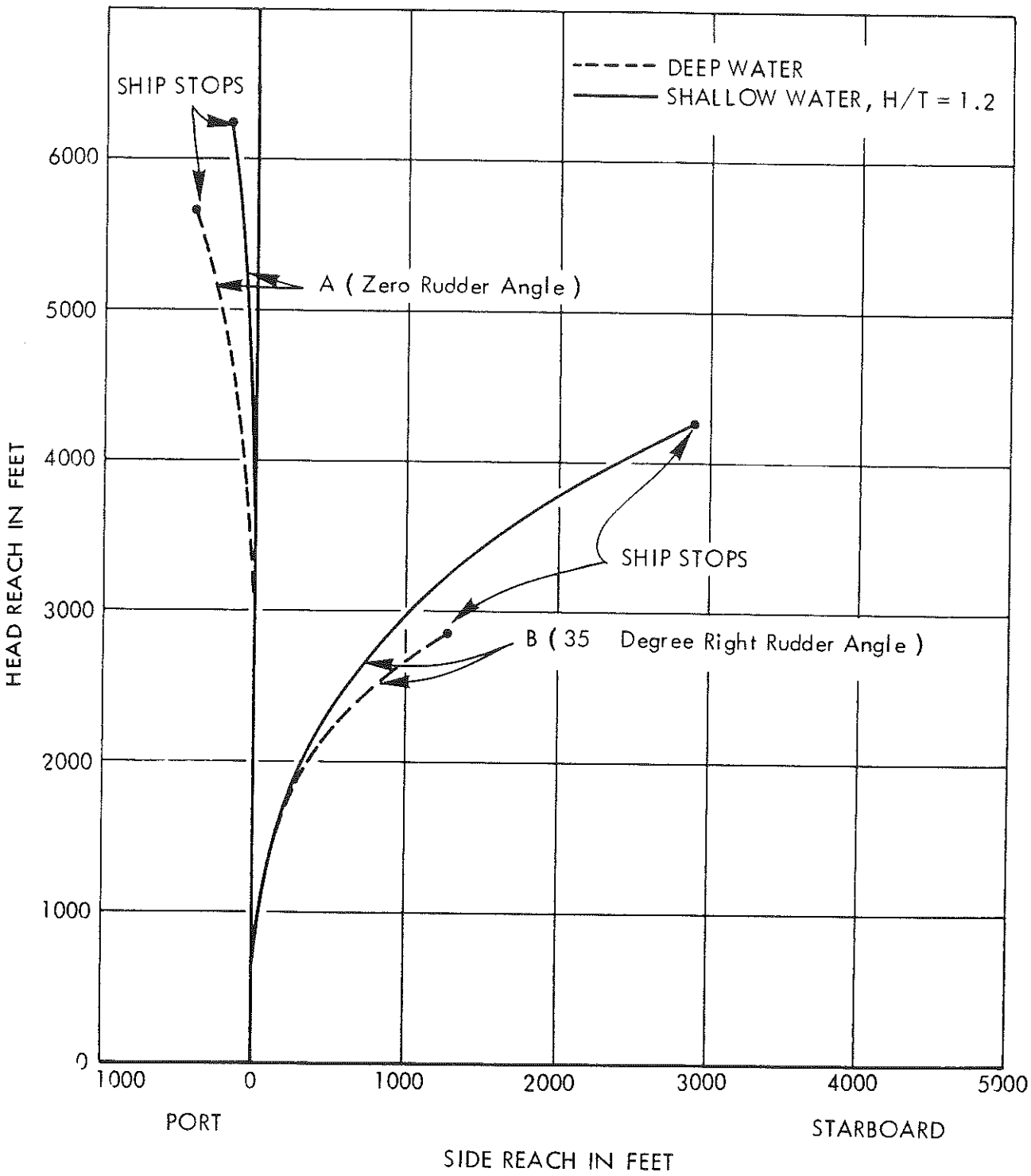

FIGURE 7-35 - COMPARISON OF PATH DURING STOPPING MANEUVERS FOR SHIP E IN DEEP AND SHALLOW WATER AT H/T = 1.2

Table 7-1

Test Conditions

(a) Dimensional Shallow Water Depth Conditions

	Condition	Model			200,000 Tons Displacement		
		H/T = 2.5	H/T = 1.5	H/T = 1.2	H/T = 2.5	H/T = 1.5	H/T = 1.2
E	Depth H, ft	3.333	2.000	1.600	141.95	85.17	68.14
	Draft T, ft	1.333	1.333	1.333	56.78	56.78	56.78
	(H-T), ft	2.000	0.667	0.267	85.17	28.39	11.36
K	Depth H, ft	2.667	1.600	1.280	122.33	73.40	58.72
	Draft T, ft	1.067	1.067	1.067	48.93	48.93	48.93
	(H-T), ft	1.600	0.533	0.213	73.40	24.47	9.79
L	Depth H, ft	2.545	1.527	1.222	108.33	65.00	52.00
	Draft T, ft	1.018	1.018	1.018	43.33	43.33	43.33
	(H-T), ft	1.527	0.509	0.204	65.00	21.67	8.67
H	Depth H, ft	3.333	2.000	1.600	130.05	78.03	62.42
	Draft T, ft	1.333	1.333	1.333	52.02	52.02	52.02
	(H-T), ft	2.000	0.667	0.267	78.03	26.01	10.40

(b) Nondimensional Values Corresponding to Ship Propulsion Point ($\eta = 1.0$)

		Nondimensional Value				Ratio to Deep-Water Value		
		H/T = ∞	H/T = 2.5	H/T = 1.5	H/T = 1.2	H/T = 2.5	H/T = 1.5	H/T = 1.2
E	F_N	0.08164	0.08164	0.08164	0.08164	1.000	1.000	1.000
	$1/J_a$	1.565	1.610	1.683	1.893	1.029	1.075	1.203
	$C_{Ti} = C_{Ts}$	2.481×10^{-3}	2.871×10^{-3}	4.009×10^{-3}	5.418×10^{-3}	1.157	1.616	2.813
K	F_N	0.07867	0.07867	0.07867	0.07867	1.000	1.000	1.000
	$1/J_a$	1.442	1.488	1.562	1.732	1.032	1.083	1.201
	$C_{Ti} = C_{Ts}$	2.217×10^{-3}	2.937×10^{-3}	4.487×10^{-3}	5.887×10^{-3}	1.325	2.024	2.655
L	F_N	0.07632	0.07632	0.07632	0.07632	1.000	1.000	1.000
	$1/J_a$	1.612	1.700	1.847	2.022	1.055	1.146	1.254
	$C_{Ti} = C_{Ts}$	2.255×10^{-3}	3.325×10^{-3}	4.975×10^{-3}	6.775×10^{-3}	1.475	2.206	3.004
H	F_N	0.07482	0.07482	0.07482	0.07482	1.000	1.000	1.000
	$1/J_a$	1.665	1.715	1.808	1.949	1.030	1.086	1.171
	$C_{Ti} = C_{Ts}$	2.138×10^{-3}	2.618×10^{-3}	3.568×10^{-3}	4.168×10^{-3}	1.224	1.669	1.949

Table 7.2

Principal Geometric Characteristics of MARAD Series Models and Corresponding 200,000 Ton Displacement Ships

Characteristic	Model				Ship			
	E	K	L	H	E	K	L	H
Hull								
Length (between perps.) L, ft	20.00	20.00	22.90	26.00	851.64	917.36	974.84	1014.42
Beam B, ft	4.00	4.00	4.58	4.00	170.33	183.47	194.97	156.06
Draft T, ft	1.333	1.067	1.018	1.333	56.78	48.93	43.33	52.02
Displacement (volume) ∇, ft^3	90.60	72.54	90.74	117.86				
Displacement, long tons					200,000	200,000	200,000	200,000
Wetted Surface (includes rudder) S, ft^2	121.762	111.599	137.582	156.988	220,782	234,790	249,327	238,975
C_B	0.85	0.85	0.85	0.85	0.85	0.85	0.85	0.85
L/B	5.00	5.00	5.00	6.50	5.00	5.00	5.00	6.50
B/T	3.00	3.75	4.50	3.00	3.00	3.75	4.50	3.00
LCB/L, percent fwd. of midships	2.50	2.50	2.50	2.50	2.50	2.50	2.50	2.50
Rudder								
Designation	B	D	E	B	B	D	E	B
Total planform area A_T, ft^2	0.8869	0.7247	0.6871	0.8869	1608.15	1524.68	1245.17	1350.08
Fixed Area A_F, ft^2	0.1117	0.0953	0.0821	0.1117	202.54	200.50	148.79	170.03
Movable Area A_M, ft^2	0.7752	0.6294	0.6050	0.7752	1405.61	1324.18	1096.38	1180.05
Mean Span $\bar{b}$, ft	1.1202	0.9153	0.8678	1.1202	47.70	41.98	36.94	43.71
Root chord, c_r	0.7917	0.7917	0.7917	0.7917	33.71	36.31	33.70	30.89
Tip chord, c_t	0.7917	0.7917	0.7917	0.7917	33.71	36.31	33.70	30.89
Geometric aspect ratio $\bar{b}^2/A_T$	1.4149	1.1560	1.0960	1.4149	1.4149	1.1560	1.1560	1.4149
Rudderstock centerline, percent chord from leading edge (located at AP)	30	30	30	30	30	30	30	30
Propeller								
Designation	B	D	D	B	B	D	E	B
Number of blades	4	4	4	4	4	4	4	4
Diameter D, ft	0.689	0.604	0.604	0.689	29.34	27.70	25.71	26.88
Diameter-to-Draft Ratio D/T	0.517	0.566	0.593	0.517	0.517	0.566	0.593	0.517

Table 7-3

Residuary Resistance Coefficients for 200,000 Tons Displacement at Various Depth Conditions

(Values of residuary resistance coefficients must be multiplied by 10^{-3})

H/T	Ship Designation			
	E	K	L	H
∞	0.780	0.530	0.580	0.470
2.5	1.170	1.250	1.650	0.950
1.5	2.308	2.800	3.300	1.900
1.2	3.717	4.200	5.100	2.500

Note: C_R values are assumed to be constant up to F_N of about 0.100. H/T = 2.5 values for Models K, L, and H are interpolated.

Table 7-4

Summary of Resistance and Propulsion Characteristics for 200,000 Ton Displacement Series Ships for Various Water Depth Conditions

Model	H/T	P/D	D/T	F_N	C_{Ts}	$1-w_T$	$1-w_Q$	$1-w$	$1-t$	e_h	e_{rr}	e_p	J_a	PC	EHP	SHP	RPM
E	∞	0.764	0.517	0.08164	0.002481	0.667	0.672	0.670	0.800	1.199	1.002	0.545	0.674	0.654	2444	3737	40.98
	2.5				0.002871	0.654	0.695	0.674	0.841	1.286	1.05	0.52	0.643	0.699	2829	4047	42.96
	1.5				0.004004	0.428	0.428	0.428	0.733	1.713	1.000	0.34	0.610	0.582	3945	6778	45.28
	1.2				0.005418	0.368	0.432	0.400	0.739	2.008	1.04	0.28	0.554	0.585	5338	9124	49.86
H	∞	0.767	0.517	0.07482	0.002138	0.718	0.690	0.704	0.775	1.084	0.975	0.521	0.627	0.548	2280	4161	48.10
	1.5				0.003568	0.502	0.487	0.494	0.657	1.309	0.991	0.370	0.540	0.480	3805	7927	55.85
	1.2				0.004168	0.419	0.390	0.404	0.650	1.551	0.984	0.285	0.513	0.435	4445	10218	58.79
K	∞	0.766	0.566	0.7867	0.002217	0.715	0.680	0.697	0.800	1.119	0.975	0.562	0.629	0.613	2322	3788	46.53
	1.5				0.004487	0.490	0.525	0.476	0.888	1.812	1.075	0.33	0.566	0.642	4701	7322	51.71
	1.2				0.005887	0.445	0.506	0.514	0.834	1.874	0.987	0.28	0.515	0.591	6168	10437	56.83
L	∞	0.759	0.593	0.07632	0.002255	0.697	0.750	0.723	0.776	1.110	1.05	0.526	0.615	0.613	2509	4092	51.27
	1.5				0.004975	0.425	0.506	0.466	0.810	1.906	1.049	0.32	0.518	0.639	5535	8662	60.87
	1.2				0.006775	0.387	0.425	0.406	0.793	2.039	1.012	0.26	0.452	0.537	7538	14037	69.76

Table 7-5

MARAD Series Model E - Nondimensional Stability and Control Derivatives, Hull Constants, and Stability Indices for Various H/T Values

(Values are based on a 200,000 ton full load displacement at a reference speed of 8 knots.)

	Nondimensional Value				Ratio to Deep Water Value			
	H/T = ∞	H/T = 2.5	H/T = 1.5	H/T = 1.2	H/T = ∞	H/T = 2.5	H/T = 1.5	H/T = 1.2
Y_v'	-0.01914	-0.02788	-0.05167	-0.13107	1.000	1.457	2.700	6.848
N_v'	-0.01072	-0.01292	-0.02756	-0.05238		1.205	2.571	4.886
Y_r'	0.00554	0.00519	0.00659	0.01278		0.936	1.190	2.307
N_r'	-0.00460	-0.00416	-0.00535	-0.00898		0.904	1.163	1.952
$Y_{\dot{v}}'$	-0.02017	-0.02547	-0.05304	-0.09543		1.263	2.630	4.731
$N_{\dot{v}}'$	0.00002	0.00004	0.00055	0.00201		2.000	27.500	100.500
$Y_{\dot{r}}'$	-0.00035	-0.00043	-0.00125	-0.00300		1.229	3.571	8.571
$N_{\dot{r}}'$	-0.00136	-0.00137	-0.00189	-0.00255		1.007	1.390	1.875
$Y_{\delta r}'$	0.00545	0.00547	0.00554	0.00650		1.004	1.017	1.193
$N_{\delta r}'$	-0.00286	-0.00287	-0.00291	-0.00293		1.004	1.017	1.024
m'	0.02267	0.02267	0.02267	0.02267		1.000	1.000	1.000
I_z'	0.001417	0.001417	0.001417	0.001417		1.000	1.000	1.000
$-Y_{\dot{v}}'/m'$	0.8897	1.1235	2.3397	4.2095		1.263	2.630	4.731
σ_{1h}'	0.3331	0.3435	0.2691	-0.5608		1.031	0.808	-1.683
σ_{2h}'	-2.4086	-2.3798	-2.4618	-2.4812		0.996	1.022	1.030
σ_{1h}''	0.07482	0.07715	0.06042	-0.1259		1.031	0.808	-1.683
t_v'	0.5601	0.4634	0.5334	0.3996		0.827	0.952	0.713
t_r'	0.2688	0.2382	0.3331	0.9098		0.886	1.239	3.384
t_d'	-0.2912	-0.2252	-0.2003	0.5102	1.000	0.773	0.688	-1.752

Table 7-6

MARAD Series Model K - Nondimensional Stability and Control Derivatives, Hull Constants, and Stability Indices for Various H/T Values

(Values are based on a 200,000 ton full load displacement at a reference speed of 8 knots.)

	Nondimensional Value				Ratio to Deep Water Value			
	H/T = ∞	H/T = 2.5	H/T = 1.5	H/T = 1.2	H/T = ∞	H/T = 2.5	H/T = 1.5	H/T = 1.2
Y_v'	-0.01294	-0.01521	-0.03771	-0.10675	1.000	1.175	1.960	8.250
N_v'	-0.00687	-0.00727	-0.02056	-0.03903		1.058	2.992	5.681
Y_r'	0.00342	0.003685	0.00659	0.01105		1.077	1.927	3.231
N_r'	-0.00314	-0.00325	-0.00411	-0.00717		1.035	1.309	2.283
$Y_{\dot{v}}'$	-0.01349	-0.01867	-0.03958	-0.06487		1.384	2.934	4.809
$N_{\dot{v}}'$	-0.00016	-0.00007	0.000596	0.00250		0.437	-3.725	-15.625
$Y_{\dot{r}}'$	-0.00024	-0.00041	-0.00105	-0.00218		1.708	4.375	9.083
$N_{\dot{r}}'$	-0.000857	-0.000865	-0.00121	-0.00166		1.009	1.412	1.937
$Y_{\delta r}'$	0.00456	0.00451	0.00477	0.00657		0.989	1.046	1.441
$N_{\delta r}'$	-0.00238	-0.00238	-0.00250	-0.00265		1.000	1.050	1.113
m'	0.01813	0.01813	0.01813	0.01813		1.000	1.000	1.000
I_z'	0.001133	0.001133	0.001133	0.001133		1.000	1.000	1.000
$-Y_{\dot{v}}'/m'$	0.7440	1.0298	2.1831	3.5780		1.384	2.934	4.809
σ_{1h}'	0.4139	0.3310	0.2393	-0.7574		0.800	0.578	-1.830
σ_{2h}'	-2.3388	-2.2799	-2.5277	-2.7236		0.975	1.081	1.165
σ_{1h}''	0.08630	0.06902	0.04988	-0.1579		0.800	0.578	-1.830
ℓ_v'	0.5309	0.4780	0.5452	0.3656		0.900	1.027	0.689
ℓ_r'	0.2126	0.2251	0.3564	1.0138		1.059	1.676	4.769
ℓ_d'	-0.3184	-0.2529	-0.1883	0.6481	1.000	0.794	0.591	-2.035

Table 7-7

MARAD Series Model L - Nondimensional Stability and Control Derivatives, Hull Constants, and Stability Indices for Various H/T Values

(Values are based on a 200,000 ton full load displacement at a reference speed of 8 knots.)

	Nondimensional Value				Ratio to Deep Water Value			
	H/T = ∞	H/T = 2.5	H/T = 1.5	H/T = 1.2	H/T = ∞	H/T = 2.5	H/T = 1.5	H/T = 1.2
Y_v'	-0.00935	-0.01269	-0.03632	-0.09770	1.000	1.357	3.884	10.449
N_v'	-0.00448	-0.00635	-0.02031	-0.03705		1.417	4.533	8.270
Y_r'	0.00251	0.00271	0.00485	0.01223		1.080	1.627	4.873
N_r'	-0.00250	-0.00259	-0.00350	-0.00632		1.036	1.400	2.528
$Y_{\dot{v}}'$	-0.00981	-0.01379	-0.02760	-0.05009		1.406	2.813	5.107
$N_{\dot{v}}'$	-0.00016	-0.00015	0.000374	0.001117		0.938	-2.356	-6.981
$Y_{\dot{r}}'$	-0.00011	0.00021	0.001033	0.002217		-1.909	-9.391	-20.154
$N_{\dot{r}}'$	-0.000586	-0.000663	-0.001104	-0.001433		1.131	1.884	2.445
$Y_{\delta r}'$	0.00359	0.00361	0.00414	0.00581		1.005	1.153	1.618
$N_{\delta r}'$	-0.001865	-0.00187	-0.00207	-0.00212		1.003	1.110	1.137
m'	0.01511	0.01511	0.01511	0.01511		1.000	1.000	1.000
I_z'	0.000944	0.000944	0.000944	0.000944		1.000	1.000	1.000
$-Y_{\dot{v}}'/m'$	0.6490	0.9126	1.8266	3.3150		1.406	2.813	5.107
σ_{1h}'	0.3740	0.4143	0.2956	-0.8506		1.108	0.790	-2.274
σ_{2h}'	-2.3186	-2.3848	-3.1516	-3.9365		1.029	1.359	1.698
σ_{1h}''	0.07338	0.08128	0.05799	-0.1669		1.108	0.790	-2.274
ℓ_v'	0.4791	0.5004	0.5592	0.3809		1.044	1.167	0.795
ℓ_r'	0.1985	0.2090	0.3414	2.200		1.053	1.720	11.083
ℓ_d'	-0.2806	-0.2914	-0.2178	1.820	1.000	1.038	0.776	-6.486